DOCTOR OF PHILOSOPHY

Rapid determination of parasite viability using AC electrokinetic techniques

Dalton, Colin

Award date:
2002

Awarding institution:
Bangor University

A THESIS SUBMITTED TO THE UNIVERSITY OF WALES
IN CANDIDATURE FOR THE DEGREE OF
DOCTOR OF PHILOSOPHY

Rapid Determination of Parasite Viability using AC Electrokinetic Techniques

BY

Colin Dalton
B. Eng. (Hons) Electronic Engineering
M.Sc. Electronic Engineering

School of Informatics
University of Wales
Bangor
Gwynedd, U.K.

12th July 2002

To my family,

and in memory of
my best friend, Chris.

Acknowledgements

There are numerous people to whom I owe a great deal for making the three years of my Ph.D. the best ever.

I am indebted to my supervisors : Prof. Ron Pethig, Prof. Huw V. Smith and Dr. Julian Burt.

I am particularly grateful to Dr. Andy Goater for his support and assistance over the years, especially with understanding the biological nature of the work.

I would also like to express my thanks to my colleagues within the group and the department : Dr. Chris Hayden, Dr. Sally Cotterill, John Tame, Dr. Paul Rees, Dr. Iestyn Pierce, James Drysdale, Alan Grant, Dr. Mark Talary, Dr. Richard Lee and especially Prof. Martin Taylor

My gratitude also to all the administration staff who put up with my idiosyncrasies over the years : Julie Boulton, Gaynor Mew, Lynne Jones, Yvonne Scutt, Sian Jones, Wendy Halstead and Mari and Mair in the Library.

To my long suffering friends - it's finally over. Thank you for all the support over the years. I don't quite know how my liver has survived! Sarah Raby, Mags Eklo, Dr. Chris Mills, Emma Leighton-Jones, Ffion Wynne Jones, Rachel Davies, Dr. Ana Galladro-Soto, Pablo Marin-Franch, Consuelo Lopez-Diez, Dr. Peter Bowen-Walker, Rebecca Dean, Ross McGregor, Viv Plank, Steph Jones, Kate Paton, Annie Riley and my godkids, Haydn and Elliot.

If I've forgotten anyone, well, you know what I'm like....

Finally, to my late friend Chris Riley - I made it, shame you can't be here.

Summary

The work described is primarily concerned with measuring the induced AC electrokinetic properties of the transmissive stages of two water- and food-borne intestinal pathogens, namely oocysts of *Cyclospora* and eggs of *Ascaris,* in order to demonstrate the applicability of electrorotation for determining the viability of the organisms.

An electrode design that maximises the space over which a uniform electric field is applied to the electrorotation chamber is described. This is important when investigating organisms that are few in number, or for investigating large, mixed populations.

It was found that *Cyclospora* viability and sporulation state could be determined using electrorotation. Since there is no vital dye assay for this emerging parasite, and its life-cycle is not fully understood, these are important findings for the water and food industries. Modelling of the electrorotational response was found to be in good agreement with the experimental data. Limited electrorotational spectra from oocysts recovered from baboons showed slight differences when compared with those of human source.

The first electrorotational studies of a complex biological organism, namely the eggs of the nematode *Ascaris*, which poses a global health problem, are presented. It was found that unfertilised and fertilised eggs rotate in opposite directions, allowing for rapid visual determination of mixed populations. Different stages in the development of fertilised *Ascaris* eggs were also observed by electrorotation. Modelling of the electrorotational response of the *Ascaris* eggs was found to be in reasonable agreement with the experimental data.

The work presented here shows that the electrorotation technique can be used for the rapid determination of the viability and sporulation state of oocysts of *C. cayetanensis,* and the fertilisation state of eggs of *A. suum.* As current viability assays are complicated and time consuming, requiring trained personnel, the electrorotation technique offers many advantages to the food and water industries, especially as it can be automated.

CONTENTS

Chapter 1

Introduction

1.1 Introduction

Increased movements of people, expansion of international trade in foodstuffs and medicinal biological products, social and environmental changes linked to urbanisation, and deforestisation are all manifestations of the rapidly changing nature of the world we live in. Add to that the rapid adaptation of micro-organisms, which has facilitated the return of old communicable diseases and the emergence of new ones, and the evolution of microbial resistance, which means that curative treatments for a wide range of parasitic, bacterial and viral infections have become less effective, and a communicable disease in one country today is the concern of all.

Water- and food-borne illness represent a serious and recurring problem in almost all parts of the world. Currently, half of the world's hospital beds are occupied by people suffering from water-borne diseases (WaterAid, 2002). There are an estimated 2.4 billion people who do not have access to basic sanitation, of which 1.1 billion are without clean water (WHO, 2000). Globally, there are approximately 4 billion cases of diarrhoea each year which cause 2.2 million deaths (WHO, 2000). In developing countries in the year 2000, 1.3 million children under five died from diarrhoeal diseases caused by unsafe water supply, sanitation and hygiene (WHO, 2002a).

Even developed countries suffer : 76 million cases of food-borne disease occur in the USA every year, with 5000 deaths and 325,000 needing hospital treatment, at an annual cost of US$35 billion in medical expenses and lost productivity (WHO 2002b). Furthermore, according to WHO Quarterly statistics surveys, food-borne diseases may be more frequent than the reported cases tend to indicate (WHO, 1997). In a single outbreak in 1993, an estimated 403,000 people in Milwaukee, Wisconsin, developed an acute diarrhoeal illness as a result of contamination of the public water supply with the protozoan parasite, *Cryptosporidium parvum*. This outbreak was

unique in two ways. First, it was by far the largest waterborne outbreak ever reported in the United States. Second, the treated water responsible for the outbreak met all the federal water quality standards of the time. In this outbreak, the median duration of diarrhoea was nine days, with a median weight loss of 4.53kg (10 lb.), and 4400 people were hospitalised as a result of their illness. Among 82 HIV-infected patients who developed cryptosporidiosis, only 34 were still alive at one year (Steiner *et al.* 1997). Among the recommendations given by a Centres for Disease Control task force in September 1994, was the requirement for improvement of current techniques for identification of *C. parvum* oocysts in the water with regard to their specificity and sensitivity for detecting infectious oocysts as well as their cost and labour requirements (Steiner, *et al.* 1997).

Cyclospora cayetanensis is a recently described protozoan parasite of man (Ashford, 1979; Ortega *et al.,* 1993) which causes diarrhoeal illness worldwide (Oretga *et al.,* 1994) and is often mistaken for *C. parvum* in stool samples (Soave, 1996; Mota *et al.,* 2000). Cyclosporiasis, the illness caused by infection with *C. cayetanensis*, is endemic in Haiti, Nepal and Peru, although the host ranges and reservoirs are as yet undefined (Miller and Paige, 1998). In recent years, the importance of *C. cayetanensis* as an emerging pathogen of humans in the developed world has been highlighted by several outbreaks in North America during 1996, 1997 and 1998 (Herwaldt, 2000). Despite improved food safety measures implemented after the 1996 outbreak, over 1,400 cases were reported in 1997, and more in 1998, due to the same source, Guatemalan raspberries (CDC, 1997 and 1998). To date, the mode of contamination of the raspberries has not been identified for any of these outbreaks, although contaminated ground water is suspected (Herwaldt, 2000). Cyclosporiasis is treatable, but is clinically indistinguishable from the illness caused by *C. parvum,* which is not treatable (Soave, 1996). This leads to confusion as to what care a patient requires if misdiagnosed, and highlights the need for better surveillance and analysis systems to be developed.

As a result of the outbreaks in the United states, the Microbiological Contaminants Research Committee of the American Water Works Association (AWWA) and the US Environmental Protection Agency (EPA), listed *C. cayetanensis* as a '*concern*' to the

water industry, and proposed more research into methods to '*determine oocyst viability, taxonomy, species identification, infectivity and virulence*', and to '*determine water treatment processes that would remove and inactivate oocysts*'. The committee also wanted to '*better understand the epidemology of cyclosporiasis in humans, such as the significance of waterborne transmission and the public health importance of exposure to low concentrations of Cyclospora oocysts*' (AWWA, 1999).

In the UK there have been no significant outbreaks associated with *Cyclospora* : only 44-66 laboratory reports of *C. cayetanensis* were reported per year between 1993 and 1998 (Cann *et al.,* 2000). However, only 68% of UK microbiology laboratories actively look for *Cyclospora*, and of those, only 58% correctly identified the organism when assessed, suggesting that *Cyclospora* may be under-diagnosed in the UK (Gill, 1997; Cann *et al.,* 2000). In the United States prior to the large multi-state outbreak in 1996, most laboratories did not routinely examine stool specimens for *Cyclospora.* Since then there has been better awareness for the need to perform the appropriate tests (Eberhard *et al.,* 1997), but a recent review states that most laboratories still only test for *Cyclospora* on request (Herwaldt, 2000). As the oocysts of *C. cayetanensis* are resistant to current water treatment procedures, including chlorination (Rabold *et al.,* 1994), and the infective dose is low, probably between 10 and 100 oocysts (Adams and Ortega, 1999), there is a need for more rapid viability assays that work at the single organism level.

The majority of food-borne illness is caused by parasitic infections, usually by worms. *Ascaris* is the common roundworm that infects man and pigs. In 1999 it was estimated that 1.5 billion people are infected globally (Crompton, 1999), up from 1 billion in 1988 (Crompton, 1988). A major factor for this increase is the resilience of the transmissive stage, the egg, in the environment, and the increase, and ease, of international travel, especially to developing countries. Once shed, eggs can survive for 6-12 months in soils (Gaspard *et al.,* 1997). Eggs have even been reported to survive in sub-arctic regions (Embil *et al.,* 1984), and Krasnosos (1978) showed that some embryonated eggs were still viable after 14 years in moist soils.

Recognition that *Ascaris* infection is deleterious to health has prompted the World Health Organisation to develop and promote control strategies based on the prudent use of anthelminthic drugs, supported by appropriate health education and realistic sanitation (WHO, 1996). Swine parasitism exerts a significant economic impact worldwide; three of the six most common food-borne parasitic diseases in the United States are associated with pork consumption (Baker *et al.,* 1994). *Ascaris* infection leads to morbidity in about 335 million of those infected, and is a global public health problem (Crompton, 2001). Cross infection of *Ascaris* from pigs to humans has been reported (Crompton, 1989; Anderson, 1995). Diagnosis of infection is by finding the characteristic eggs in faecal smears. The detection of eggs in stool samples will not work if there are only immature worms, males or old females present in the small intestine as these worms do not produce eggs. There is at present no convenient method for discriminating between an *Ascaris* egg from a human, known as *Ascaris lumbricoides,* or from a pig, known as *Ascaris suum* (Crompton, 2001).

Despite our increased knowledge of hygiene today, 'foodborne disease is perhaps the most widespread health problem in the world' (WHO, 1992). One of the major means of addressing the concerns about communicable disease in both industrialised and developing countries is through the 'development of strong surveillance systems' (WHO, 1998). This requires new and improved detection systems to better protect water and food supplies.

1.2 Electrorotation

Electrorotation has been successfully used to investigate the properties of protozoal pathogens of man (e.g. Gascoyne *et al.*, 1997b; Goater *et al.*, 1997). As an investigative tool, electrorotation has several advantages over conventional techniques. Electrorotation is non-invasive, allowing it to become part of a series of sequential investigations. Electrorotation functions at the single organism level, which can be extremely important when accurate viability information for low numbers of organisms is required, as is the case for water testing. Electrorotation allows the real time assessment of particle viability of individual cells (Gundel *et al.*, 1989; Zhou *et al.,* 1995; Hodgson and Pethig, 1998; Dalton *et al.,* 2001). As well as

the rapid (a few seconds per cell) straightforward assessment of the viability of individual cells, the viability of larger numbers of cells (e.g. 30 cells in a field of view at a magnification of x100) can also be assessed simultaneously. To assist the analyst, automatic measurement of the rotation rate or for a full spectrum is also possible (Schnelle *et al.* 1997; Zhou *et al.,* 1998; DeGasperis *et al.*, 1998, Reichle *et al.,* 2000). A full frequency electrorotation spectrum, which can be thought of as a 'fingerprint' for heterogenous particles like oocysts, provides information not only about the viability of the particle, but also the conductivity and permittivity of the various 'compartments' within its structure (Chan *et al.,*1997).

After electrorotation analysis the particle remains intact and unchanged, and because electrorotation is a non-invasive method the particle can be subjected to further holistic or destructive analytical methods. Other techniques, such as fluorogenic dyes, have several disadvantages, such as cost, the requirement for an incubation stage, specialist storage and handling, as well as a fluorescent microscope in a dark room. The majority of flourogenic dyes are also usually carcinogenic and require refrigeration. Culture-based viability techniques generally take more than one week (Gaspard *et al.,*1996) and conventional microbiological methods are generally slow, largely because incubations in cultural stages are required to generate detectable concentrations of cells, taking days. Electrorotation, by comparison, is a quick and simple technique, with a sample preparation time of less than 15 minutes, which is also faster than a reverse transcriptase polymerase chain reaction test (RT-PCR). Although the particle suspension for electrorotation analysis requires sufficient purification to avoid particle-debris interaction, electrorotation has found many application, with both biological and synthetic particles (Table 1.1).

A variety of particle types, including the transmissive stages of parasites can be investigated by electrorotation. Indeed, whereas there is often the need to develop viability stains, molecular methods or excystation protocols for determining the viability of newly investigated cell types, electrorotation probes a common difference between all dead and viable cells, namely membrane integrity. Potential applications also include distinguishing between sub-types or strains of particles, whose surface or membrane properties differ, for example distinguishing between the cysts of the non-

invasive *Entamoeba dispar* from the potentially invasive *E. histolytica* in which specific transmembrane proteins have been identified (Walderich *et al.*, 1998).

PARTICLE TYPE		EXAMPLES
ACELLULAR	Virus	Virus erythrocyte interaction (Gimsa *et al.*,1989)
PROKARYOTES	Bacteria	Investigation of the flagellar motor torque of *E. coli* (Berry & Berg, 1996) Biocide treatment of bacterial biofilms (Zhou *et al.*, 1996) Viability studies of *E. coli* (Hodgson *et al.*, 1998)
EUKARYOTES	Protozoa	*Plasmodium falciparum* infected erythrocytes (Gascoyne *et al.*, 1997b) *Cryptosporidium spp.* oocysts (Goater *et al.*,1997) *Giardia intestinalis* cysts (Dalton *et al.*, 2001)
	Yeast	*Saccharomyces cerevisiae* comparison of wild type and vacuole deficient mutant (Asami & Yonezawa, 1996) *Saccharomyces cerevisiae* in an automated system (Reichle *et al.*, 2000)
	Algae	*Neurospora* slime (Gimsa *et al.*, 1991) Coccal green alga *Chlorococcum mimutum* (Reichle *et al.*, 2000)
	Plant cells	Barley Mesophyll protoplasts (Arnold & Zimmermann, 1982)
	Insect cell line	Effect of osmotic and mechanical stresses and enzymatic digestion on IPLB-Sf cell line of the Fall Armyworm (*Spodoptera frugiperda,* Lepidoptera) (Freitag *et al.*, 1989)
Mammalian cells	Cell lines	MDA-231 human breast cancer cells (Gascoyne *et al.*, 1997a)
	Lymphocyte	Influence of membrane events (Ziervogel *et al.*, 1986) Automated measurement system (Reichle *et al,* 2000)
	Erythrocyte	Erythrocytes parasitised by *Plasmodium falciparum* (Gascoyne *et al.*, 1997b) α-dispersion studies (Georgieva *et al,* 1998)
	Platelet	Influence of activators (Egger & Donath, 1995) α and β dispersion model comparison (Neu *et al.*, 2002)
	Trophoblast	Mononuclear cells also investigated (Chan *et al.*, 2000)
OTHER PARTICLES	Liposomes	Liposomes with 1 to 11 bilayers (Chan *et al.*, 1997)
	Latex bead	Effect of surface conductance (Arnold *et al.* 1987) Surface charge investigation (Maier, 1997)

Table 1.1 – Different particle types investigated by electrorotation (updated from Goater, 1999).

Electrorotation also overcomes several problems of commonly used impedance methods. Electrode polarisation does not influence the results since particle polarisation and consequently particle movement is measured relative to the suspending medium. Electric and hydrodynamic particle-particle interactions can be avoided since the measuring effect is independent of the solution volume and one particle is sufficient for measurements.

1.3 Overview of research in Electrorotation

In 1978 Pohl suggested that non-uniform fields can sometimes induce a torque on a particle, causing it to rotate. The term electrorotation was first used to describe the method of inducing controlled cellular spin by subjecting a cell to a rotating electrical field in 1982 (Arnold & Zimerman, 1982; Mischel *et al.* 1982). Electrorotation has been reviewed in several journal articles (Arnold and Zimmerman, 1988; Pethig, 1991a; Schnelle *et al.,* 1997) and has been described in several books (Jones, 1995; Pethig, 1991b and 1994). The electrotational force on a particle depends on the dielectric properties of the particle and the suspending medium. A dielectric is defined as a material in which both electrical conduction losses and charge storage (polarisation) occurs when it is exposed to an electric field.

In brief, the magnitude and direction of the electrorotational force on a particle suspended in a dielectric medium depends on a number of factors including the particle permittivity and conductivity, the medium permittivity and conductivity and the applied field strength and frequency.

The generation of rotating electric fields was considered over 100 years ago, for example Meyer (1877) (quoted in Heydweiler, 1897) described how to make a simple rotating electric field by the circular motion of an electrostatically charged rod. Using this method he induced anti-field motion of a solar radiometer. Electrical generation of rotating fields, more suitable for scientific or technical purposes, was described by Arno (1892) and later improved by v. Lang (1906) (for greater detail see the review by Arnold & Zimmermann, 1988).

Some important historical work concerning the rotation of objects in electric fields are listed in Table 1.2.

Hertz (1881)	Stated that a rotating body exposed to a steady electric field would experience a retarding torque (electromagnetic braking).
Heydweiler (1897)	Predicted that a rotating field would produce torque in a body.
v. Lang (1906)	Demonstrated that the direction of rotation of an insulating dielectric cylinder in a rotating electric field could be either anti- or co-field, depending on the conductivity of the suspending liquid.
Lampa (1906)	Following v. Lang's observations, Lampa wrote a detailed theory on how rotating electric field measurements could be interpreted.
Teixeira-Pinto *et al.* (1960)	Observed orientational movement of suspended, non-spherical, biological cells in linear electric fields.
Pohl (1978)	Stated that non-uniform (inhomogeneous) fields can sometimes induce cellular spin.
Arnold & Zimmermann (1982)	Demonstrated the rotation of a single biological particle in a rotating electric field.

Table 1.2 – Important historical work concerning the rotation of objects in electric fields (adapted from Goater, 1999).

A great deal of work has been carried out to elucidate the nature of the electrorotation force, in connection with dielectrophoresis (Wang *et al.,* 1992; Wang *et al.,* 1993) and travelling wave dielectrophoresis (Huang *et al.* 1993; Wang *et al.,* 1994). Specifically designed electrorotation electrodes have been used to characterise the dielectric properties of cells, starting with Arnold & Zimmermann's work on isolated plant cells (Arnold and Zimmerman, 1982).

Electrorotation data from non-biological particles, such as artificial liposomes (Chan *et al.,* 1997), have been of use in verifying the theoretical nature of the electrorotation force, as these are simple membraned cellular particles. Latex micro-particles have similarly been of use in probing the effects of surface groups and charges on the electrorotation spectra (Maier, 1997).

The use of electrorotation for particle characterisation and for determining viability are explored in this thesis, using the water- and food-borne pathogens *Cyclospora cayetanensis* and *Ascaris suum.* To date, the phylum nematoda, which includes the economically important *Ascaris*, is not known to have been investigated by electrorotation.

1.4 Thesis outline

Chapter 2 contains a brief description of the biology of the oocysts of *C. cayetanensis* and the eggs of *A. suum* that is essential to understanding how the particles interact with the electrorotation assay. Chapter 3 reviews the dielectric theory and the electric field techniques used in this thesis. Chapter 4 presents a review of the mathematical model of the electrorotation assay, develops the model for the biological organisms under investigation, and predicts the electrorotational responses of the organisms. Chapter 5 explains the methods and materials used in this work. Chapter 6 presents electrorotational results of *C. cayetanensis* oocysts, showing that electrorotation can determine viability and sporulation state. Chapter 7 describes the electrorotational studies of *A. suum* eggs, showing that electrorotation can determine fertility state. Conclusions based on this work and the direction of future studies are given in Chapter 8. Detailed background information and recent research into *C. cayetanensis* and *A. suum* are given in Appendices A and B, respectively. Appendix C lists the journal publications and conference presentations that have arisen from this work.

1.5 References

Adams, A., and Y. R. Ortega. **(1999)** *Cyclospora. In* R. K. Robinson, C. A. Batt, and P.D. Patel (ed.), *Encyclopaedia of Food Microbiology*. Academic Press Limited, London, UK.

Anderson, T. J. C **(2001)** The dangers of using single locus markers in parasite epidemiology : *Ascaris* as a case study. *TRENDS in Parasitology* **17(4)** 183-188

Arno, R. **(1892)** Campo elettrico rotanto per mexxo di differenze di potenziali alternative. *Atti Accad. Naz. Lincei Rend.* **1** 139-142.

Arnold, W. M. & Zimmermann, U. **(1982)** Rotating-field-induced rotation and measurement of the membrane capacitance of single mesophyll cells of *Avena sativa. Zeitschrift fur Naturforschung C* **37** 908-915.

Arnold, W. M., Schwan, H.P. & Zimmermann, U. **(1987)** Surface conductance and other properties of latex particles measured by electrorotation. *J. Phys. Chem.* **91** 5093-5098.

Arnold, W. M. and Zimmermann, U. **(1988).** Electro-rotation: Development of a technique for dielectric measurements on individual cells and particles. *J. Electrostatics.* **21** 151-191.

Asami, K. and Yonezawa, T. **(1996)** Dielectric behaviour of wild-type yeast and vacuole deficient mutant over a frequency range of 10kHz to 10GHz. *Biophys. J.* **71** 2192-2200.

Ashford, R. W. **(1979)** Occurrence of an undescribed coccidian in man in Papua New Guinea. *Ann. Trop. Med. Parasitol.* **73** 497-500.

AWWA **(1999)** Committee Report : emerging pathogens – viruses, protozoa and algal toxins. *J. American Water Works Association* **91 (9)**110-121.

Baker, D. G., Bryant, J. D., Urban, J. F. and Lunney, J. K. **(1994)** Swine Immunity to selected parasites. *Veterinary immunology and immunopathology* **43(1-3)** 127-133

Berry, R. M. and Berg, H. C. **(1996)** Torque generated by the bacterial flagellar motor close to stall. *Biophysical Journal.* **71** 3501-3510.

Cann, K. J., Chalmers, R. M.,Nichols, G., O'Brien, S. J. **(2000)** *Cyclospora* infections in England & Wales 1993-1998. *Commun.Dis & Public Health* **3(1)** 46-49.

CDC **(1997)** Update : Outbreaks of Cyclosporiasis – US and Canada. *Morbidity and Mortality Weekly* **46(23)** Centres for Disease Control, Atlanta.

CDC **(1998)** Outbreak of Cyclosporiasis – Ontario, Canada, May 1998. *Morbidity and Mortality Weekly* **47(38)** Centres for Disease Control, Atlanta.

Chan, K. L., Gascoyne, P. R. C., Becker, F. F. & Pethig, R. **(1997)** Electrorotation of liposomes: verification of dielectric multi-shell model for cells. *Biochim. Biophys. Acta-Lipids and Lipid metabolism.* **1349** 182-196.

Chan, K. L., Morgan, H., Morgan, E., Cameron, I. T. and Thomas, M. R. **(2000)** Measurements of the dielectric properties of peripheral blood mononuclear cells and trophoblast cells using AC electrokinetic techniques. *Biochim. Biophys. Acta.* **1500** 313-322

Crompton, D. W. T. (**1988)** The prevalence of ascariasis. *Parasit.Today* **4** 162-169

Crompton, D. W. T. **(1999)** How much human helminthiasis is there in the world? *J. Parasitol* **85 (3)** 397-403.

Crompton, D. W. T. (**2001)** *Ascaris* and ascariasis. *Adv. Parasitol.* **48** 285-375

Dalton, C., Goater, A. D., Pethig R., & Smith H.V. **(2001)** Viability of *Giardia intestinalis* cysts and viability and sporulation state of *Cyclospora cayetanensis* oocysts determined by Electrorotation. *Appl. Environ. Microbiol* **67** (2) 586-590.

DeGasperis, G., Wang, X. B., Yang, J., Becker, F. F. and Gascoyne, P. R. C. **(1998)**, *Meas. Sci. Tech.* **9** 518

Eberhard, M. L., Pieniazek, N. J. and Arrowood, M.J. **(1997)** Laboratory diagnosis of *Cyclospora* infections. *Archiv. Pathol. Lab. Med.* **121** 792-797.

Egger, M. and Donath, E. **(1995)** Electrorotation measurements of diamide-induced platelet activation changes. *Biophys. J.* **68** 364-372.

Embil, J. A., Pereira, C. H. and White, F. H. **(1984)** Prevalence of *Ascaris lumbricoides* infection in a small Nova Scotian community. *Am. J. Trop. Med. Hyg.* **33** 595-598

Freitag, R., Schügerl, K., Arnold, W. M. & Zimmermann, U. **(1989)** The effect of osmotic and mechanical stress and enzymatic digestion on the electrorotation of insect cells (*Spodoptera frugiperda*). *J. Biotech.* **11** 325-336.

Gascoyne, P. R. C., Wang, X-B., Huang, Y. & Becker, F. F. **(1997a)** Dielectrophoretic separation of cancer cells from blood. *IEEE Tran. Ind. Appl.* **33** 670-678.

Gascoyne, P., Pethig, R., Satayavivid, J., Becker, F. F. & Ruchirawat, M. **(1997b)** Dielectrophoretic detection of changes in erythrocyte membranes following malarial infection. *Biochim. Biophys. Acta -Biomembranes.* **1323** 240-252.

Gaspard, P., Wiart, J. & Schwartzbrod, J. **(1996)** A method for assessing the viability of nematode eggs in sludge. *Environmental technology.* **17:** 415-420.

Gaspard, P., Ambolet, Y. and Schwartzbrod, J. **(1997)** Urban sludge reused for agricultural purposes : Soils contamination and model development for the parasitological risk assessment. *Bulletin de L'Academie Nationale de Medicine* **181(1)** 43-57

Georgieva, R., Neu, B., Shilov, V. M., Knippel, E., Budde, A., Latza, R., Donath, E., Kiessewetter, H. and Bäumler, H. **(1998)** Low Frequency Electrorotation of fixed Red Blood Cells. *Biophys. J.* **74** 2114-2120

Gill, N. **(1997)** Cyclosporiasis in Europe : Underdiagnosed? *EuroSurveillance Weekly* 21.8.97

Gimsa, J., Marszlatek, P., Loewe, U. & Tsong, T. Y. **(1991)** Dielectrophoresis and electrorotation of *Neurospora* slime and murine myeloma cells. *Biophys. J.* **60** 749-760.

Goater, A. D., Burt, J. P. H. and Pethig, R. **(1997)** A combined electrorotation and travelling wave device: applied to the concentration and viability of *Cryptosporidium. Journal of Physics D-Applied Physics.* **33:** L65-L70.

Goater, A. D. **(1999)** A.C. Electrokinetic Bioassays. Development of Electrorotation Assay for Analyets in Water. *Ph.D. Thesis,* University of Wales.

Gundel, J., Wicher, D. and Matthies, H. **(1989)** Electrorotation as a viability test for isolated single animal cells. *Stud. Biophys.* **133** 5-18

Hertz, H. **(1881)** Uber die vertheilung der electricitat auf der oberflache bewegter leiter. *Wied. Ann.* **13** 266-275.

Herwaldt, B. L. **(2000)** *Cyclospora cayetanensis :* A review focussing on the outbreaks of cyclosoriasis in the 1990s. *Clin. Infect. Dis.* **31** 1040-1057.

Heydweiler, A. **(1897)** Ueber Rotationen im constanten electrishen Felde. *Verh. Dtsch. Phys. Ges.* **16** 32-36.

Hodgson, C. E. & Pethig, R. **(1998)** Determination of the Viability of *Escherichia coli* at the single organism level by electrorotation. *Clin. Chem.* **44** 2049-2051.

Huang, Y., Wang, X-B, Tame, J. & Pethig, R. **(1993)** Electrokinetic behaviour of colloidal particles in travelling electric fields: Studies using yeast cells. *J. Phys. D-Appl. Phys.* **26** 1528-1535.

Jones, T.B. **(1995)** *Electromechanics of Particles.* Cambridge University Press, Cambridge. p 212.

Krasnosos, L. N. **(1978)** Long term survival of ascarid eggs – *Ascaris lumbricoides* L. 1758 – in the soil of Samarkand. *Meditinskaya Parazitologicya I Parasitarnye Bolezni* **47** 103-105

Lampa, A. **(1906)** Ueber rotationen im elektrostatischen drehfelde. *Wien, Ber.* 2a **115** 1659-1690.

Lang, V. V. **(1906)** Vershuche im elektrostatishcen drehfelde *Wien, Ber.* **115** 211-222.

Maier, H. **(1997)** Electrorotation of colloidal particles and cells depends on surface charge. *Biophys. J.* **73** 1617-1626.

Miller, M. A. and Paige, J. C. **(1998)** Other foodborne infections. *Veterinary Clinics of North America Food Animal Practice* **14(1)** 71-+.

Mischel, M., Voss, A. & Pohl, H. A. **(1982)** Cellular spin resonance in rotating electric fields. *J.Biol. Phys.* **10** 223-226.

Mota, P., Rauch, C. A. and Edberg, S. C. **(2000)** *Microsporidia* and *Cyclospora* : epidemiology and assessmnt of risks from the environment. *Crit. Rev. Microbiol.* **26** 69-90.

Neu, B., Georgieva, R., Meiselman, H. J. and Baümler, H. **(2002)** Alpha- and beta-deispersion of fixed platlets : comparison with a structure-based theoretical approach. *Colloids and Surfaces A : Physiochem. Eng. Aspects.* **197** 27-35

Ortega, Y. R., Sterling, C. R., Gilman, R. H., Cama V. A., and Diaz F. **(1993)** *Cyclospora species*: A new protozoan pathogen of humans. *New Eng. J. Med.* **328** 1308-1312.

Ortega, Y. R., Gilman R. H., and Sterling, C. R. **(1994)** A New Coccidian Parasite (Apicomplexa : Eimeriidae) from Humans. *J. Parasitol.* **80** 625-629.

Pethig, R. **(1991a)** Biological electrostatics - Dielectrophoresis and Electrorotation. *Inst. Phys. Conf. Ser.* **118** 13-26.

Pethig, R. **(1991b)** Application of AC electrical fields to the manipulation and characterisation of cells. In: *Automation in biotechnology*. (ed. *Karube, I.*), pp. 159-185. Elesevier, Amsterdam.

Pethig, R. **(1994)** *Dielectric and A.C. Electrodynamic properties of cells.* In: *Bioelectrodynamics and biocommunication.* (Eds. M.W. Ho, F-A. Popp & U. Warnke) Ch. 9, pp. 229-249.

Pohl, H.A. **(1978)** *Dielectrophoresis.* Cambridge University Press, Cambridge.

Rabold, G., Hoge C. W., Shlim D. R., Kefford C., Rajah R., & Echeverria P. **(1994)** *Cyclospora* outbreak associated with chlorinated drinking water. *Lancet.* **344** 1360.

Reichle, C., Schnelle, T., Müller, T., Leya, T. and Fuhr, G. **(2000)** A new microsystem for automated electrorotation measurements using laser tweezers. *Biochim. Biophys. Acta.* **1459** 218-229

Schnelle, T., Glasser, H. & Fuhr, G. **(1997)** Opto-electronic technique for automatic detection of electrorotational spectra of single cells. *Cellular Engineering.* **2** 33-41.

Soave, R. **(1996)** State of the Art Clinical Article : *Cyclospora,* and overview. *Clin. Inf. Dis.* **23** 429-437.

Steiner, T. S., Theilman, N. M. & Geurrant, R. L. **(1997)** Protozoal agents: What are the dangers for the public water supply? *Annual Review of Medicine.* **48:** 329-340.

Teixeira-Pinto, A. A., Nejelski, L. L., Cutler, J. L. & Heller, J H. **(1960)** The behaviour of unicellular organisms in an electromagnetic field. *Experimental Cell Research.* **20** 548-564.

Wang, X-B, Pethig, R. & Jones, T. B. **(1992)** Relationship of dielectrophoretic and electrorotational behaviour exhibited by polarised particles. *J. Phys. D-Appl. Phys.* **25** 905-912.

Wang, X-B., Huang, Y., Burt, J. P. H., Markx, G. H. & Pethig, R. **(1993)** Selective dielectrophoretic confinement of bioparticles in potential energy wells. *J. Phys. D-Appl. Phys.* **26** 1278-1285.

Wang, X-B., Huang, Y., Becker, F. F. & Gascoyne P. R. C. **(1994)** A unified theory of dielectrophoresis and travelling wave dielectrophoresis. *J. Phys. D-Appl. Phys.* **27** 1571-1574.

WaterAid **(2002)** *The Human Waste.* Report by WaterAid and Tearfund, WaterAid, London.

WHO **(1992)** *Report of the Panel on Food and Agriculture* (WHO/EHE/92..2:191), World Health Organisation, Geneva.

WHO **(1996)** *Report of the WHO Informal Consultation on hookworm infection and anaemia in girls and women.* (WHO/CTD/SIP/96.1) World Health Organisation, Geneva.

WHO **(1997)** *World Health Statistics Quarterly,* Vol. **50,** N 1/2., World Health Organization, Geneva.

WHO **(1998)** Global Infectious Disease Surveillance, *Fact Sheet N° 200 (June 1998),* World Health Organization, Geneva.

WHO **(2000)** *Global Water Supply and Sanitation Assessment 2000 Report*, World Health Organisation, Geneva.

WHO **(2002a)** *Press Release* for the WHO Bangkok Conference on Child Mortality and Morbidity linked to Unhealthy Environments (WHO/12, 3 March 2002), World Health Organisation, Geneva.

WHO **(2002b)** Food Safety and Foodborne Illness, *Fact Sheet N° 237 (revised January 2002),* World Health Organisation, Geneva.

Zhou, X-F., Markx, G. H., Pethig, R. & Eastwood, I. M. **(1995)** Differentiation of viable and nonviable bacterial biofilms using electrorotation *Biochim. Biophys. Acta -General subjects.* **1245** 85-93.

Zhou, X-F., Markx, G. H. and Pethig, R. **(1996)** Effect of biocide concentration on electrorotation spectra of yeast cells. *Biochimica Biophysica Acta- Biomembranes.* **1281** 60-64.

Zhou, X-F., Burt, J. P. H. and Pethig, R. **(1998)** Automatic cell electrorotation measurements: Applied to studies of the biological effects of low-frequency magnetic fields and of heat shock. *Physics in Medicine and Biology.* **43** 1075-1090.

Ziervogel, H., Glaser, R., Schadow, D. & Heymann, S. **(1986)** Electrorotation of lymphocytes, the influence of membrane events and nucleus. *Bioscience Reports.* **6** 973-982.

Chapter 2

Organisms Investigated

2.1 Introduction

The behaviour of bioparticles such as cells in electric fields is dependent on the electrical properties of the cell and its structure. The organisms studied in this work are eukaryotic, possessing a well characterised internal organisation. Cells are usually discussed in terms of their major components, the cell wall (where present), cell membrane and cytoplasmic content. The two organisms investigated, oocysts of *Cyclospora cayetanensis* and eggs of *Ascaris suum,* are briefly described in this chapter. For more detailed biological background information and the most recent research regarding these organisms, see Appendices A and B.

2.2 *Cyclospora* species

C. cayetanensis was first reported in humans by Ashford *et al.* in 1979. The name *C. cayetanensis* was validated in 1994 when a complete morphological description was published (Ortega *et al.,* 1994). The work by Eberhard *et al.* (1999) suggests that there are two distinct groupings of cyclosporans. The first that infects insectivores and rodents producing large, oblong oocysts and the second, that infects primates and produces small, spherical oocysts (see Appendix A for a complete list of sizes and species). A notable point made by Eberhard *et al.* was that the primate species were easily distinguished at the molecular level, but not at the light microscope level. Based on an 18S rDNA sequence of *Cyclospora* oocysts collected from baboons and humans, Lopez *et al.* (1999) suggested that two different species designations might be warranted for these two primate-associated cyclosporans, Cyc-bab and Cyc-hu, respectively. Lopez *et al.* also noted that 'Cyc-bab' and 'Cyc-hu' are not freely shared between baboons and humans and speculated that baboons might not support the development of the human-associated *Cyclospora.*

A major constraint on research is the limited supply of *C. cayetanensis* oocysts available for study (Herwaldt, 2000; Quintero-Betancourt *et al.*, 2002). Currently, infected humans are the only known source of oocysts, and methods are not yet available for propagating them in culture or in animals (Eberhard *et al.*, 2000; Quintero-Betancourt *et al.*, 2002).

2.2.1 *Cyclospora* Identification

Identification of *C. cayetanensis* oocysts (the environmentally-resistant stage) is through a combination of accurate size measurement, autofluorescence in ultraviolet light and excystation (Ortega *et al.*, 1994) (Figures 2.1 and 2.2).

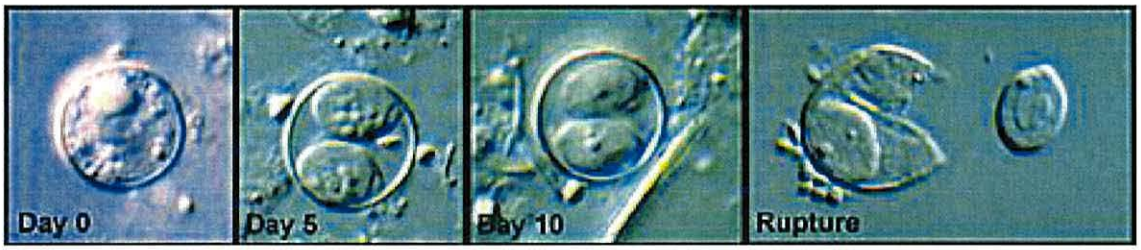

A B C D

Figure 2.1 – Sporulation and excystation, under laboratory conditions, of an oocyst of *C. cayetanensis*. A – unsporulated oocyst, B – sporulated oocyst, C – sporulated oocyst containing sporozoites and D – excystation. Times refer to days after the oocyst is subjected to the right environmental conditions (CDC, 2002a).

Molecular techniques, for example polymerease chain reaction (PCR), can be used for identification purposes (Lopez *et al.*, 1999), but there are often distinct differences between laboratory and field data (Smith, 1998), in contrast to the similar coccidian pathogen, *Cryptosporidium parvum.* There are no monoclonal antibodies available to detect *Cyclospora* oocysts in environmental samples, and acid-fast staining techniques that are commonly used for other cysts in faecal samples are problematic and sometimes lead to misidentification of the parasite in the clinical setting (Mota *et al.*, 2000; Quintero-Betancourt *et al.*, 2002). No successful viability assays using vital dyes or a suitable animal model have yet been reported for *C. cayetanensis* oocysts (Eberhard *et al.*, 2000; Quintero-Betancourt *et al.*, 2002). While the excystation

method provides a means of viability determination, this typically takes between 1 and 2 weeks (Smith *et al.*, 1997), since the oocysts have to sporulate first.

Only viable, sporulated oocysts of *C. cayetanensis* are responsible for the transmission of infection. Unsporulated oocysts (immature, with undifferentiated cytoplasm) are passed into the environment from the host in faeces (Figure 2.1A). The oocysts are remarkably uniform in size (8-10 μm) and do not change size upon sporulation (Figures 2.1A and B). Egested oocysts sporulate within 2-3 weeks in the environment, in the presence of higher atmospheric oxygen concentrations and a temperature of approximately 30°C. Each sporulated oocyst contains two ovoidal sporocysts (4.0 x 6.3 μm, Figure 2.1B). After maturation, two sporozoites (the infective stages) develop in each sporocyst (Figure 2.1C, Ortega *et al.*, 1998). When the right environmental conditions are met (i.e. in the natural life-cycle, when an oocyst is exposed to biochemical cues from the host intestine), the cell wall splits and releases the infectious sporozoites (Figure 2.1D).

By using epifluorescent illumination with a 350 nm excitation filter, the organisms appear as distinctive bright, pale blue circles in stool samples (Figure 2.2) and with a 450-490 nm excitation filter the oocysts appear as green circles (Ortega *et al.* 1994). However, this autofluoressence appears to decline over time. Most laboratories that test water supplies do not perform this test unless specifically requested (Cann *et al.*, 2000).

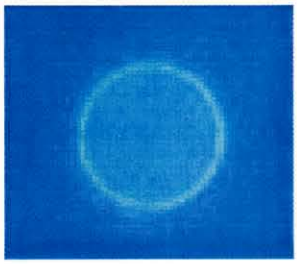

Figure 2.2 – Autofluoresence of *C. cayetanensis* oocyst under UV illumination (365 nm excitation filter) (CDC, 2002a).

2.2.2 Oocyst Wall

From transmission electron microscope studies (Ortega *et al.,* 1993), it has been shown that *C. cayetanensis* oocysts have a bilayered wall 113 nm thick, consisting of a rough outer wall of 63 nm and a smooth inner wall 50 nm thick. The bilayered wall structure is similar to other coccidian parasites, such as *Cryptosporidium parvum*. However, the wall thickness for *C. parvum* is more than twice that for *C. cayetanensis,* at 300 nm. The oocyst wall surrounds the inner, cytoplasmic membrane, maintaining the shape of the oocyst and protecting the cytoplasmic membrane from mechanical damage and rupture due to the high internal osmotic pressure generated by the cytoplasm. The oocyst wall has many other uses apart from providing mechanical strength. For example, it can store essential ions by attraction to the many ionisable groups within the porous cell wall, as well as acting as a molecular sieve to protect the plasma membrane from harmful molecules such as antibiotics. The exact composition of the oocyst wall for *C. cayetanensis* is not known. However, from studies of other coccidian parasites, such as *C. parvum* (Smith and Ronald, 2001), it can be predicted that the oocyst wall will contain protein, glycoprotein, lipid/lipid-conjugates and carbohydrates.

2.2.3 Cytoplasmic Membrane

The cytoplasmic membrane acts as a selective permeability barrier between the cytoplasm and the cell environment. It is able to maintain unequal concentrations of ions on either side, yet at the same time selectively allows certain large molecules to pass through. It is also the site at which many important and indispensable cellular activities occur, and contains sensing molecules which give the cell information about its surroundings. All biological membranes share a similar structure, varying in thickness from 5-10 nm, consisting primarily of phospholipids and protein, although the exact membrane composition depends on the cells of origin. The basic framework of the cytoplasmic membrane is the phospholipid bilayer. Hydrophilic groups occur on either side of the bilayer while hydrophobic chains occur within it (Figure 2.3).

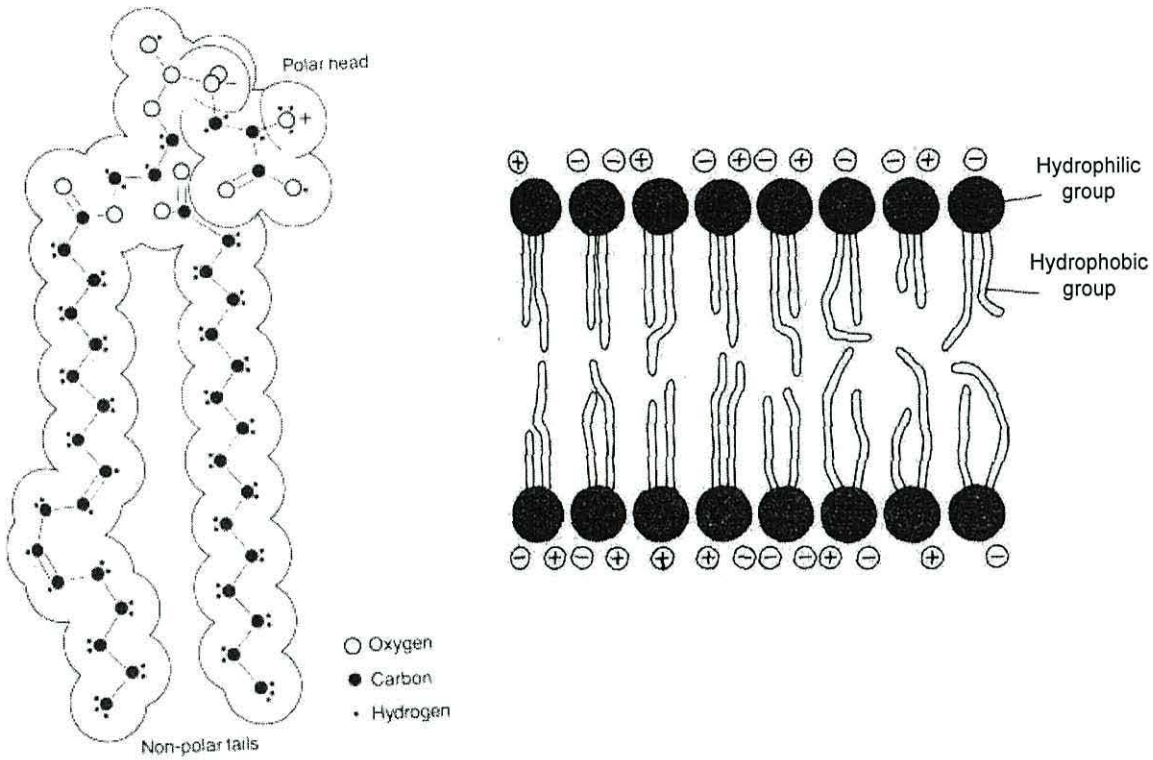

Figure 2.3 – A phospholipid molecule (left) and a phospholipid bilayer (right) (Thain and Hickman, 1994).

Thus a sheet is formed in which a hydrophobic layer is sandwiched between two hydrophilic layers. In a typical cell, the membrane is made up of three types of lipids – phospholipids, cholesterol and glycolipds (Figure 2.4).

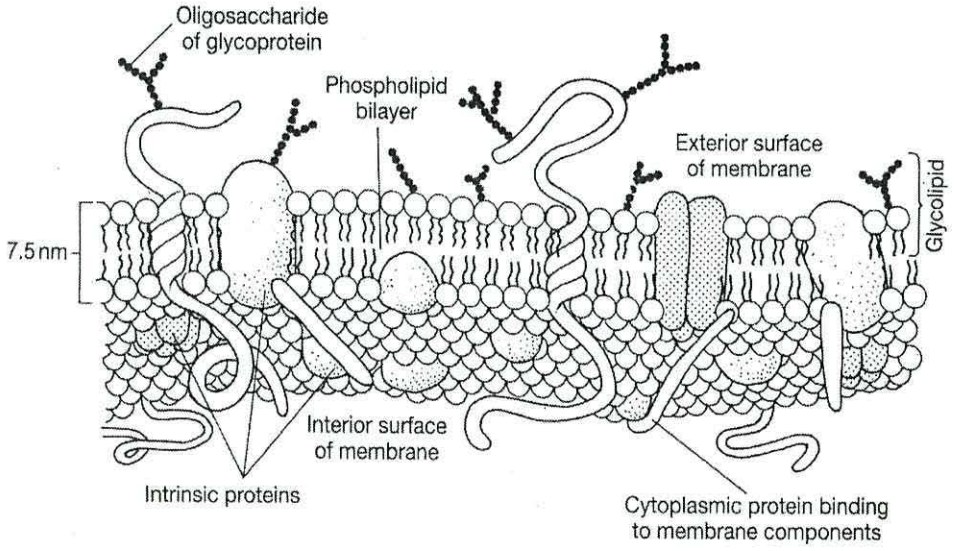

Figure 2.4 – Diagrammatical representation of a cell membrane showing the bilayer structure of phospholipids, cholesterol and glycoplipids (Thain and Hickman, 1994).

About 75% of the membrane lipids are phospholipids (lipids that contain phosphate groups). Present in smaller amounts are cholesterol, a steroid with an attached –OH (alcohol) group, and various glycolipids, lipids that have sugary carbohydrate groups attached. Cholesterol is incorporated within the bilayer to provide a degree of rigidity. The cholesterol molecule is a small, rigid molecule which is able to orientate itself between phospholipid molecules in the bilayer, with its polar head close to the polar head of the phospholipid. The rigid steroid ring tail of the cholesterol molecule interacts with the fatty acid chain of the phospholipid to immobilise the parts of the fatty acid chain close to the polar head of the lipid. Glycolipids are found on the outer surface of the plasma membrane and are similar to phospholipids with two hydrocarbon chain tails, but have a head group consisting of one or more sugar residues. The exact function of the glycolipids is not known, however, one group, the gangliosides, have a net negative charge.

The lipids act as a barrier to the entry or exit of polar substances while some of the proteins regulate the traffic of polar molecules and ions into and out of the cell. Membrane proteins are typically 50 times larger than membrane lipids. The exact membrane composition is unknown for *C. cayetanensis.*

The lipid bilayer is not a rigid structure. The lipid molecules are actually in a fluid state; they can diffuse freely in a lateral direction through the membrane, but they cannot passively flip from one side of the bilayer to the other. Some of the proteins in the membrane are associated with one side or the other, whilst others are embedded within it. The cell membrane also contains enzymes involved in the synthesis of new cell and cell membrane components. The proteins are made of sequences of amino acids and also contain carbohydrate at their terminations, usually in the form of covalently bonded sugar or sialic acid residues located on the outer surface of the membrane. This region of high carbohydrate concentration close to the surface of the cell is referred to as the cell glycocalyx.

The hydrophobic interior of the lipid bilayer helps the membrane to serve as an impermeable barrier to polar molecules, so preventing most of the water soluble contents of the cell escaping. In biological membranes the controlled movement of

molecules across the membrane is carried out by the membrane proteins. Small non-polar molecules and water are able to diffuse through the membrane. However, larger molecules and other polar molecules must cross the membrane via transport proteins. There are three principal mechanisms for membrane transport. All involve the movement of molecules through channels in the membrane formed by the proteins. The simplest form is passive diffusion of large molecules through protein channels. In this case the concentration gradient of the molecule governs the direction of transport. A more complex form of transport is involved for the movement of polar molecules, where a concentration gradient and an electrochemical gradient, provided by the transmembrane potential, control transport. The difference in electrochemical potential across biological membranes is caused by the well-documented sodium-potassium pump mechanism, which provides the third means of membrane transport, referred to as active transport. The Na^+-K^+ pump protein system maintains a higher concentration of sodium ions outside the membrane than inside, while simultaneously maintaining a higher concentration of potassium ions inside the cell. The regulation of ion movement provides an electrochemical potential difference across the membrane such that the interior of the cell is ~70mV more negative than the exterior of the cell.

2.2.4 Cytoplasm

The oocyst interior is the region lying within the cytoplasmic membrane. It has a relatively high conductivity due to the presence of large amounts of salts. It also contains a variety of molecules including DNA, RNA, protein, macromolecular precursors and other low molecular weight metabolites. The organisation of these molecules within the cell interior is complex, in particular for eukaryotic cells, in which many of the life processes such as energy production are defined in organelles. Together these components participate in a variety of catabolic and anabolic processes that are essential for growth.

2.2.5 Oocyst Schematic

Based on the Transmission Electron Micrograph (TEM) work by Ortega *et al.* (1993 and 1994) and a review of *C. parvum* (Smith and Ronald, 2001), an oocyst of *C. cayetanensis* can be schematically represented as shown in Figure 2.4. The cytoplasm is enclosed by the cytoplasmic membrane which is itself surrounded by the oocyst wall. The oocyst wall is presented to the external environment (either in water, on food or in the stomach). For experiments carried out on oocysts by electrorotation, the oocysts are suspended in a liquid media of known conductivity and permittivity.

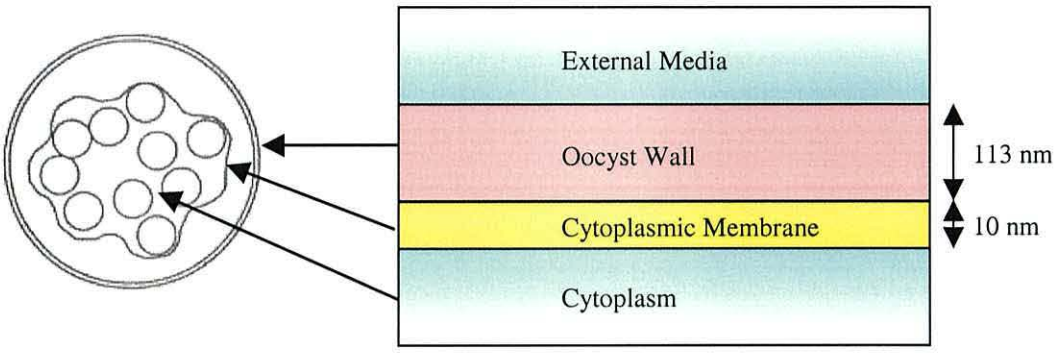

Figure 2.4 – Schematic representation of an unsporulated *C. cayetanensis* oocyst, and a cross-sectional representation of the oocyst structure.

2.3 *Ascaris* species

Common parasitic roundworms of pigs and humans are in the genus *Ascaris*. Tyson (1683) first described *Ascaris* in humans scientifically as *Lumbricoides teres*, but Linnaeus (1758) proposed that it be known as *A. lumbricoides*. Not long after, Goeze (1782) published his description of *Ascaris* in pigs, which he called *A. suum*. The two species continue to be discussed today as if they are separate, although there are difficulties in distinguishing them (Crompton, 1989) and there is a debate in the literature as to whether they are actually separate species or not (Crompton, 2001; Anderson, 2001).

2.3.1 *Ascaris* : the worm and egg

The male worm has a hooked tail and is approximately 15-30 cm long and about 0.5 cm in diameter. The adult female is longer, approximately 25-35cm, and has a smooth tail (Figure 2.5).

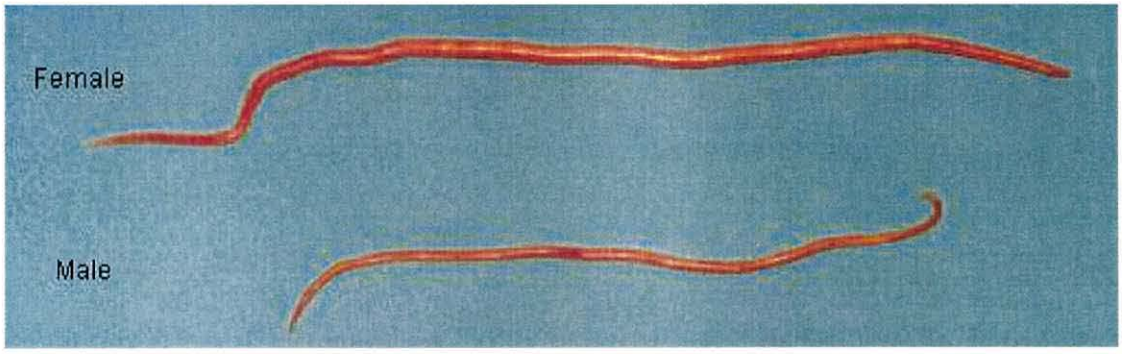

Figure 2.5 – Adult male (bottom) and female (top) worms of *Ascaris lumbricoides*. The male is clearly distinguished by the hooked tail (CDC, 2002b).

Adult worms live in the small intestine of the mammalian host and the female worm lays approximately 200,000 unembryonated eggs per day for about a year (Crompton, 1989), which are shed in faeces. Figure 2.6 shows micrographs of the eggs.

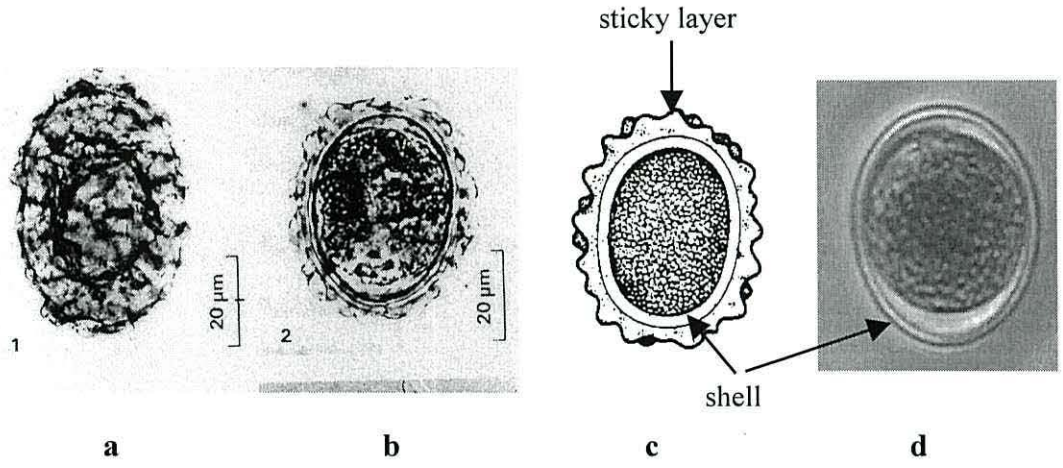

Figure 2.6 – *Ascaris* eggs - (a) unfertilised egg, (b) fertilised egg, (c) schematic and (d) a fertilised, viable egg after decortication (a, b, c – Katz, 1988).

When observed microscopically, fertile eggs of *A. lumbricoides* (Figure 6.3 b) appear slightly elliptical in shape with dimensions of between 50-70 by 40-50 µm. The fertilised eggs clearly possess a thick shell, and an outer surface that appears rough or irregular. The unfertilised eggs (Figure 6.3 a) have a generally thinner shell, are larger and more elongated, measuring about 60-100 by 40-60 µm. They are easily distinguished from fertile eggs by the lack of signs of a zygote or embryo. The parent female deposits an uneven layer of sticky mucopolysacharide on the outer surface of the eggs as they are laid, known as the uterine layer (Foor, 1967).

2.3.2 Egg Shell Composition

The egg shell consists of an outer, sticky uterine layer, a vitelline layer (which may not be visible by light microscopy), a chitinous layer and an innermost lipid layer (Figure 2.7). The chitinous layer provides strength, support and protection and also contains protein. The lipid layer resists desiccation and penetration by polar molecules. The lipid layer also contains molecules called ascarosides, glycosides of ascaryl alcohol, that resist entry by all molecules except lipids and gases.

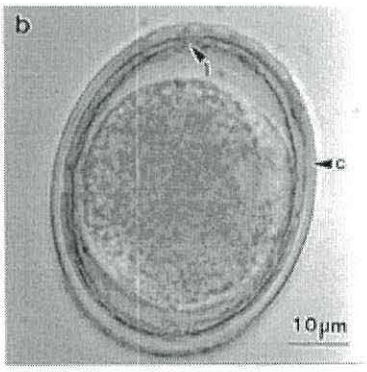

Figure 2.7 –A fertilised, undeveloped egg showing chitinous layer (c) and the lipid layer (l). Note the uterine layer has been removed and the vitelline layer is not visible (Darben, 2002).

2.3.2.1 Uterine Layer

This layer is the most variable of all the egg-shell components between nematode species. In *Ascaris* it is a homogenous mass of mucopolysaccharides. The exact role of the uterine layer is not known, but it has been proved that it is not essential to the continued survival of the embryo (Izumi, 1952). Jasoski (1952) theorised that the uterine layer provided an important auxillary barrier to the penetration of harmful chemicals into the egg, and Prociv (1990) suggested the uterine layer acted to prevent desiccation. Fairbairn (1957) stated that one function of the layer was to adhere to surfaces, thus increasing the chances of transmission. Since the seminal work by Foor (1967) on the ultrastructure of *Ascaris* eggs, very little work has been published on the uterine layer since.

2.3.2.2 Vitelline Layer

The vitelline layer is little understood, infrequently described and the chemical nature remains unclear (Darben, 2002). It is thought that in *Ascaris lumbricoides*, the vitelline layer is composed of a non-keratinous scleroprotein (Foor, 1967). However, no definitive tests have been performed. TEM studies show that the vitelline layer is 400 nm thick (Rogers, 1956). No specific purpose or function for the layer has been proposed and it is assumed to be a residual structure left over from egg-shell formation. After fertilisation, the vitelline layer thickens slightly.

2.3.2.3 Chitinous Layer

The chitinous layer is the thickest and most prominent layer in the nematode egg-shell, approximately 1.6 μm thick (Darben, 2002). The chitinous layer is formed after the thickening of the vitelline layer following fertilisation (Sromova and Lysek, 1990). It is composed of a polymer of acetyl-glucosamine residues, and provides protection against mostly physical stresses (Wharton, 1980). Deshelled eggs are permeable to non-polar solvents (Kunert, 1992), while whole eggs are impermeable, suggesting an additional barrier function of the chitinous layer.

2.3.2.4 Lipid Layer

The lipid layer of nematode eggs is the structure that has attracted the most research. The lipid layer is the last of the three endogenous layers to form, being deposited on the inner surface of the newly formed chitinous layer after fertilisation, and is about 100 nm thick (Darben, 2002). The lipid layer prevents entrance of harmful chemicals and the loss of water. Polar solvents and other water soluble ovicidal agents, capable of pasing through the outer protein and chitinous layers, cannot penetrate the inner lipid layer. However, since the membrane must allow the passage of respiratory gasses (carbon dioxide and oxygen), it must also allow the passage of the smaller water molecule. Clarke and Perry (1980) stated that the lipid layer of the egg-shells of

Ascaris suum eggs was a semi-permeable membrane. They found that *Ascaris suum* eggs were slightly permeable to water and therefore were open to osmotic effects. Therefore, the decorticated eggs, whilst still remarkably chemically resistant and often infective, need the outer layers of protein and chitin to act as a guard against the loss of vital water from the embryo.

In the eggs of *Ascaris lumbricoides*, the lipid layer is composed of 75% 'free' ascarosides and 25% protein (Fairbairn, 1957). Jaskoski (1962) concluded that the presence of amino acids in the lipd layer was suggestive of the presence of a lipoprotein structure, and that this structure must be strongly resistant to hypochlorite, in order to survive the decortication process. Tarr and Fairbairn (1973a) reported that almost all ascarosides in the ovaries of *Ascaris suum* occurred as esters. Later, these authors (Tarr and Fairbairn, 1973b) showed that the levels of ascaroside esters steadily decreased as the egg developed, accompanied by a subsequent increase in the levels of 'free' ascarosides. Tarr and Fairbairn also noted a possible biological role for the differentiation of the esterified and non-esterified forms : 'free' ascarosides melt at 80-90°C, thus giving greater protection than would the esterified forms, which melt at approximately 40°C.

Electron micrographs of the egg-shell are shown in Figures 2.8 and 2.9.

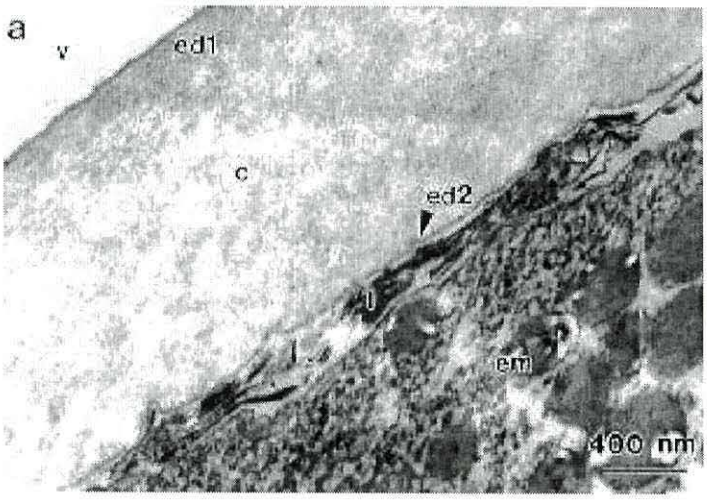

Figure 2.8 - Transmission electron micrograph of the egg wall of an *Ascaris suum* egg. Note that the uterine layer has been removed for ease of handling. (v - vitelline layer, ed1- electron dense infiltration of the chitinous layer in the region of the vitelline layer, c - chitinous layer, ed2 - electron dense infiltration of the chitinous layer in the region of the lipid layer, l - lipid layer, em - undeveloped embryo) (Darben, 2002).

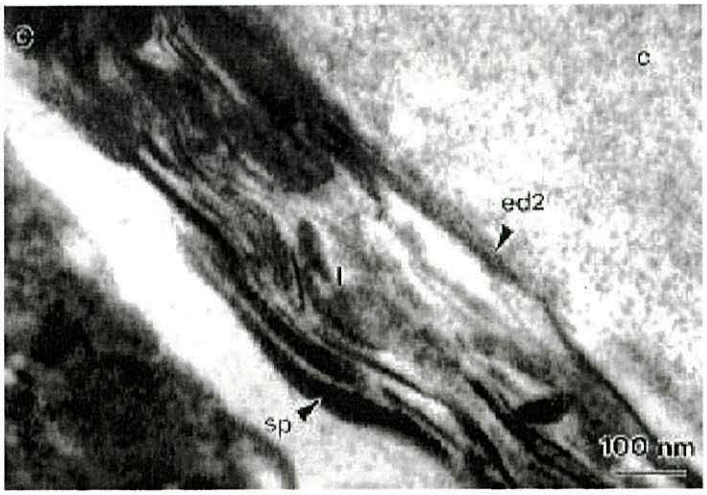

Figure 2.9 - Transmision electron micrograph showing details of the lipid layer of the egg-shell of *Ascaris suum*. Note the complex lamellated arrangement of this structure (c - chitinous layer, ed2 - electron dense infiltration of the chitinous layer in the region of the lipid layer, l - lipid layer, sp - spindle body) (Darben, 2002).

2.3.3 Embryonation

During embryonation, the single fertilised cell inside the egg divides into progressively more cells which become organised into a larval worm (Figure 2.10). An important factor to consider for electrorotational studies is that the single large cell in Figure 2.10a divides into progressively smaller cells. These smaller cells each have a membrane, and interact with each other for cell division to occur. The final larval stage (Figure 2.10c) is a very complex organism made up of thousands of cells after some 100+ divisions.

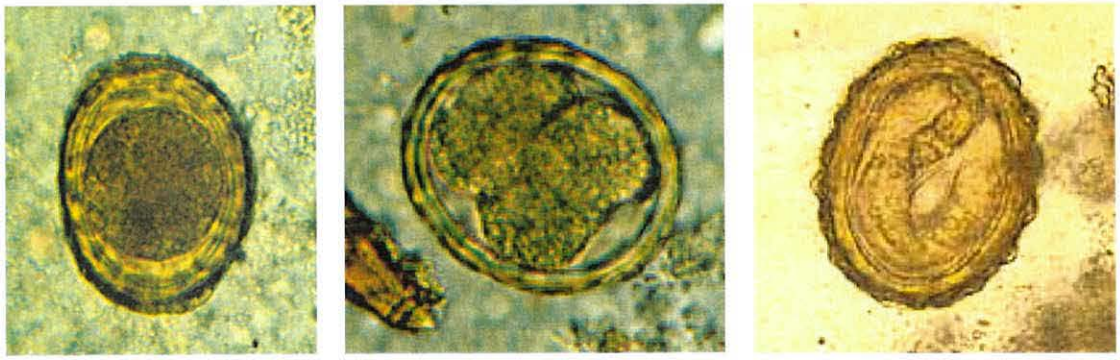

a **b** **c**

Figure 2.10 – Stages of development within the egg from (a) unicellular through (b) multi-cellular to (c) larval stage (CDC, 2002b).

2.3.4 Egg Shell Schematic

Based on the work of Rogers (1956), Foor (1967) and Darben (2002), the structure of fertilised and unfertilised eggs of *A. suum* can be schematically represented as shown in Figure 2.11. The internal contents of an unfertilised egg are surrounded by the vitelline layer, which is in turn surrounded by the sticky uterine layer. Upon fertilisation, the chitinous and lipid layers form between the internal contents and the vitelline layer, which also thickens slightly.

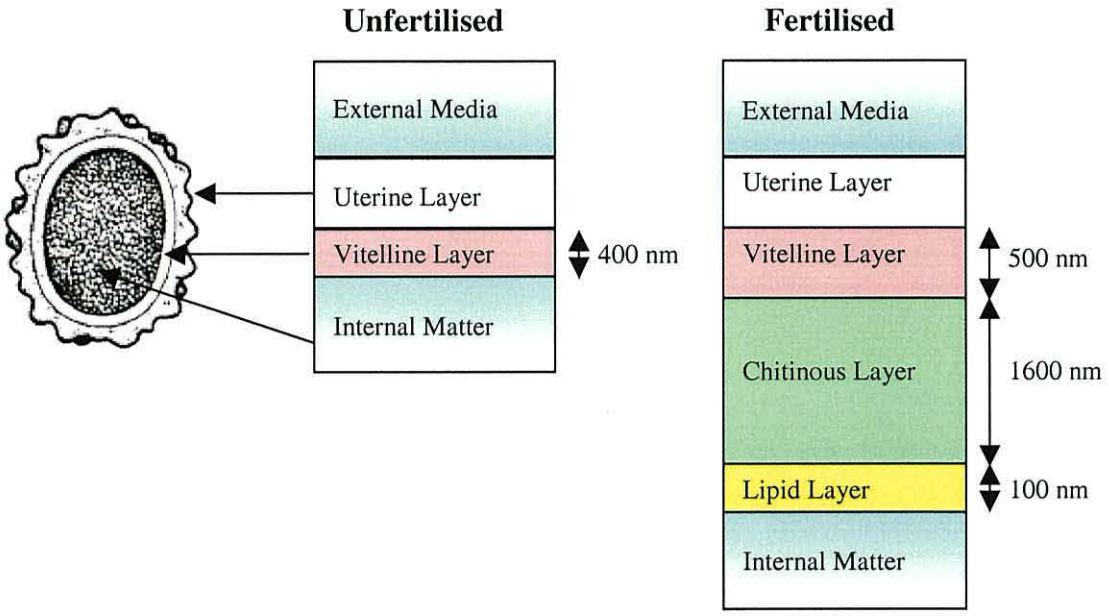

Figure 2.11 – Schematic representation of an unfertilised *A. suum* egg, and a cross sectional representation of the egg structure for a fertilised and an unfertilised egg.

2.4 Conclusions

In this chapter, up to date descriptions of the biological structure of *C. cayetanensis* oocysts and *A. suum* eggs have been described. It has been shown that the basic structure of the oocysts and eggs can be represented schematically as a series of layers. Each layer will have unique dielectric properties, due to the differences in their biochemical make-up. This layer structure can then be modeled mathematically, allowing for simulations of the expected electrorotational response of oocysts and eggs. The model is described in detail in Chapter 4, and the dielectric theory that supports the model, and the electrorotation technique, is described in the next Chapter, 3.

2.5 References

Anderson, T. J. C **(2001)** The dangers of using single locus markers in parasite epidemiology : Ascaris as a case study. *TRENDS in Parasitology* **17(4)** 183-188

Ashford, R. W., Warhurst, D. C. and Reid, G. D. F. **(1979)** Human infection with cyanobacterium-like bodies. *Lancet* **34** 1034.

Cann, K. J., Chalmers, R. M.,Nichols, G., O'Brien, S. J. **(2000)** *Cyclospora* infections in England & Wales 1993-1998. *Commun.Dis & Public Health* **3(1)** 46-49.

CDC **(2002)** Centres for Disease Control and Prevention. *Identification and diagnosis of parasites of public health concern.* Retrieved May 14th, 2002, from the World Wide Web : http://www.dpd.cdc.gov/dpdx/HTML/Cyclosporiasis.htm

CDC **(2002b)** Centres for Disease Control and Prevention. *Identification and diagnosis of parasites of public health concern.* Retrieved April 5th, 2002, from the World Wide Web : http://www.dpd.cdc.gov/dpdx/HTML/Ascariasis.htm.

Clarke, A. J. and Perry, R. N. (**1980)** Egg_shell permeability and the hatching of *Ascaris suum. Parasitology* **80** 447-456

Crompton, D. W. T. (**1989)** Prevalence of ascariasis. In : *Asariasis and it prevention and control.* Taylor and Francis, London.

Crompton, D. W. T. (**2001)** *Ascaris* and ascariasis. *Adv. Parasitol.* **48** 285-375

Darben, P. **(2002)** *Personnel communication* based on unpublished, confidential commercial work carried out at the Queensland University of Technology, Australia

Eberhard, M. L., da Silva, A. J., Lilley, B. G. and Pieniazek N. J. **(1999)** Morphologocical & molecular characterisation of New *Cyclospora* species from Ethiopian monkeys *: C. cercopitheci sp.n., C. colobi sp.n* and *C. papionis sp.n. Emerging Infectious Dis.* **5 (5)** 651-658.

Eberhard, M.L., Ortega, Y. R., Hanes, D. E., Nace, E. K., Do, R. Q., Robl M. G., Won, K. Y., Gavidia, C., Sass, N.L., Mansfield, K., Gozalo, A., Grigiths, J., Gilman, R. and Sterling C. R. **(2000)** Attempts to establish *Cyclospora cayetanensis* infection in laboratory animals. *J. Parasitol.* **86(3)** 577-582.

Fairbairn, D. **(1957)** The biochemistry of *Ascaris. Experimental Parasitol.* **6** 491-554

Foor, W. E. **(1967)** Ultrastructural aspects of oocyte development and shell formation in *Ascaris lumbricoides. J. Parasitol* **53** 1245-1261

Herwaldt, B. L. **(2000)** *Cyclospora cayetanensis :* A review focussing on the outbreaks of cyclosoriasis in the 1990s. *Clin. Infect. Dis.* **31** 1040-1057.

Goeze, J. A. E. **(1782)** *Versuch einer Naturgeschichte der Eingeweidewurmer thierischer Korper.* Blankenburg : PA Pape.

Izumi, S. **(1952)** Biological studies on *Ascaris* eggs. II. On the penetrating activity of various chemicals to *Ascaris eggs. Japanese Medical Journal* **5** 21-36

Jaskoski, B. J. **(1952)** The protein coat in development of *Ascaris lumbricoides* eggs. *Experimental Parasitology* **1** 291-302

Jaskoski, B. J. **(1962)** Paper chromatography of some fractions of *Ascaris suum. Experimental Parasitology* **12** 19-24

Katz, M., Despommier, D. D. and Gwadz, R. **(1988)** *Parasitic Disease* 2nd Ed. Springer-Verlag, New York.

Kunert, J. **(1992)** On the mechanism of penetration of ovicidal fungi through egg_shells of parasitic nematodes. Decomposition of chitinous and ascaroside layers. *Folia Parasitologica* **39** 61-66

Linnaeus, C. **(1758)** *Systema Naturae* Laurentill Salvii, Holmiae

Lopez, F. A., Manglicmot, J., Schmidt, T. M., Yeh, C., Smith, H. V. and Relman, D. A. **(1999)** Molecular characterisation of *Cyclospora*-like organisms from baboons. *J. Infect. Dis.* **179** 670-676.

Mota, P., Rauch, C. A. and Edberg, S. C. **(2000)** *Microsporidia* and *Cyclospora* : epidemiology and assessmnt of risks from the environment. *Crit. Rev. Microbiol.* **26** 69-90.

Ortega, Y. R., Sterling, R., Gilman, R. H., Lama, V. A. and Diaz, F. **(1993)** *Cyclospora* Species – A New Protozoan Pathogen of Humans. *New Eng. J. Med.*1306 – 1312.

Ortega, Y. R., Gilman, R. H. and Sterling, C. R. **(1994)** A new coccidian parasite (apicomplaxe:Eimeriidae) from humans. *J. Parsitology* **80(4)** 625-629.

Ortega, Y. R., Stirling, C. R. and Gilman, R. H. **(1998)** *Cyclospora cayetanensis. Adv. Parasitol.* **40** 399-418.

Prociv, P. **(1990)** Observations on the morphology of *Toxocara pteropodis* eggs. *J. Helminthology* **64** 271-277

Quintero-Bentacourt, W., Peele, E. R. and Rose, J. B. **(2002)** *Cryptosporidium parvum* and *Cyclospora cayetanensis* : a review of laboratory methods for detection of these waterborne parasites. *J. Microbiol. Meth.* **49** 209-224

Rogers, R. A. (**1956)** A study of eggs of *Ascaris lumbricoides* var. *suum* with the electron microscope. *J. Parasitol.* **42** 97-103

Smith, H. V., Paton, C. A. Mtambo, M. A. and Girdwood, R. W. A. **(1997)** Sporulations of *Cyclospora* Sp. Oocysts. *App. Environ. Microbiol.* 1631-1632.

Smith, H. V**. (1998)** Detection of parasites in the environment. *Parasitol.* **117** S113-S141.

Smith, H. V. and Ronald, A. **(2001)** *Cryptosporidium* : The Analytical Challenge. In *: Cryptosporidium : The Analytical Challenge.* Eds Smith, M. and Thompson, K. C. , Royal Society of Chemistry, Cambridge, UK.

Šromová, D. and Lýsek, H. **(1990)** Visualisation of chitin/protein layer formation in *Ascaris lumbricoides* egg shells. *Folia Parasitologica* **37** 77-80

Tarr, G. E. and Fairbairn, D. **(1973a)** Ascarosides of the ovaries and eggs of *Ascaris lumbricoides* (Nematoda). *Lipids* **8** 7-16

Tarr, G. E. and Fairbairn, D. **(1973b)** Conversion of ascaroside esters to free ascarosides in fertilised eggs of *Ascaris suum* (Nematoda). *J. Parasitol.* **59** 429-433

Thain, M. and Hickman, M. (1994) *Dictionary of Biology 9th Ed.,* Penguin Book Ltd.

Tyson, E. **(1683)** *Lumbricoides teres*, or some anatomical observations on the roundworm bred in human bodies. *Phil. Trans. Roal Soc. London* **13** 152-161

Wharton, D.A. **(1980)** Studies on the function of the oxyurid egg_shell. *Parasitology* **81**103-113

Chapter 3

Theory

3.1 Introduction

This chapter describes the relevant background theory to AC electrokinetics, and focuses on the chosen method of investigation for this work, namely electrorotation.

The motion of electrically charged biological particles in electric fields was first observed over 100 years ago (e.g. Loretet, 1896). Indeed the phenomenon, known as *electrophoresis,* is widely used for separating and identifying biological molecules such as proteins e.g. Polyacrylamide Gel Electrophoresis (PAGE) in uniform electric fields. When electrically neutral particles are exposed to a uniform electric field they simply polarise. However, in the presence of a non-uniform field the particle will experience a resultant force and will move in the field gradient, irrespective of whether a time-independent or alternating electric field is applied. Observations of this effect, known as *dielectrophoresis*, date back to 1923 (Hateschek & Thorpe, 1923), but the first major study was not until 1951, when Herbert Pohl published his paper on '*The Motion and Precipitation of Suspensoids in Divergent Electric Fields*' (Pohl, 1951). Theoretical aspects of dielectrophoresis, mainly established by Pohl (1978), have been further developed by many other workers, including Jones and Kallio (1979), Benguigui and Lin (1982), Sauer and Schlögl (1985). Of particular interest is the change in particle behaviour often observed when the frequency of the applied field is increased (Pethig, 1991; Wang *et al.,* 1992 and Jones, 1995).

In 1978 Pohl suggested that the polarisation of particles in non-uniform fields can sometimes induce a torque on a particle, causing it to rotate. If a particle is exposed to an external, *rotating,* electric field, a rotational torque is produced on the particle. The term electrorotation was first used in 1982 (Arnold & Zimerman, 1982; Mischel *et al.* 1982) to describe the method of inducing controlled cellular spin by subjecting a cell to a rotating electrical field.

In the present work, the rotating electric field is generated by energising four microelectrodes with sinusoidal voltages with 90° phase separation (see Chapter 5 for details of the experimental set up). This results in a rotational movement of the particle at certain frequencies. The rate and direction of the resulting motion is dependent on the dielectric properties of the particle and the suspending medium, as will be shown in this chapter.

3.2 Dielectric Materials

In response to an applied electric field, free charges within a conducting material move in such a direction as to neutralise the field within the conductor. In dielectric materials, or insulators, the charges are bound – the electrons are localised in the process of bonding atoms together. Thus covalent, ionic or van der Waals bonding between closed-shell atoms all give rise to the dielectric or insulating properties. There are no free charge carriers and the application of an electric field, unless it is very high, will produce no free charge carriers. However, an electrical dipole is produced when the bound charges in the atoms of a dielectric are displaced slightly from their normal charge centres by the action of an external electrical field. Dielectrophoresis arises from the interaction of this induced dipole with the external field. In the following sections, these concepts are explored.

3.3 Dielectric Properties of Materials

Consider a capacitor with its plates separated by a dielectric material. The presence of a charge on the surface of the metal plates attracts charges of opposite polarity within the dielectric. Since the charges in the dielectric are not able to move freely, they cannot participate in conduction processes. Only slight electrical displacement can occur, giving rise to polarisation of the dielectric as exemplified by the generation of induced electrical dipoles in Figure 3.1.

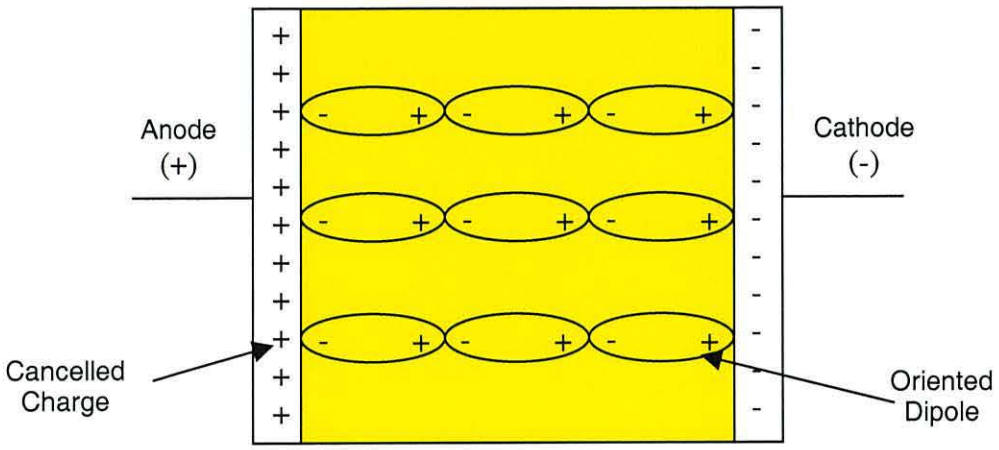

Figure 3.1 – Two parallel plates separated by a dielectric to form a capacitor. Orientated dipoles within the dielectric effectively cancel a proportion of the charge on the metal plates.

An important property of the dielectric is its resistivity, which is a measure of the resistance, R, a charge experiences travelling through the material. The inverse of the resistance is known as the conductance, G, which is the ease with which charge is transported through the material. The charge storage capacity of the dielectric, i.e. its capacitance, C, and the conductance, G, are given by

$$C = \frac{Q}{V} = \frac{\varepsilon_0 \varepsilon_r A}{d} \tag{3.1}$$

and

$$G = \frac{1}{R} = \frac{\sigma A}{d} \tag{3.2}$$

where A is the capacitor plate surface area, d is the distance between the plates, σ is the electrical conductivity of the material, Q is the charge on the capacitor, V is the voltage between the plates, ε_0 is the permittivity of free space and ε_r is the relative permittivity of the dielectric material compared to free space.

The relative permittivity of a medium is the ratio of the capacitance of the appropriate dielectric to the capacitance of a vacuum. The action of a dielectric, therefore, is to increase the charge storage capability of a capacitor, and the relative permittivity is a measure of the polarisability of the material.

3.4 Complex Permittivity and *tan* δ

If a sinusoidal alternating electric field of relatively low frequency is applied to a dielectric, the dipoles will try to align themselves along the field lines at the same frequency as the applied field. If the electric field and the dipole moment are sufficiently large, then the dipoles will align themselves along the field lines and the displacement current (the electromagnetic energy) will be transmitted through the material with no loss. As the frequency of the applied field increases, the dipoles find it harder to align themselves to the field, due to the various polarisation mechanisms. At this stage, some of the electromagnetic energy is lost, being converted into Joule heating of the dielectric. This is known as dielectric loss. In addition, the amount of charge stored by the capacitor decreases, as the dipoles are no longer polarised to the maximum extent, resulting in a decrease in permittivity. It is useful to express the dielectric loss in terms of *tan* δ. Consider the equivalent circuit for a real capacitor, i.e. one that has losses (Figure 3.2).

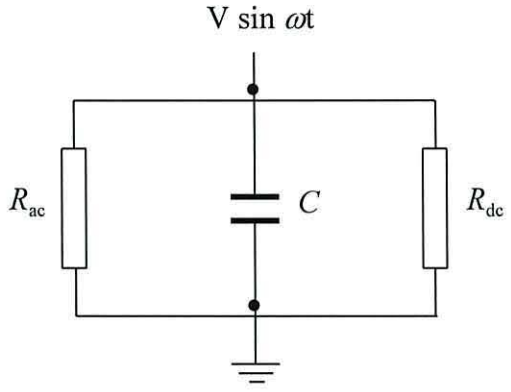

Figure 3.2 – Equivalent circuit of a real capacitor.

If the dipoles dissipate energy on oscillation, this can be represented by a resistor R_{ac}, in parallel with a perfect capacitor, C. Thus the power loss is due to the current through the resistor. In a 'real' dielectric some charge transport will also occur, represented by the resistor R_{dc}. However, for simplicity, it is assumed that the dielectric is a perfect insulator against DC current, so R_{dc} is infinitely large and can be ignored. The currents through the resistor and capacitor can be represented by a phasor diagram (Figure 3.3).

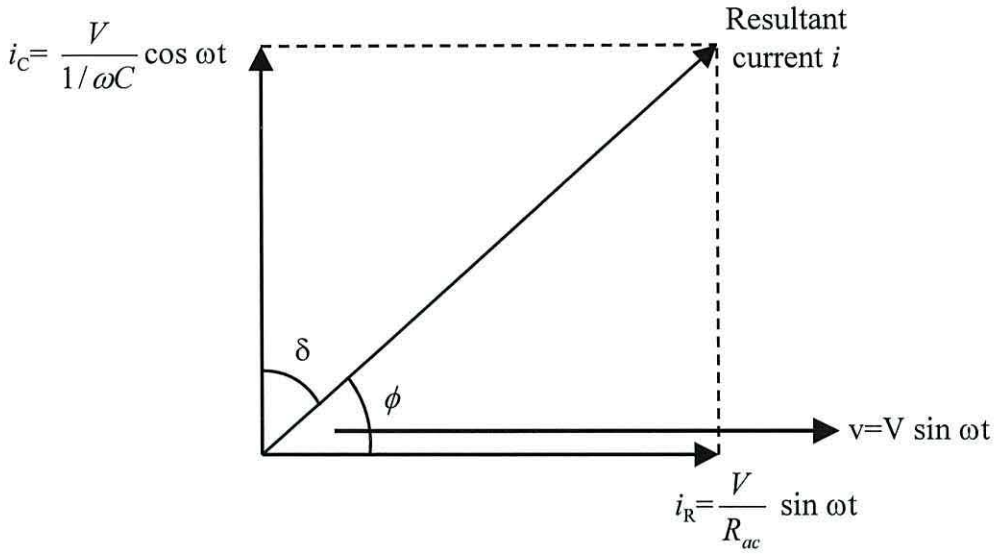

Figure 3.3 – Phasor diagram for the equivalent circuit of a real capacitor.

As can be seen from the diagram, the resultant current is not in phase with the capacitor current, but is displaced by a small angle δ. In the situation where the dipoles experience no lag with the alternating field, R_{ac} is considered infinitely large, resulting in no current flow through the resistor. As there is no i_R component, the resultant current is in phase with the capacitor current, i.e. the current is 90° out of phase with the voltage. Thus, the product $V \times i = 0$, and so all the electromagnetic energy is transmitted without loss. As the frequency increases, a component i_R develops. Thus the resultant current is no longer 90° out of phase with the voltage and the product $V \times i > 0$.

From a mathematical analysis of the energy stored by a perfect capacitor at any instant of time and the instantaneous power dissipated through R_{ac}, $tan\ \delta$ can be described by the ratio

$$\tan \delta = \frac{\text{energy lost per cycle}}{2\pi \times \text{maximum energy stored per cycle}} = \frac{1}{\omega C R_{ac}} \qquad (3.3)$$

where ω is the angular frequency.

3.5 Dielectric Polarisation

For the capacitor in Figure 3.1, the polarisation, P, in the dielectric can be described as the additional surface charge density (or electric flux density, D) produced when an electric field is applied to the dielectric

$$P = D_R - D_0 \tag{3.4}$$

where D_R is the displacement within the dielectric of permittivity ε_r and D_0 is the displacement in the absence of a dielectric. Since $D = \varepsilon_0 \varepsilon_r E$, then for an externally applied field E, the polarisation can be written as

$$P = \varepsilon_0 \varepsilon_r E - \varepsilon_o E \tag{3.5}$$

$$= \varepsilon_0 (\varepsilon_r - 1) E \tag{3.6}$$

which may be written as

$$P = \varepsilon_0 \chi E \tag{3.7}$$

where χ is the susceptibility of the medium.

The polarisation, P, may also be defined as the induced dipole moment per unit volume (Cross, 1987), i.e.

$$P = Nm \tag{3.8}$$

where N is the number of dipoles per unit volume and m is the dipole moment, given by

$$m = \alpha_T E_{loc} \tag{3.9}$$

where α_T is the total polarisability of a dipole and E_{loc} is the local field strength experienced by the dipole. From Equations (3.6), (3.8) and (3.9), the relative permittivity of a dielectric can be written as

$$\varepsilon_r = 1 + \frac{N \alpha_T E_{loc}}{\varepsilon_0 E} . \tag{3.10}$$

In order to quantitatively relate the macroscopic permittivity of a material to molecular quantities such as its polarisability α_T, the relationship between the microscopic field intensity E_{loc} and the macroscopic field intenstity E must be obtained. In dense materials such as liquids and solids, E_{loc} is not equal to the applied field, since P is large and the total field experienced by a molecule has contributions from both the applied field and the fields due to the polarisation of atoms in its neighbourhood. The relationship has been simplified for materials with a high degree of crystal symmetry or complex molecular disorder (Alison, 1971), to arrive at the Clausius-Mossotti equation

$$\frac{\varepsilon_r - 1}{\varepsilon_r + 2} = \frac{N\alpha_T}{3\varepsilon_0}. \tag{3.11}$$

3.6 Polarisation Mechanisms

The total polarisability, α_T, of a homogenous dielectric consists of the sum of the electronic, α_e, atomic, α_a and orientational polarisation, α_o, which are related to molecular properties. For a heterogeneous material, consisting of dissimilar elements with different dielectric properties, extra polarisation mechanisms occur, which are included in the interfacial polarisation term, α_i, that depends on the macroscopic size and distribution of the various phases in the material.

Each of the polarisation processes have their own characteristic time constants, and will contribute to the series of dielectric dispersions seen as the frequency of the applied field is increased (Figure 3.4).

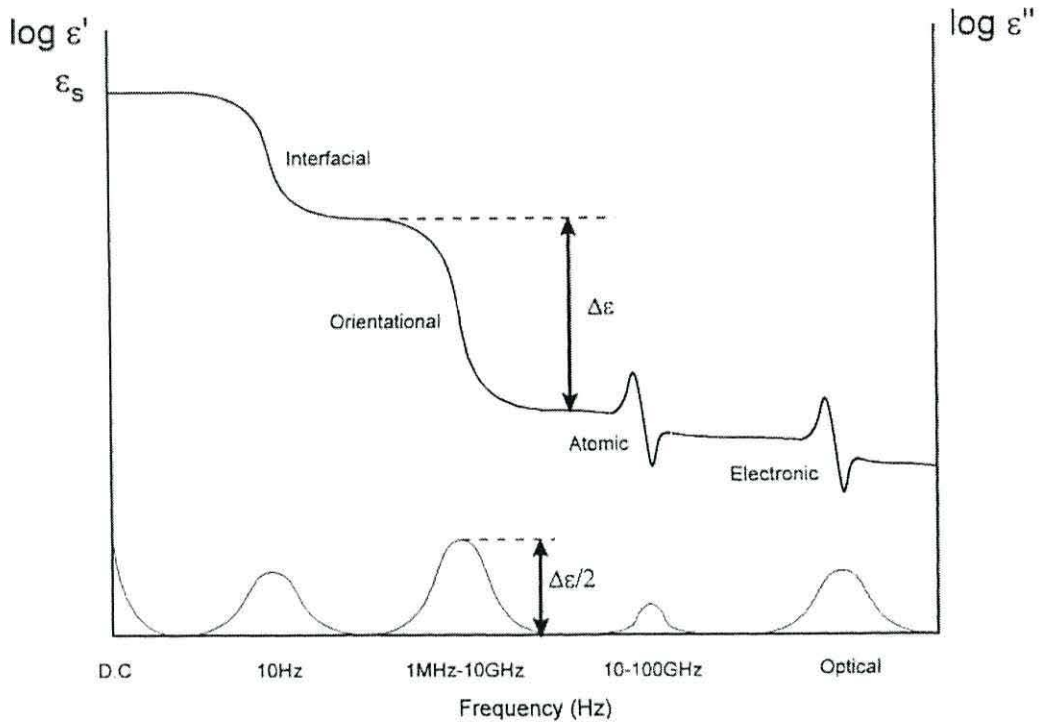

Figure 3.4 – Variations of the real and imaginary parts of the complex permittivity for a dielectric exhibiting a number of dispersion processes (adapted from Burt, 1990)

3.6.1 Electronic Polarisation

Every dielectric material exhibits electronic polarisation (α_e) when an ac field is applied, which causes the displacement of electrons in an atom relative to the positive nucleus. The displacement is small since the applied fields, in the order of 10^6 V/m, are considerably smaller than those within the atom, which are about 10^{11} V/m. The displacement of the charges is therefore only in the order of 10^{-8} Å. This resonance process leads to a constant permittivity for applied alternating electric fields up to ~10^{15} Hz and, since it is a function of molecular structure, it is largely independent of temperature.

3.6.2 Atomic Polarisation

The atomic polarisation process (α_a) arises from the displacement of charged ions with respect to each other in a crystal lattice. An applied electric field will cause positive ions to move relative to the negative ions, inducing a dipole moment and associated polarisation in the dielectric. Consider an ionic solid such as sodium chloride. The sodium ions move relative to the chloride ions when subjected to an external electric field, inducing a dipole moment within the solid. Similar atomic polarisation processes can contribute greatly to the total polarisation in inorganic compounds, whilst in organic materials, where ions are absent, this type of polarisation only makes a small contribution to the total. Again, this resonance process leads to a constant relative permittivity for applied frequencies up to ~10^{13} Hz.

3.6.3 Orientational Polarisation

Orientational polarisation only occurs in polar materials which contain permanent dipoles in their structure, arising from the separation of charged groups within the molecule. A good example is the asymmetrical water molecule (Figure 3.5a). Molecules such as carbon dioxide, which are symmetrical, have no overall charge asymmetry, and therefore have no net dipole (Figure 3.5b).

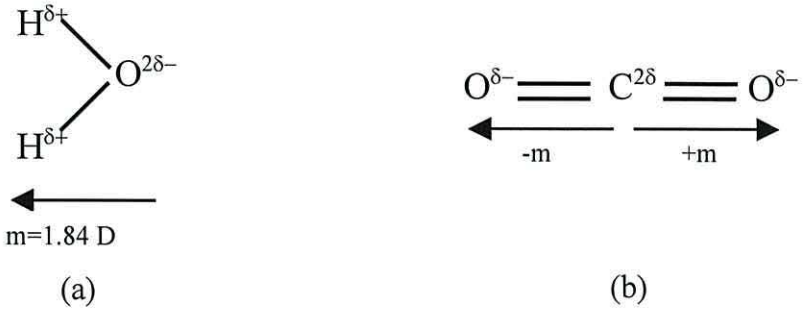

Figure 3.5 – Examples of the overall dipole moments (m) possessed by (a) a non-symmetrical water molecule and (b) a symmetrical carbon dioxide molecule.

If no electric field is present the polar molecules are randomly aligned. When an electric field is applied, the dipoles experience a torque and will try to align themselves with the field. The frequency range over which dipolar polarisations occur is dependent on the size of the molecule, from 10^5 Hz for large molecules, such as a protein in solution, to approximately 10^9 Hz for smaller molecules such as amino acids. Liquid water has a dielectric constant of ~80 for frequencies below 10^9 Hz at room temperature, whilst at frequencies above 10^{11} Hz the dielectric constant falls to a value of ~4.5. This polarisation process is temperature dependent.

The permittivity, ε', and the dielectric loss, ε'', are related by a complex equation known as the Debye equation, after the work of Debye (1929), who originally described the frequency dependence of polarisation processes analytically. Thus the complex permittivity, $\varepsilon^*(\omega)$, is given by

$$\varepsilon^*(\omega) = \varepsilon' - j\varepsilon'' = \varepsilon_\infty + \left(\frac{\varepsilon_S - \varepsilon_\infty}{1 + j\omega\tau}\right) \tag{3.12}$$

where ε_S is the low-frequency relative permittivity, ε_∞ is the high-frequency relative permittivity and τ is the relaxation time, given by $\tau = 1/2\pi f_r$, where f_r is known as the relaxation frequency.

The real and imaginary parts can be equated to give the permittivity and dielectric loss as

$$\varepsilon' = \varepsilon_\infty + \frac{\varepsilon_S - \varepsilon_\infty}{1 + \omega^2\tau^2} \tag{3.13}$$

$$\varepsilon'' = \frac{(\varepsilon_S - \varepsilon_\infty)\omega\tau}{1 + \omega^2\tau^2} \tag{3.14}$$

Equations (3.13) and (3.14) are known as the *Debye equations* and describe a single relaxation process where equilibrium is attained exponentially with time when a constant external field is applied to the dielectric material, and has a half-height frequency width of 1.14 decades. When applying a DC voltage across the dielectric

material (ω=0), the real part of the complex permittivity reduces to the steady state permittivity ($\varepsilon^*=\varepsilon_s$), whilst at very high frequencies the real part reduces to the permittivity ε_∞. By considering the energy storage properties of the dielectric in an AC field and considering the first law of thermodynamics that deals with the conservation of energy, it has been shown (Fröhlich, 1958) that the imaginary term ε'' in the complex permittivity is a measure of the energy loss from the applied electric field. The phase lag between the polarisation and the applied field leads to this absorption of energy and joule heating, and is equivalent to the rate of conversion of the electrical energy to heat in the material. This is referred to as the dielectric loss factor.

The frequency dependence of both ε' and ε'' is shown in Figure 3.6.

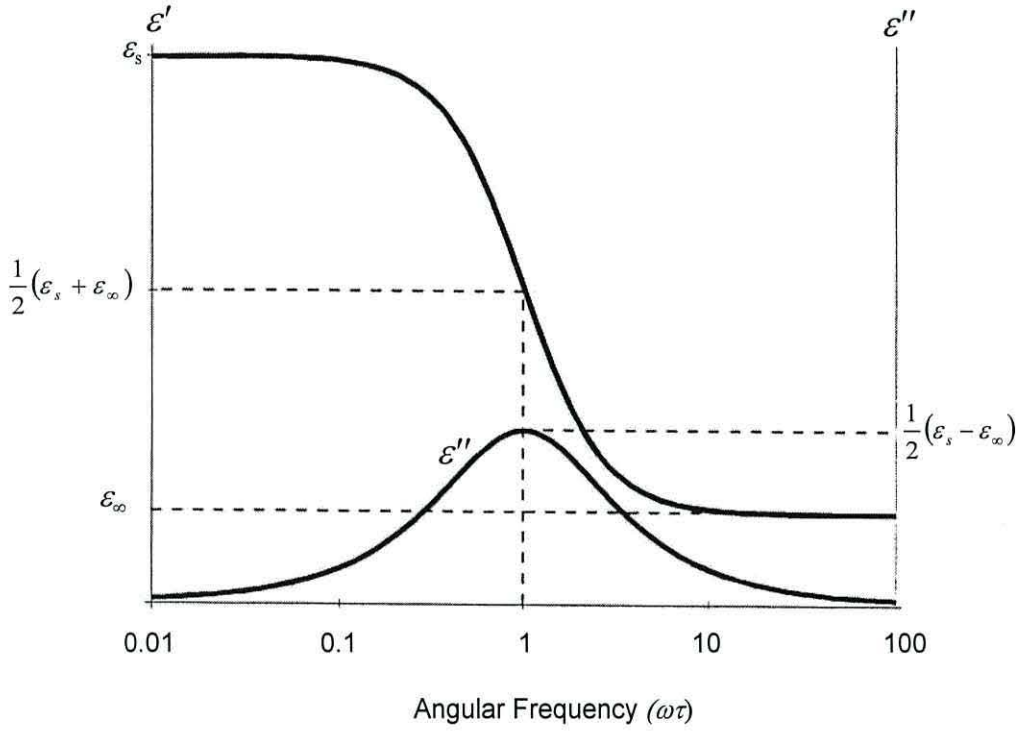

Figure 3.6 – The variation of the real and imaginary part of the complex permittivity as described by the Debye equations (a) – dielectric permittivity, ε' and (b) dielectric loss, ε'', with angular frequency.

3.6.4 Maxwell-Wagner Interfacial Polarisation

Interfacial polarisation arises from the accumulation of charges at a structural interface between dissimilar phases within a dielectric, and gives rise to the formation of charge double layers at the boundaries. This polarisation process is referred to as Maxwell-Wagner polarisation after the work of Maxwell (1892), who first recognised the phenomenon for DC fields, and Wagner (1914, 1924) who extended the theory to include AC fields. This type of polarisation is common in heterogeneous biological systems, which are composed of molecules exhibiting many different permittivities and conductivities. The simplest form of the Maxwell-Wagner interfacial polarisation is a parallel plate capacitor with two dielectrics of different thicknesses (d_1, d_2), permittivities (ε_1, ε_2) and conductivities (σ_1, σ_2) (Figure 3.7).

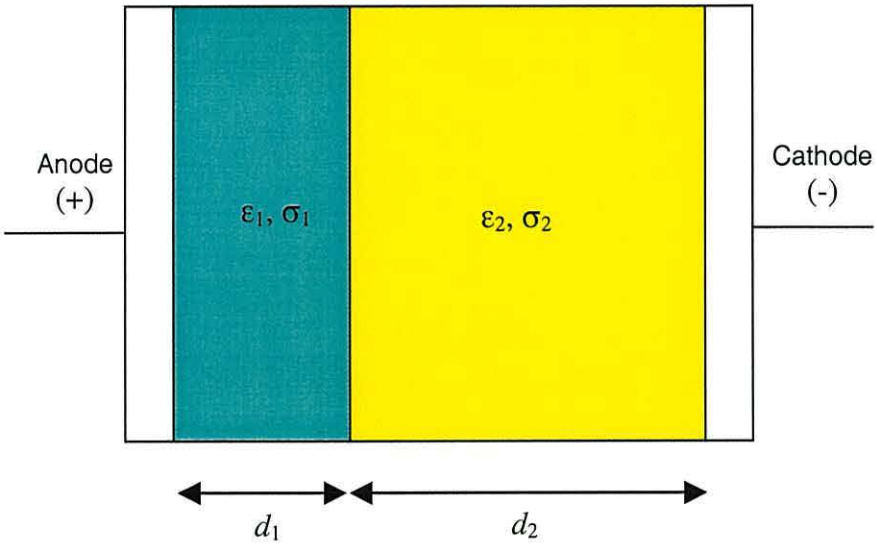

Figure 3.7 – A parallel plate capacitor separated by two differing dielectrics.

The mechanism by which interfacial polarisation occurs can be explained in terms of the non-uniform distribution of charges across the interface between the two differing dielectrics. The build up of charge at the interface causes polarisation in the dielectric system, which is frequency dependent.

By assuming that σ_2 is negligibly small and that ε_1, ε_2 and σ_1 are frequency independent, it is possible to obtain a simple expression for the behaviour of the dielectric system. The system can be regarded as two capacitors in series, so that the total capacitance is given by

$$\frac{1}{C} = \frac{1}{C_1} + \frac{1}{C_2} \tag{3.15}$$

where the capacitance of the two capacitors is given by (Pethig, 1979)

$$C_1 = \frac{A\varepsilon_0\left(\varepsilon_1 - \frac{j\sigma_1}{\omega\varepsilon_0}\right)}{d_1} \tag{3.16}$$

and

$$C_2 = \frac{A\varepsilon_0\varepsilon_2}{d_2} \tag{3.17}$$

giving a total capacitance of

$$C = \frac{A\varepsilon_0\varepsilon_2\left(\varepsilon_1 - \frac{j\sigma_1}{\omega\varepsilon_0}\right)}{d_2\left(\varepsilon_1 - \frac{j\sigma_1}{\omega\varepsilon_0}\right) + d_1\varepsilon_2}. \tag{3.18}$$

From Equations (3.1) and £.18) it can be seen that in the low frequency limit $(\omega \to 0)$, the effective permittivity, ε_s, is given by

$$\varepsilon_s = \frac{\varepsilon_2 d}{d_2} \tag{3.19}$$

where $d=d_1+d_2$.

For the high frequency limit $(\omega \to \infty)$ the effective permittivity ε_∞ is given by

$$\varepsilon_\infty = \frac{\varepsilon_1 \varepsilon_2 d}{d_2 \varepsilon_1 + d_1 \varepsilon_2} \tag{3.20}$$

from which it can be seen that $\varepsilon_s > \varepsilon_\infty$ indicating that the system exhibits a dielectric dispersion. In fact the dielectric dispersion of a two layer system can be described in terms of the Debye equations (van Beek, 1960) where

$$\varepsilon' = \varepsilon_\infty + \frac{\varepsilon_s - \varepsilon_\infty}{1 + \omega^2 \tau^2} \tag{3.21}$$

and

$$\varepsilon'' = \frac{(\varepsilon_s - \varepsilon_\infty)\omega\tau}{1 + \omega^2 \tau^2} \tag{3.22}$$

with

$$\varepsilon_s = \frac{d\left(\varepsilon_1 d_1 \sigma_2^2 + \varepsilon_2 d_2 \sigma_1^2\right)}{\left(\sigma_1 d_2 + \sigma_2 d_1\right)^2}, \tag{3.23}$$

$$\varepsilon_\infty = \frac{d\varepsilon_1 \varepsilon_2}{\varepsilon_1 d_2 + \varepsilon_2 d_1} \tag{3.24}$$

and

$$\tau = \frac{\varepsilon_0\left(\varepsilon_1 d_2 + \varepsilon_2 d_1\right)}{\sigma_1 d_2 + \sigma_2 d_1}. \tag{3.25}$$

The conductivity of the interfacial system as a whole is given by

$$\sigma = \frac{d\sigma_1 \sigma_2}{\sigma_1 d_2 + \sigma_2 d_1}. \tag{3.26}$$

3.7 Dielectric Dispersion

Polarisation rates are limited, so that as the frequency of the applied electric field is increased, some polarisation processes will no longer be able to maintain their DC or low frequency values (Figure 3.4). The slowest induced polarisation mechanism is always the first polarisation term to disappear as frequency is increased as the dipoles are no longer able to orientate themselves fully with the alignment of the electric field. This results in a reduction in the total polarisability from α_T to $(\alpha_T - \alpha_o)$. This fall in the polarisability with its associated change in the permittivity of the material and the absorption of energy is referred to as dielectric dispersion.

3.8 Manipulation of particles using non-uniform electric fields

Consider a sphere of radius r, composed of an ideal (zero conductivity) dielectric of relative permittivity $\varepsilon_{p,}$ suspended in an ideal dielectric fluid medium with a relative permittivity of ε_m and subjected to a homogeneous field E. The field in the fluid is uniform before the insertion of the sphere. The sphere distorts this field to give a field E_{in} interior to the sphere boundary given by

$$E_{in} = \left(\frac{3\varepsilon_m}{\varepsilon_p + 2\varepsilon_m} \right) E . \tag{3.27}$$

The induced polarisation, P, per unit volume becomes

$$P = \varepsilon_0 \left(\varepsilon_p - \varepsilon_m \right) E_{in} . \tag{3.28}$$

For a volume V, the induced dipole moment, m, is the product of the volume and the polarisation,

$$m = VP . \tag{3.29}$$

For the case where the neutral dielectric body is homogeneously, linearly and isotropically polarisable, then

$$m = \alpha VE \tag{3.30}$$

where α is the polarisability. From Equations (3.29) and (3.30) we obtain

$$VP = \alpha VE \tag{3.31}$$

yielding

$$\alpha = \frac{P}{E}. \tag{3.32}$$

Substituting for E_{in} from Equation (3.27) and P from Equation (3.28) gives the polarisability, α, per unit volume as

$$\alpha = 3\varepsilon_0\varepsilon_m \frac{\left(\varepsilon_p - \varepsilon_m\right)}{\left(\varepsilon_p + 2\varepsilon_m\right)}. \tag{3.33}$$

For a homogeneous spherical particle of radius r, and complex permittivity ε_p^*, suspended in a medium of complex permittivity ε_m^*, the magnitude of the dipole moment for the induced interfacial charges produced is given by (Wagner, 1914)

$$m = 4\pi\varepsilon_m \left(\frac{\varepsilon_p^* - \varepsilon_m^*}{\varepsilon_p^* + 2\varepsilon_m^*} \right) r^3 E \tag{3.34}$$

where E is the applied electric field strength. The complex permittivity takes account of the fact that the particle and suspending medium exhibit both conduction and dielectric properties when exposed to electrical fields, and has the form

$$\varepsilon^* = \varepsilon - j(\sigma/\omega) \tag{3.35}$$

where ω is the angular frequency of the applied field, $j(=\sqrt{-1})$ indicates that the dielectric displacement current leads the conduction current by a phase angle of 90° and σ is the finite conductivity of the particle or suspending medium.

Equation (3.34) reveals that the magnitude and polarity of the induced dipole moment depends on the frequency of the applied electric field and on the relative magnitudes of ε_p, ε_m, σ_p and σ_s (Wang *et al.*, 1993). If the magnitude of ε_p^* is less than that of ε_m^* then the effective polarisability of the particle is less than that of its suspending solution, and the induced charges on the particle are as shown in Figure 3.8a, with the induced dipole moment **m** directed against the applied field. Conversely, as shown in Figure 3.8b, if the permittivity of the particle is greater than that of the suspending medium, then the arrangement of the induced charge produces a dipole moment in the same direction as the applied field. The resultant electric field patterns within and around the particle for the different cases are shown.

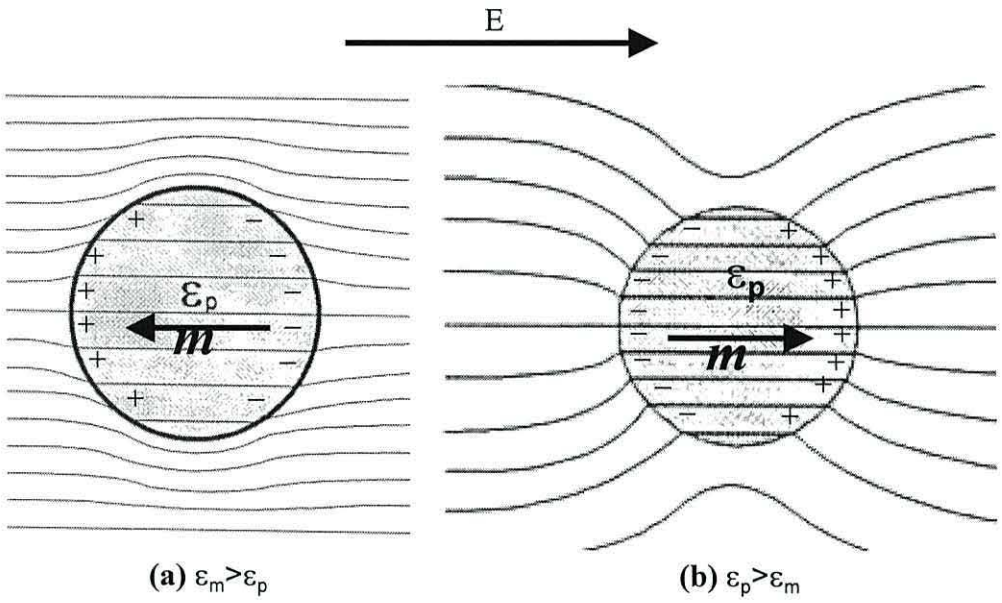

Figure 3.8 – Two particles of different permittivity shown in a uniform AC electric field created between parallel electrodes. The distribution of electric charges induced at the surface of the particles and the direction of the resulting dipole moment, *m*, are shown (a) where the permittivity of the particle is less than the surrounding medium ($\varepsilon_m > \varepsilon_p$) and (b) where the permittivity of the particle is greater than the surrounding medium ($\varepsilon_p > \varepsilon_m$) (adapted from Talary, 1994).

The relaxation time, τ, of this Maxwell-Wagner system is characterised by (Wang *et al.*, 1993; Pethig, 1994)

$$\tau = \left(\frac{\varepsilon_p^* - 2\varepsilon_m^*}{\sigma_p^* + 2\sigma_m^*} \right) \tag{3.36}$$

and the frequency dependence of the dipole moment is described by the term

$$K(\omega) = \frac{\varepsilon_p^* - \varepsilon_m^*}{\varepsilon_p^* + 2\varepsilon_m^*}. \tag{3.37}$$

Equation (3.37) is known as the Clausius-Mossotti factor. This holds true under conditions where the characteristic size of the electric field is large compared to the size of the particle and the particle is sufficiently far away from other dielectric objects so as not to be influenced by their dipole moments.

3.9 Dielectrophoresis

Dielectrophoresis is defined as the translational motion of electrically neutral particles caused by the polarisation effects of non-uniform electric fields (Pohl 1978, Pethig 1979). This is quite distinct from electrophoresis which is an electrostatic response to the free charges on particles in an electric field.

3.9.1 Dielectrophoretic Force

The polarisation of dielectric materials has been shown to be frequency dependent, with characteristic dielectric dispersion regions occurring as the frequency is increased from dc conditions (Figure 3.4). These dispersions affect the translational motion of the particle as the frequency of the applied electric field is changed, giving rise to a characteristic dielectrophoretic spectrum that is dependent on the dielectric properties of the particle. Pohl (1978) provided a simplified theory for the force exerted on an electrically neutral particle suspended in a homogeneous fluid medium when exposed to a non-uniform field. The brief treatment given here is based on that given by Pohl (1978) and Pethig (1979).

In a static field, the net translational force on a neutral small body with a dipole moment **m** (induced or permanent) at equilibrium is given by

$$F = (m \bullet \nabla)E \tag{3.38}$$

where ∇ is the del vector operator and E is the external field. Combining Equations (3.38) and (3.30) gives

$$F = \alpha V (E \bullet \nabla)E \tag{3.39}$$

$$= \frac{\alpha V}{2} \nabla |E|^2 \tag{3.40}$$

substituting for α from Equation (3.33) into Equation (3.40) gives the dielectrophoretic force, F,

$$F = 2\pi r^3 \varepsilon_0 \varepsilon_m \frac{\left(\varepsilon_p^* - \varepsilon_m^*\right)}{\left(\varepsilon_p^* + 2\varepsilon_m^*\right)} \nabla |E|^2 \tag{3.41}$$

which can be rewritten as

$$F = 2\pi r^3 \varepsilon_o \varepsilon_m \, \mathrm{Re}[K(\omega)] \nabla E^2 \tag{3.42}$$

where $K(\omega)$ is the Clausius-Mossotti factor described in Equation (3.37). When the permittivity of the particle is greater than that of the suspending medium ($\varepsilon_p > \varepsilon_m$), then $K(\omega) > 0$ and the particle is attracted to electric field maxima and repelled from the field minima. This effect is known as positive dielectrophoresis and is illustrated schematically in Figure 3.9. When the permittivity of the particle is less than that of the suspending medium ($\varepsilon_p < \varepsilon_m$), then $K(\omega)$ is less than zero and the particle is attracted to electric field minima and repelled from the maxima. This effect is known as negative dielectrophoresis and is illustrated schematically in Figure 3.10.

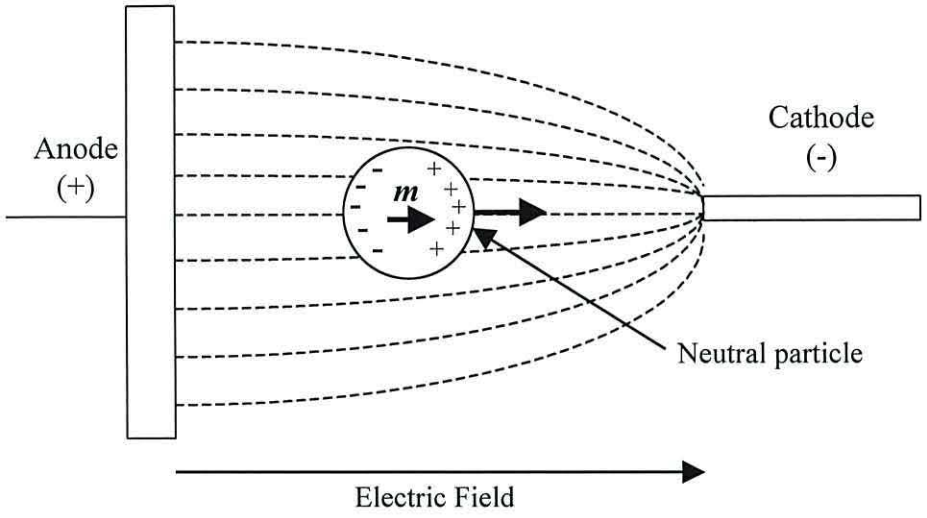

Figure 3.9 – Motion of a polarised neutral particle by positive dielectrophoresis where the permittivity of the particle is greater than that of the suspending medium ($\varepsilon_p > \varepsilon_m$).

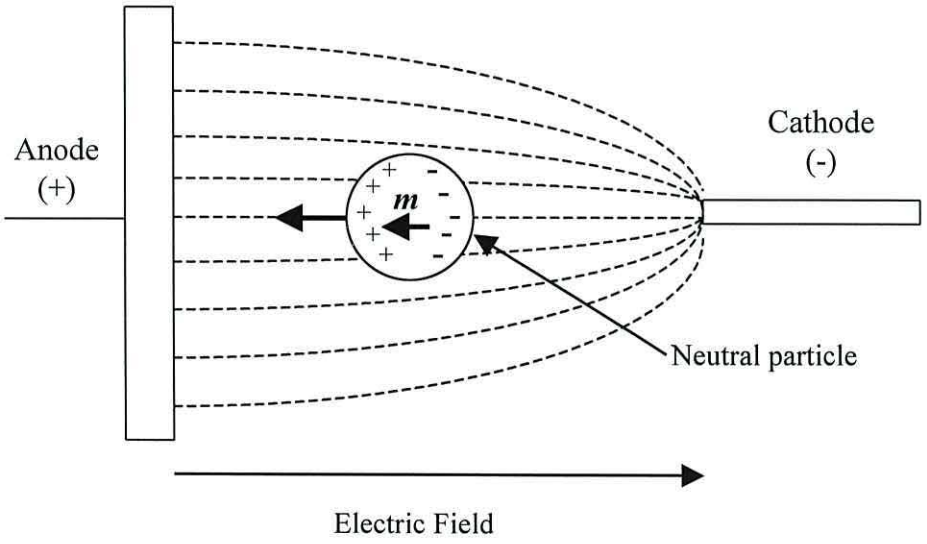

Figure 3.10 – Motion of a polarised neutral particle by negative dielectrophoresis where the permittivity of the particle is less than that of the suspending medium ($\varepsilon_p < \varepsilon_m$).

3.10 Electrorotation

Pohl (1978) suggested that non-uniform fields can also sometimes induce a torque on a particle, causing it to rotate. However, the first reports of controlled particle rotation, using a uniform (homogenous) rotating electric field, were given by Arnold and Zimmerman (1982) and Mischel *et al.* (1982).

3.10.1 Description of a rotating field

When two sinusoidally varying, linear electrical fields, directed at right angles to each other and differing in phase by exactly 90°, are superimposed, a rotating electric field E is produced (Figure 3.11).

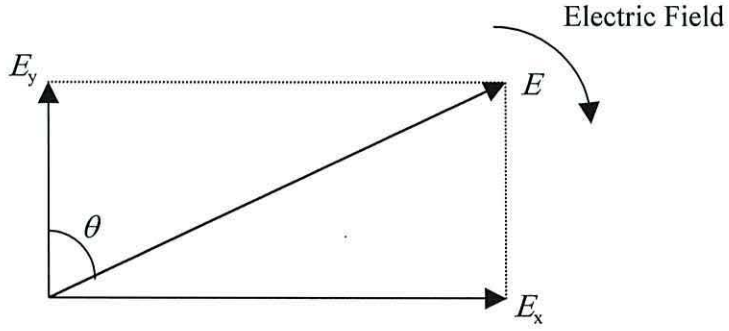

Figure 3.11 – The superposition of two orthogonal linear field vectors and the resultant field, E, at a given instant in time. θ is the angle of E with respect to the y-vector.

This is readily shown by assuming both fields have a peak amplitude E_0 (V/cm) and angular frequency ω (rad/s) so that

$$E_y = E_0 \cos \omega t \tag{3.43}$$

and

$$E_x = E_0 \cos\left(\omega t - 90^o\right) \tag{3.44}$$

$$= E_0 \sin \omega t\,. \tag{3.45}$$

The amplitude of the resultant is given by

$$E^2 = E_0^2\left(\cos^2 \omega t + \sin^2 \omega t\right) = E_0 \tag{3.46}$$

and therefore constant.

The angle θ is given by

$$\tan\theta = \frac{E_0 \sin\omega t}{E_0 \cos\omega t} \tag{3.47}$$

$$= \tan\omega t\,. \tag{3.48}$$

Therefore

$$\theta = \omega t\,. \tag{3.49}$$

The resultant field rotates at an angular frequency ω but has a constant instantaneous amplitude E_0, which is the peak value of the component fields.

3.10.2 Frequency dependence of the torque

Holzapfel *et al.* (1982) states that a linear alternating field

$$E_y = E_0 \cos\omega t \tag{3.50}$$

will induce a linear dipole, m_y, in a particle given by

$$m_y = \frac{G}{1+(\omega\tau)^2}\left(\cos\omega t + \omega\tau \sin\omega t\right) \tag{3.51}$$

where $G = -2\pi\varepsilon_0 r^3$ and r is the radius of the particle.

Similarly, if a second linear field E_x with a 90° phase delay is imposed at right angles to E_y, a second dipole is induced, given by

$$m_x = \frac{G}{1+(\omega\tau)^2}\left(\sin\omega t - \omega\tau\cos\omega t\right). \tag{3.52}$$

The amplitude of the resultant dipole is given by (Arnold and Zimmerman, 1982)

$$m = \left(m_y^2 + m_x^2\right)^{\frac{1}{2}} \tag{3.53}$$

$$= \frac{G}{1+(\omega\tau)^2}\left[\sin^2\omega t - \cos^2\omega t + (\omega\tau)^2\sin^2\omega t + \cos^2\omega t\right]^{\frac{1}{2}} \tag{3.54}$$

$$= G\left[1+(\omega\tau)^2\right]^{-\frac{1}{2}}. \tag{3.55}$$

If the instantaneous dipole m and instantaneous field E are not co-linear, a torque will result whose magnitude depends on their angular displacement, ϕ, where

$$\tan(\phi) = \frac{\mathrm{Im}(m)}{\mathrm{Re}(m)}. \tag{3.56}$$

Here Im(m) and Re(m) represent the imaginary and real parts of the induced dipole moment, respectively (Figure 3.12).

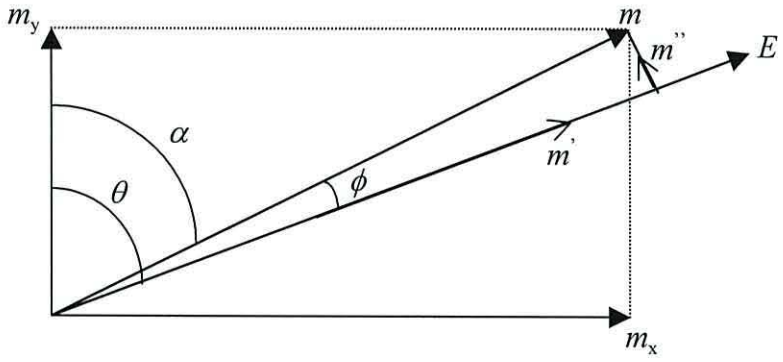

Figure 3.12 – The superposition of two orthogonal linear dipoles resulting from dielectric polarisation involving component fields from Figure 3.11. ϕ is the phase lag of the resultant dipole with respect to the resultant field (E).

If the angle $\alpha = \tan^{-1}(m_x/m_y)$ describes the instantaneous position of the dipole vector with respect to the axes, then

$$\sin\phi = \sin(\theta - \alpha) \tag{3.57}$$

$$= \sin\theta\cos\alpha - \cos\theta\sin\alpha \tag{3.58}$$

$$= \frac{m_y}{m}\sin\theta - \frac{m_x}{m}\cos\theta. \tag{3.59}$$

Substituting using Equations (3.51), (3.52) and (3.55) gives

$$\sin\phi = \left[1+(\omega\tau)^2\right]^{-\frac{1}{2}}\left(\omega\tau\sin^2\theta + \omega\tau\cos^2\theta\right) \tag{3.60}$$

$$= \omega\tau\left[1+(\omega\tau)^2\right]^{-\frac{1}{2}}. \tag{3.61}$$

From Equations (3.55) and (3.61) we see that, for constant ω, the induced dipole is of constant amplitude and rotates with a constant phase difference behind the field.

The torque, Γ, exerted on the dipole m by the field E at angle ϕ is given by

$$\Gamma = Em\sin\phi\,. \tag{3.62}$$

Substituting from Equations (3.55) and (3.61) then gives

$$\Gamma = EG\frac{\omega\tau}{1+(\omega\tau)^2}, \tag{3.63}$$

from which it is seen that the maximum torque occurs at $\omega\tau = 1$. If $\omega\tau$ is very large or very small, the torque reduces to an insignificant level.

3.10.3 Electrorotation torque and velocity

When the imposed field E is a rotating electric field, electrorotation occurs as the result of the rotational torque exerted on a polarised particle. The rotating electric field can be generated by addressing electrodes with 4 sinusoidal voltages, each separated by a 90° phase angle as shown in Figure 3.13. In theory three, five or even more electrodes can be used to generate the rotating field, however the production of the necessary phase shifts over a wide frequency range would require complex generator circuitry.

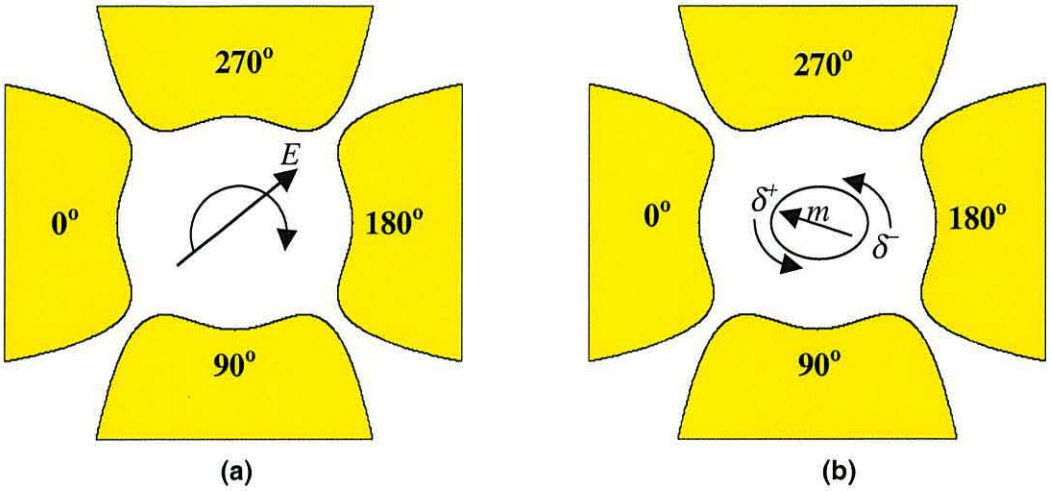

Figure 3.13 – A quadrature electrode structure (a) which creates a rotating electric field, *E*, which produces anti-field rotation (b) in a particle (not to scale) in the centre.

For a homogeneous particle of radius r in an imposed electric field E of angular frequency ω, the electrorotational torque is given by (Fuhr, 1985; Saur and Schlögl, 1985)

$$\Gamma(\omega) = -4\pi\varepsilon_m r^3 \,\mathrm{Im}\left(\frac{\varepsilon_p^* - \varepsilon_m^*}{\varepsilon_p^* + 2\varepsilon_m^*}\right) E^2 \tag{3.64}$$

where ε_p^* and ε_m^* are the complex permittivities of the particle and suspending medium respectively. Substituting for the dipole moment from Equation (3.34) gives the rotational torque in the form

$$\Gamma(\omega) = -\mathrm{Im}\{m(\omega)\}E \tag{3.65}$$

Thus it is the imaginary component of the dipole moment that determines the rate and sense of the induced electorotation. If the imaginary component of the Clausius-Mossotti factor is positive then the torque exerted will be negative and the particle rotates in a direction that opposes that of the rotating field (anti-field rotation). If the imaginary component is negative, then the torque exerted will be positive and the particle rotates in the same sense as the electric field (co-field rotation).

The sense and magnitude of the rotation, as seen from Equation (3.64), are dependent on the relative dielectric properties of the particle and the suspending medium and the frequency of the applied field. These affect the phase angle of the field induced dipole moment. When the dipole moment lags the electric field by an angle lying between 0 to 180°, co-field rotation is observed. However, if the dipole moment lags the field by more than 180° then anti-field rotation takes place (Huang *et al.* 1992).

When the electrorotational torque is balanced by the opposing viscous drag of the suspending medium, the magnitude of the steady-state electrorotation velocity $V(\omega)$ is derived as (Arnold and Zimmerman, 1988)

$$V(\omega) = -0.5\frac{\varepsilon_m}{R}\mathrm{Im}\left(\frac{\varepsilon_p^* - \varepsilon_m^*}{\varepsilon_p^* + 2_m^*}\right)E^2 \tag{3.68}$$

where R is the friction co-efficient whose value depends on the viscosity of the surrounding medium and on the geometry and surface frictional properties of the particle (Kakutani *et al.*, 1993).

3.11 Dielectric properties of cells

The dielectric properties of cell suspensions have been studied by many workers in the frequency range of ~5 Hz to 30 GHz (Fricke *et al.* 1956, Schwan 1957, Grant *et al.* 1978, Pethig 1979, Pethig and Kell 1987). Generally three major dispersion regions are displayed, referred to as α, β and γ dispersions. These dispersions arise from the polarisation mechanisms that occur at the cell exterior, cell membrane and the cell interior (aqueous cytoplasmic) (Grant *et al.* 1978) (Figure 3.14).

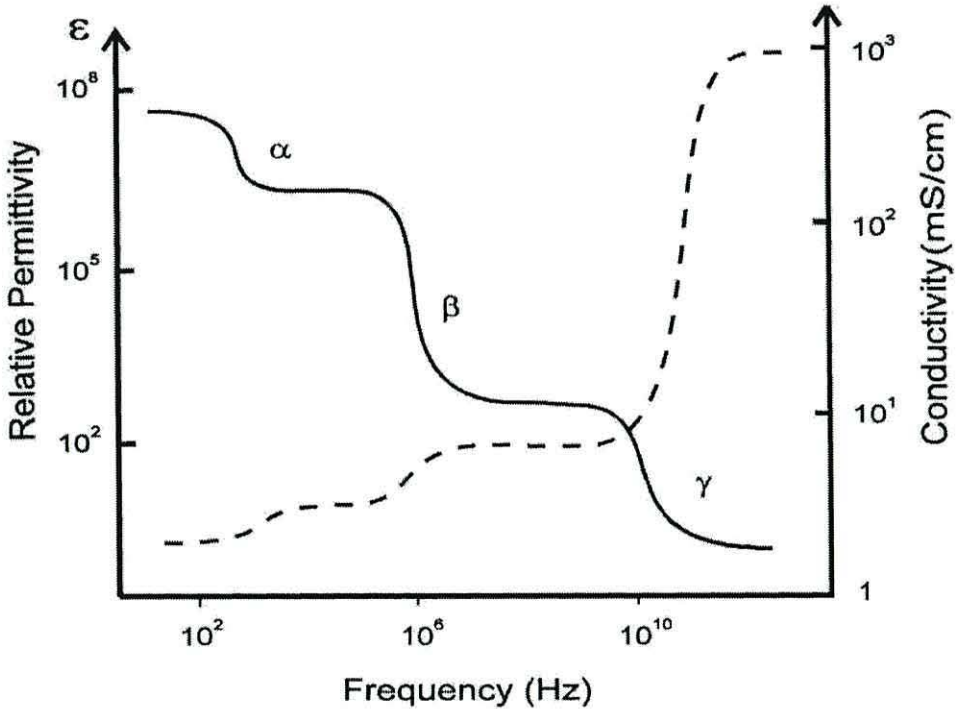

Figure 3.14 – Frequency variation in the relative permittivity ε, and conductivity, σ, of muscle showing the presence of three distinct α, β and γ dispersions. Solid line indicates relative permittivity and dashed line indicates conductivity (Schwan, 1957).

The α-dispersion, which occurs in the frequency range below 10 kHz, is generally considered to be associated with the relaxation of the ionic double layer at the interfaces of the cells (Schwan *et al.*, 1962; Schwarz, 1962). When cells are suspended in an aqueous medium, they acquire a net surface charge due to the presence of negatively charged head groups on the lipids, proteins and sugars that reside on the membrane surface. An electrical double layer is formed close to the cell surface as mobile counter-ions in the suspending medium are electrostatically attracted to the charged cell surface (Figure 3.15).

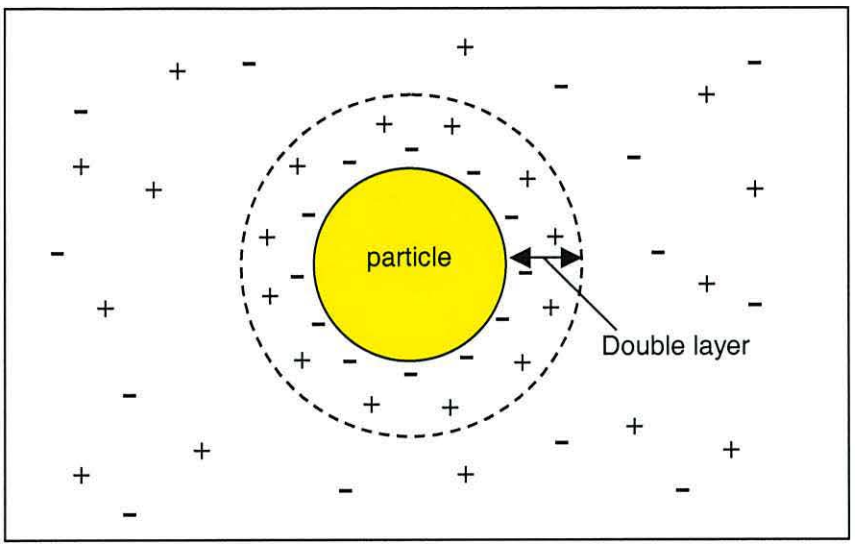

Figure 3.15 – The diffuse electrical double layer formed around a suspended particle in an ionic medium with no field applied.

On the application of an electric field, the ions surrounding the particle are displaced about the centre of the cell forming a very large induced dipole (Figure 3.16).

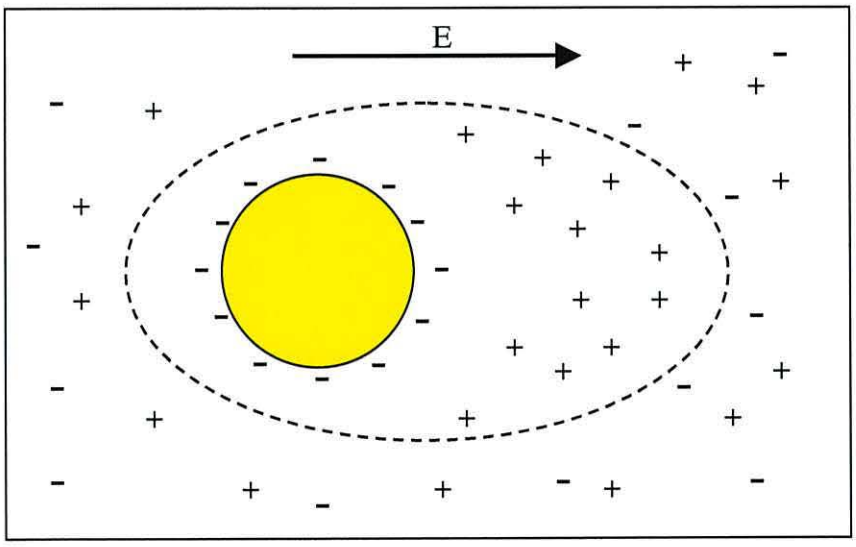

Figure 3.16 – The greatly exaggerated displacement of ions in the diffuse electrical double layer after the application of an electric field.

The displacement of the ions in the double layer takes a finite time known as the characteristic relaxation time. The relaxation frequency of such a dispersion is typically 1 kHz. At higher frequencies the mobilities of ions in the double layer are too low to follow the applied field. The relaxation process is controlled by factors such as surface charge density, ionic mobility (which varies with temperature) and ionic concentration in the suspending medium and on the surface of the cell.

The β-dispersion occurs in the frequency range of 1 MHz to 10 MHz and is considered to be associated with the interactive charge build up at the interfaces between the poorly conducting cytoplasmic membrane and the suspending medium (Irimajiri *et al.*, 1979; Pethig and Kell, 1987). The relaxation mechanisms that arise are associated with the interfacial polarisation processes. The relaxation that occurs at the membrane interface between the suspending media and the charge build-up on the outer surface of the cell are identical to the interfacial Maxwell-Wagner relaxation. There will also be relaxation processes associated with the interface between the inner surface of the cell membrane and the cell cytoplasm. The cytoplasmic membrane, as described in Chapter 2, consists mainly of lipids and protein molecules and is relatively non-conducting. The average thickness of a lipid bilayer membrane is around 6 nm and the permittivity of the phospohlipids which make up the bilayer is around $2.5\varepsilon_0$ (Pethig, 1979). This gives an average membrane capacitance of ~0.5 μFcm^{-2}. The widely held textbook value of membrane capacitance is 1.0 μFcm^{-2} (Pethig, 1979), which was originally found by extracellular electrode measurements. Transmembrane electrode techniques have found the membrane capacitance to be probably no more than 0.6 μFcm^{-2}, with the lateral electrophoresis of proteins within the plane of the membrane affecting the effective permittivity of the membrane (Pethig and Kell, 1987). In parallel with this capacitance is some degree of conductivity caused by the movement of ions through the membrane, either by diffusion or via the membrane transport proteins. A typical membrane resistance is 20 Ωm^{-2} (Asami *et al.*, 1989) which for a membrane thickness of 5 nm is equivalent to a conductivity of 0.25 nSm^{-1}.

At low frequencies, the high resistance of the cell membrane insulates the cytoplasm from the external electric field, and no DC current is induced within the cell interior as shown in Figure 3.17a. At higher frequencies, the short-circuiting effect of membrane capacitance allows the electric field to penetrate into the cell, Figure 3.17b, until at sufficiently high frequencies the effective membrane resistance becomes vanishingly small and the cell appears as a sphere with the dielectric properties of the cell cytoplasm and radius of the cell without its membrane (Figure 3.17c). This β–dispersion need not constitute a single relaxation mechanism but may also include polarisation processes attributed to the rotation of protein molecules within the plane of the membrane (Kell and Harris, 1985).

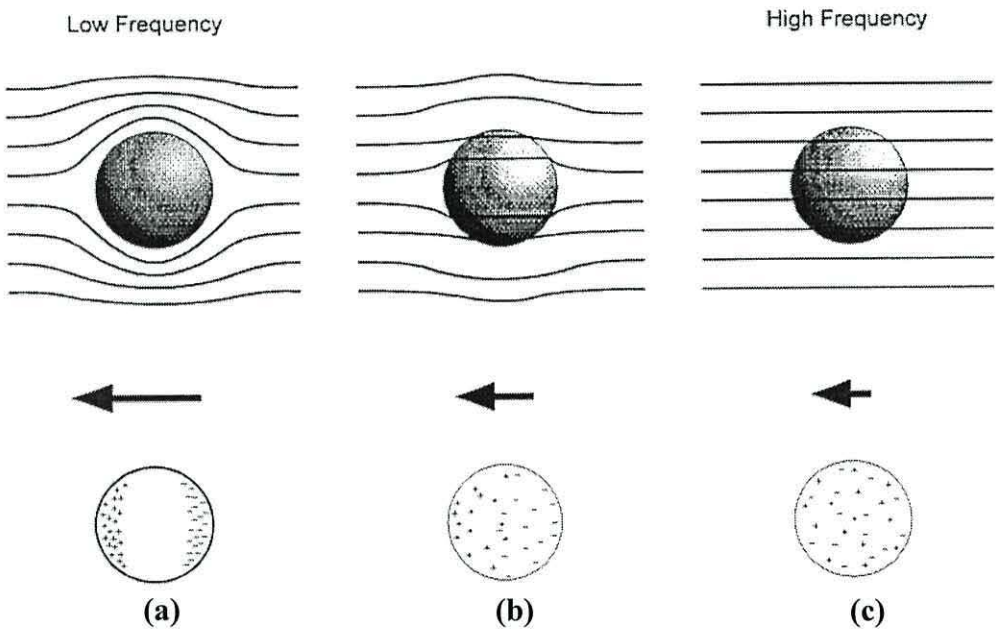

Figure 3.17 – Schematic indicating current flow at various frequencies and magnitude of induced dipole (adapted from Talary, 1994)

The γ-dispersion appears in the very high frequency range (> 1GHz) and is associated with the relaxation of water molecules within the cytoplasm (Grant *et al.*, 1978). Water bound to proteins and other biomacromolecular structures exhibits dielectric dispersions at frequencies lower that the γ-dispersion of free water molecules (which occur at ~20 GHz), and this can sometimes be observed as a small δ-dispersion in the region 0.1 – 1 GHz (Grant, 1965).

3.12 Conclusions

The dielectric theory, applied to cells, has been presented in this Chapter. Combined with the biological information from Chapter 2, this is developed in Chapter 4 into a mathematical model of a biological cell in a rotating electric field which can be used to simulate the electrorotational response of *Cyclospora cayetanensis* and *Ascaris suum.* The simulations will then be compared to experimental data in order to determine the changes in the dielectric properties of the organisms.

3.13 References

Alison, J. **(1971)** *Electronic Engineering Materials and Devices,* McGraw-Hill, London

Arnold, W. M. and Zimmermann, U. **(1982)** Rotating-field-induced rotation and measurement of the membrane capacitance of single mesophyll cells of *Avena sativa. Zeitschrift fur Naturforschung C* **37** 908-915.

Arnold, W. M. and Zimmermann, U. **(1988).** Electro-rotation: Development of a technique for dielectric measurements on individual cells and particles. *Journal of Electrostatics.* **21** 151-191

Asami, K., Hanai, T. and Koizumi, N. **(1980)** Dielectic approach to suspensions of ellipsoidal particles covered with a shell in particular reference to biological cells. *Jap. J. Appl. Phys.* **19** 359-365

Asami, K. Takahashi, Y. and Takashima, S. **(1989)** Dielectric properties of mouse lymphocytes and erythrocytes. *Biochim. Biophys. Acta.* **1010** 49-55

Benguigui, L. and Lin, I. J. **(1982)** More about dielectrophoretic force. *J. Appl. Phys.*53 **1141-1143**

Burt, J. P. H. **(1990)** Biotechnological Applications of Dielectrophoresis *PhD Thesis,* University of Wales.

Cross, J. A. **(1987)** *Electrostatics : principles, problems and applications,* Adam Hilger, Bristol

Debye, P. **(1929)** *Polar molecules.* Chemical Book Company, New York

Fricke, H., Schwan, H. P. and Bryson, V. **(1956)** A dielectric study of the low-conductance surface membrane of *E. coli. Nature* **177** 134-135

Fröhlich, H. **(1958)** *Theory of Dielectrics.* 2nd. Ed., Clarendon Press, Oxford.

Fuhr, G. **(1985)** Über die Rotation dielktrisher Körper in rotierenden Felderd. *Ph.D Dissertation*, Humboldt-Universität, Berlin.

Grant, E. H. **(1965)** The structure of water neighbouring proteins, peptides and amino acids as deduced from dielectric measurements. *Ann. N. Y. Acad. Sci.* **125** 418-427

Grant, E. H., Sheppard, R. J. and South, G. P. **(1978)** *Dielectric Behaviour of Biological Molecules in Solution.* Clarendon Press, Oxford.

Hateschek, E and Thorne, P. C. L. **(1923)** Metal Sols in Non-dissociating Liquids Part 1. Nickel in Toluene and Benzene. *Proc. Roy. Soc.* **103** 276-284

Höber, R. (**1913)** Messungen der inneren Leitfähigkeit von Zellen. *Pfl. Physiol. Archiv. Mensch. Tiere* **150** 15-45

Holzapfel, C., Vienken, J. and Zimmermann, U. **(1982)** Rotation of cells in an electric field – Theory and experimental proof. *J. Membrane. Biol.* **67(1)** 13-26

Huang, Y., Hölzel, R., Pethig, R. and Wang, X.B. **(1992)** Differences in the ac electrodynamics of viable and non-viable yeast cells determined through combined dielectrophoresis and electrorotation studies. *Phys. Med. Biol.* **37(7)** 1499-1517

Irimajiri, A., Hanai, T. and Inouya, A. **(1979)** A dielectric theory of 'multi-stratified shell' model with its application to a lymphoma cell. *J. Theor. Biol.* **78** 251-269

Jones, T. B. and Kallio, G. A. **(1979)** Dielectrophoretic levitation of spheres and shells. *J. Electrostat.* **6** 207-224

Jones, T. B. **(1995)** *Electromechanics of Particles.* Cambridge University Press, Cambridge

Kakutani, T., Shibatani, S. and Sugai, M. **(1993)** Electrorotation of non-spherical cells : theory for ellipsoidal cells with an arbitrary number of shells. *Bioelectrocehem. Bioenerg.* **31** 131-145

Kell, D. B. and Harris, C. M. **(1985)** On the Dielectrically observable consequences of the diffusional motions of lipids and proteins in membranes *Eur. Biophys.J.* **12** 181-197

Lortet, M **(1896)** Influences des courants induits sur l'orientation des bacteries vivantes. *Comptes Rendus de L'Academie des Sciences.* **112** 892-894

Maxwell, J. C. **(1892)** *A Treatise on Electricity and Magnetism,* 3rd ed., Vol. 1, Clarendon Press, Oxford.

Mischel, M., Voss, A. & Pohl, H. A. **(1982)** Cellular spin resonance in rotating electric fields. *J.Biol. Phys.* **10** 223-226.

Pethig, R. **(1979)** *Dielectric and Electronic Properties of Biological Materials.* John Wiley and Sons, Chichester

Pethig, R. and Kell, D. B. **(1987)** The Passive Electrical Properties of Biological Systems : their significance in physiology, biophysics and biotechnology. *Phys. Med. Biol.* **32** 933-970

Pethig, R. **(1991)** Biological electrostatics : dielectrophoresis and electrorotation. *IOP Conference Series* **118(1)** 13-26

Pohl, H. A. **(1951)** The Motion and Precipitation of Suspensoids in Divergent Electric Fields. *J. Appl. Phys.* **22** 869-871

Pohl, H. A. **(1978)** *Dielectrophoresis*, Cambridge University Pres, Cambridge.

Sauer, F. A. and Schlögl, R. W. **(1985)** Torques exerted on cylinders and spheres by external electromagnetic field : A contribution to the theory of field induced cell rotation. *In* Interactions between electromagnetic fields and cells. (Eds. Chiabera, A., Nicolini, C. & Schwan, H. P.) 203-251. New York, Plenum.

Schwan, H. P. **(1957)** Electrical properties of tissues and cells suspensions *Adv. Biol. Med. Phys.* **5** 147-209

Schwan, H. P., Schwarz, G., Maczuk, J. and Pauly, H. **(1962)** On the low frequency dielectric dispersion of colloid particles in electrolyte solution. *J.Phys. Chem.* **66** 2626-2636

Schwarz, G. **(1962)** A theory of the low frequency dielectric dispersion of colloidal particles in electrolyte solution. *J. Phys. Chem.* **66** 2636-2642

Talary, M. S. **(1994)** Automatic Dielectrophoretic Characterisation of Cells *PhD Thesis,* University of Wales.

Van Beek, L. K. H. **(1960)** *Dielectric Behaviour of Heterogeneous Systems, in Progress in Dielectrics,* Ed. J. B. Birks, 7 69, Heywood, London

Wagner, K. W. **(1914)** Erklarung der dielectrischen Nachwirkungsvorgange auf grund Maxwellsher Forstellungen. *Archiv. Electrotechnik* **2** 371-89

Wagner, K. W. **(1924)** *Die Isolierstoffe der Electrotechnik*, Ed. H. Schering, Springer, Berlin. (as cited by Pohl H. A., 1978)

Wang, X. B., Pethig, R. and Jones, T. B. **(1992)** Relationship of dielectrophoretic and electrorotation behaviour exhibited by polarised particles. *J. Phys. D : Appl. Phys.* **25** 905-912

Wang, X. B., Huang, Y., Hölzel, R., Burt, J. and Pethig, R. **(1993)** Theoretical and experimental investigations of the interdependence of the dielectric, dielectrophoretic and electrorotational behaviour of colloid particles. *J. Phys. D: Appl. Phys.* **26** 312-322

Chapter 4

Modelling

4.1 Introduction

The chosen modelling method for biological organisms subjected to electrorotation is described in detail in this chapter. The effects of changing the model parameters and what information can be deduced about the organism under investigation are discussed. Based on model parameters taken from the relevant literature, comparisons are made with preliminary electrorotational data to show the validity of the chosen model for the organisms under investigation. A brief overview of other types of mathematical models available are also given.

4.2 Spherical Dielectric Multi-Shell Model

For a homogeneous particle of radius r subjected to an imposed electric field E of angular frequency ω, the effective dipole moment m, time-averaged dielectrophoretic force F and rotational torque $\Gamma(\omega)$ are related through Equations (3.34), (3.42) and (3.65), respectively, as shown in Chapter 3.

However, cells are not homogeneous in their electrical and physical properties. Höber (1913) showed, to a good approximation, that red blood cells could be represented as a conducting sphere surrounded by a resistive membrane. Maxwell (1892) had already demonstrated that such a concentric system could be replaced by a homogeneous sphere of the same outer radius having an effective resistance r_p. When placed in an electrical field, the 'smeared out' sphere can be substituted for the heterogeneous sphere without altering the field. Maxwell and later Wagner (1914) extended this philosophy to derive the effective complex permittivity of a system composed of

particles dispersed in a dielectric medium. This means that the interfacial charging effect that occurs for a homogeneous particle is reflected in the overall dielectric property of the heterogeneous mixture.

The multi-shell model of a cell was formulated based on dielectric theories by Fricke (1924), Hanai (1960) and Irimajiri *et al.* (1979), whereby a heterogeneous particle can be described in terms of a homogeneous *smeared out sphere* exhibiting frequency dependent dielectric and conductive properties. This concentric-spheroid model of a cell was used to calculate (Irimajiri *et al.,* 1979) the effective electrical properties of cells in suspension, and later adapted for the calculation of the electrorotational torque acting on a cell in a rotating electric field by Fuhr and Kuzmin (1986). Using this approach, Equations (3.34), (3.42) and (3.65), for homogeneous particles can be used to describe the case for heterogeneous ones, by the simple process of replacing the frequency independent permittivity and conductivity parameters by frequency dependent ones. A formal proof that this approach gives the same (but more practically useful) results as those of the effective dipole-moment method of Fuhr and Kuzmin (1986) is given in Huang *et al.* (1992).

The multi-shell model of a cell is shown in Figure 4.1a in the form of concentric dielectric spheres with a permittivity of ε_i, conductivity σ_i (i = 1,2,…,N+1) and radius R_i for each shell i, respectively, where i = 1 is the innermost sphere (Huang *et al.,* 1992). The effective, frequency dependent, complex permittivity of such multi-shelled particles can be determined using the following *smeared out sphere* approach.

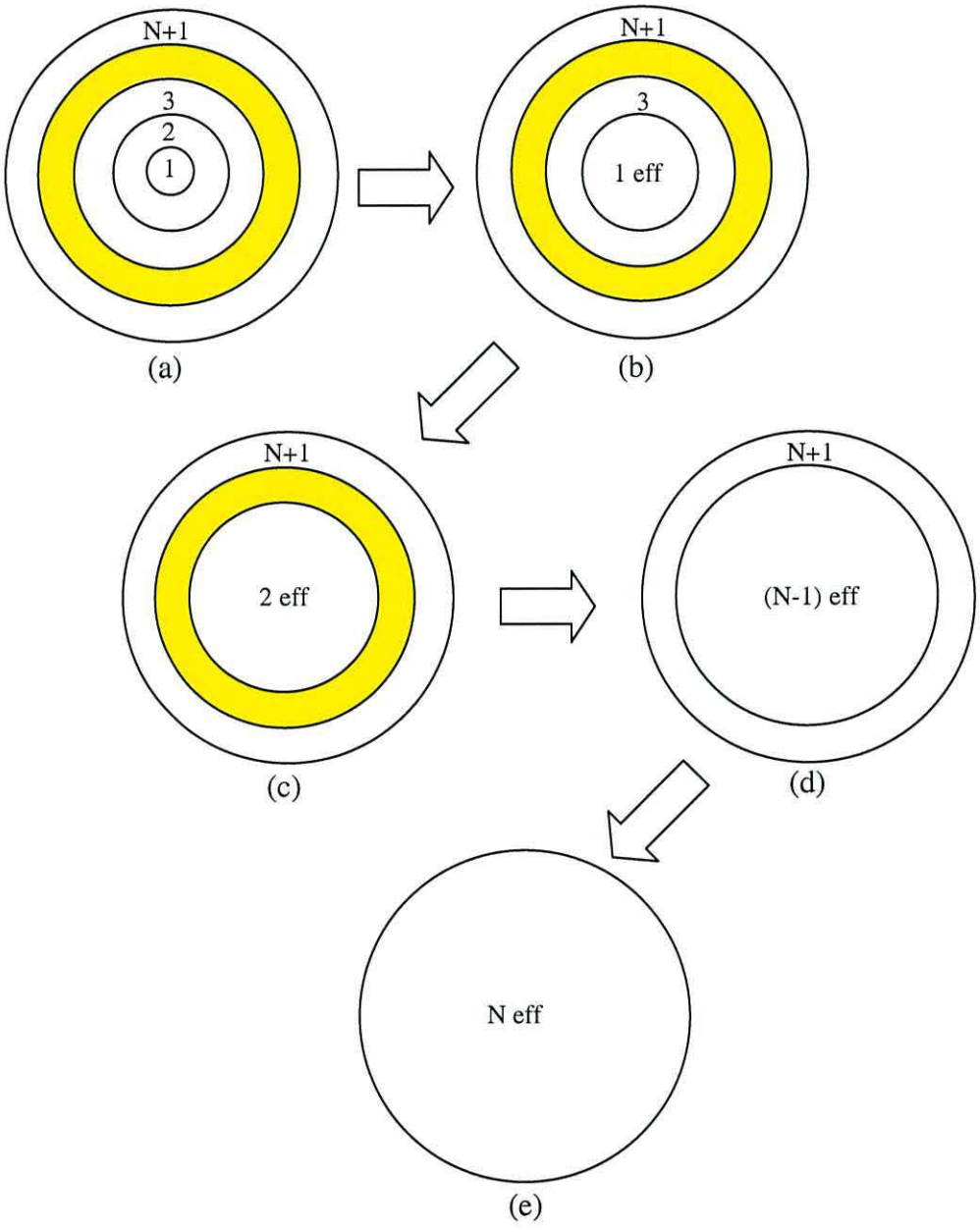

Figure 4.1 – A *smeared out sphere* approach for determining the effective permittivity of a N shell sphere, showing the progressive simplification to a simple homogeneous sphere having an effective frequency dependent, complex permittivity (Equation 4.10) that mimics the dielectric properties of the multi-shell sphere.

If we initially consider the case of the inner-most shell (1), with a complex permittivity of ε_1^*, surrounded by the next shell (2) with complex permittivity ε_2^*, we can replace the inner-most shell (Figure 4.1b) with an effective shell of complex permittivity

$$\varepsilon_{1eff}^* = \varepsilon_2^* \frac{\left(\frac{R_2}{R_1}\right)^3 + \frac{2\left(\varepsilon_1^* - \varepsilon_2^*\right)}{\left(\varepsilon_1^* + 2\varepsilon_2^*\right)}}{\left(\frac{R_2}{R_1}\right)^3 - \frac{\varepsilon_1^* - \varepsilon_2^*}{\left(\varepsilon_1^* + 2\varepsilon_2^*\right)}} \tag{4.1}$$

$$= S\left(\varepsilon_1^*, \varepsilon_2^*, R_1, R_2\right) \tag{4.2}$$

where the function S is defined as

$$S(a,b,c,d) = b\frac{\left(\frac{d}{c}\right)^3 + \frac{2(a-b)}{(a+2b)}}{\left(\frac{d}{c}\right)^3 - \frac{(a-b)}{(a+2b)}}. \tag{4.3}$$

This effective shell completely describes the frequency dependent dielectric properties of the first sphere within the second. The process can be repeated as shown in Figure 4.1c by considering the first effective shell with a complex permittivity of ε_{1eff}^*, surrounded by the next shell (3) with a complex permittivity of ε_3^*. We can replace the inner-most effective shell with an effective shell of complex permittivity

$$\varepsilon_{2eff}^* = \varepsilon_3^* \frac{\left(\frac{R_3}{R_2}\right)^3 + \frac{2\left(\varepsilon_{1eff}^* - \varepsilon_3^*\right)}{\left(\varepsilon_{1eff}^* + 2\varepsilon_3^*\right)}}{\left(\frac{R_3}{R_2}\right)^3 - \frac{\varepsilon_{1eff}^* - \varepsilon_3^*}{\left(\varepsilon_{1eff}^* + 2\varepsilon_3^*\right)}} \tag{4.4}$$

$$= S\left(\varepsilon_{1eff}^*, \varepsilon_3^*, R_2, R_3\right) \tag{4.5}$$

$$= S(S\left(\varepsilon_1^*, \varepsilon_2^*, R_1, R_2\right), \varepsilon_3^*, R_2, R_3). \tag{4.6}$$

By continuing this process of replacing the inner spheres by effective shells, eventually the outer shell will be reached at which point the shell-spheres will have been reduced to an equivalent *smeared out sphere*, as shown in Figure 4.1e, whose effective permittivity is given by

$$\varepsilon^*_{peff} = \varepsilon^*_{Neff} = \varepsilon^*_{N+1} \frac{\left[\left(\frac{R_{N+1}}{R_N}\right)^3 + 2f\left(\varepsilon^*_{N-1eff}, \varepsilon^*_{N+1}\right)\right]}{\left(\frac{R_{N+1}}{R_N}\right)^3 - f\left(\varepsilon^*_{N-1eff}, \varepsilon^*_{N+1}\right)} \tag{4.7}$$

$$= S\left(\varepsilon^*_{N-1eff}, \varepsilon^*_{N+1}, R_N, R_{N+1}\right) \tag{4.8}$$

$$= S\left(S\left(\varepsilon^*_{N-2eff}, \varepsilon^*_N, R_{N-1}, R_N\right), \varepsilon^*_{N+1}, R_N, R_{N+1}\right) \tag{4.9}$$

$$= S\left(S\left(S\left(...S\left(\varepsilon^*_1, \varepsilon^*_2, R_1, R_2\right)..\right), \varepsilon^*_N, R_{N-1}, R_N\right), \varepsilon^*_{N+1}, R_N, R_{N+1}\right) \tag{4.10}$$

where $f(a,b)$, defined as $(a-b)/(a+2b)$, is the Clausius-Mossotti factor of Equation (3.37), ε^*_{N+1} is the complex permittivity of the outer-most shell and ε^*_{N-1eff} represents the effective complex permittivity of the inner-most N spheres after they have been 'smeared' together.

By inserting Equation (4.10) into Equations (3.34), (3.42) and (3.65), it is theoretically possible to calculate the electrorotation frequency spectra of a spherical particle with any number of shells. Ermolina *et al.* (2000) performed an analysis of the model and determined that the dielectric parameters of the exterior cell structures influence the low-frequency part of the electrorotational spectrum, and the parameters of the interior structures affect the high frequency region.

4.3 Ellipsoidal Dielectric Multi-Shell Model

The two-shell model has been well tested for both spherical and ellipsoidal cells possessing a wall and membrane (Irimajiri *et al.,* 1979; Asami *et al.,* 1980; Huang *et al.,* 1992; Kakutani *et al.,* 1993; Zhou *et al.,*1996) (Figure 4.2).

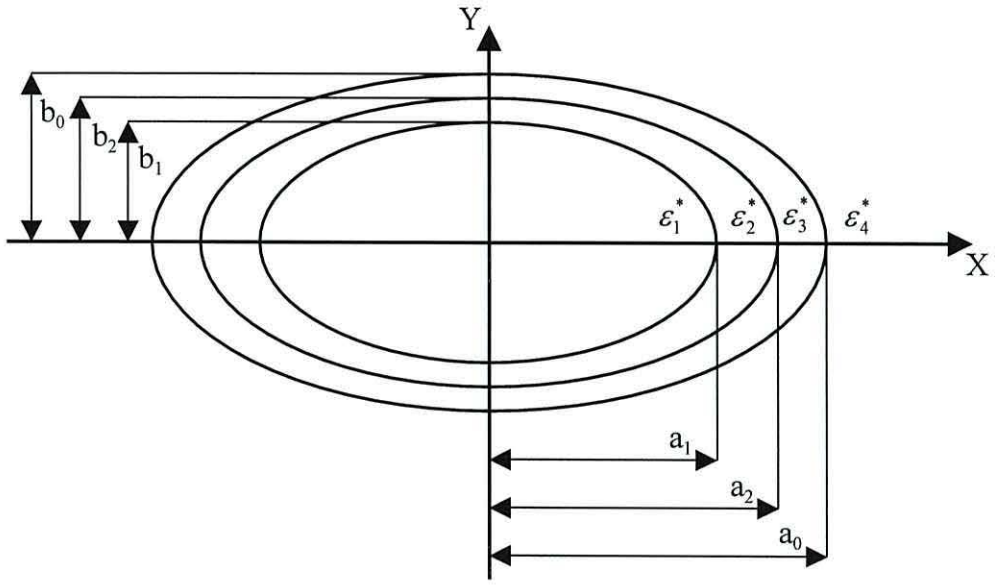

Figure 4.2 – Cross-section of an ellipsoidal two-shell model representing a simple cell (e.g. yeast) in the x-y plane. $\varepsilon_4^*, \varepsilon_3^*, \varepsilon_2^*$ and ε_1^* represent the complex permitivitties of the suspending medium, cell wall, cytoplasmic membrane and cell interior, respectively.

The complex AC permittivity of the suspending medium, the cell wall, the cytoplasmic membrane and the interior of the cell are represented by ε_4^*, ε_3^*, $\varepsilon_2^*$and ε_1^* respectively. They are determined by

$$\varepsilon_i^* = \varepsilon_i - j\frac{\sigma_i}{\omega} \tag{4.11}$$

where ε_i and σ_i are the relative permittivity and conductivity, respectively, of the i^{th} phase (i=1,2,3 and 4). The surfaces of the shells are represented by three confocal ellipsoids and an ellipsoidal co-ordinate system is introduced by assuming the outermost surfaces of the shelled ellipsoid to be a standard ellipsoid with semi-axis a_0, b_0 and c_0 (Kakutani *et al.* 1993), where

$$\frac{x^2}{a_0^2+\xi}+\frac{y^2}{b_o^2+\xi}+\frac{z^2}{c_0^2+\xi}=1 \tag{4.12}$$

where ξ is a parameter representing a family of surfaces of confocal ellipsoids. When $\xi=0$ and $\xi=-\delta_i$, equation (4.12) represents the outermost and i^{th} surfaces respectively of the shelled ellipsoid (Asami *et al.,* 1980; Kakutani *et al.,* 1993). The semi-axis a_i, b_i and c_i of the i^{th} surface are given by

$$a_i=\left(a_o^2-\delta_i\right)^{\frac{1}{2}} \qquad b_i=\left(b_o^2-\delta_i\right)^{\frac{1}{2}} \qquad c_i=\left(c_o^2-\delta_i\right)^{\frac{1}{2}} \tag{4.13}$$

A cell, such as yeast, can be considered as a homogeneous ellipsoid surrounded by a cytoplasmic membrane and a cell wall. For such a particle in an imposed electric field E of angular frequency ω, the electrorotation torque $\Gamma(\omega)$ is given by (Kakutani *et al.* 1993)

$$\Gamma(\omega)=0.5v_c\varepsilon_m\,\mathrm{Im}[\chi_\alpha(\omega)]E^2(\alpha=x,y) \tag{4.14}$$

where V_c is the volume of the ellipsoid given by

$$V_c=\frac{4\pi a_0 b_0 c_0}{3} \tag{4.15}$$

and $\chi_\alpha(\omega)(\alpha=x,y)$ is given by

$$\chi_\alpha(\omega)=\frac{\varepsilon_{effp}^*-\varepsilon_4^*}{\left(\varepsilon_{effp}^*-\varepsilon_4^*\right)A_{0\alpha}+\varepsilon_4^*}(\alpha=x,y) \tag{4.16}$$

where ε_4^* is the complex permittivity of the suspending medium and $A_{i\alpha}(i=0,1,2;\alpha=x,y)$ is the depolarising factor along the x and y axis given by

$$A_{ix}=0.5a_ib_ic_i\int_0^\infty\frac{d\xi}{(a_i+\xi)R_i} \tag{4.17}$$

$$A_{iy} = 0.5 a_i b_i c_i \int_0^{\infty} \frac{d\xi}{(b_i + \xi) R_i} \tag{4.18}$$

with

$$R_i = \left[\left(a_i^2 + \xi\right)\left(b_i^2 + \xi\right)\left(c_i^2 + \xi\right) \right]^{\frac{1}{2}} (i = 0,1,2). \tag{4.19}$$

ε^*_{effp} is the effective complex permittivity of the two-shelled ellipsoid along the $\alpha(\alpha = x, y)$axes, and is given by

$$\varepsilon^*_{effp} = \varepsilon^*_3 \frac{\varepsilon^*_3 + \left(\varepsilon^*_{ieff} - \varepsilon^*_3\right)\left[A_{1\alpha} + \upsilon_1\left(1 - A_{0\alpha}\right)\right]}{\varepsilon^*_3 + \left(\varepsilon^*_{ieff} - \varepsilon^*_3\right)\left(A_{1\alpha} - \upsilon_1 A_{0\alpha}\right)} \tag{4.20}$$

where ε^*_{ieff} represents the effective complex permittivity of the innermost ellipsoids after they have been *smeared* together and is given by

$$\varepsilon^*_{ieff} = \varepsilon^*_2 \frac{\varepsilon^*_2 + \left(\varepsilon^*_1 - \varepsilon^*_2\right)\left[A_{2\alpha} + \upsilon_2\left(1 - A_{1\alpha}\right)\right]}{\varepsilon^*_2 + \left(\varepsilon^*_1 - \varepsilon^*_2\right)\left(A_{2\alpha} - \upsilon_1 A_{2\alpha}\right)} \tag{4.21}$$

with

$$\upsilon_j = \frac{a_j b_j c_j}{a_{j-1} b_{j-1} c_{j-1}} (j = 1,2) \tag{4.22}$$

where the subscripts 1, 2 and 3 represent the internal phase, cytoplasmic membrane and the wall of the biological cell, respectively.

4.4 Limitations of Model

Gascoyne *et al.* (1995) performed a numerical analysis of the three-shell model and highlighted several important limitations. The shell model assumes that the dielectric surfaces are smooth and perfectly concentric. A biological surface, such as the cytoplasmic membrane, has a complicated, folded structure and will therefore have a larger surface area than is assumed by the idealised model. It is unclear to what extent such deviations from an ideal smooth surface may affect the shape of the electrorotation spectra, although Gascoyne *et al.* suggest a broadening of the anti-field peak (β-dispersion) could result. To minimise the effects of cell ionic leakage during the course of an electrorotation experiment, Gascoyne *et al.* stated that the electrorotational spectrum should be measured from the high-frequency end downwards. Gascoyne *et al.* also stated that to determine the interior parameters of the particle accurately, the frequency spectrum should be taken to as high a value as possible, to encompass the co-field peak. Gascoyne *et al.* concluded that the model was limited for characterising particles of complex structure, but offered a reasonable approximation for simple particles.

Co-field electrorotation effects at frequencies typically below 1 kHz (α-dispersion) have been observed for latex beads (Wang *et al.,* 1993), artificial vesicles (Wicher and Gundel, 1989), yeast (Arnold and Zimmerman, 1989) and red blood cells (Georgieva *et al.,* 1998; Neu *et al,* 2002). The single-shell model does not predict such low-frequency co-field electrorotation. Grosse and Shilov (1996 and 1998) realised that in addition to the total torque acting on the particle together with its double layer, a motion of the outer part of the double layer relative to the particle can also cause rotation. This electroosmotic slip velocity theory of low frequency electrorotation was tested by Georgieva *et al.* (1998) and by Neu *et al.* (2002) and found to be consistent with experimental data.

The traditional isotropic dielectric single-shell model was further extended in the low frequency region to account for plasma membrane anisotropy by Sukhorukov *et al.* (2001). The anisotropy can be caused by the partition of hydrophobic ions into the membrane of the cell. Numerical calculations by Sukhorukov *et al.* demonstrated that

the tangential conductivity related to the lateral ion motion can introduce significant deviations from the conventional isotropic model in the low frequency region.

Chan *et al.* (1997) performed a series of reliability tests of the single- and multi-shell models using liposomes. Chan *et al.* reported that the single shell model provided close agreement between experiment and theory for unilamellar liposomes, and that the three-shell model provided a good theoretical description of the oligolamellar liposomes (two distinct compartments). Chan *et al.* also reported that decreasing confidence levels were found for the parameters with increasing model complexity, reflecting a deterioration of the conditioning of the solution system. This deterioration was attributed to the complex, recursive nature of the dielectric equations and Chan *et al.* concluded that increasing the complexity of models beyond 4 or 5 layers could lead to complete degeneracy among parameters in the solution set, and that the dielectric multi-shell model was a realistic model for relatively simple cells only.

4.5 Organisms modelled

Various *simple* organisms have been modelled using the multi-shell model (Table 4.1) and good correspondence with experimental data has been obtained.

T-Lymphocytes (white blood cells)	Becker *et al.*, 1995
Erythocytes (red blood cells)	Becker *et al.*, 1995; Gimsa and Wachner, 1998; Huang *et al.*, 1999
Yeast (viable and non-viable)	Huang *et al.*, 1992; Wang *et al.*, 1992; Zhou *et al.*, 1996, Talary *et al.*, 1996
Mammalian cell line DS19 (viable and non-viable)	Gascoyne *et al*, 1993, Wang *et al.*, 1994, Gascoyne *et al.*, 1994
Mammalian cell line R1 (viable and non-viable)	Gascoyne *et al.*, 1993 and 1994
Mammalian cell line (human lymphoid Jurkat)	Suckorukov *et al.*, 2001
Breast cancer cells (MDA 231)	Becker *et al.*, 1995
Liposomes	Chan *et al.*, 1997
Bacteria	Morgan *et al*, 1987; Holzel, 1999
Trophoblasts	Chan *et al.*, 2000

Table 4.1 – Some biological organisms investigated by electrorotation and modelled using the multi-shell model.

4.6 Modelling of a 2 shell Biological Organism

Electrorotation spectra of a biological organism were modelled here using a 2-shell model based on the simple structure of an unsporulated, spherical oocyst of *C. cayetanensis*as as described in Chapter 2. The physiological data used to model *C. cayetanensis* is given in Table 4.2, and was taken from the relevant literature. The suspending medium conductivity was assumed to be 1.0 mS/m and the relative permittivity to be 79 (Huang *et al.,* 1992).

	Conductivity (Sm^{-1})	
	Viable	**Non-viable**
Cytoplasm	0.5[a]	0.1[a]
Cell Membrane	$1\ e^{-6}$[a]	$1\ e^{-4}$[a]
Cell Wall	0.025[b]	0.025[b]
	Relative Permittivity	
Cytoplasm	50[c]	50[c]
Cell Membrane	6[d]	6[d]
Cell Wall	60[c]	60[c]

References : *a* – Goater, 1999; *b* - Talary *et al.,* 1996; *c* – Huang *et al.,* 1992 and *d* – Pethig *et al.*, 1995

Table 4.2 – Physiological values used to model oocysts of *Cyclospora cayetanensis.*

All *C. cayetanensis* modelling was carried out using the spherical two-shell model in MatLab (MathWorks Ltd, UK). An initial simulation using the values listed in Table 4.2 bears a close resemblance to preliminary experimental electrorotation spectra of 4 morphologically identical unsporulated oocysts of *C. cayetanensis* (Figures 4.3 and 4.4).

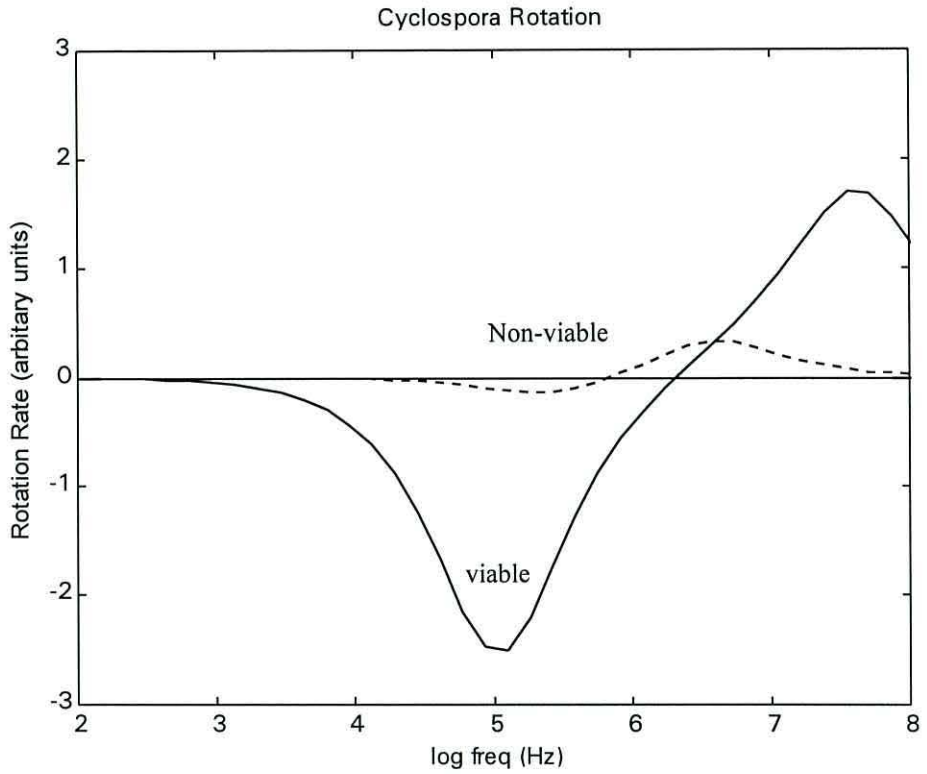

Figure 4.3 – Viable (solid line) and non-viable (dashed line) MatLab simulation of the electrorotational response of unsporulated oocysts of *C. cayetanensis* based on the physiological values given in Table 4.2.

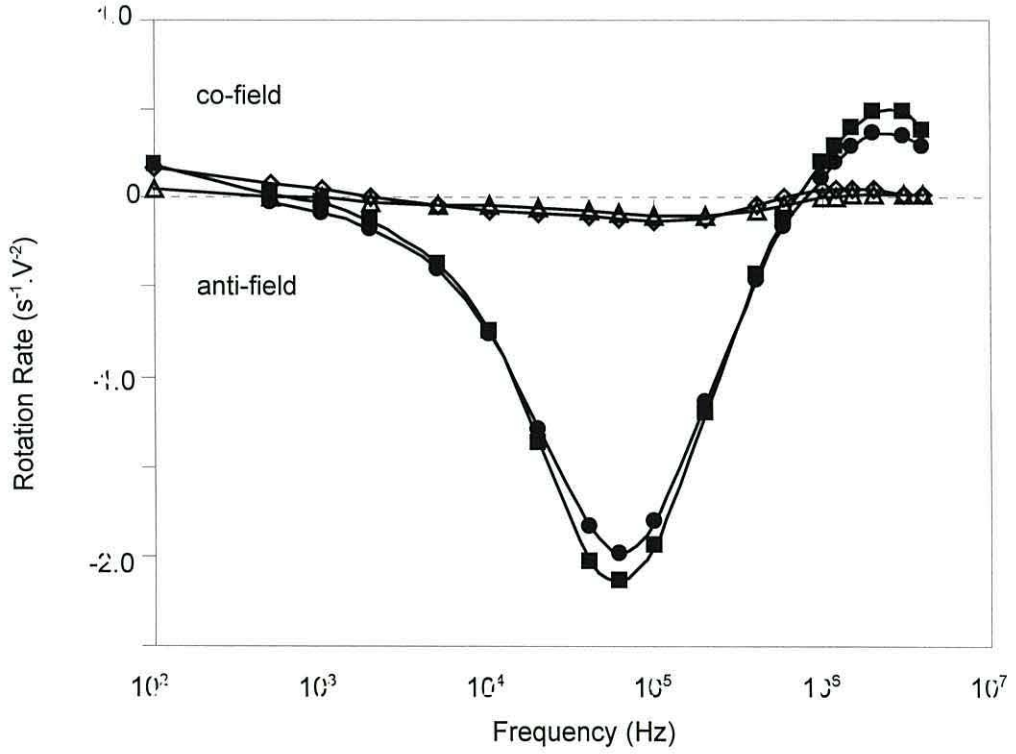

Figure 4.4 – Rotation spectra of 4 unsporulated oocysts showing the difference between viable (■, ●) and putative non-viable (Δ, ◊) oocysts. (conductivity 0.6 mS/m).

It is not possible to distinguish morphologically between viable and non-viable *C. cayetanensis* oocysts. The membrane of a viable oocyst is selectively-permeable to ions and non-lipid, soluble molecules, so the internal composition of the cell is quite different from the exterior medium. Upon cell death, membrane integrity is lost, and the cell freely exchanges material with the external suspending medium. As a result, fewer induced charge differences occur between the inside of the oocyst and the exterior medium, and this greatly affects the rotation spectra produced. The difference in the magnitude of rotation rate (Figure 4.4) between oocysts designated viable and non-viable is similar to that reported by Goater *et al.,* (1997) for *Cryptosporidium parvum*, a coccidian pathogen with a similar structure to *C. cayetanensis*. Goater confirmed that this observation was due to differences in oocyst viability by a fluorogenic vital dye assay (Goater, 1999). The viability of *C. cayetanensis* oocysts cannot be independently verified by such methods as none have yet been developed. The close correlation between the modelled viable and non-viable oocysts and the experimental data is a good indication that the model is reliable for simulating *C. cayetanensis* oocysts.

The effects on the simulated *C. cayetanensis* oocyst electrorotation spectra of changing model parameters is shown in Figures 4.5 to 4.12 These simulated spectra will be used later (Chapters 6 and 7) to indicate what may be causing the effects observed in experimental spectra.

4.6.1 Effect of Changing Suspending Medium Conductivity

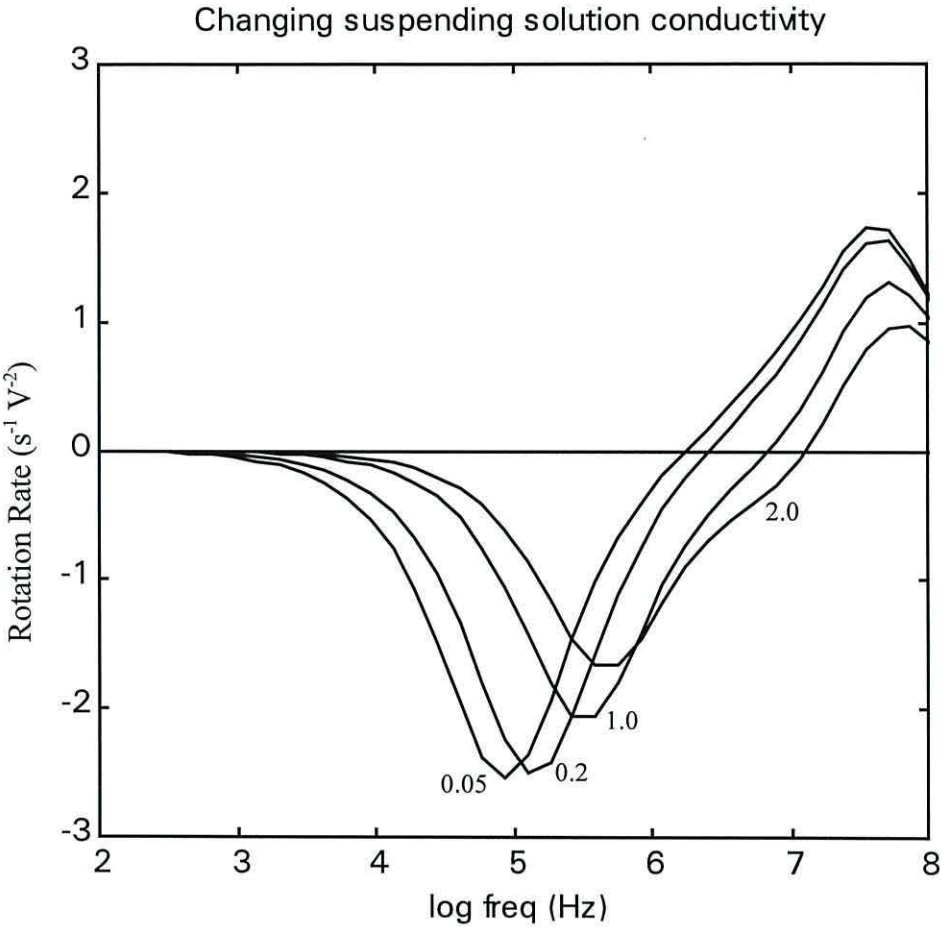

Figure 4.5 – Effect on a model viable, unsporulated *C. cayetanensis* oocyst rotation spectra of changing the conductivity of the suspending solution from 0.05 to 2.0 mS/m.

Figure 4.5 shows that increasing the conductivity of the suspending solution will increase the anti-field peak rotation frequency, decrease the anti-field peak rotation rate, increase the high frequency cross-over point and decrease the co-field peak rotation rate. The model assumes a constant wall conductivity, which for walled particles such as yeast cells (Markx *et al.,* 1995) has been shown to vary with suspending medium conductivity. Carstensen *et al.* (1965) suggested that at low suspending medium conductivities the conductivity of the wall has a lower limit determined by counterions of the fixed charge of the cell wall, whereas for higher conductivities, ions from the medium invade the cell wall causing an increase in its conductivity so that it takes on values roughly proportional to that of the suspending medium. As most of the work described is performed in low suspending medium conductivities, an assumption was made that the wall conductivity would be a constant near to its lower limit, and that the model was valid.

4.6.2 Effect of Changing Membrane Conductivity

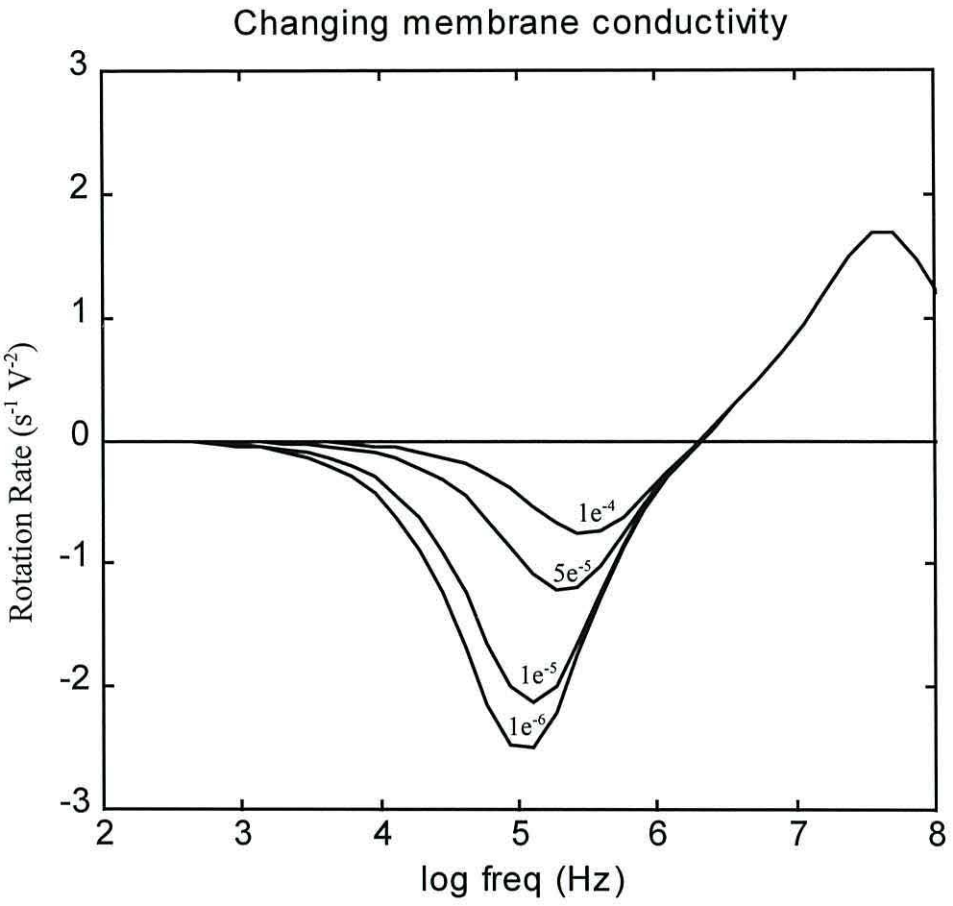

Figure 4.6 - Effect on a model, viable, unsporulated *C. cayetanensis* oocyst rotation spectra due to changing the conductivity of the membrane from $1x10^{-6}$ to $1x10^{-4}$ S/m.

Figure 4.6 shows that as the membrane conductivity increases, a large reduction in the anti-field rotation rate is seen. As a *C. cayetanensis* oocyst undergoes sporulation, a reorganisation of the interior occurs, with the membrane bound cytoplasm becoming two membrane bound sporocysts, each containing sporozoites that possess their own organised contents and membranes. Thus the membrane dielectric properties will be very different between unsporulated and sporulated oocysts, and the model predicts that the unsporulated oocysts should have a greater anti-field peak rotation rate compared to the sporulated oocysts.

4.6.3 Effect of Changing Wall Conductivity

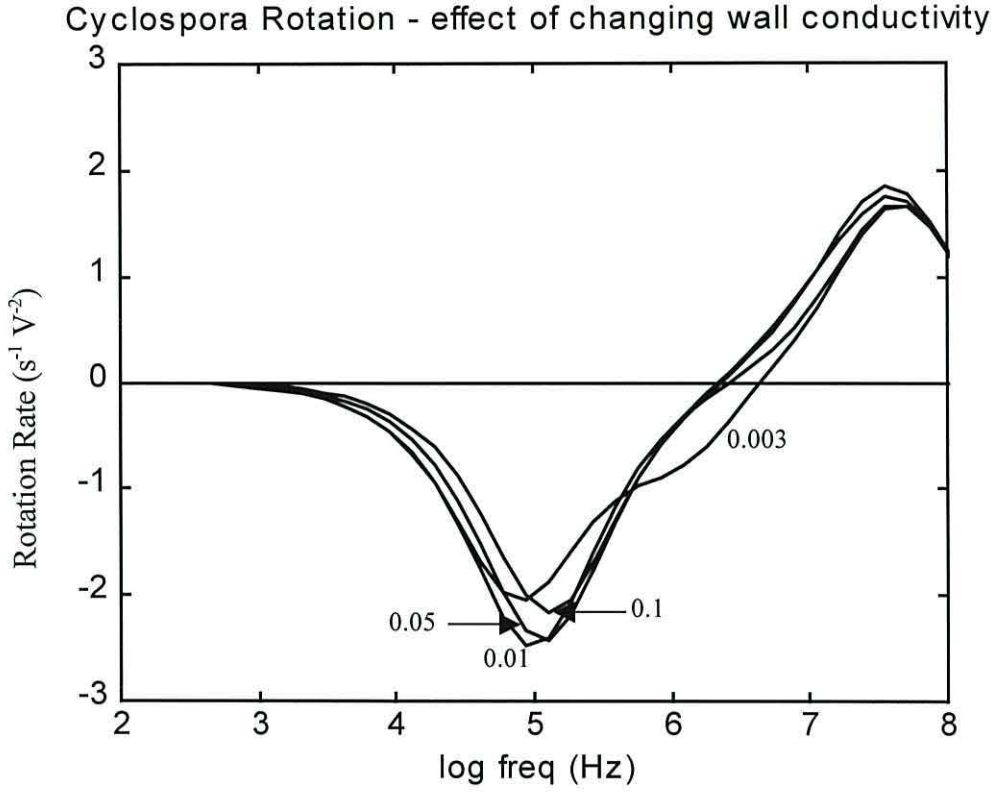

Figure 4.7 – Effect on a model viable, unsporulated *C. cayetanensis* oocyst rotation spectra due to changing the wall conductivity from 0.1 to 0.003 S/m.

Figure 4.7 shows the effect on the model of changing the conductivity of the oocyst wall. In comparison with other factors, changing the cell wall conductivity has little effect on the electrorotation spectra.

4.6.4 Effects of Changing the Interior Conductivity

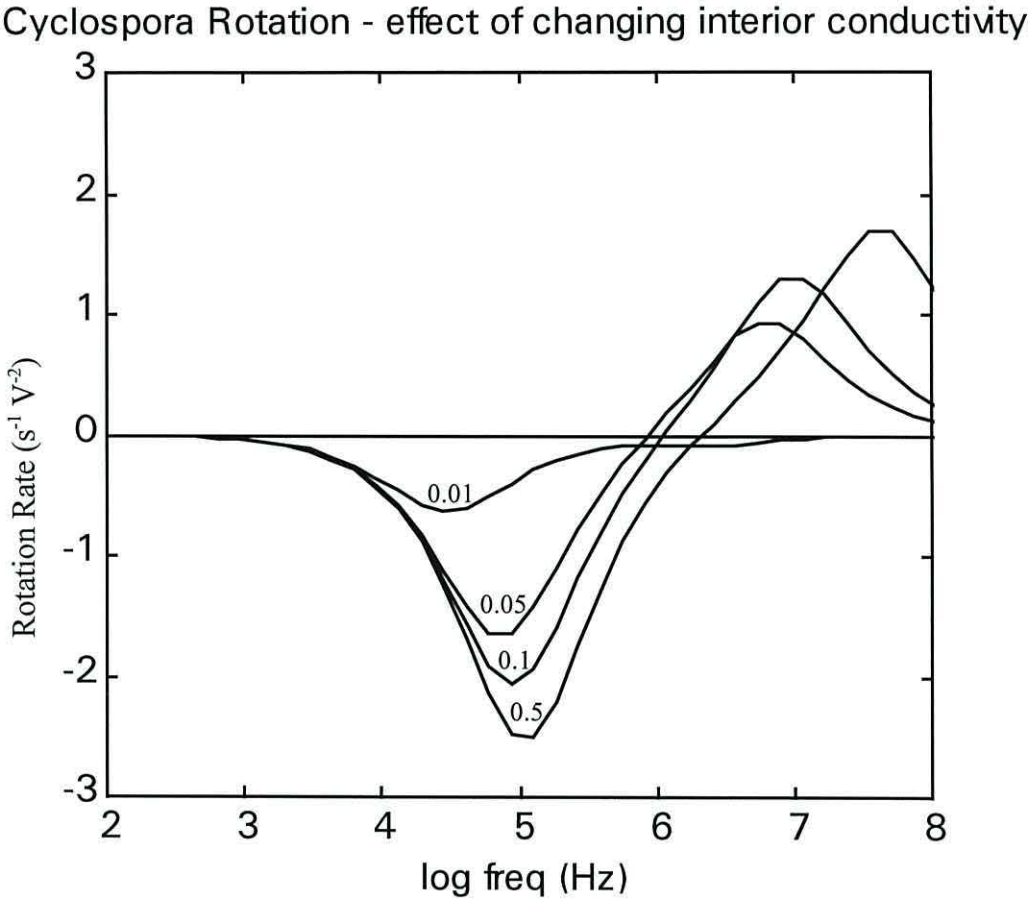

Figure 4.8 – Effect on a model viable, unsporulated *C. cayetanensis* oocyst rotation spectra due to changing the interior conductivity from 0.5 to 0.01 S/m.

Figure 4.8 shows the effect on the model of changing the interior conductivity of the oocyst. As the interior conductivity decreases, the anti-field rotation rate greatly reduces and the peak rotation frequency shifts from 100 kHz to about 20 kHz. In a viable oocyst, the interior conductivity is high compared to the suspending medium due to the high concentration of salts present. When an oocyst becomes non-viable, membrane integrity is lost, and the oocyst freely exchanges material with the external suspending medium, lowering the interior conductivity. The model predicts that the interior conductivity of an oocyst is a major factor influencing the difference between the spectra of viable and non-viable organisms.

4.6.5 Effect of Changing the Interior Permittivity

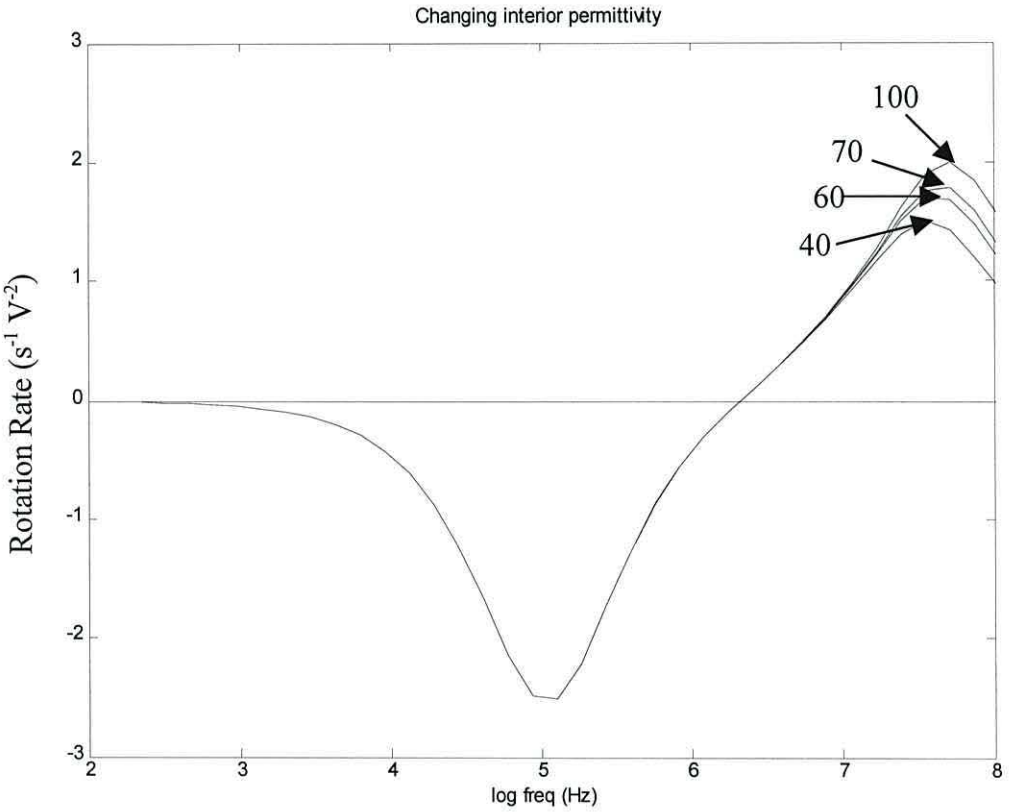

Figure 4.9 – Effect on a model viable, unsporulated *C. cayetanensis* oocyst rotation spectra due to changing the interior permittivity from 40 to 100.

Figure 4.9 shows the effect on the model of changing the relative permittivity of the oocyst interior. As the interior permittivity decreases, so does the co-field peak rotation rate. There is no effect on the anti-field peak rotation rate. In comparison with other factors, changing the interior cell permittivity has little effect on the electrorotation spectra.

4.6.6 Effect of Changing the Wall Permittivity

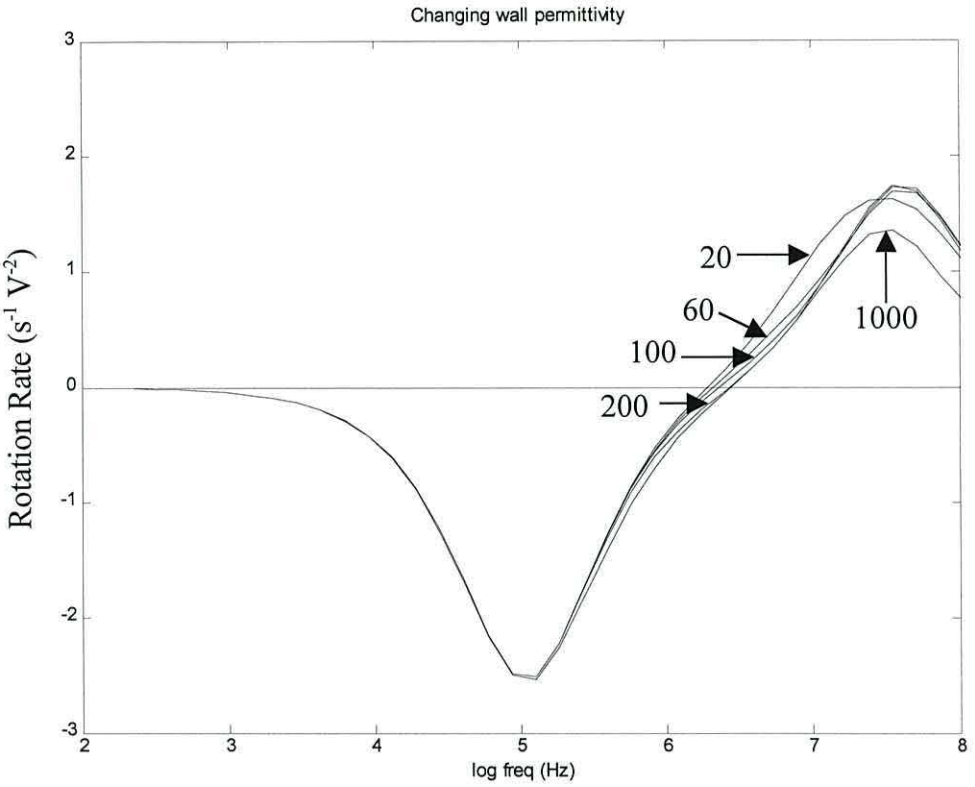

Figure 4.10 – Effect on a model viable, unsporulated *C. cayetanensis* oocyst rotation spectra due to changing the wall relative permittivity from 20 to 1000.

Figure 4.10 shows the effect on the model of changing the relative permittivity of the oocyst wall. In general, as the wall permittivity decreases, the co-field peak rotation rate increases. There is little effect on the anti-field peak rotation rate. Significant increases in the wall permittivity are necessary to effect even a small increase in the cross-over frequency.

4.6.7 Effect of Changing the Membrane Permittivity

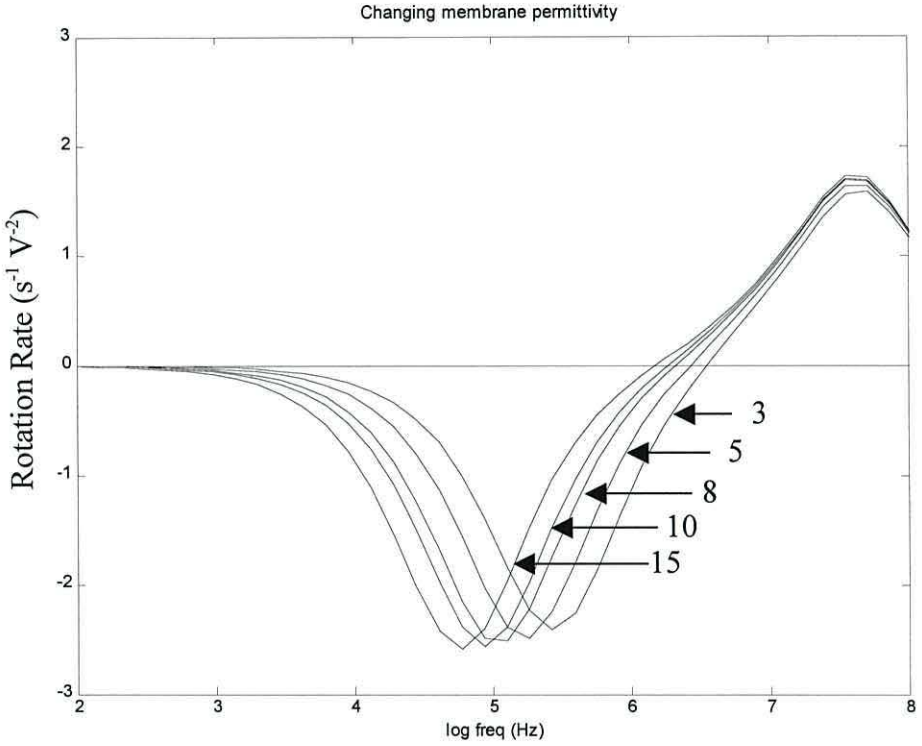

Figure 4.11 – Effect on a model viable, unsporulated *C. cayetanensis* oocyst rotation spectra due to changing the membrane relative permittivity from 3 to 15.

Figure 4.11 shows the effect on the model of changing the relative permittivity of the oocyst membrane. As the permittivity of the membrane increases, the anti-field peak rotation frequency decreases. There is also a slight increase in the rate of rotation at the peak rotation frequency. The cross-over frequency also decreases with an increase in the membrane permittivity. There is little effect upon the co-field peak rotation rate or frequency.

4.6.8 Effect of Changing the Suspending Medium Permittivity

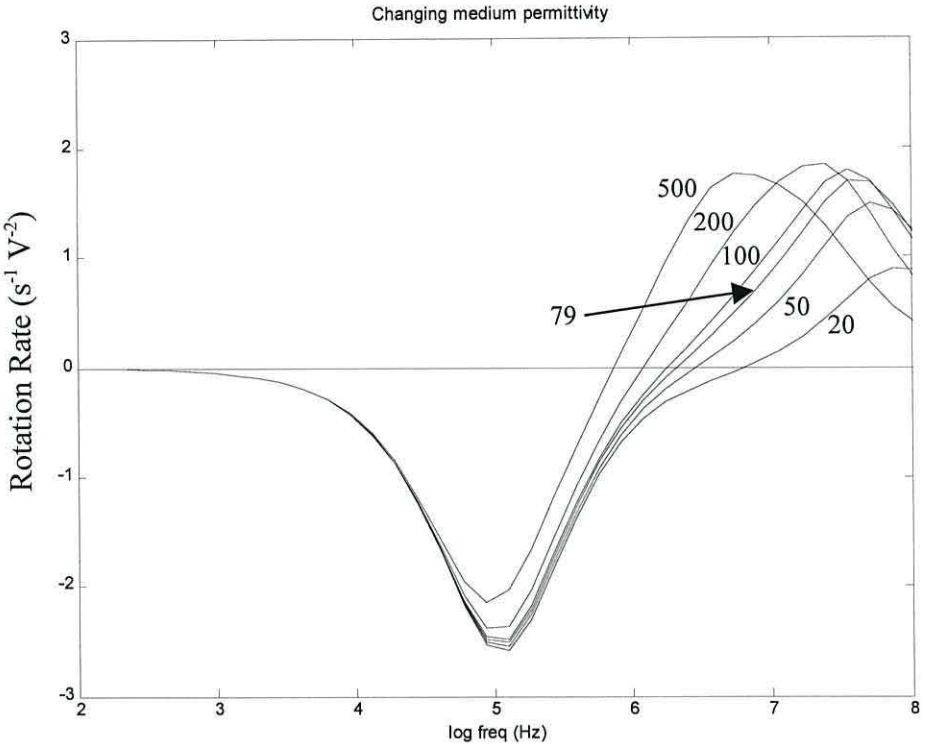

Figure 4.12 – Effect on a model viable, unsporulated *C. cayetanensis* oocyst rotation spectra due to changing the medium relative permittivity from 20 to 500. A value of 79 is typical for the suspending solutions used in this work.

Figure 4.12 shows the effect on the model of changing the relative permittivity of the suspending medium. As the permittivity of the medium decreases, the co-field peak rotation frequency increases, the co-field peak rotation rate decreases and the cross-over frequency increases.

4.6.9 Summary of Modelling Changes

These simulations show the type of differences that could appear in the rotation spectra for oocysts of *Cyclospora cayetanensis* due to changes in the oocysts' physiological and morphological state. By observing the changes in actual spectra it is hoped that a better understanding of the processes occurring within the oocysts can be obtained.

The changes in the model parameters shown in this chapter can also be used to explain effects observed in the spectra of *Ascaris suum* eggs.

4.7 Other Models

There are other methods to model a biological particle subjected to a rotating electric field, and some a briefly described here.

4.7.1 Resistor-Capacitor Model

Gimsa and Wachner first proposed a resistor-capacitor model for the structural polarisations for homogeneous and single-shell spheroids with the symmetry axis orientated perpendicular to the field (Gimsa and Wachner, 1998). All geometrical constituents were described by parallel circuits of a capacitor and resistor. Model predictions were consistent with experiments on human red blood cells. The model assumes that the disturbance of the external field due to polarisation may project into the medium to a characteristic distance, the 'influential radius'. This parameter is related to the axis ratio of the spheroid and allows the geometry for a finite resistor-capacitor model to be determined. From the model, the potential at the spheroids surface is obtained, and the local field inside a homogeneous spheroid is determined. In the single shell case, this is the dependent induced dipole moment. This approach allowed Gimsa and Wachner to develop simple equations for homogeneous and single-shell spheroids, which they expanded in 1999 to include both oblate and prolate

homogeneous spheroids (Gimsa and Wachner, 1999). The model has been further expanded by Gimsa for ellipsoidal cells (Gimsa, 2001).

The single shell RC model is shown in Figure 4.13.

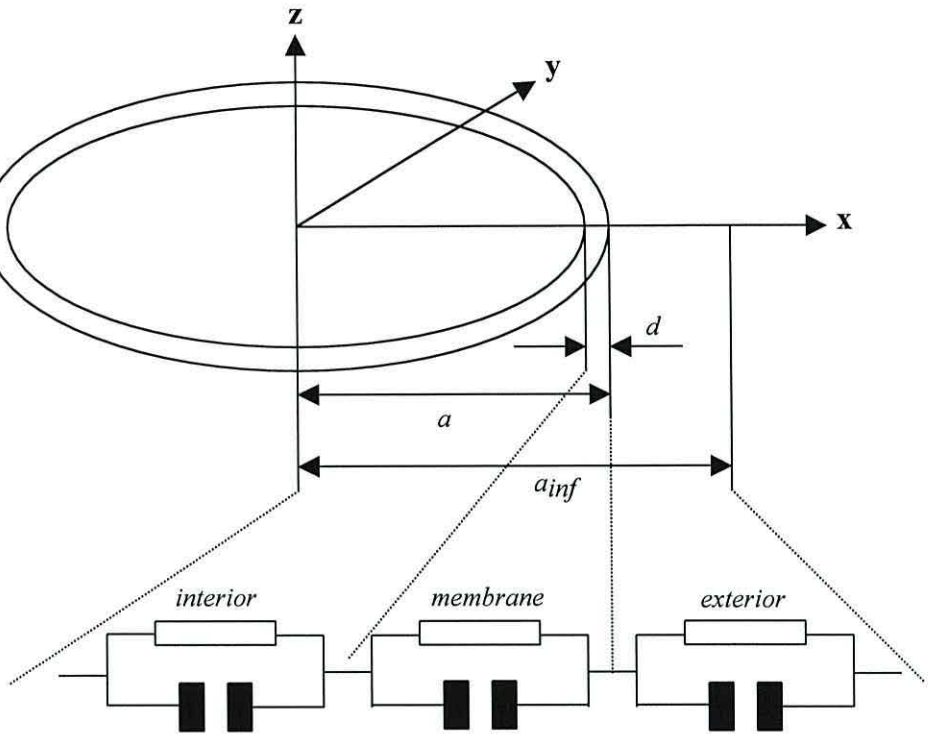

Figure 4.13 – Single shell model of general ellipsoidal shape with constant shell (membrane) thickness *d*. The principal axes *a*, *b* and *c* are orientated in the *x*, *y* and *z* directions, respectively. a_{inf} is the influential radius along axis *a*. The equivalent resistor-capacitor model is shown (Gimsa, 2001).

The RC model has been shown to be consistent with simple biological organisms such as red blood cells (Gimsa, 2001). However, Gimsa states that a much more complicated problem is the extension of the model to multi-shell objects with additional structural (interfacial) dispersions, since for the internal structures an influential radius cannot easily be defined. Such investigations are underway (Gimsa, 2001), but so far have not been published.

4.7.2 Spectral Representation

Recently, Huang and Yu (2002) have proposed a model based on the use of spectral representation for analysing the electrorotation spectra of particle in suspensions. The spectral representation is a rigorous mathematical formalism for the effective dielectric constant of a two-phase composite material (Bergman, 1978). It offers the advantage of the separation of material parameters (namely the dielectric constant and conductivity) from the cell structure information. Huang and Yu compared their theoretical calculations for a simple spheroid system to results obtained by Burt *et al.* (1996) for anti-body coated latex beads, and stated they had good agreement. Huang and Yu concluded that their spectral representation model could easily be extended to a multi-shell model. However, they then state that '*we believe that the multi-shell nature of a cell may have only minor effect on the electrorotation spectrum*'. It has been shown experimentally (Goater, 1999) and theoretically (Gascoyne *et al.,* 1995; Chan *et al.,* 1997), that the electrorotation spectrum is greatly affected by more complex biological organisms (with more shells and interfacial polarisation mechanisms), and casts doubt on the validity of the spectral representation model for anything other than a simple particle.

4.8 Conclusions

As the organisms that are being investigated, *Cyclospora cayetanensis* and *Ascaris suum*, are complex, having several layers (shells), the established multi-shell model was used in this work. The advantages and limitations of this modeling method have been described in this Chapter. In Chapters 6 and 7, the best fits of the spherical and ellipsoidal multi-shell models are made to the experimental data obtained for *C. cayetanensis* oocysts and *A. suum* eggs, respectively.

4.9 References

Arnold, W. M. and Zimmerman, U. **(1989)** *Proc. 1st Int. Conf. On Low Cost Experiments on Biophysics,* Cairo University, UNESCO

Asami, K., Hanai, T. and Koizumi, N. **(1980)** Dielectic approach to suspensions of ellipsoidal particles covered with a shell in particular reference to biological cells. *Jap. J. Appl. Phys.* **19** 359-365

Becker, F. F., Wang, X. B., Huang, Y., Pethig, R., Vykoukal, J. and Gascoyne, P. R. C. **(1995)** *Proc. Natl. Acad. Sci. USA* **92** 860-864

Bergman, D. J. **(1978)** *Phys. Rep.* **43** 379

Burt, J. P. H., Chan, K. L., Dawson, D., Parton, A. and Pethig, R. **(1996)** *Ann. Biol. Clin.* **54** 253

Carstensen, E. L., Cox Jr., H. A., Mercer, W. B. and Natale,L. A. **(1965)** *Biophys. J.* **5** 289-300

Chan, K. L., Gascoyne, P. R. C., Becker, F. F. & Pethig, R. **(1997)** Electrorotation of liposomes: verification of dielectric multi-shell model for cells. *Biochim. Biophys. Acta-Lipids and Lipid metabolism.* **1349** 182-196.

Chan, K. L., Morgan, H., Morgan, E., Cameron, I. T. and Thomas,M. R. **(2000)** Measurements of the dielectric properties of peripheral blood mononuclear cells and trophoblast cells using AC electrokinetic techniques. *Biochim. Biophys. Acta.* **1500** 313-322

Ermoline, I., Polevaya, Y. and Feldan, Y. **(2000)** Analysis of dielectric spectra of eukaryotic cells by computer modelling. *Eur. Biophys. J.**29** 141-145*

Fricke, H. **(1924)** A mathematical treatment of the electric conductivity and capacity of disperse systems. *Phys. Rev.* **24** 575-87

Fuhr, G. and Kuzmin, P. I. **(1986)** Behaviour of cells in rotating electric fields with account to surface charges and cell structures. *Biophys. J.* **50** 789-794

Gascoyne, P. R. C., Pethig, R., Burt, J. P. H. and Becker, F. F. **(1993)** *Biochim. Biophys. Acta.* **1149** 119-126

Gascoyne, P. R. C., Noshari, J. Becker, F. F. and Pethig, R. **(1994)** Use of dielectrophoretic collection spectra for characterising differences between normal and cancerous cells. *IEEE Trans. Industry. Appl.* **30(4)** 829-834

Gascoyne, P. R. C., Becker, F. F. and Wang, X-B. **(1995)** Numerical analysis of the influence of experimental condtions on the accuracy of the dielectric parameters derived from electrorotation measurements. *Bioelectrochem. Bioenerg.* **36** 115-125

Georgieva, R., Neu, B., Shilov, V. M., Knippel, E., Budde, A., Latza, R., Donath, E., Kiessewetter, H. and Bäumler, H. **(1998)** Low Frequency Electrorotation of fixed Red Blood Cells. *Biophys. J.* **74** 2114-2120

Gimsa, J. and Wachner, D. **(1998)** A unified RC model for impedance, Dielectrophoresis, electrorotation and induced transmembrane potential. *Biophys. J.* **75** 1107-1116

Gimsa, J. and Wachner, D. **(1999)** A Polarisation model overcoming the geometric restrictions of the Laplace solution for speroidal cells : Obtaining new equations for field-induced forces and transmembrane potential. *Biophys. J.* **77** 1316-1326

Gimsa, J. **(2001)** A comprehensive approach to electro-orientation, electrodeformation, Dielectrophoresis and electrorotation of ellipsoidal particles and biological cells. *Bioelectrochem.* **54** 23-31

Goater, A. D., Burt, J. P. H. and Pethig, R. **(1997)** A combined electrorotation and travelling wave device: applied to the concentration and viability of *Cryptosporidium. Journal of Physics D-Applied Physics.* **33:** L65-L70.

Goater, A. D. **(1999)** A.C. Electrokinetic Bioassays. Development of Electrorotation Assay for Analyets in Water. *Ph.D. Thesis,* University of Wales.

Grosse, C. and Shilov, V. N. (**1996)** Theory of the low frequency electrorotation of polystyrene particles in electrolyte solution. *J. Phys. Chem.* **100** 1771-1778

Grosse, C. and Shilov, V. N. **(1998)** Theory of the low frequency electrorotation of disperse particles in electrolyte solution. *Colloid and Surfaces A : Physiochemical and Engineering Aspects* **140** 199-207

Hanai, T. **(1960)** Theory of the dielectric dispersion due to the interfacial polarisation and its appliation to emulsion. *Kolloid Z.* **171** 23-31

Höber, R. (**1913)** Messungen der inneren Leitfähigkeit von Zellen. *Pfl. Physiol. Archiv. Mensch. Tiere* **150** 15-45

Hölzel, R.**(1999)** Non-invasive determination of bacterial single cell properties by electrorotation. *Biochim. Biophys. Acta.* **1450** 53-60

Huang, Y., Hölzel, R., Pethig, R. and Wang, X.B. **(1992)** Differences in the ac electrodynamics of viable and non-viable yeast cells determined through combined dielectrophoresis and electrorotation studies. *Phys. Med. Biol.* **37(7)** 1499-1517

Huang, Y., Yang, J., Wang, X-B, Becker, F. F. and Gascoyne, P. R. C. **(1999)** The removal of human breast cancer cells from hematopoietic CD34(+) stem cells by dielectrophoretic field-flow-fractionation. *J. Hematother. Stem. Cell Res.* **8** 481-490

Huang, J. P. and Yu, K. W.**(2002)** First principles approach to electrorotation assay. *J. Phys. Condens. Matter* **14** 1213-1221

Irimajiri, A., Hanai, T. and Inouya, A. **(1979)** A dielectric theory of 'multi-stratified shell' model with its application to a lymphoma cell. *J. Theor. Biol.* 78 251-269

Kakutani, T., Shibatani, S. and Sugai, M. **(1993)** Electrorotation of non-spherical cells : theory for ellipsoidal cells with an arbitrary number of shells. *Bioelectrocehem. Bioenerg.* **31** 131-145

Markx, G. H., Zhou, X-F. and Pethig, R**. (1995)** Dielectrophoretic manipulation of micro-organisms in micro-electrode arrays. *Institute of Physics Conference Series* **143** 145-148

Maxwell, J. C. **(1892)** *A Treatise on Electricity and Magnetism,* 3rd ed., Vol. 1, Clarendon Press, Oxford.

Morgan, H., Green, N. G., Hughes, M. P., Monaghan, W. and Tan, T. C. (**1997)** Large-area travelling-wave dielectrophoresis particle separator. *Journal of Micromechanics and Microengineering.* **7** 65-70

Neu, B., Georgieva, R., Meiselman, H. J. and Baümler, H. **(2002)** Alpha- and beta-deispersion of fixed platlets : comparison with a structure-based theoretical approach. *Colloids and Surfaces A : Physiochem. Eng. Aspects.* **197** 27-35

Pethig, R. and Huang, Y. **(1995)** Dielectrophoretic and electrorotation behaviour of cells – Theory and experiment. *Bioelectrochem. Cell. Tissues 208-244*

Sukhorukov, V. L., Meedt, G., Kürschner, M. and Zimmermann, U. **(2001)** A single-shell model for biological cells extended to account for the dielectric anisotropy of the plasma membrane. *J. Electrostatics* **50** 191-204

Talary, M. S., Burt, J. P. H., Tame, J. A. & Pethig, R. **(1996)** Electromanipulation and separation of cells using travelling electric fields. *Journal of Physics D-Applied Physics.* **29** 2198-2203

Wagner, K. W. **(1914)** Erklarung der dielectrischen Nachwirkungsvorgange auf grund Maxwellsher Forstellungen. *Archiv. Electrotechnik* **2** 371-89

Wang, X.B., Huang, Y., Hölzel, R., Burt, J. and Pethig, R. **(1993)** Theoretical and experimental investigations of the interdependence of the dielectric, dielectrophoretic and electrorotational behaviour of colloid particles. *J. Phys. D: Appl. Phys.* **26** 312-322

Wang, X.B., Huang, Y., Gascoyne, P. R. C., Becker, F. F., Hölzel, R. and Pethig, R. **(1994)** *Biochim. Biophys. Acta.* **1193** 330-

Wicher, D. and Gundel, J. **(1989)** *Bioelectrochem. Bioenerg.* **21** 279-

Zhou, X-F, Markx, G. H., and Pethig, R. **(1996)** Effect of biocide concentration on electrorotation spectra of yeast cells. *Biochimice et Biophysica Acta – Biomembranes* **1281** 60-64

Chapter 5

Materials and Methods

5.1 *Cyclospora* spp.

Purified *Cyclospora cayetanensis* oocysts were supplied by the Scottish Parasite Diagnostic Laboratory (SPDL, Glasgow, UK). Samples were collected from infected humans in the Glasgow area who had recently travelled abroad (2 male, 1 female). One of the major challenges during purification is to separate the oocysts from debris in the sample, without simultaneously losing most of the relatively few oocysts present (Herwaldt, 2000). The samples were purified by a water-ether sedimentation protocol followed by a sucrose flotation method (Bukhari & Smith, 1995). Oocysts were then washed in deionised water and stored at 4°C in 2% potassium dichromate solution to prevent bacterial growth.

To obtain reproducible electrorotation data, oocysts were first washed and resuspended in a solution of well defined chemical composition and conductivity. To reduce electrical heating effects the magnitude of the rotating field was also kept as low as possible.

For this work, phosphate buffered saline (PBS, pH 7.4, 10 mM phosphate buffer, 27 mM KCl, 137 mM NaCl, Sigma Chemical Co.) solution adjusted to a conductivity of 1 mS m^{-1} was used as the suspending medium. At this conductivity, rotation rates were easily measurable at modest applied voltages in the frequency range 100 Hz to10 MHz. The washing procedure (repeated three times) consisted of diluting a 100 µl aliquot of oocyst suspension in ultra pure water (conductivity 0.1 mS m^{-1}) to 1.5 ml, vortexing for 30 seconds, microcentrifuging for 1 minute (3300 $\times g$) and then aspirating to 100 µl. After the final wash the sample was resuspended in PBS solution which had been diluted with ultra pure water to give a conductivity of 1 mS m^{-1}. The suspending medium conductivity was then checked by testing 200 µl of supernatant following centrifugation using a calibrated Hanna Instruments Pure

Water Tester™, modified to reduce the volume of the sample chamber. Working particle density concentrations were typically 5 x 10^3 oocysts ml^{-1}. All experiments were carried out at 19°C in an air conditioned, class 2 biological hazard laboratory.

5.2 *Ascaris* spp.

Adult female *Ascaris suum* roundworms were collected from the intestines of slaughtered pigs from a local abattoir (Cig Arfon, Caernarfon, Wales). The worms were stored in 5% formalin solution at 4°C. Fertilised and unfertilised eggs were collected from the female worms by dissection of the uterus, and stored in water at 4°C. The highly adhesive, debris coated glycosaminoglycan outer cortical layer was removed by adding an equal volume of 12% sodium hypochlorite to the suspension, and incubated at 37°C for 30 minutes. Following this process (known as decortication), the eggs were stored in ultra pure water at 4°C. Prior to electrorotation, the eggs were washed three times in ultra pure water and suspended in solutions of phosphate buffered saline (PBS). The PBS was diluted to a conductivity of 0.65 ±0.1 mS/m, to reduce electrical heating effects at the electrodes.

5.3 Electrode Design

A frequent practical problem with electrorotation is that the particle is seldom positioned in the exact centre of the electrode array. Also, groups of particles cannot all be in the exact centre of the array, so many potential spectra are lost, as the uniformity of the field cannot be guaranteed over the whole region of the electrode chamber. Different electrode geometries have been investigated theoretically in an attempt to overcome this problem (Hughes, 1998). For the present work an electrode geometry was chosen that provides a uniform field over the central region of the electrode chamber. The 'bone' electrode design is optimised for electrorotation by making the chamber enclosed by the electrode edges near circular in shape. The electrode shapes are described by the 4th order polynomial

$$y(x) = x^4 - 0.75x^2 + 1. \qquad (5.1)$$

The shape provides a near uniform electric field in the central region and reduces unwanted dielectrophoretic forces that the particle may experience. This is confirmed by an electric field analysis in the X-Y plane for the electrode system (Maxwell™, Ansoft) (Figure 5.1 a-d).

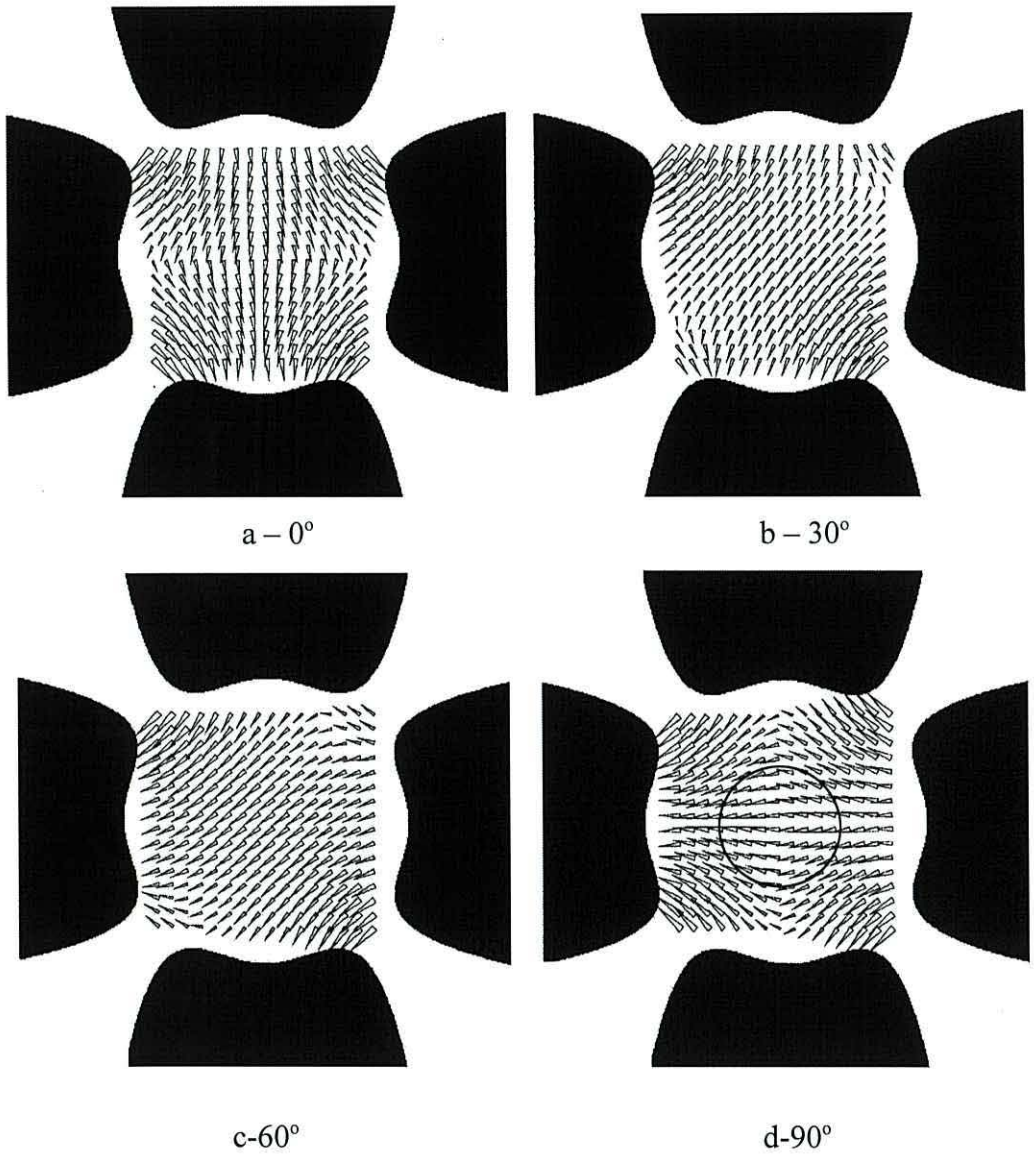

Figure 5.1 - The bone electrode array as described by equation 3.1 with an electric field analysis in the x-y plane. The applied voltages progress through the first quarter of a cycle in 30° steps, a – 0°, b – 30°, c – 60°, d – 90°. The magnitude of the vectors in the central region as the field changes direction remain constant.

The field vectors within the central section of the chamber do not change magnitude, confirming that the bone electrode design generates a highly uniform field within the central area. A greater number of spectra can be acquired with this design. This is especially important for obtaining data from samples with limited numbers of

organisms, such as the oocysts of *C. cayetanensis*, which has no animal model available for amplification. The bone electrode design is also advantageous in creating a uniform field over as large an area as possible in the centre of the chamber, since using low conductivity suspending media results in disruptive positive dielectrophoretic forces over a wider frequency range than are observed for higher conductivity solutions. Indeed, for high conductivity media, negative dielectrophoresis may be observed over the whole frequency range of interest, in which case highly angular electrode tips are an advantage as they assist in keeping the particle in the centre of the chamber (Fuhr *et al.,* 1994). However, this is not helpful with multiple particles in a chamber, as they are pushed together.

5.4 Electrode Manufacture

The bone electrodes were manufactured using a photolithographic process. A microscope slide was cleaned in an ultrasonic bath for 5 minutes in a 1:4 solution of Decon 90™ (Scientific Services/BDH, UK) and ultra pure water. A thin layer of chromium (~5 nm) was evaporated onto the microscope slide using an Edwards Auto 306 Turbo Evaporator (Severn Science, Bristol). A gold layer was then evaporated on top of the chromium layer, to a thickness of ~70 nm. The chromium layer is used as an adhesion layer between the glass of the microscope slide and the gold layer (Figure 5.2a). A 2μm layer of positive photo-resist (Shipley 1818, Chestech, Rugby, Warickshire) was then spun onto the slide (Figure 5.2b). The photoresist was then soft-baked at 116°C for 1 minute to remove any solvents and stresses. The slide was exposed to a collimated UV source (436 nm, g-line) for 25 seconds (Presima Tamarack MAS 12 mask aligner) through a 1:1 mask of the bone electrode design (Figure 5.2c). Where the ultraviolet light strikes the positive resist, it weakens the polymer through chain scission. The weakened polymer was washed away by developing solution (MF 319, Shipley, UK) leaving a positive image of the mask on the resist layer (Figure 5.2d). The slide was then placed in a gold etching solution (aqua regia for ~20s). The gold not protected by a resist layer was removed, exposing the chromium layer beneath. Next, the chrome layer was etched using chrome etch

removed using acetone, leaving a set of gold/chromium electrodes on the microscope slide in the pattern of the bone electrode mask (Figure 5.2f).

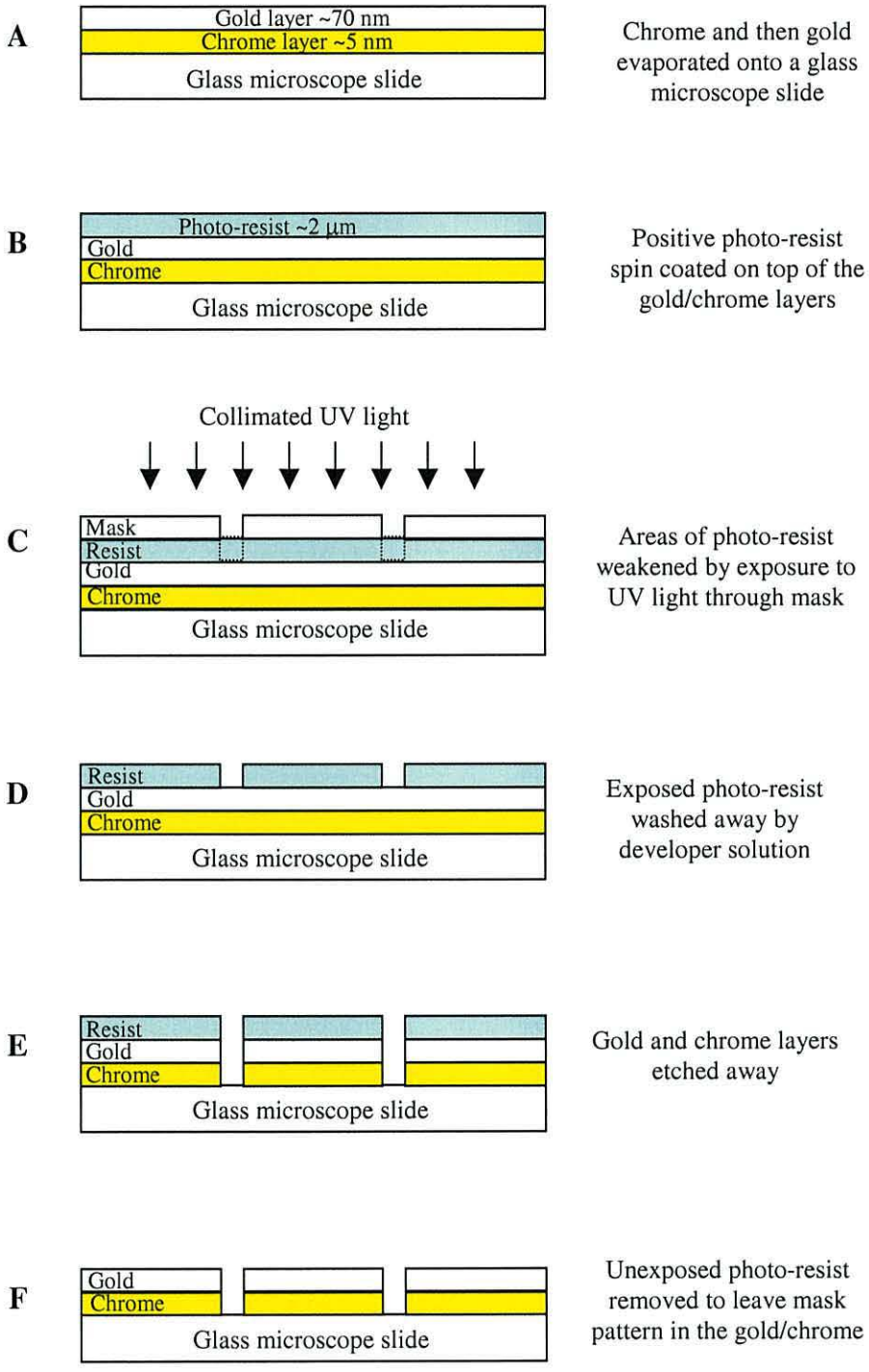

Figure 5.2 – Photolithographic production process to fabricate bone electrodes.

For the experiments carried out in this work, an inter-electrode gap of 2 mm was used (Figure 5.3), to maximise the number of organisms exposed to the uniform field region.

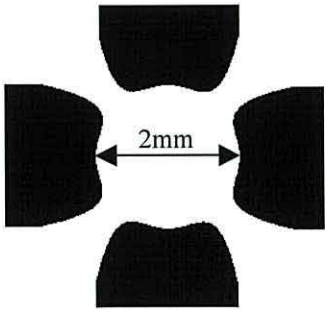

Figure 5.3 – Plan view of bone electrodes showing the 2mm electrode gap.

5.5 Experimental Set Up

The microscope slide with gold electrodes was coated in a 30 μm layer of dry-film resist (Laminar 5000, Shipley, UK), which was exposed to provide a 5 mm hole around the bone electrode tips. The resist coated slide was then heated slowly to 270°C and baked for 2 hours. The resist provided protection for the electrode contacts during experimentation. A circular PVC layer was added around the electrode tips to form a chamber ~100 μm deep. During experimentation, the chamber was sealed using a circular coverslip (Figure 5.4).

Electric fields in the frequency range 100 Hz to 10 MHz. were generated by connecting a custom made four phase sinusoidal signal generator to the electrodes. Particle identification and motion in the electric field were visualised using phase contrast microscopy with a total magnification of × 400 for the *Cyclospora* oocysts, and ×100 for the *Ascaris* eggs (Nikon Optiphot-2 microscope with JVC model TK-1280E colour video camera attachment and ×2.4 zoom tube) and recorded by video for later analysis and timing by stopwatch (Figure 5.4).

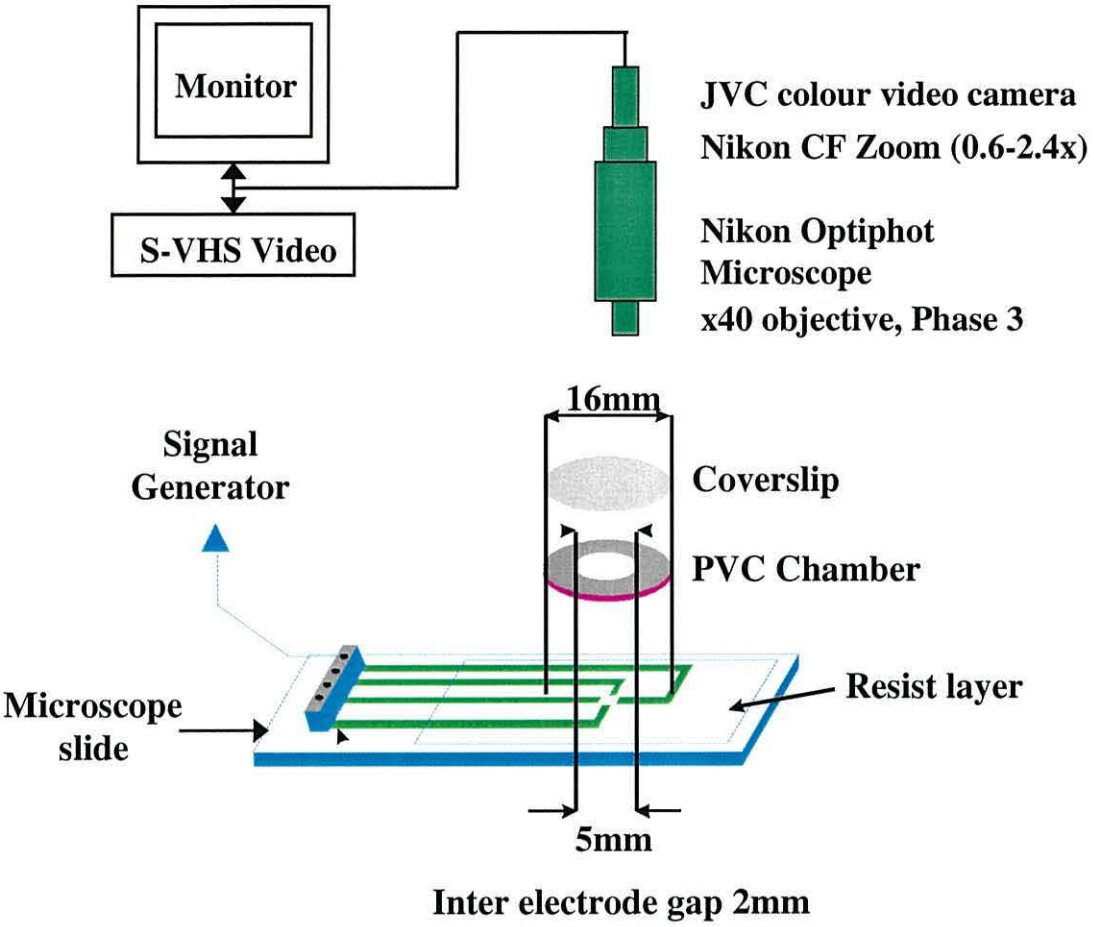

Figure 5.4 – Experimental set up for rotation experiments (Goater, 1999).

5.6 Experimental Procedure

At the start of each experimental session, a haemocytometer grid of known size was recorded to video tape at various zoom settings. By measuring the grid on the TV screen, the total magnification of the system (microscope, video camera, zoom and TV) was known. When the video tape of an experiment was paused, the dimensions of the particle could be measured directly from the TV screen. This system of measurement had the advantage of being accurate even if the video tape was played in a different video player and displayed on a different TV screen.

20 µl of sample suspension was pipetted into the electrorotation chamber. The chamber was then sealed with a microscope coverslip. After 1 minute, to allow particle sedimentation onto the glass, particles within the central region of the chamber (Figure 5.1d) and greater than 3 particle diameters from other particles were selected for the full frequency spectrum. 20 approximately equidistant frequency points on a log scale were chosen between 100 Hz and 10 MHz, and particles were rotated for approximately 20 s at each frequency.

The applied field was kept on while changing frequencies as this helped prevent particle-substrate adhesion. As electrophoretic effects, which cause particle drift, were more noticeable at lower frequencies, <1kHz, each spectrum was recorded from high to low frequency. There was no significant difference between a spectrum recorded in this manner and one recorded with a random frequency order. The shape and magnitude of the spectra obtained are known to be affected by the particle position in the chamber and by the presence of debris on the particle surface (Goater, 1999). Particles were therefore excluded from analysis if they were positioned outside the central region of the chamber, drifted more than three times their own diameter during the recording or had debris, e.g. bacteria, on their surface. These selection criteria, coupled with an electrode design that minimised particle drift, improved the proportion of oocysts or eggs from which reliable data could be obtained.

After each aliquot had been examined and spectra recorded, the chamber was washed with ultra pure water and dried under a stream of nitrogen gas. The chamber was then reused. Due to electrolysis effects at the electrode edges, a chamber was only used for 30 experiments and then replaced before significant deterioration occurred.

5.7 Results Analysis

5.7.1 Normalisation of the Rotation Rate

Due to limitations in the signal generator, the data collected at different frequencies was not always obtained at the same voltage. During each experiment, the phase angle of the signals and the actual applied voltage were measured using an oscilloscope (Hameg 20MHz storage oscilloscope, Model HM 205-3, RS Components, UK). As the rotation rate has been shown to scale with the square of the applied voltage (Arnold *et al.,* 1987), the rate of rotation was normalised by dividing by V^2 as shown

$$ROT_{rate} = 100 \times \left[\frac{\frac{Rotations}{Time}}{(V_{pk})^2} \right] \tag{5.2}$$

5.7.2 Results Plotting

Results were plotted on a log frequency scale and the standard deviation, a measure of how widely values are dispersed from the mean value, was calculated using the 'nonbiased' or 'n-1' method, using the following formula

$$\sigma = \sqrt{\frac{\sum_i (x_i - \bar{x})^2}{n}} \tag{5.3}$$

where x is the population of size n.

The 95% confidence level was then found from the standard deviation. This is the degree of confidence that a parameter lies in the given interval. If $\bar{x}$ is the mean of a random sample of size n from a population with variance σ^2 a central 95% confidence interval for the population mean is given by

$$\bar{x} \pm \frac{1.96\sigma}{\sqrt{n}} \tag{5.4}$$

Results of measurements carried out as described above are presented in Chapters 6 and 7 for oocysts of *Cyclospora cayetanensis* and eggs of *Ascaris suum*, respectively.

5.8 References

Arnold, W. M., Schwan, H.P. & Zimmermann, U. **(1987)** Surface conductance and other properties of latex particles measured by electrorotation. *J. Phys. Chem.* **91** 5093-5098.

Bukhari, Z. and Smith, H. V. **(1995)** Effect of 3 concentration techniques on viability of *Cryptosporidium parvum* oocysts recovered from bovine faeces. *J. Clin. Microbiol.* **33** 2592-2595

Fuhr, G., Glasser, H., Müller, T. and Schnelle, T. **(1994)** Cell manipulation and cultivation under AC electric field influence in highly conductive culture media. *Biophys. Biochim. Acta – General Subjects* **1201** 353-360

Goater, A.D. **(1999)** AC Electrokinetic Bioassays. Development of Electrorotational Assay for Analytes in Water. *Ph.D Thesis* University of Wales, Bangor

Herwaldt, B. L. **(2000)** *Cyclospora cayetanensis* : A review focussing on the outbreaks of cyclosoriasis in the 1990s. *Clin. Infect. Dis.* **31** 1040-1057

Hughes, M. P. **(1998)** Computer aided analysis of conditions for optimising practical electrorotation. *Phys. Med. Biol.* **43** 3639-3648

Chapter 6

Electrorotation of *Cyclospora cayetanensis*

6.1 Introduction

In this Chapter, electrorotation spectra for three isolates of *C. cayetanensis* oocysts from humans and two isolates from baboons are presented. A comparison is made between spectra from sporulated and unsporulated oocysts, human source and baboon source oocysts and viable and non-viable oocysts. Using the spherical multi-shell model described in Chapter 4, the electrorotational response of oocysts are modelled and compared to experimental spectra to provide a better understanding of the physiological changes that are occurring within the oocysts.

Due to the limited numbers of *C. cayetanensis* oocysts available to work with, spectra were recorded of any oocysts found within the middle third of the electrorotation chamber that were reasonably free of debris. Of the 200+ spectra obtained, only about 100 were from oocysts that were clean enough to be analysed, the others possessed some form of debris attached to the oocyst wall, either bacteria or particulate matter from the original stool sample. The spectra presented in this Chapter are therefore of clean oocysts, except where specifically mentioned otherwise.

6.2 Analysis of Human Isolate C1

30 initial spectra were obtained from a human isolate designated C1 and were used for familiarisation with the experimental procedure, described in detail in Chapter 5, the experimental equipment, the organism and the model.

6.2.1 Effect of surface debris

Since the samples were badly contaminated with particulate matter, the effect on the rotation spectra of small amounts of debris on the oocyst wall was investigated (Figure 6.1). The spectra of three oocysts with similar amounts of debris were compared to the spectra of an uncoated oocyst (Figure 6.2). The spectra were taken at the same suspending medium conductivity (1.3 mS/m). The peak rotation frequency, and the rotation cross-over frequency values were the same for the debris-coated and uncoated oocysts. The debris-coated oocysts rotated in the same direction but at a slower rate than that for than the uncoated oocyst.

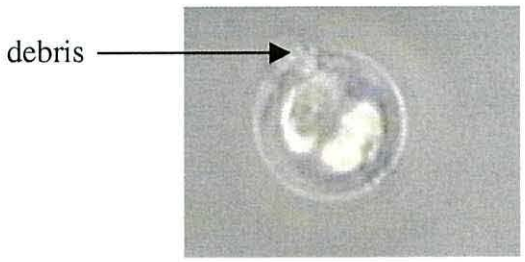

Figure 6.1 – Debris on the surface of a sporulated oocyst.

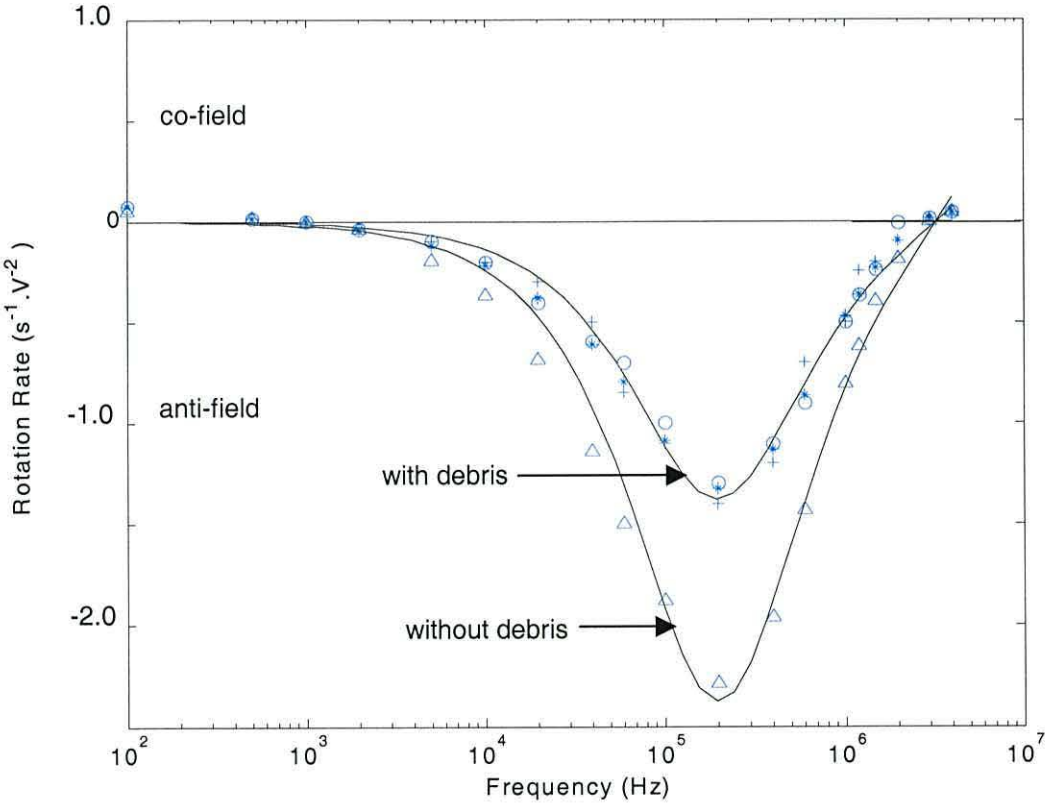

Figure 6.2 – Rotation spectra of a single, debris free, unsporulated oocyst (Δ) compared to 3 debris coated, unsporulated oocysts (*, o, +). The solid line is the best fit for the single shell model using the parameters given in Table 6.1, but with the value of the viscous drag increased from 2.3 $x10^{-18}$ to 4.5 $x10^{-18}$ for the debris coated oocysts (conductivity 1.3 mS/m).

	Cyclospora cayetanensis			
	Unsporulated		Sporulated	
	Viable	Non-viable	Viable	Non-viable
Dimensions (μm)	9[a]	9[a]	9[a]	#
Wall thickness (nm)	113[a]	113[a]	113[a]	#
Membrane thickness (nm)	9[b]	9[b]	9[b]	#
Permittivity (ε_r)				
Interior	50[c]	50[c]	50[c]	#
Membrane	5[c]	3[e]	5[c]	#
Wall	60[c]	60[c]	60[c]	#
Conductivity (S/m)				
Cytoplasm	0.5[d]	0.2 ± 0.03[e]	0.5[d]	#
Membrane	$(1\pm0.3)\times10^{-6}$ [e]	$(2\pm0.1)\times10^{-5}$ [e]	$(8\pm0.5)\times10^{-6}$ [e]	#
Wall	0.09 ± 0.01[e]	0.01 ± 0.004[e]	0.09 ± 0.01[e]	#

none observed
reference *a*-Ortega *et al.*, 1993; *b*- Pethig *et al*, 1995; *c* – Huang *et al.*, 1992; *d* – Huang *et al.*, 1993 and *e* - fitted

Table 6.1 - Particle dimensions and initial dielectric parameter values used in the modelling of the electrorotation spectra shown in Figures 6.2, 6.3, 6.4 and 6.5.

Other than changing the value of the viscous drag term in the model, the parameters defining the electrical properties of the oocyst and the suspending medium were not changed, indicating that the reduction in rotation velocity due to the presence of debris on the oocyst surface can be attributed to drag alone. Goater (1999) reported that the presence of small amounts of particulate matter on the surface of a *Cryptosporidium parvum* oocyst reduced the rotation rate by a significant amount, and attributed the effect to drag. Mitchell (2001) showed that the addition of a single bacterium to a latex bead changed the sense rotation of the latex bead. As such a change is not seen here, merely a reduction in the rate of rotation, it is clear that the addition of small amounts of faecal debris, not bacteria, will reduce the rate of rotation of the anti-field peak, but will not change the anti-field peak frequency, or the high frequency cross over frequency.

6.2.2 Biological Variance

The effect of biological variance is shown in Figure 6.3, which shows a comparison of seven unsporulated, debris-free oocysts at the same solution conductivity.

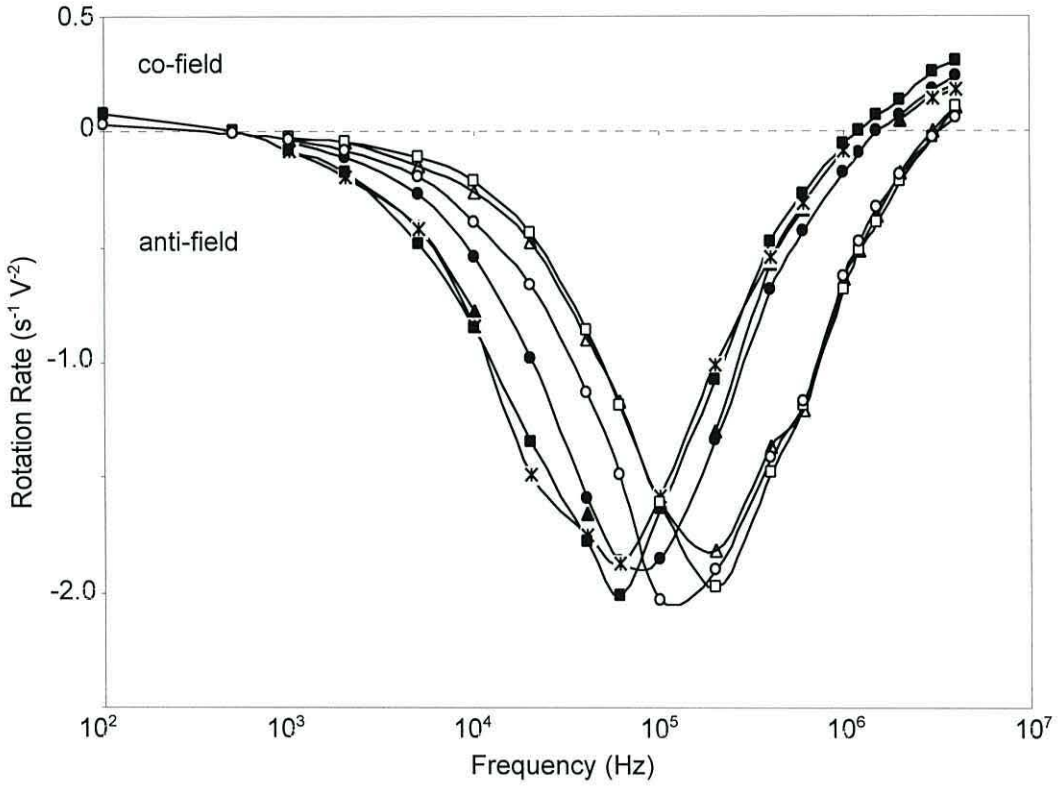

Figure 6.3 – Rotation spectra of seven debris free, unsporulated oocysts showing similar anti-field peak rotation rates, but differences in the anti-field peak rotation frequency of 60 kHz to 200 kHz (conductivity 0.4 mS/m).

The anti-field peak rotation rate varies by ~10% between the seven oocysts. The oocysts show a variety of peak rotation frequencies, between 60 kHz and 200 kHz. There appear to be two populations in the upper cross-over frequency region, one at 1.5 MHz (solid symbols) and one at 3 MHz (open symbols). This data suggests a difference between the oocysts, other than solution conductivity and sporulation state, that is not discernable visibly. This difference may be due to biological variance between oocysts, highlighting the sensitivity of the electrorotation technique. The 'kink' in the three open symbol spectra at ~800 kHz is also similar to an effect observed in Figure 4.7 for a very low conductivity of the oocyst wall (0.003 S/m) and could be attributed to another dispersion process. The modelleing also showed the increase in the high frequency cross-over frequency, as seen here for the three open symbols (Figure 6.3).

6.2.3 Unsporulated and Sporulated Oocysts

Rotation spectra for three unsporulated and two sporulated debris free oocysts are shown in Figure 6.4. The unsporulated oocysts rotate at a higher rate than the sporulated oocysts. The frequency at which the direction of rotation reverses from anti-field to co-field at high frequencies is significantly different between unsporulated and sporulated oocysts, at 800 kHz and 2 MHz respectively. Thus, at 1 MHz the unsporulated oocysts will rotate in the opposite direction to the sporulated oocysts, allowing rapid discrimination. The values used for the model are listed in Table 6.1.

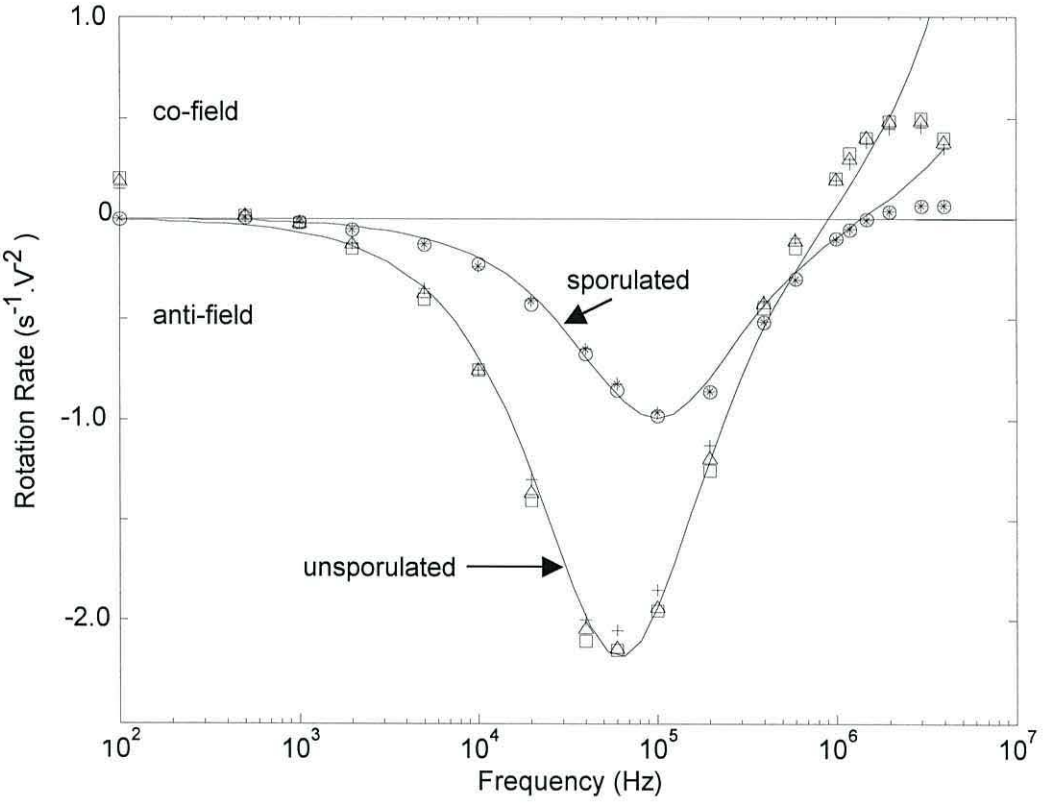

Figure 6.4 – Rotation spectra of three debris free, unsporulated oocysts (+, Δ, □), which rotate at a higher rate than two debris free, sporulated oocysts in the anti-field region (*, o). Solid line indicates the best fit with the model using the values listed in Table 6.1 (conductivity 1.0 mS/m).

From Table 6.1, which shows the values of best fit from the model, it can be seen that the major difference between sporulated and unsporulated oocysts is a difference in the conductivity of the membrane. The increase in the conductivity of the membrane corresponds to the changes occurring within the oocyst during sporulation, namely the formation of the two sporocysts, as detailed in Chapter 2, Figure 2.1. At high

frequencies, > 2 MHz, the model does not match the experimental data well, and for frequencies below 1 kHz, the model does not show the slight co-field rotation observed experimentally for unsporulated oocysts. The limitations of the model at low frequencies and for complex organisms at high frequencies was discussed in Chapter 4. However, for the frequency range 1 kHz to 2 MHz, the model fits the experimental data well, and the difference in magnitude of the peak rotation frequency, and the difference in the high frequency cross-over point, can be used to distinguish between unsporulated and sporulated oocysts.

6.2.4 Viable and non-viable oocysts

The spectra for four debris free, unsporulated oocysts, at the same conductivity (0.9 mS/m) were significantly different (Figure 6.5). Two of the oocysts (Δ, □) gave characteristic rotation spectra as seen previously for unsporulated oocysts (Figure 6.4). The spectra of the other 2 oocysts (o, *) were characteristic of non-viable oocyst spectra, as reported and verified for *Cryptosporidium parvum* by Goater (1999).

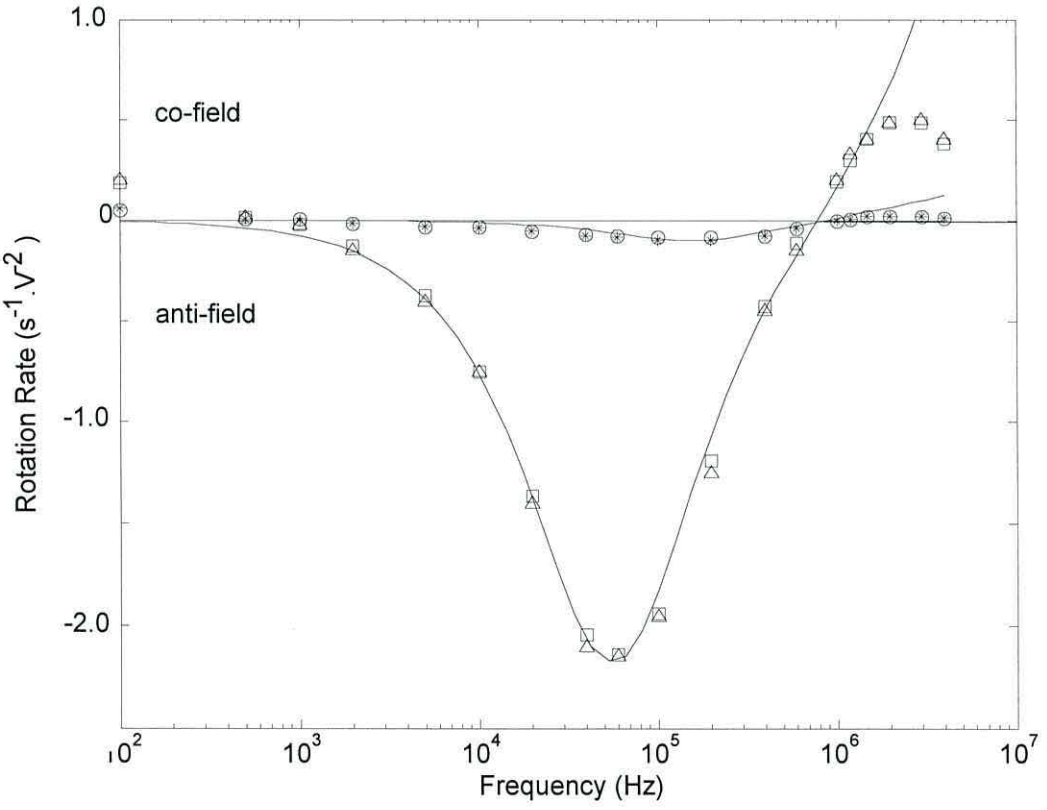

Figure 6.5 – Rotation spectra of 2 debris free, viable, unsporulated oocysts (Δ, □), and 2 putative non-viable, unsporulated oocysts (*, o). Mean rates of rotation shown. Solid line indicates the best model fit using the values listed in Table 6.1 (conductivity 0.9 mS/m).

From the model data (Table 6.1), the difference between the two types of oocysts is a reduction in the membrane permittivity, an increase in the membrane conductivity, a decrease in the cytoplasm conductivity and a decrease in wall conductivity. These changes are consistent with a membrane that has ceased to function and can be attributed to differences in the viability of the oocysts. The membrane of a viable oocyst is selectively-permeable to ions and non-lipid soluble molecules, so the internal composition of the cell is quite different from the exterior medium. Upon cell death, membrane integrity is lost, and the cell freely exchanges material with the external suspending medium. As a result, fewer induced charge differences occur between the inside of the oocyst and the exterior medium, and this greatly affects the rotation spectra produced. This difference in the magnitude of rotation rate (Figure 6.5) between oocysts designated viable and non-viable is similar to that reported by Goater *et al.* (1997) for *Cryptosporidium parvum*, a coccidian pathogen with a similar structure to *C. cayetanensis*. Goater confirmed that this observation was due to differences in oocyst viability by a fluorogenic vital dye assay (Goater, 1999). As the viability of *C. cayetanensis* oocysts cannot be independently verified by such techniques, as methods have yet to be developed, and it is not possible to distinguish morphologically between viable and non-viable oocysts, this result could have significant implications for detection and assessment of this organism in the water and food industries.

6.2.5 Effect of suspending solution conductivity

The conductivity of the supporting medium was found to affect the anti-field peak rotation frequency and rotation rate, and the high frequency cross-over point, at which the oocyst changes direction of rotation. Increasing the conductivity of the suspending solution increased the anti-field peak rotation frequency, decreased the anti-field peak rotation rate, increased the high frequency cross-over point and decreased the co-field peak rotation rate, as predicted in Chapter 4, Section 4.6.1. (Figure 6.6).

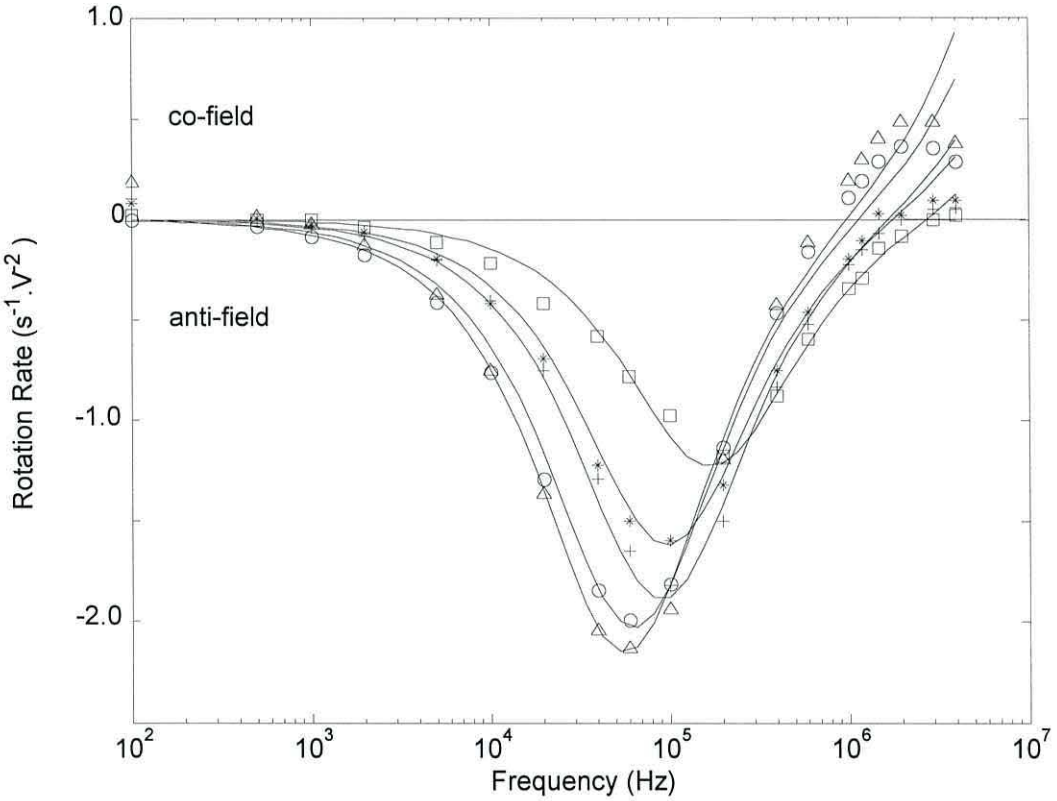

Figure 6.6 – Electrorotation spectra for debris free, unsporulated oocysts of *C. cayetanensis* (Δ, 0.4 mS/m; o, 0.6 mS/m; +, 0.8 mS/m; * 0.95 mS/m; □, 1.1 mS/m). Solid lines indicate the best fit of the model parameters listed in Table 6.1, with only the solution conductivity varied.

As the conductivity of the solution increases the upper frequency cross-over point shifts from ~800 kHz to ~2 MHz. The conductivity of the suspending medium was the only model parameter varied, and the effects observed in Figure 6.6 highlight the importance of maintaining a constant suspending medium conductivity during experiments. Due to biological variance (Figure 6.3), oocyst spectra with conductivities varying by ± 0.1 mS/m can be compared with confidence.

6.2.6 Effects of storage

Oocysts of isolate C1 were stored in 2.5% potassium dichromate solution at 4°C after the initial spectra shown in Figure 6.2 were obtained. Due to the limited number of oocysts available to work on, it is important to know if long term storage affects the oocysts, or the rotation spectra. Eight months later, electrorotation spectra of oocysts from this isolate were measured again to investigate the effect of storage on the spectra (Figure 6.7).

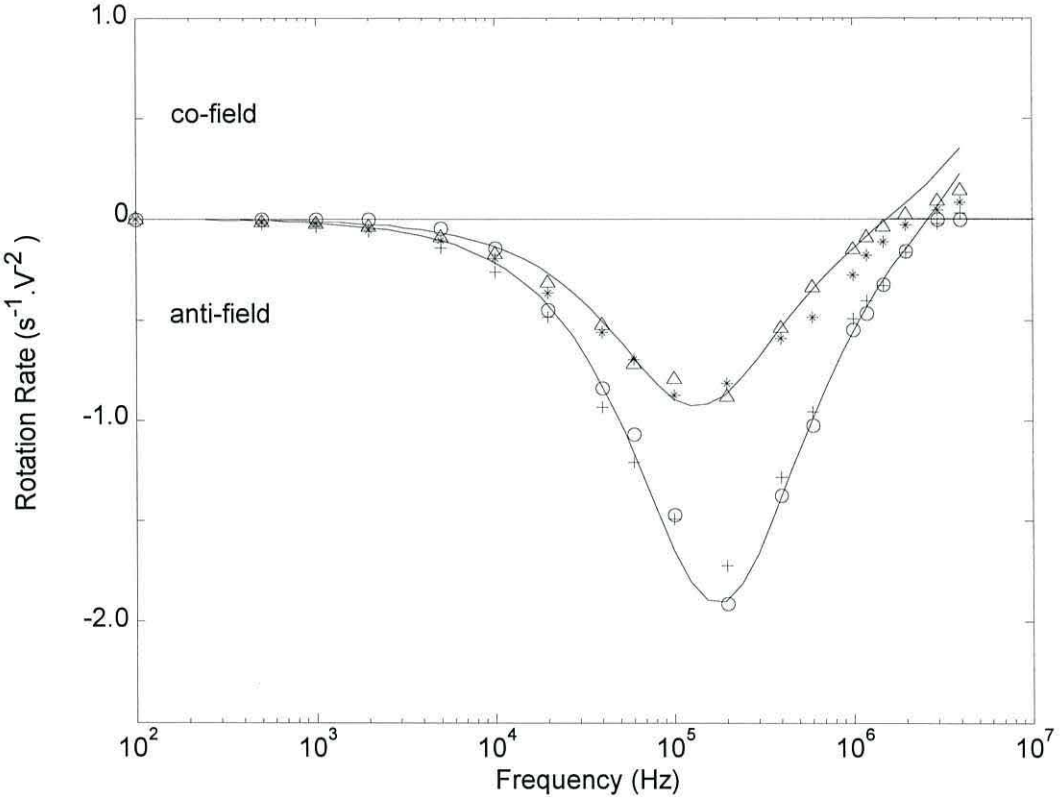

Figure 6.7 – Rotation spectra of 2 debris free, unsporulated (+, o) and 2 debris free, sporulated (*, Δ) oocysts after storage in 2.5% potassium dichromate solution for 8 months at 4°C (conductivity 0.6 mS/m). Solid lines indicate the best fit of the model using the values listed in Table 6.2.

The anti-field peak rotation rate for the unsporulated oocysts is greater than that of the sporulated oocysts, as seen previously (Figure 6.4). The magnitude of the anti-field rotation rate has decreased slightly (~10%) for both the unsporulated and sporulated oocysts compared to before storage (Figure 6.4). The anti-field peak rotation frequency for the sporulated oocysts shows a slight increase compared to that seen before storage, from 100 kHz to 150 kHz. The high frequency cross-over frequency, at ~1.5 MHz, is the same for sporulated oocysts before and after storage.

For unsporulated oocysts, the high frequency cross-over frequency has changed to 3 MHz compared to 800 kHz seen previously (Figure 6.4). Thus the previous assertation that the difference in direction of rotation at 1 MHz indicated sporulation state is no longer valid. However, the ability to distinguish between sporulated and unsporulated oocysts by the difference in magnitude of the anti-field peak rotation rate is still valid, even after storage for 8 months.

The model shows that, after storage, for the sporulated oocysts there is a slight increase in the conductivity of the wall, and a slight decrease in the membrane permittivity that corresponds to these changes in the rotation spectra (Table 6.2).

	Cyclospora cayetanensis			
	Unsporulated		Sporulated	
	Before storage	After storage	before storage	After storage
Permittivity (ε_r)				
Membrane	5[a]	4[c]	5[a]	4[c]
Conductivity (S/m)				
Cytoplasm	0.4 ± 0.1[c]	0.8 ± 0.1[c]	0.5[b]	
Wall	0.09 ± 0.01[c]	0.2 ± 0.01[c]	0.09 ± 0.01[c]	0.12± 0.01[c]

none observed
reference *a* – Huang *et al.*, 1992; *b* – Huang *et al.*, 1993 and *c* – fitted

Table 6.2 - Changes to the dielectric parameter values from Table 6.1 used in the modelling of the electrorotation spectra shown in Figure 6.7.

The high frequency section of the spectrum is usually associated with the internal dielectric properties of cells, as explained earlier (Chapter 4). The shift in the high frequency cross-over frequency from 800 kHz to 3 MHz for the unsporulated oocysts before and after storage corresponds to an increase in the conductivity of the interior of the unsporulated oocysts. The model also indicates that there is an increase in the conductivity of the oocyst wall after storage, which is associated with the shift in the peak anti-field rotation frequency from 60 kHz to 200 kHz.

The experiments performed on the oocysts after storage were performed at a suspending medium conductivity of 0.6 mS/m. The experiments prior to storage were conducted at a suspending medium conductivity of 1.0 mS/m. Based on the observed and modelled effect of the suspending medium conductivity on the electrorotation spectra of oocysts (Figures 6.6 and 4.5), it would be expected that the peak anti-field rotation rate would be reduced for the oocysts after storage, and that the high frequency cross over frequency would be reduced also. That these trends are not followed implies that the differences between Figures 6.4 and 6.7 could be greater still, if the experiments had been performed at the same suspending medium conductivity.

Unlike previous spectra (Figures 6.2, 6.4, 6.5 and 6.6), there is no low frequency co-field rotation observed for either unsporulated or sporulated oocysts after storage (Figure 6.7). As mentioned in Chapters 3 and 4, the low frequency area of the rotation spectrum is related to the surface charge of a particle, and is not fully understood. This data suggests that storage in 2.5% potassium dichromate solution reduces the surface charge of the oocysts.

Taking into account biological variance and the limited number of oocysts studied before and after storage, it is reasonable to assume that the sporulated oocysts were not affected greatly by storage. Indeed, a sporulated oocyst is capable of surviving in hostile environments until the right environmental conditions are met and excystation can occur. In contrast, certain physiological changes have to occur to an unsporulated oocyst as it undergoes sporulation in the environment. Artificial sporulation usually takes place after 7-20 days at a temperature between 26-30°C (Smith *et al.,* 1997). Since the unsporulated oocysts investigated were kept at 4°C, the life-cycle processes will have been drastically reduced, due to immobilisation of proteins on the surface of the oocyst. This would result in the conductivity of the oocyst wall increasing, as seen in the modelling data.

Long term storage in potassium dichromate does not affect the viability of *C. cayetanensis* oocysts, as oocysts will sporulate in 2.5% potassium dichromate solution (Smith *et al.,* 1997). However, the data presented here shows that, although the oocysts may remain viable, their dielectric properties are affected by the storage medium and temperature.

6.2.7 Ruptured Oocysts

Oocysts with ruptures in their cell walls, as shown in Figure 6.8, are non-viable.

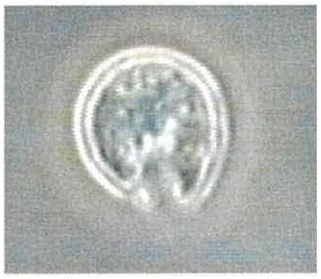

Figure 6.8 – Unsporulated oocyst with a rupture in the cell wall.

The interior of a ruptured oocyst may be partially or wholly at the same conductivity as the surrounding solution. Therefore spectra of ruptured oocysts are useful for comparison with whole, putative non-viable oocyst spectra. When an oocyst becomes non-viable, it loses membrane integrity, and material is exchanged freely between the interior of the oocyst and the exterior solution. Figure 6.9 shows rotation spectra of three ruptured oocysts, a debris free, viable unsporulated oocyst and a putative non-viable oocyst.

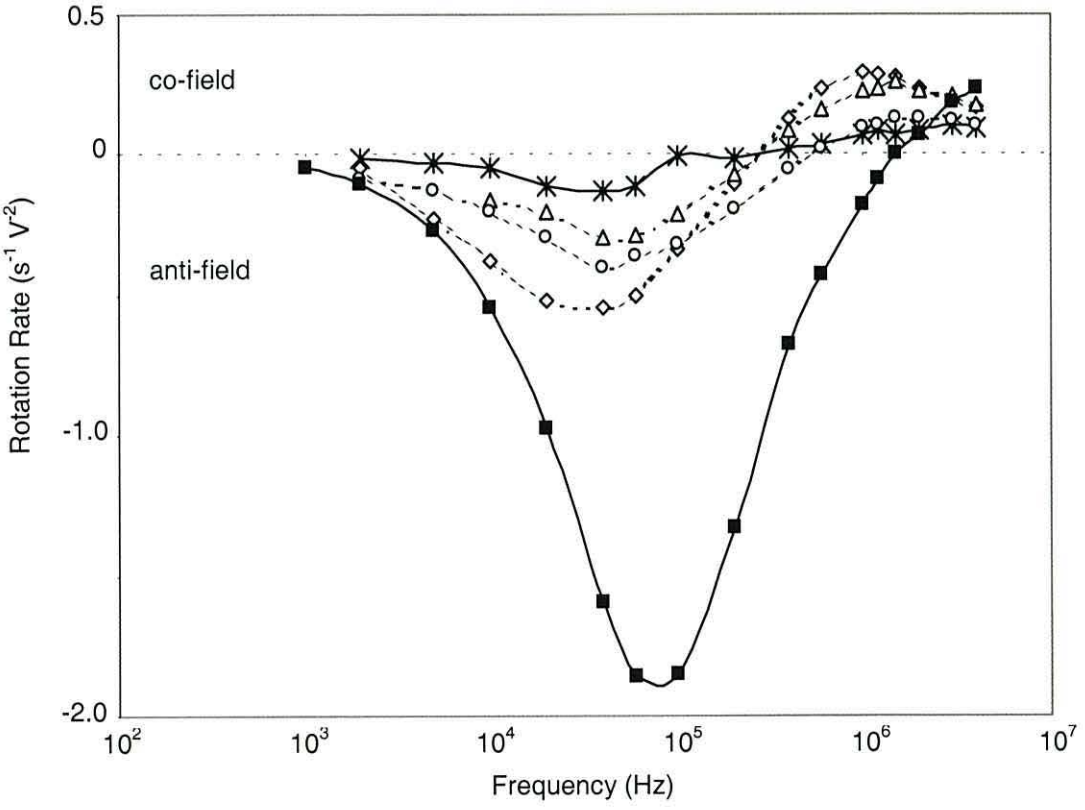

Figure 6.9 – Rotation spectra of three oocysts that have a rupture in the oocyst wall (◊, o, Δ), a centrally located viable, unsporulated oocyst (■), and a putative non-viable oocyst (*) (Conductivity 0.4 mS/m).

Compared to the unsporulated, viable oocyst, the ruptured oocysts all have low anti-field rotation rates and low cross-over frequencies, which correspond with the characteristics observed by Goater (1999) to indicate non-viable oocysts, as discussed earlier (Section 6.2.4). Based on the work of Goater (1999), and the response of the ruptured oocysts, it is assumed that the intact, morphologically indistinguishable, unsporulated oocyst that has a very low rotation rate and low cross-over frequency is non-viable, as has been modelled previously (Figure 6.5)

The differences in the rotation rates of the ruptured oocysts can be attributed to varying stages of cell death, with sections of the membrane still being resistive in places, and/or differences in the size of the rupture. The effect on the rotation spectra of changes in the conductivity of the cell membrane were shown in Figure 4.6, which showed a decrease in the rate of rotation with increasing membrane conductivity. The rupture in the oocyst wall allows the interior contents of the oocyst, such as salts and DNA, to be freely exchanged with the external, suspending medium. Thus the interior of the ruptured oocyst has a conductivity similar to that of the suspending medium. Figure 4.8 showed the effect on the rotation spectra of reducing the interior conductivity of an oocyst, namely a large reduction in the anti-field rotation rate, a reduction in the anti-field peak rotation frequency and a reduction in the cross-over frequency. All of these effects are observed in Figure 6.9.

6.3 Baboon *Cyclospora* Spectra

A limited number of baboon *Cyclospora* oocysts were obtained from the Scottish Parasite Diagnostic Laboratories (SPDL), and investigated. *Cyclopora* oocysts from baboons are morphologically indistinguishable from oocysts recovered from humans, and are considered to be the same species. For more information on the taxonomic classification of *Cyclospora*, see Appendix A.

6.3.1 1998 Baboon Isolate

Oocysts were collected in April 1998 from baboons in Africa and stored in formalin at the SPDL. The samples were known to contain viable and non-viable oocysts (Smith *et al.*, 1997). However, due to the amount of time in storage, and the storage method (no antibiotics), the samples were contaminated with particulate matter and bacteria. Very few oocysts could be isolated that were free from debris or bacteria and very few rotation spectra could be obtained. Of oocysts supplied from four different baboons, only one isolate contained reasonably clean oocysts, and from this, only three unsporulated oocysts were clean enough to be investigated. The few spectra from the debris free oocysts revealed a distinct difference in rotation rate and the peak rotation frequency between the viable and putative non-viable oocysts (Figure 6.10). With such a small sample number, this is not a conclusive result.

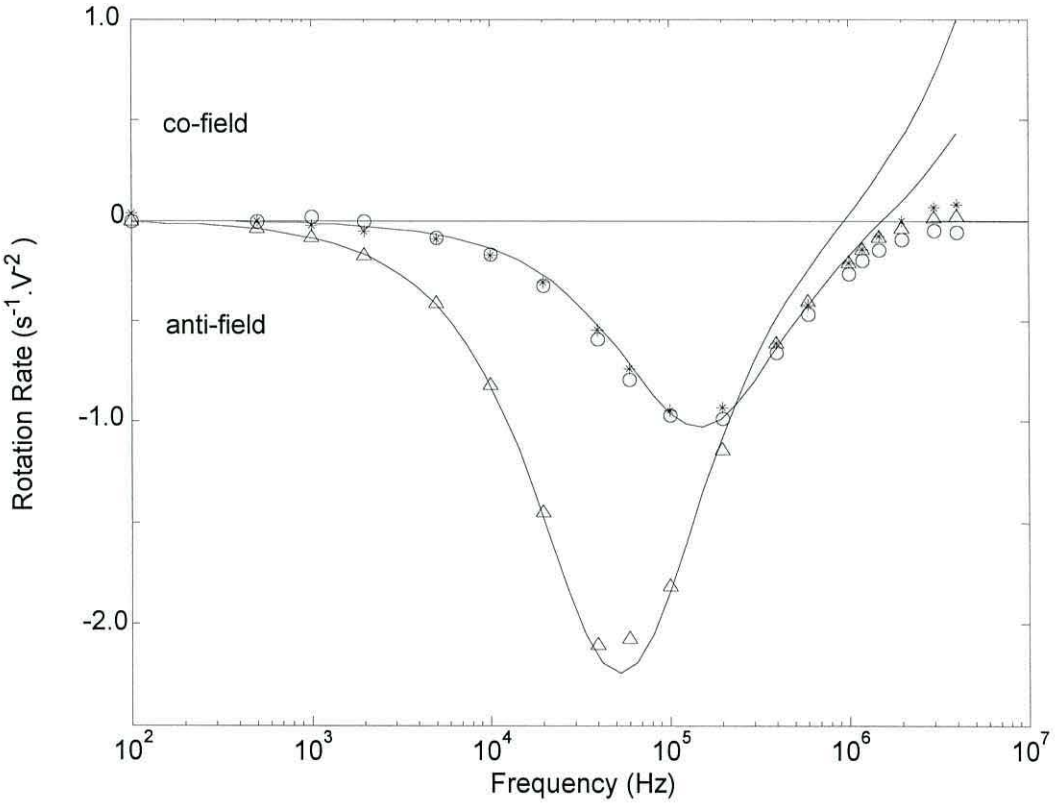

Figure 6.10 – Rotation spectra of three unsporulated oocysts collected from baboons in April 1998. The faster rotating oocyst (Δ) is probably viable, while the slower rotating oocysts (o, *) are putative non-viable. Solid lines show the best fit to the model using the parameters listed in Table 6.3 (conductivity 0.8 mS/m).

The putative non-viable spectra are rotating in a manner that is not expected or consistent with non-viable oocysts, which are expected to exhibit much lower rotation rates in the anti-field region as seen previously in Figure 6.5. The speed of rotation is comparable to that of a sporulated oocyst (Figure 6.4), however, the baboon oocysts were confirmed as unsporulated morphologically at the time of the experiments and afterwards by examination of the video tape. One possible explanation is that, unlike the human *Cyclospora* oocysts, the baboon oocysts were stored in formalin (37% formaldehyde) for transport from Africa to the SPDL, which affected their physico-chemical properties. When the oocysts were stored in formalin, they were viable. The formalin has somehow preserved the integrity of the membrane, whilst at the same time rendering the organism non-viable.

	Baboon source *Cyclospora*	
	Unsporulated	
	Viable	Non-viable
Dimensions (μm)	9[a]	9[a]
Wall thickness (nm)	113[a]	113[a]
Membrane thickness (nm)	9[b]	9[b]
Permittivity (ε_r)		
Interior	50[c]	50[c]
Membrane	4[d]	4[d]
Wall	60[c]	60[c]
Conductivity (S m^{-1})		
Cytoplasm	0.8 ± 0.1[d]	0.5 ± 0.03[d]
Membrane	$(1 \pm 0.3) \times 10^{-6}$ [d]	$(8 \pm 0.1) \times 10^{-6}$ [d]
Wall	0.1 ± 0.01[d]	0.15 ± 0.02[d]

reference
a-Ortega *et al.*, 1993; *b*- Pethig *et al*, 1995; *c* – Huang *et al.*, 1992; and *d* - fitted

Table 6.3 - Particle dimensions and initial dielectric parameter values used in the modelling of the electrorotation spectra shown in Figure 6.10 for unsporulated oocyst from baboons.

The model data, shown in Table 6.3, for the unsporulated, viable baboon oocysts is similar to that shown for the unsporulated, viable human oocysts that were stored in 2.5% potassium dichromate solution (Table 6.2). The only difference is that the wall conductivity for the viable, unsporulated baboon oocysts is 0.1 S/m, while for the viable, unsporulated human oocysts it is 0.2 S/m. This difference may be due to the formalin affecting the surface charge of the oocyst in a different way to that of the potassium dichromate. The modeling data for the putative non-viable oocysts show

dielectric properties that would be associated with sporulated oocysts (a much lower wall conductivity would be expected for a non-viable oocyst). This suggests that there are either differences between the baboon and human source oocysts that cannot be identified by light microscopy, or that the storage in formalin has greatly changed the physiological properties of the oocysts. Formaldehyde is used to fix and preserve cells, and it has been reported that formaldehyde affects the plasma membrane of mammalian cells (Burt, 1990). In high concentrations formaldehyde produces inter- and intra-molecular cross linking in proteins (Schauenstein *et al.*, 1977; Zubay, 1983). This treatment effectively stops the membrane proteins from functioning by fixing their structure and possibly their position in the membrane, so making the membrane more rigid. This could explain the effects in the spectra observed for formalin stored baboon oocysts.

6.3.2 1994 Baboon Isolate

Figure 6.11 shows rotation spectra of three unsporulated oocysts obtained from a baboon source collected in 1994 compared to two unsporulated oocysts from a human source. Again, there were problems obtaining enough clean oocysts from such a contaminated source. The baboon spectra show a remarkable uniformity of rotation rate and peak rotation frequency, despite being from oocysts stored in formalin for five years at 4°C. The spectra are also similar to those in Figure 6.10, which were from oocysts stored for a shorter time (one year). The oocysts collected in 1994 were confirmed non-viable by the excystation protocol (Ortega *et al.*, 1993) carried out at the SPDL. This indicates that the previous designation of non-viable oocysts was correct (Figure 6.10), and shows that non-viable baboon oocysts have a higher anti-field rotation rate than non-viable human oocysts, although this may be an effect of the storage conditions. The peak rotation frequency for non-viable, unsporulated oocysts of baboon and viable, unsporulated human oocysts is the same (~80 kHz). Further investigation into these effects, as well as comparisons with fresh samples of baboon oocysts, is required before any conclusions can be drawn. Low frequency co-field rotation is observed for the baboon oocysts suggesting that the effect formalin has on the surface charge is different to the effect potassium dichromate has, as mentioned earlier.

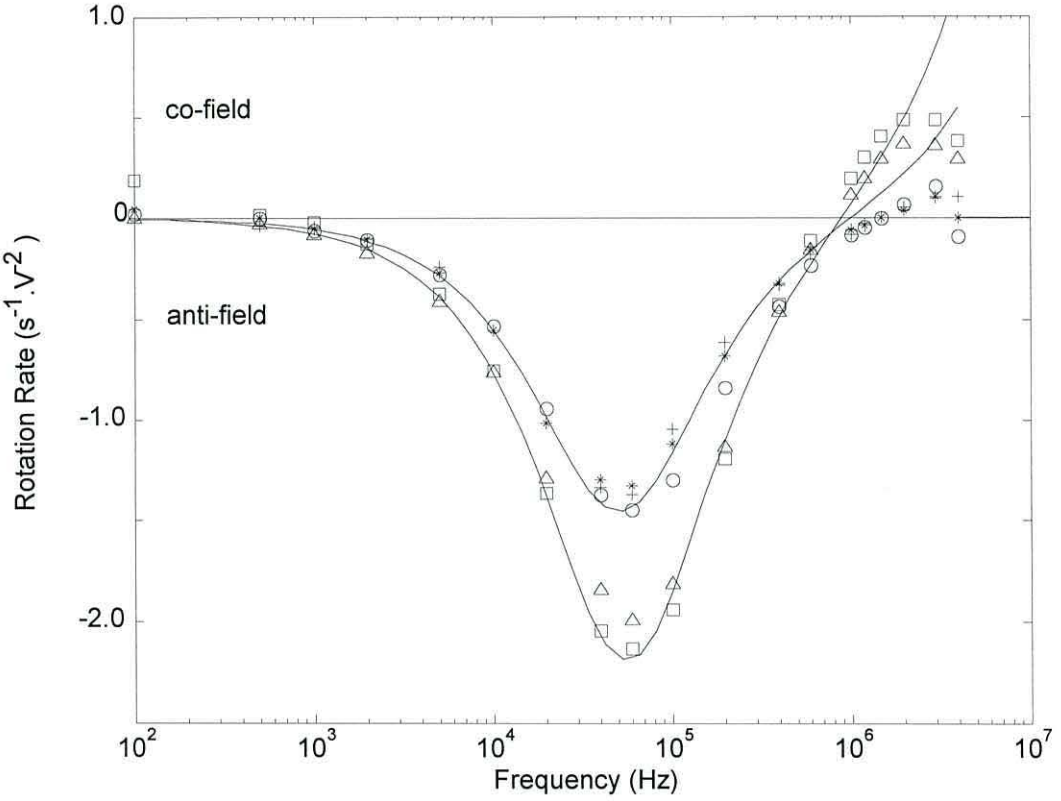

Figure 6.11 – Spectra of 3 debris free, non-viable, unsporulated, baboon *Cyclospora* oocysts (0, *, +) collected in 1994 and stored in formalin at 4°C compared to 2 debris free, unsporulated human source oocysts (□, Δ). Solid lines show the best fit of the model using the parameters listed in Table 6.4 (conductivity 0.5 mS/m).

	Unsporulated *Cyclospora*	
	Human	Baboon
Dimensions (μm)	9[a]	9[a]
Wall thickness (nm)	113[a]	113[a]
Membrane thickness (nm)	9[b]	9[b]
Permittivity (ε_r)		
Interior	50[c]	50[c]
Membrane	5[c]	5[c]
Wall	60[c]	60[c]
Conductivity (S m^{-1})		
Cytoplasm	0.4 ± 0.1[d]	0.8 ± 0.03[d]
Membrane	$(1\pm0.3)\times10^{-6}$ [d]	$(1\pm0.1)\times10^{-6}$ [d]
Wall	0.09 ± 0.01[d]	0.09 ± 0.04[d]

reference

a-Ortega *et al.*, 1993; *b*- Pethig *et al*, 1995; *c* – Huang *et al.*, 1992; and *d* - fitted

Table 6.4 - Particle dimensions and dielectric parameter values used in the modelling of the electrorotation spectra shown in Figure 6.11 for unsporulated oocysts from baboons and humans.

The parameters used to model the human unsporulated oocysts are the same as listed in Table 6.1. The difference between the human and baboon model parameters is an increase in the conductivity of the cytoplasm. Whether this is due to a difference between very similar species of *Cyclospora*, or an artefact of the storage remains to be investigated. Lopez *et al.* (1999) recently reported finding differences in the ribosomal DNA between morphologically indistinguishable, unsporulated oocysts recovered from humans and baboons. It is interesting to note that the oocysts that Lopez *et al.* performed their studies on are from the same source as the oocysts investigated here. Figure 6.11 concurs with Lopez's findings, but a more comprehensive investigation with many more oocysts is required before any firm conclusions can be drawn.

6.4 Analysis of Human Isolate C2

34 spectra were obtained from isolated C2 at a suspending medium conductivity of 1 mS m^{-1}. The spectra recorded for 19 oocysts which were in an unsporulated state and were morphologically indistinguishable are shown in Figure 6.12. However, the rotation spectra were of two distinct types, 17 oocysts that have a rapid anti-field rotation rate, and two oocysts that have very slow rotation rates. As seen previously (Figure 6.5) the two types can be designated viable and non-viable. The distinct spectra of two unsporulated oocysts (open symbols) designated non-viable are similar to the spectrum of an oocyst that had no observable structural contents (*, Figure 6.12) and which was considered non-viable, as discussed in Section 6.2.7. Minor differences between spectra can be attributed to differing states of deterioration following oocyst death.

Estimations of the electrical parameters of the different oocyst components for the viable and non-viable best model-fits shown in Figure 6.12 are listed in Table 6.5. Similar trends to those of *C. parvum* oocysts (Goater, 1999) are found for the *C. cayetanensis* oocysts, namely an increase in membrane conductivity with a corresponding decrease in the interior conductivity as oocysts die. This provides further evidence that the change in shape of the spectra from viable to non-viable is indeed due to differences in physiological state.

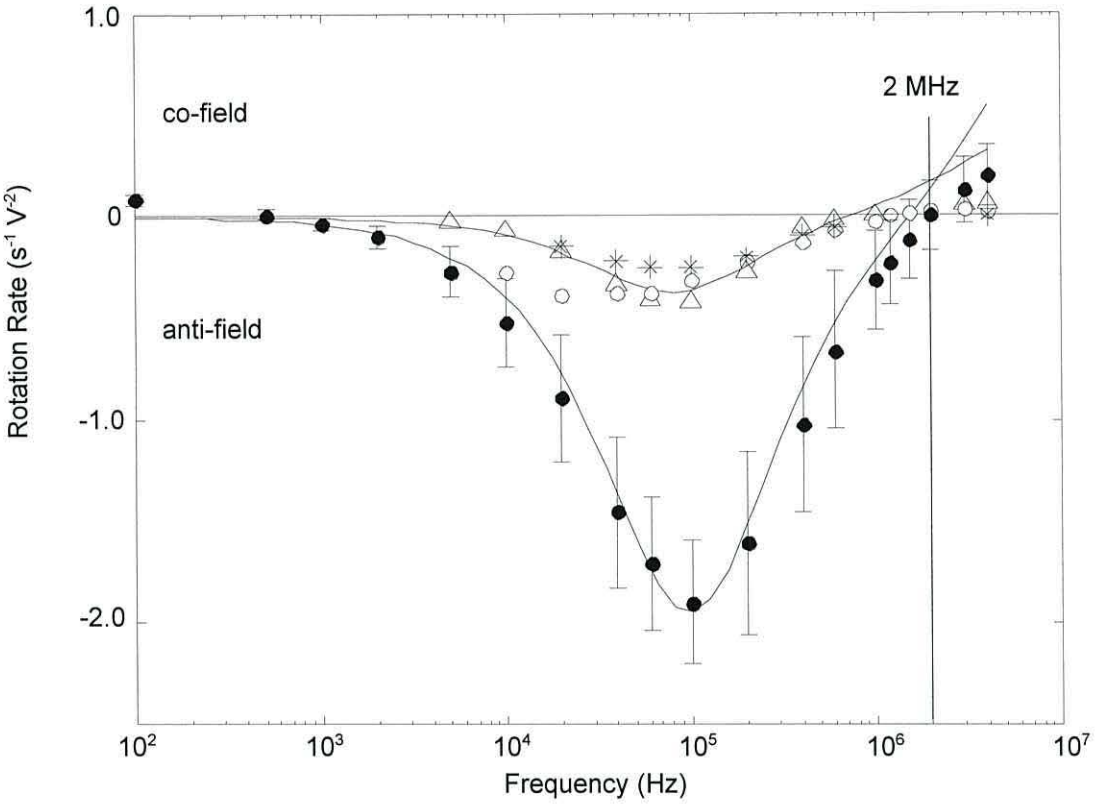

Figure 6.12 - Rotation spectra of 19 debris free, unsporulated oocysts showing two distinct populations (●, *n=17*) and (o, Δ). Also shown is the spectrum for an oocyst without internal contents (*). Solid lines show the best fit from the multi-shell model using values listed in Table 6.5. Mean rotation rate shown, with error bars representing one standard deviation (conductivity 1 mS m^{-1}).

	Cyclospora cayetanensis			
	Unsporulated		Sporulated	
	Viable	Non-viable	Viable	Non-viable
Dimensions (μm)	9[a]	9[a]	9[a]	#
Wall thickness (nm)	113[a]	113[a]	113[a]	#
Membrane thickness (nm)	9 ± 0.5[c]	9 ± 0.5[c]	9 ± 0.5[c]	#
Permittivity (ε_r)				
Interior	50[b]	50[b]	50[b]	#
Membrane	4 ± 0.5[c]	4 ± 0.5[c]	4 ± 0.5[c]	#
Wall	60[b]	60[b]	60[b]	#
Conductivity (S m^{-1})				
Cytoplasm	0.8 ± 0.1[c]	0.2 ± 0.03[c]	0.8 ± 0.1[c]	#
Membrane	(5.5±0.3)×10^{-6} [c]	(1± 0.1)×10^{-5} [c]	(8±0.5)×10^{-6} [c]	#
Wall	0.09 ± 0.01[c]	0.01 ± 0.004[c]	0.09 ± 0.01[c]	#

none observed
reference *a*-Ortega *et al.*, 1993; *b* – Huang *et al.*, 1992 and *c* - estimated

Table 6.5 - Particle dimensions and dielectric parameter values used in the modelling of the electrorotation spectra for isolates C2 and C3 shown in Figures 6.12, 6.13, 6.14 and 6.16.

C. cayetanensis oocysts of isolate C2 were stored at room temperature (~ 20°C) to induce sporulation. 30% were found sporulated after 14 days. Excystation studies (Ortega *et al.*, 1993) on these sporulated oocysts performed at the SPDL showed that 75% excysted, indicating that the isolate contained both viable and non-viable oocysts.

A comparison between unsporulated and sporulated oocysts is shown in Figure 6.13.

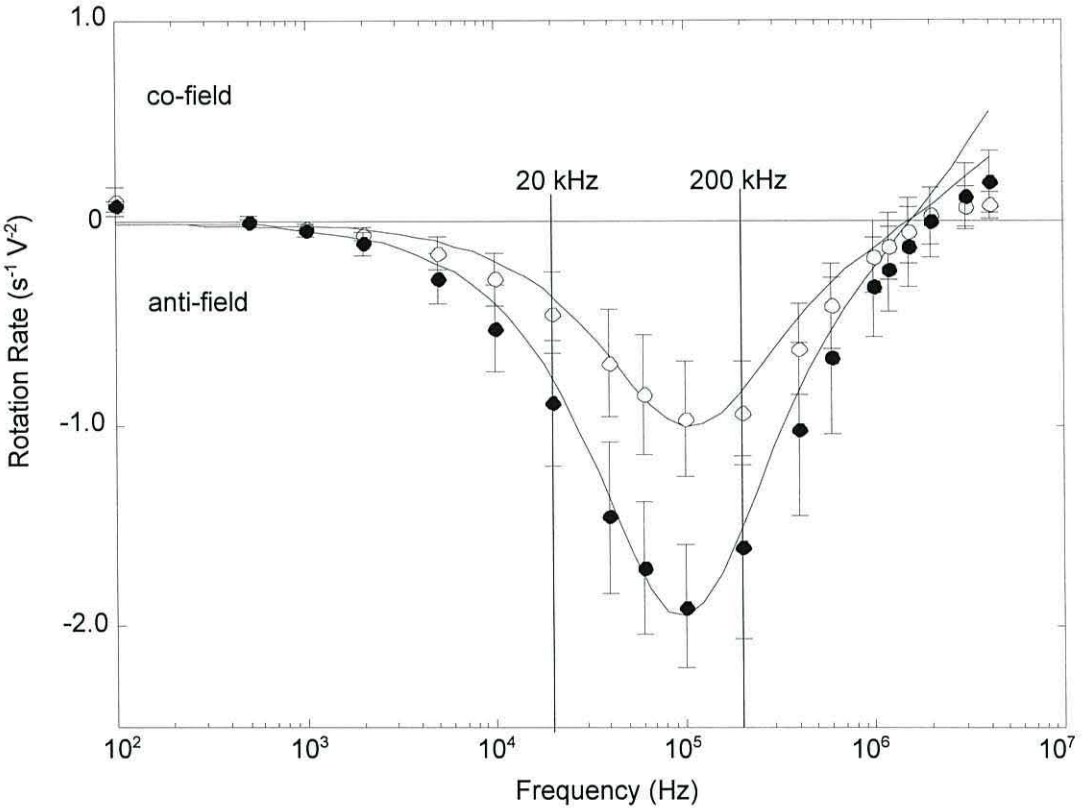

Figure 6.13 - Rotation spectra comparing 14 debris free, sporulated oocysts (o) and 17 debris free, unsporulated oocysts (•). Solid lines show the best fit from the multi-shell model using values listed in Table 6.5. Mean rotation rate shown, with error bars representing one standard deviation (conductivity 1 mS m^{-1}).

The sporulation state was determined by the presence/absence of two sporocysts within the oocyst wall as identified using phase contrast microscopy. Significant differences in the spectra are found in the frequency window from 20 kHz to 200 kHz, with a much reduced rotational velocity for the sporulated oocysts in this range. The previous spectra, for isolate C1, indicated that at a frequency of 1 MHz, unsporulated and sporulated oocysts rotate in opposite directions (Figure 6.4). Although this conclusion was valid for the limited numbers of spectra obtained for isolate C1, this

distinction is not possible for isolate C2. Importantly, however, the distinction based on the rate of rotation in the frequency window 20 kHz to 200 kHz holds for both isolates.

From the model, the change in the spectra upon sporulation can be considered to be primarily associated with a slight increase in oocyst membrane conductivity. It must be noted, however, that whereas the multi-shell model enables accurate determinations to be made of the dielectric properties of the outermost membrane and wall of the oocyst, at best it can only provide an approximate indication of any changes occurring in the properties or level of complexity of internal structures (Chan *at al.,* 1997).

From TEM studies (Ortega *et al.,* 1994), a sporulated oocyst is described as possessing a two layered oocyst wall (63 and 50 nm thick respectively) surrounding two sporocysts, each with walls 62 nm thick surrounding a plasma membrane. Within each sporocyst are two membrane-bound sporozoites. These complex internal features may explain the deviation of the fitted curves in Figure 6.13 from the experimental observations at the higher frequencies, where the electrorotation properties are regarded as being more sensitive to the internal structure of particles (Pethig, 1991).

To verify this assumption another shell was added to the model, to represent a sporocyst wall, and the membrane thickness increased to represent the sporocyst membranes (Figure 6.14). The approximation is useful to observe the effects the extra shell has on the model. The parameter values used were taken from Table 6.1 for an unsporulated oocyst. The sporocyst wall was given the same properties as the oocyst wall. Figure 6.14 shows that the addition of an extra shell reduces the anti-field rotation rate. The addition of the sporocyst wall shell and thickening of the membrane reduces the anti-field rotation rate, increases the anti-field peak rotation frequency and increases the high frequency cross-over frequency.

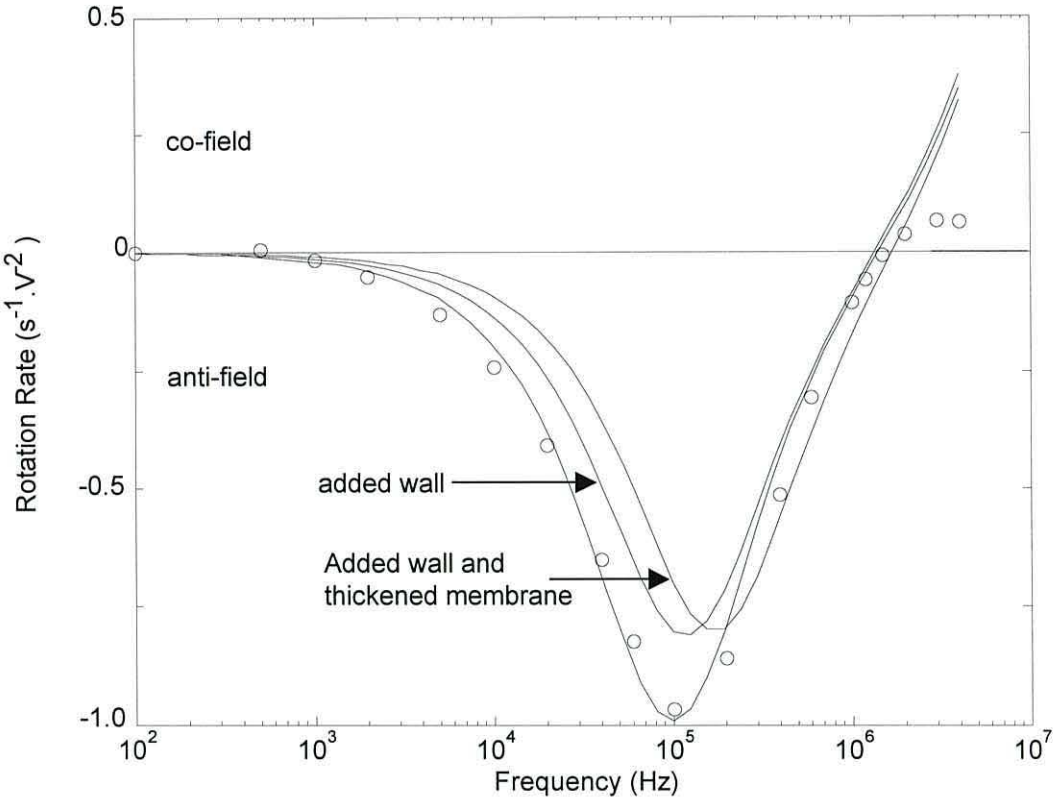

Figure 6.14 – Effect of adding a new wall and thickened membrane shell to the model. Solid lines indicate model fits using the data from Table 6.1 for a sporulated oocyst. Experimental data for a debris free, sporulated oocyst are given for comparison (o) (conductivity 1.0 mS/m).

To obtain a better fit to the experimental data, the parameters were modified from those listed in Table 6.1. The new fitted parameters are given in Table 6.6, but at frequencies > 1 MHz there is still not a good fit to the experimental data (Figure 6.15). The relative permittivity of the membrane had to be increased from 5 to 7, which is consistent with a thicker lipid structure with more proteins and carbohydrates. The interior conductivity of the oocyst had to be reduced to 0.3 S/m, which is also consistent with a reduction in the amount of conductive material bound within the two sporozoites within each sporocyst. A reduction in the membrane conductivity, from 8×10^{-6} S/m to 1×10^{-6} S/m could indicate that the membranes of the sporozoites perform different functions compared to the unsporulated oocyst membrane, which needed to interact with the external environment in order for the oocyst to sporulate. The conductivity and permittivity of both walls remained the same. Above 1 MHz the model still does not follow the experimental data well.

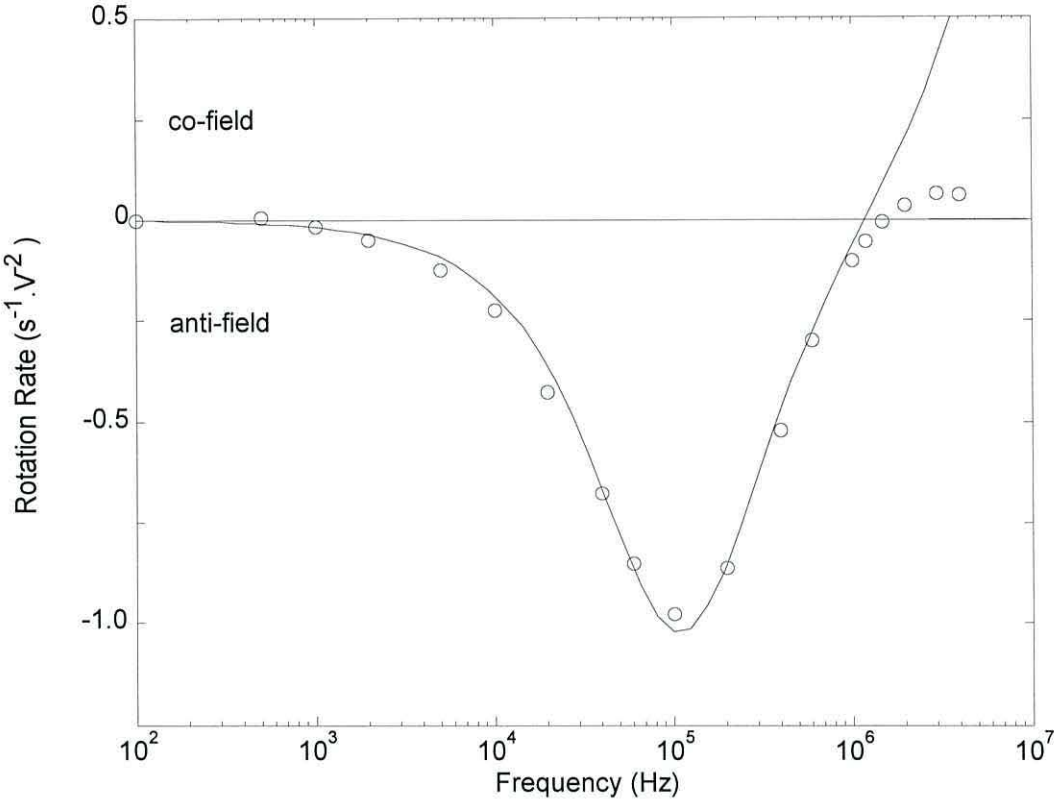

Figure 6.15 – Best fit of the 3-shell model using the data from Table 6.6 for a sporulated oocyst compared to the experimental data for a sporulated oocyst (o) (conductivity 1.0 mS/m).

	Sporulated *Cyclospora*	
	2 shell model	3 shell model
Dimensions (μm)	9[a]	9[a]
Oocyst wall thickness (nm)	113[a]	113[a]
Sporocyst wall thickness (nm)	n/a	62[b]
Membrane thickness (nm)	9[c]	15[d]
Permittivity (ε_r)		
Interior	50[e]	50[e]
Membrane	5[e]	7[d]
Oocyst wall	60[e]	60[e]
Sporocyst wall	n/a	60[e]
Conductivity (S m^{-1})		
Cytoplasm	0.4 ± 0.1[d]	0.3 ± 0.03[d]
Membrane	$8 \times 10^{-6} \pm 0.3$[d]	$1 \times 10^{-6} \pm 0.1$[d]
Oocyst Wall	0.09 ± 0.01[d]	0.09 ± 0.01[d]
Sporocyst wall	n/a	0.09 ± 0.01[d]

reference
a-Ortega *et al.*, 1993; *b*- Ortega et al., 1994; *c* - Pethig *et al*, 1995; *d* - fitted and *e* – Huang *et al.*, 1992.

Table 6.6 - Particle dimensions and dielectric parameter values used in the modelling of the electrorotation spectra shown in Figure 6.15 for a sporulated oocyst.

6.5 Analysis of Human Isolate C3

41 spectra of unsporulated oocysts were obtained from isolate C3 at a suspending medium conductivity of 1 mS m^{-1}. The spectra are shown in Figure 6.16 and are of two distinct types, corresponding to viable and non-viable oocysts. These electrorotational spectra confirm that the best method to distinguish between viable and non-viable oocysts is by the characteristic difference in the peak anti-field rotation rate. The high frequency cross-over point is not a reliable indicator of viability, as it varies between isolates (Figures 6.4, 6.12 and 6.16).

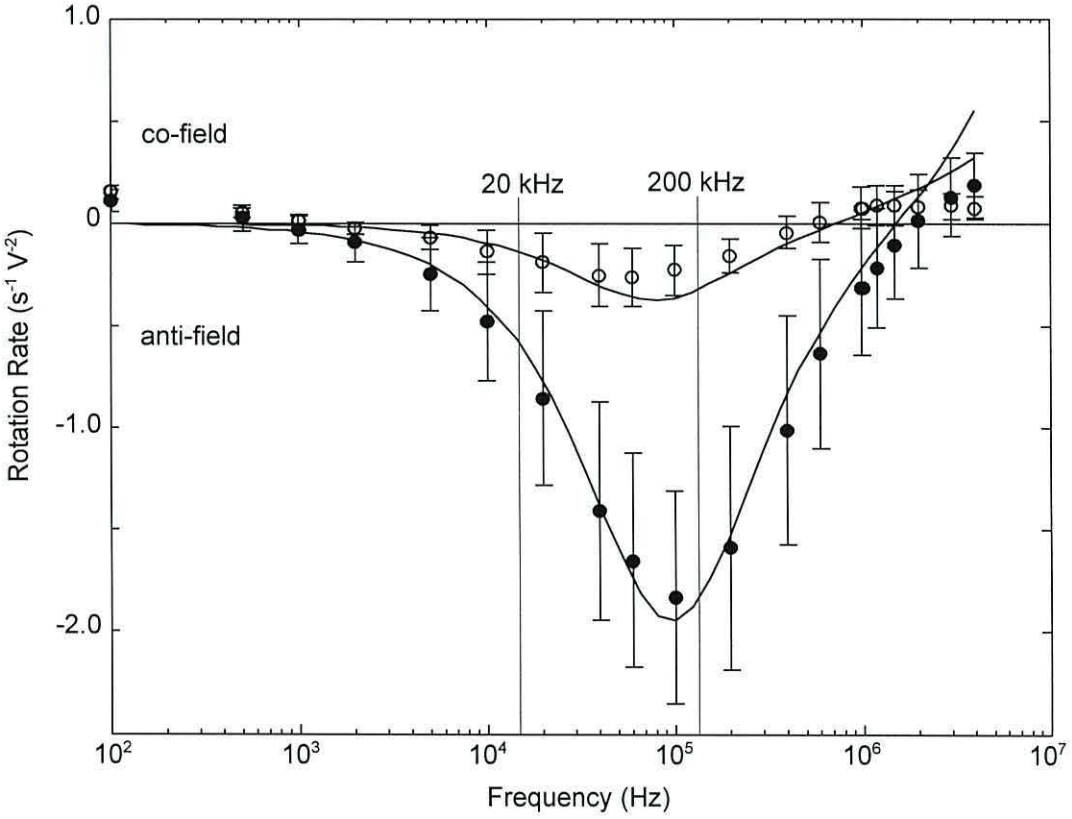

Figure 6.16 – Rotation spectra of 41 debris free, unsporulated oocysts showing two distinct populations, viable (•, *n=29*) and non-viable (o, n=12). Solid lines show the best fit from the multi-shell model using values listed in Table 6.5. Mean rotation rate shown, with error bars representing one standard deviation (conductivity 1 mS m^{-1}).

6.6 Conclusions

While storage in 2.5% potassium dichromate solution does not affect biological viability, it has been shown that the dielectric properties of the human source oocysts are affected, especially at the oocyst surface. Storage in formalin has been shown to affect the dielectric properties of baboon source oocysts. Differences observed between baboon and human source oocysts need further investigation, but indicate that the electrorotation technique can detect differences in the species of oocyst investigated, which may be of importance in risk determination of water and food where species are differentially infective to humans.

In the absence of any vital dye staining technique, electrorotation velocity at the anti-field maxima can be used to determine *C. cayetanensis* oocyst viability. Previously published electrorotation data from other protozoans (Goater *et al.,* 1997), fungi (Huang *at al.,* 1992) and animal cells (Gundel *et al.,* 1989) support this.

The ability to determine the sporulation state of *C. cayetanensis* oocysts has also been demonstrated with electrorotation. This detection of internal content compartmentalisation is of importance as the oocysts are only potentially infectious following sporulation. Determining oocyst viability and sporulation state is therefore important in assessing the risk associated with potentially contaminated water. Currently only trained laboratory workers can identify the degree of sporulation by observing morphological indicators, as oocysts of *C. cayetanensis* do not change their overall dimensions upon sporulation. Electrorotation has a clear advantage over PCR, as Herwaldt (2000) has shown that PCR cannot distinguish between sporulated and unsporulated oocysts.

Within the known limitations of the multi-shell model for characterising bioparticles of complex structure (Chan *et al.,* 1997), the fitted data indicates that the membrane conductivity of non-viable *C. cayetanensis* oocysts is significantly greater than that of viable ones. The corresponding decrease in the internal conductivity of the oocysts confirms that this loss of viability is associated with a physical degradation of the membrane and the loss of its ability to act as a barrier to passive ion flow.

6.7 References

Burt, J. P. H. **(1990)** Biotechnological Applications of Dielectrophoresis. *PhD Thesis*. University of Wales, Bangor

Chan, K. L., Gascoyne, P. R. C., Becker, F. F. and Pethig, R. **(1997)** Electrorotation of liposomes : verification of dielectric multi-shell model for cells. *Biochim. Biophys. Acta* **1349** 182-196

Goater A. D., Burt, J. P. H. and Pethig R. **(1997)** A combined travelling wave dielectrophoresis and electrorotation device : applied to the concentration and viability of *Cryptosporidium*. *J. Phys. D : Appl. Phys.* **30** L65-L69

Goater, A.D. **(1999)** AC Electrokinetic Bioassays. Development of Electrorotational Assay for Analytes in Water. *Ph.D Thesis* University of Wales, Bangor

Gundel, J., Wicher, D. and Matthies, H. **(1989)** Electrorotation as a viability test for isolated single animal cells. *Stud. Biophys.* **133** 5-18

Herwaldt, B. L. **(2000)** *Cyclospora cayetanensis* : A review focussing on the outbreaks of cyclosoriasis in the 1990s. *Clin. Infect. Dis.* **31** 1040-1057

Huang, Y., Hölzel, R., Pethig, R. and Wang, X.B. **(1992)** Differences in the ac electrodynamics of viable and non-viable yeast cells determined through combined dielectrophoresis and electrorotation studies. *Phys. Med. Biol.* **37(7)** 1499-1517

Huang, Y., Wang, X-B, Tame, J. & Pethig, R. **(1993)** Electrokinetic behaviour of colloidal particles in travelling electric fields: Studies using yeast cells. *J. Phys. D-Appl. Phys.* **26** 1528-1535.

Lopez, F. A., Manglicmot, J., Schmidt, T. M., Yeh, C., Smith, H. V. and Relman, D. A. **(1999)** Molecular characterisation of *Cyclospora*-like organisms from baboons. *J. Infect. Dis.* **179** 670-676

Mitchell, C. **(2001)** AC Electrokinetic Bioassays. Development of electrorotation assay for detection of viable and non-viable bacteria and macromolecules. *PhD Thesis, University of Wales.*

Ortega, Y. R., Sterling, R., Gilman, R. H., Lama, V. A., Diaz, F. **(1993)** *Cyclospora* Species – A New Protozoan Pathogen of Humans. *New Eng. J. Med.*1306 – 1312

Ortega, Y. R., Gilman, R. H. and Sterling, C. R. **(1994)** A new coccidian parasite (apicomplaxe:Eimeriidae) from humans. *J. Parisitology* **80(4)** 625-629

Pethig, R. **(1991)** Applications of A.C. electrical fields to the manipulation and characterisation of cells. **In** Karube, I. (ed.) Automation in Biotechnology. Elsevier, Amsterdam, The Netherlands.

Pethig, R. and Huang,Y. **(1995)** Dielectrophoretic and electrorotation behaviour of cells – Theory and experiment. *Bioelectrochem. Cell. Tissues* 208-244

Schauenstein, E., Esterbauer, H. and Zollner, H. **(1977)** *Aldehydes in Biological Systems.* Pion, London.

Smith, H. V., Paton, C. A., Mtambo, M. M. A. and Girdwood, R. W. A**. (1997)** Sporulation of *Cyclospora* sp. Oocysts. *App. Environ. Microbiol.* **63(4)** 1631-1632

Zubay, G. L. **(1983)** *Biochemistry*. Addison-Wesley, London.

Chapter 7

Electrorotation of *Ascaris suum*

7.1 Introduction

In this chapter, the electrorotation spectra for eggs of three isolates of *Ascaris suum* are presented. A comparison is then made between the spectra from unfertilised and fertilised eggs and the results from an investigation into sets observed in the fertilised spectra using the ellipsoidal multi-shell model are reported.

7.2 Effect of decortication

Initial attempts to obtain electrorotation spectra of *A. suum* eggs were unsuccessful due to their large size and highly adhesive outer uterine layer. Removing this layer by decortication, as described in Section 5.2, spectra were successfully obtained. However, it was not possible to reliably reproduce the decortication process, as for each isolate differing thicknesses of the uterine layer were removed. For some isolates, the decortication process removed the vitelline and uterine layers and killed the organisms (Figure 7.1a, b). To obtain reliable data, only spectra from eggs from the same isolate, that had been decorticated at the same time and had the presence of the vitelline layer confirmed by optical microscopy, were compared.

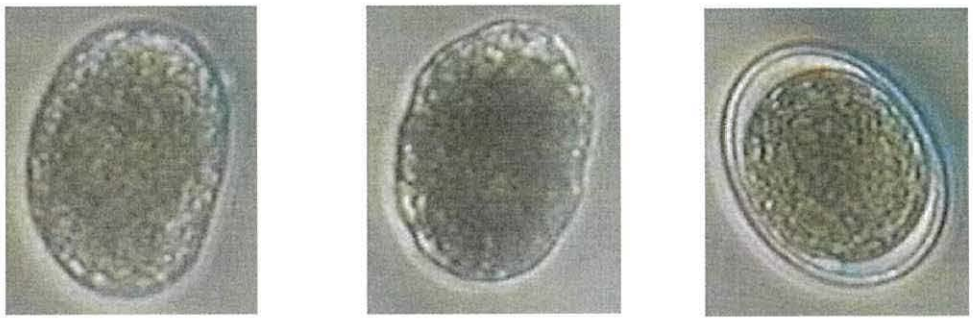

a b c

Figure 7.1 – *Ascaris suum* isolate A8 eggs (a and b), damaged by the decortication process, compared to an egg from isolate A2 (c), with a visibly intact vitelline layer.

7.3 Ruptured Eggs

Fertilised eggs with a rupture in the vitelline, chitinous and lipid layers, which allows the interior to be filled with the suspending medium and the majority of the contents to disperse, are non-viable and known as shells (Figure 7.2).

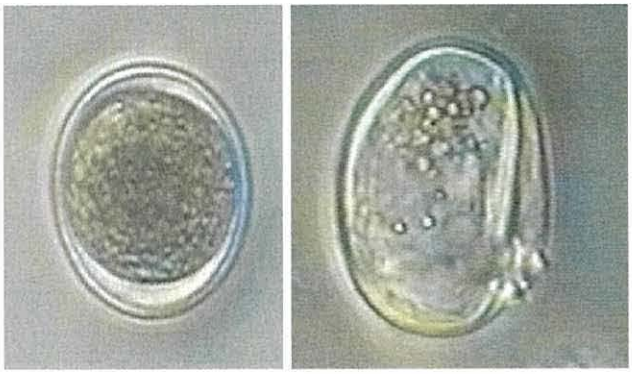

Figure 7.2 – A fertilised, viable egg (left), compared to a non-viable shell (right). Note the uniformly distributed contents of the viable egg, and the intact, refractile wall.

An egg which has been ruptured will still have a resistive membrane for a period of time after the damage. Hence, the shell spectrum should have a reduced rotation rate compared to a viable egg, and a faster rotation rate when compared to a cell whose membrane is no longer functioning. There should be significant differences between the spectra of shells and viable eggs besides a change in the rotation rate, due to the change in the membrane and interior dielectric properties. This is observed for two shell spectra compared to unruptured, intact, similarly sized eggs with contents in Figure 7.3. The shell spectra have a reduced anti-field rotation rate, a reduced anti-field peak rotation rate frequency, a much reduced high frequency cross-over frequency, a higher co-field rotation rate and a reduced co-field peak rotation rate frequency. As expected, the modelling data (Table 7.1) show that the differences between the two spectra are due to an increase in the lipid layer conductivity and a decrease in the conductivity of the vitelline and chitinous layers, as expected in the non-viable shell samples. Thus at 800 kHz, a viable, fertilised egg should rotate in the anti-field region, and a non-viable egg in the co-field direction, allowing for rapid discrimination.

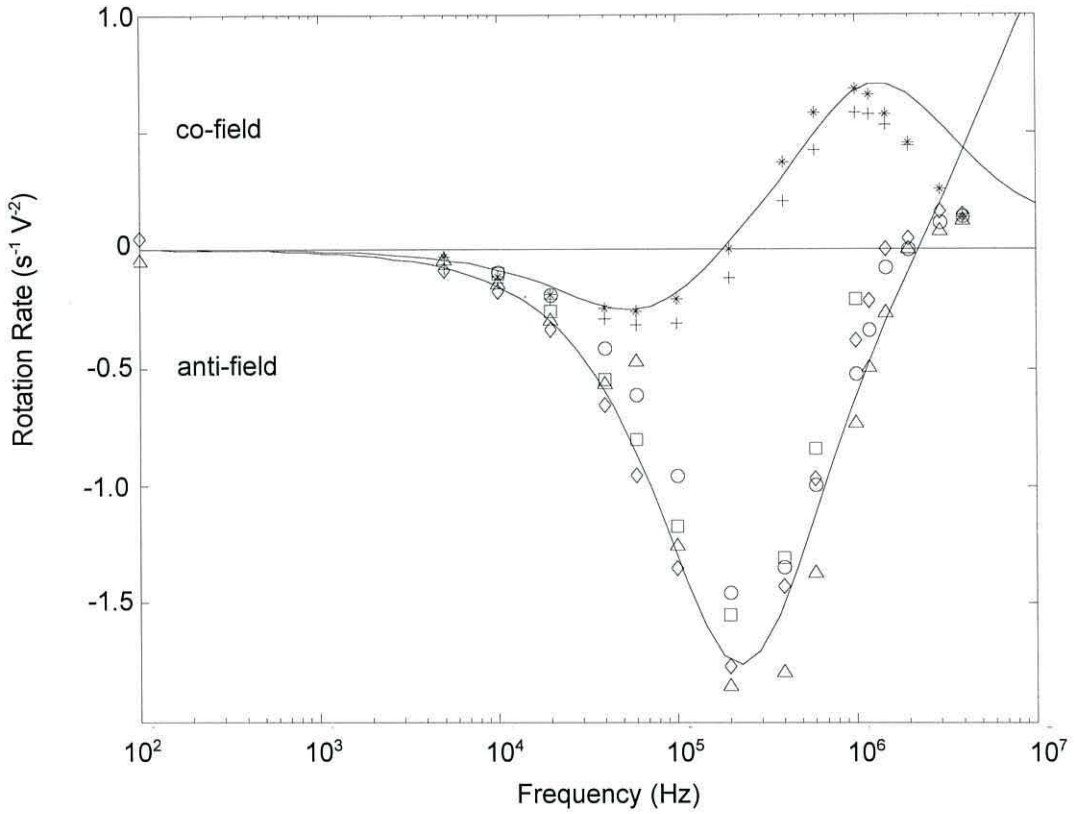

Figure 7.3 – Electrorotation spectra of 4 fertilised eggs (open symbols) of isolate A1 compared with the 2 shell spectra (+, *) (conductivity 0.4 mS/m).

	Fertilised *Ascaris suum*	
	non-viable (shell)	viable
Dimensions (μm)	60 x 44[a]	60 x 44[a]
Vitelline Layer thickness (nm)	500[b]	500[b]
Chitinous Layer thickness (nm)	1600[b]	1600[b]
Lipid Membrane thickness (nm)	100[b]	100[b]
Relative Permittivity (ε_r)		
Vitelline Layer	60[c]	60[c]
Chitinous Layer	60[c]	60[c]
Lipid Membrane	6[c]	6[c]
Cytoplasm	50[c]	50[c]
Conductivity (S/m)		
Vitelline Layer	0.02[d]	0.05[e]
Chitinous Layer	0.03[d]	0.05[e]
Lipid Membrane	5×10^{-6} [d]	1×10^{-7} [f]
Cytoplasm	0.01[d]	0.8[g]

References : *a* - Foor, 1967; *b* – Darben, 2002; *c* - Huang *et al.*, 1992; *d* –fitted *e* – Asami *et al.*,1976; *f* - Gimsa *et al.*, 1991; g – Wang *et al.*, 1994

Table 7.1 - Values used for initial modelling of *A. suum* spectra in Figure 7.3.

7.4 Effect of high suspending medium conductivity

Figure 7.4 shows spectra for fertilised eggs only at a higher conductivity of 2.2 mS/m. Here, the peak rotation frequencies shift towards higher frequencies compared to the spectra seen in Figure 7.3, as predicted in the modelling Chapter (Section 4.6.1).

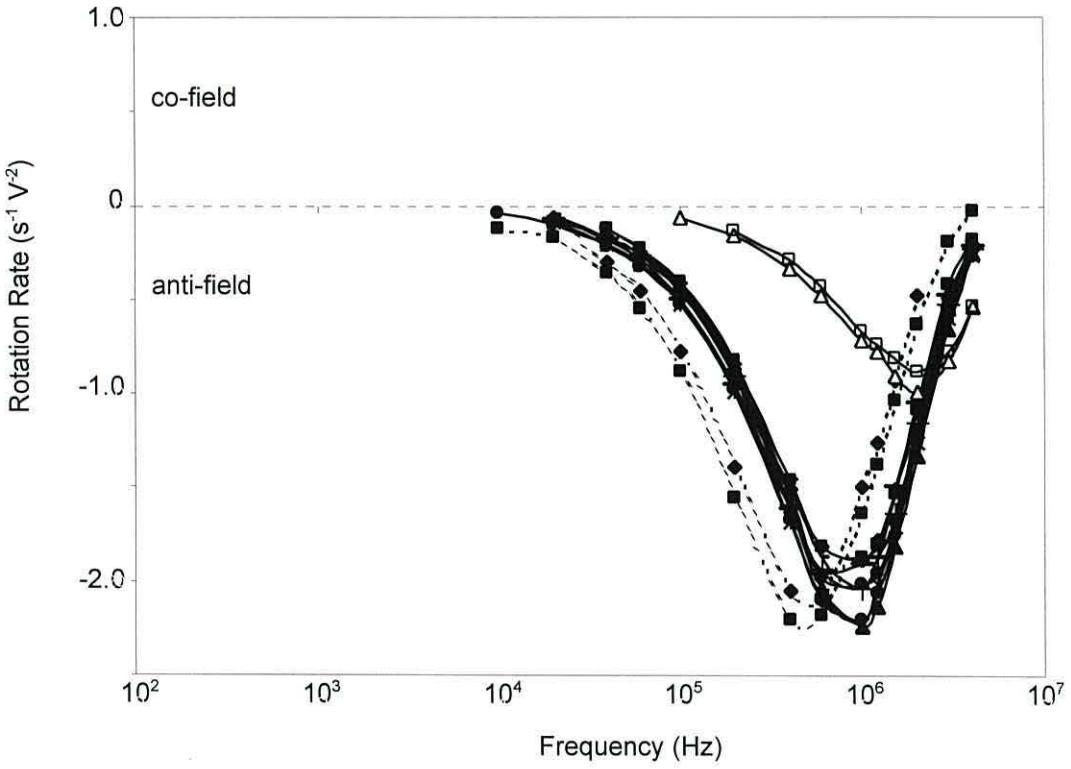

Figure 7.4 – Rotation spectra of 11 fertilised eggs of isolate A1 (conductivity 2.2 mS/m).

There were no co-field rotations observed at either low or high frequencies as seen previously in Figure 7.3. With a higher conductivity suspending medium, there are less charge differences between the interior of the egg and the exterior solution. This results in the induced torque being less than that for the lower external conductivity situation (Figure 7.3). This reduced torque is unable to overcome the drag and friction between the egg and the chamber base, resulting in no low frequency rotation. High frequency co-field rotation would be observed if the frequency generator used in this work could reliably provide frequencies greater than 5 MHz.

There are 3 sets grouped around three different anti-field peak rotation frequencies to note in the spectra, which are discussed in more detail in the next sections.

7.5 Analysis of Spectra of Isolate A2

124 spectra of *A. suum* isolate A2 were obtained. Figure 7.5 shows spectra of 22 unfertilised and fertilised eggs at a conductivity of 0.55 mS/m. Four sets can be seen in the spectra; the three sets seen previously (Figure 7.4) that rotate in the anti-field region with peak rotation frequencies of 200 kHz (solid lines, open symbols), 600 kHz (dashed lines, solid symbols) and 1.2 MHz (solid lines) and a fourth set that rotates in the co-field direction with a peak rotation frequency of 1 MHz,

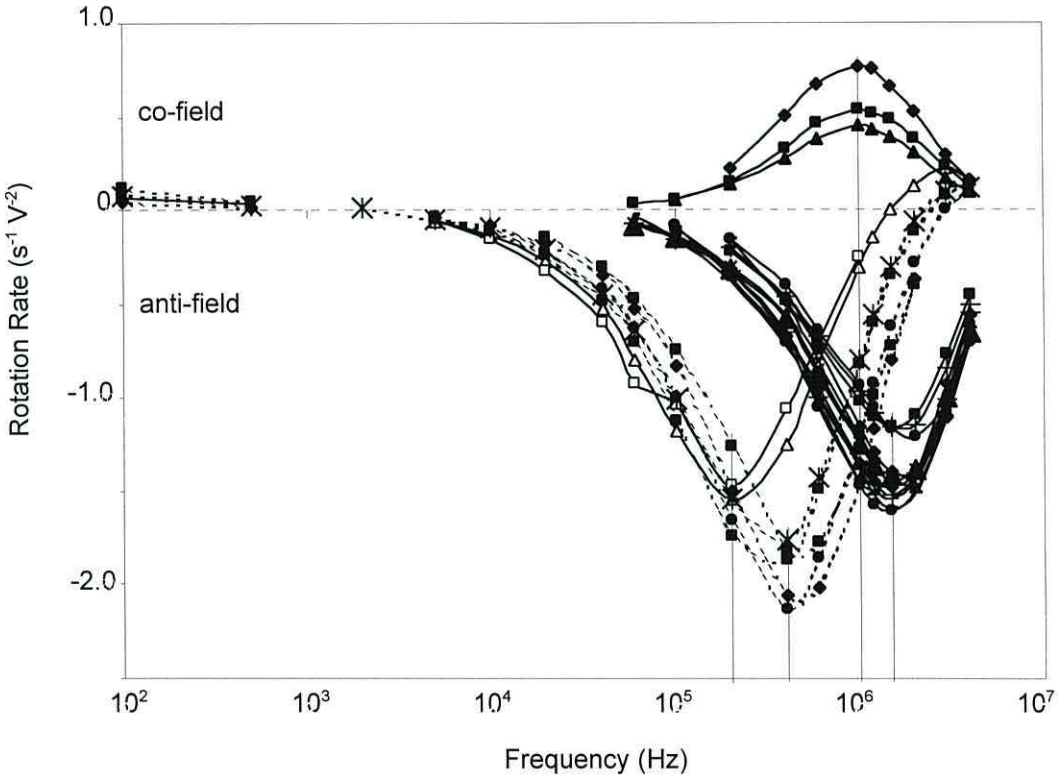

Figure 7.5 – Electrorotation spectra of 22 decorticated *A. suum* eggs, isolate A2, showing three sets in the anti-field region, and one in the co-field region (conductivity 0.55 mS/m).

The spectra with the co-field high frequency peak at 1 MHz represent unfertilised eggs only, as determined by morphological indicators. All of the spectra in the anti-field region are from fertilised eggs. The difference in direction of rotation between fertilised and unfertilised eggs can be used for easy identification of the fertilisation state at frequencies greater than 10 kHz and less than 1 MHz. Differences between the three anti-field spectra sets based on the size of the eggs or visible egg contents could not be attributed. The lack of data around 1 KHz is due to the induced torque being unable to overcome the friction between the eggs and the rotation chamber base.

Further spectra of the same isolate at a different conductivity (0.65 mS/m) are shown in Figure 7.6.

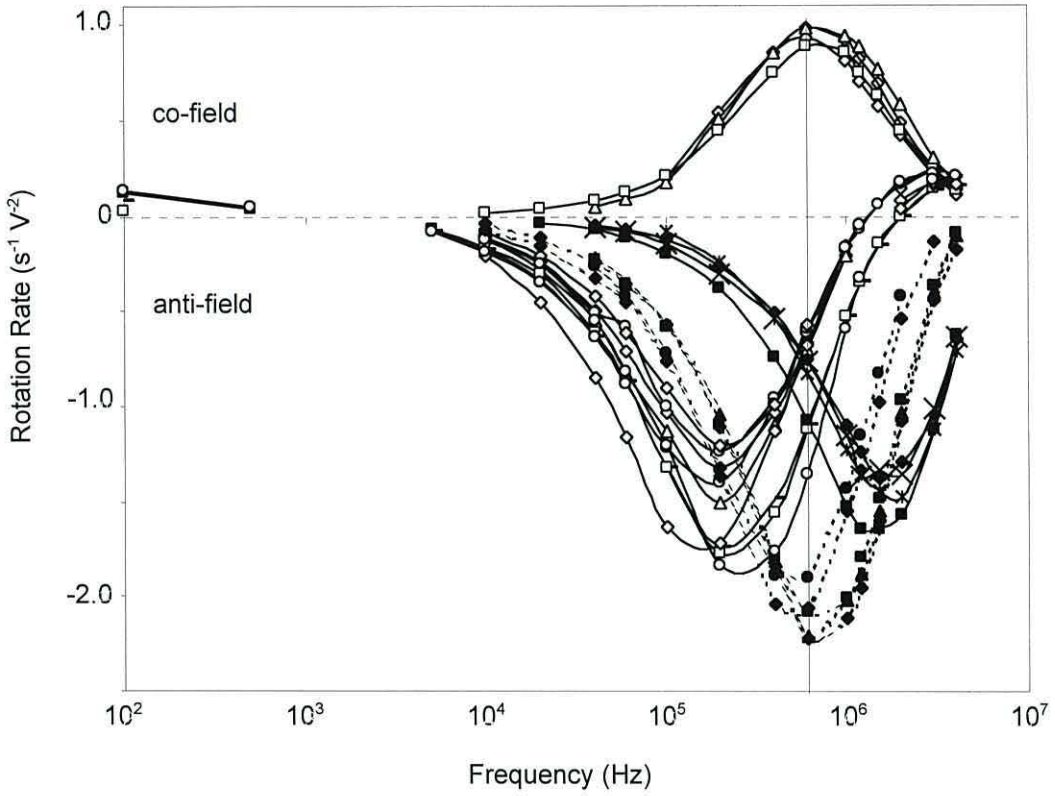

Figure 7.6 – Electrorotation spectra of 26 eggs of isolate A2 eggs (conductivity 0.65 mS/m).

The unfertilised eggs again rotate only in the co-field region. Their peak rotation frequency has decreased slightly, to 800 kHz, from the 1 MHz seen previously (Figure 7.5). There are again three sets in the anti-field peak rotation region, at 200 kHz, 600 kHz and 1.2 MHz, all associated with fertilised eggs. Differences between the three anti-field sets based on the size of the eggs or visible egg contents could not be attributed. There appear to be no common factors linking the eggs in each anti-field peak-rotation frequency set. The differences are probably due to the development of the egg, such as the thickening of the vitelline layer and the changes in the lipid layer properties as discussed in Chapter 2. To investigate the possible causes of these three sets, the electrorotational response was modelled using the ellipsoidal multi-shell model.

7.6 Modelling

Of the 124 spectra obtained of debris free eggs of isolate A2, 118 were in the conductivity range 0.65 ± 0.1 mS/m, and so could be compared, and 113 were accurately measured by a calibrated haemocytometer (as described in Chapter 5). There are two distinct morphological types of *A. suum* eggs, fertilised eggs that are oval, and unfertilised eggs that are more elliptical. By plotting the length and widths of these eggs it is easy to see the difference between the two types (Figure 7.7). The mean values of the sizes of the two types of eggs were used in the ellipsoidal multi-shell model.

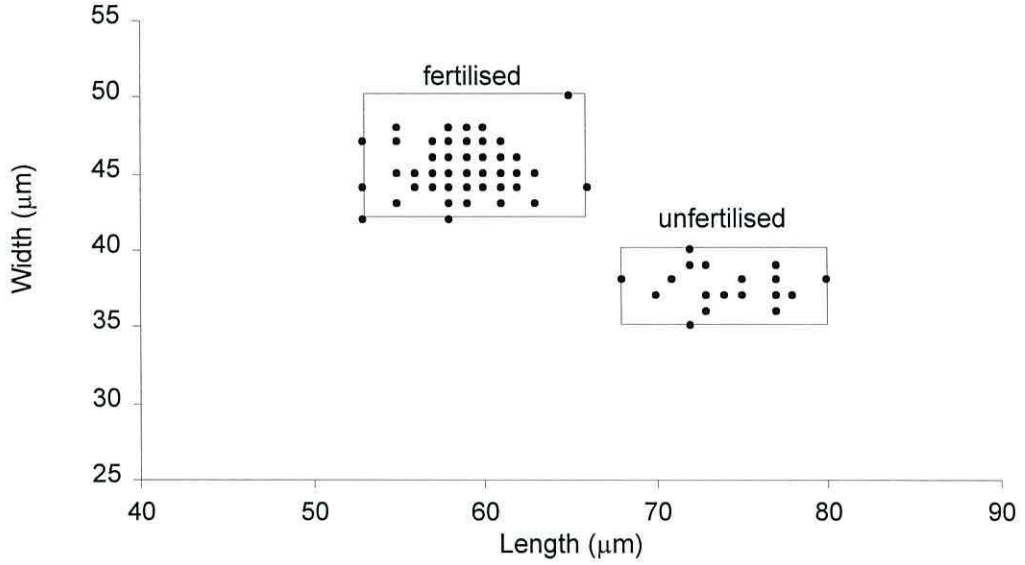

Figure 7.7 – Dimensions of 113 eggs of *A. suum* isolate A2, showing two distinct types, unfertilised and fertilised. The boxes indicate the maximum and minimum values measured.

Using the ellipsoidal multi-shell model described in Chapter 4, electrorotation spectra of fertilised and unfertilised eggs of *A. suum* were simulated (Figure 7.8). The physiological data used is given in Table 7.2, and was taken from the relevant literature. As can be seen from Figure 7.8, the model fits reasonably well with the fertilised spectra data, but poorly with the unfertilised spectra data above 2 MHz. To obtain the unfertilised spectra fit, a value of 0.01 mS/m for the cytoplasm conductivity was required, which is typically associated with a non-viable organism, suggesting that the model used might not be able to accurately predict the behaviour of unfertilised *Ascaris* spectra. As there is a large degree of variance in the fertilised spectra data, the data was split into the three peak anti-field rotation sets and the model used to investigate the differences between them.

	Ascaris suum	
	Unfertilised	Fertilised
Dimensions (μm)	74 x 38[a]	60 x 44[a]
Vitelline Layer thickness (nm)	400[b]	500[b]
Chitinous Layer thickness (nm)	-	1600[b]
Lipid Membrane thickness (nm)	-	100[b]
Relative Permittivity (ε_r)		
Vitelline Layer	60[c]	60[c]
Chitinous Layer	-	60[c]
Lipid Membrane	-	6[c]
Cytoplasm	50[c]	50[c]
Conductivity (S m^{-1})		
Vitelline Layer	0.05[d]	0.05[d]
Chitinous Layer	-	0.05[d]
Lipid Membrane	-	1×10^{-7}[e]
Cytoplasm	0.01[f]	0.8[g]

References : *a* - Foor, 1967; *b* – Darben, 2002; *c* - Huang *et al.*, 1992; *d* – Asami *et al.*, 1976; *e* - Gimsa *et al.*, 1991; *f* - fitted and *g* – Wang *et al.*, 1994;

Table 7.2 - Values used for modelling of *A. suum* spectra shown in Figure 7.8.

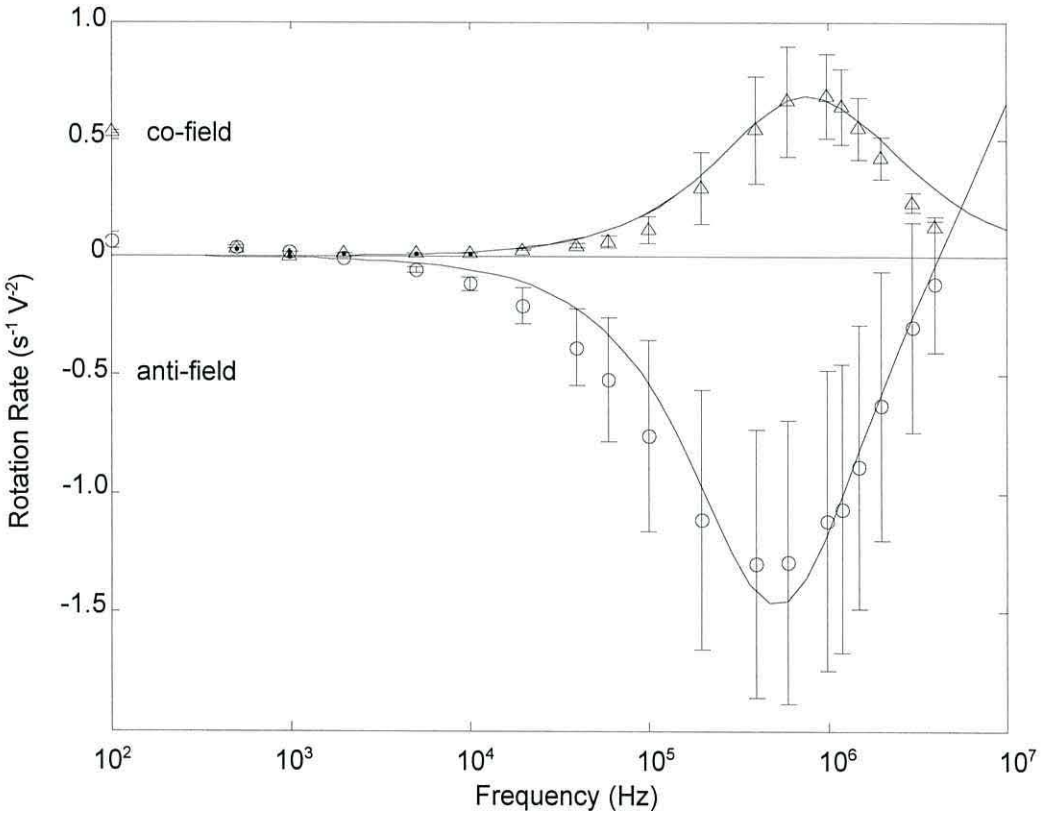

Figure 7.8 – Rotation spectra of *Ascaris suum* eggs comparing 14 unfertilised (Δ) and 104 fertilised (o) eggs. Error bars represent the mean rotation rate and one standard deviation. Solid lines show the best fit from the multi-shell model using values listed in Table 7.2 (conductivity 0.65 ±0.1 mS/m).

7.6.1 Unfertilised egg spectra

Using the physiological values given in Table 7.2 for the unfertilised eggs, the difference between the largest egg (80x40 μm) and the smallest (68x34 μm) egg were modelled, to investigate how this would affect the spectra (Figure 7.9).

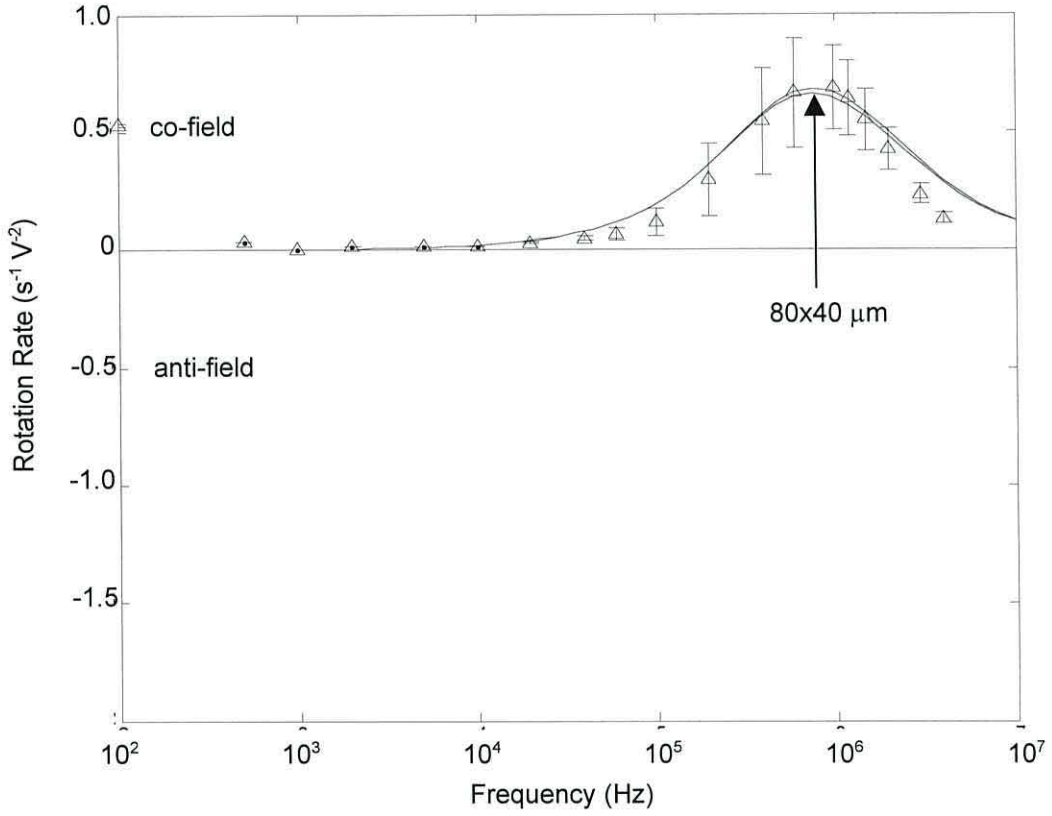

Figure 7.9 – Effect of changing the size of the unfertilised egg from the largest size observed (80 x 40 μm) to the smallest (68 x 34 μm). Solid lines show the best fit from the multi-shell model using values listed in Table 7.2 for the two limiting particle sizes. Error bars represent the mean rotation rate and one standard deviation (conductivity 0.65 ±0.1 mS/m).

Although there is an increase in the mass of the cytoplasm, and to a lesser extent, the mass of the various layers, the difference in size does not affect the unfertilised spectra to any significant degree.

7.6.2 Fertilised egg spectra

Due to the lack of attributable trends in the fertilised eggs that produced the three sets in the anti-field spectra (Figures 7.5 and 7.6), the spectra were examined on a more global basis. The number of spectra obtained for each specific peak rotation frequency was plotted (Figure 7.10).

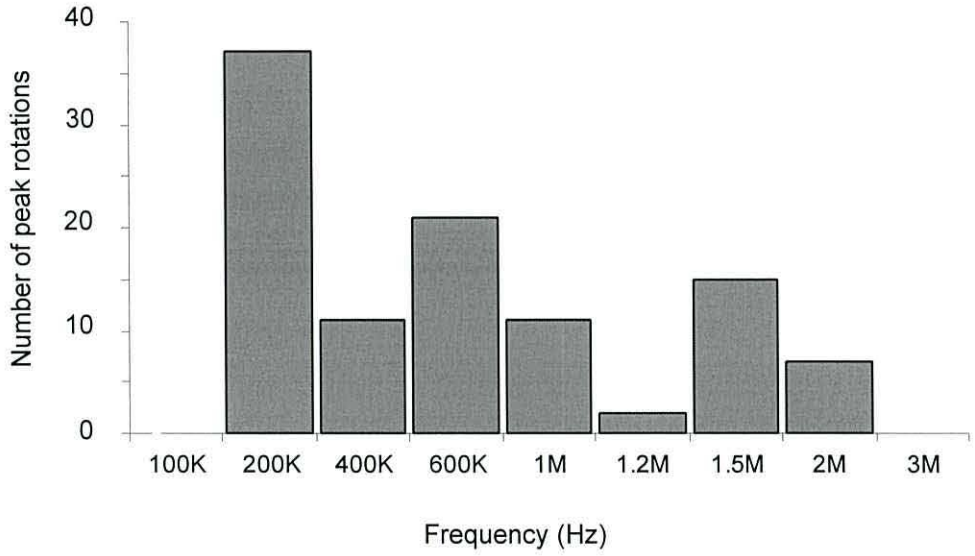

Figure 7.10 – A histogram of anti-field peak frequency distribution among 104 fertilised eggs. There are three regions of interest around the frequencies 200 kHz, 600 kHz and 1.5 MHz.

There are three regions of interest, around the peak rotation frequencies of 200 kHz, 600 kHz and 1.5 MHz. The spectra from these three regions were separated into individual plots and modelled (Figures 7.11 to 7.13).

7.6.3 Fertilised egg spectra – 200 kHz peak

To obtain the best fit of the model to the experimental data for the fertilised eggs with a peak rotation frequency of 200 kHz, a number of modelling parameters had to be changed (Table 7.3, Figure 7.11). The effects of the variations in size from the largest observed egg (61x48 μm) and the smallest egg (53x42 μm) are also shown.

	Initial values	New values
Cytoplasmic conductivity (Sm^{-1})	0.8	0.5
Lipid membrane conductivity (Sm^{-1})	1×10^{-7}	5×10^{-6}
Chitinous Layer conductivity (Sm^{-1})	0.05	0.09
Lipid membrane permittivity (ε_r)	6	15

Table 7.3 – Changes in parameter values from those listed in Table 7.2 needed to obtain the best fit of the model to the fertilised egg peak rotation frequency of 200 kHz shown in Figure 7.11.

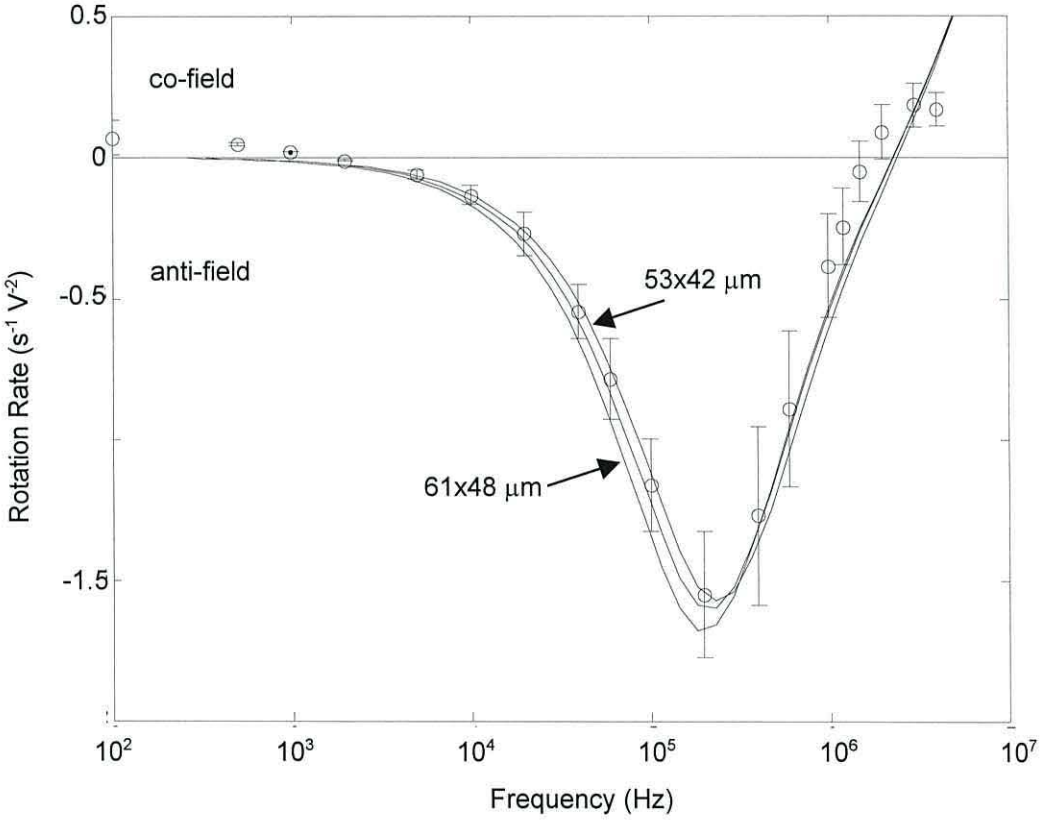

Figure 7.11 – Rotation spectra of 36 fertilised *A. suum* eggs with the peak rotation frequency 200 kHz. Solid lines show the best fit from the multi-shell model as listed in Tables 7.2 and 7.3. Error bars represent the mean rotation rate and one standard deviation (conductivity 0.65±0.1 mS/m).

The majority (92%) of the eggs that produced these spectra had internal contents that did not touch the egg wall, indicating a possible developmental stage that corresponds to this peak rotation frequency.

7.6.4 Fertilised egg spectra – 600 kHz peak

To obtain the best fit of the model to the experimental data for the fertilised egg peak rotation frequency of 600 kHz, again a number of parameters had to be changed (Table 7.4, Figure 7.12). The effects of the variations in size from the largest observed egg (65x50 μm) and the smallest egg (55x43 μm) are also shown. Only 71% of these eggs had internal contents that did not touch the egg wall.

	Initial values	New values
Lipid membrane conductivity (Sm^{-1})	1×10^{-7}	1×10^{-6}
Chitinous Layer conductivity (Sm^{-1})	0.05	0.04
Lipid membrane permittivity (ε_r)	6	4

Table 7.4 – Changes in parameter values from those listed in Table 7.2 needed to obtain the best fit of the model to the fertilised egg peak rotation frequency of 600 kHz shown in Figure 7.12.

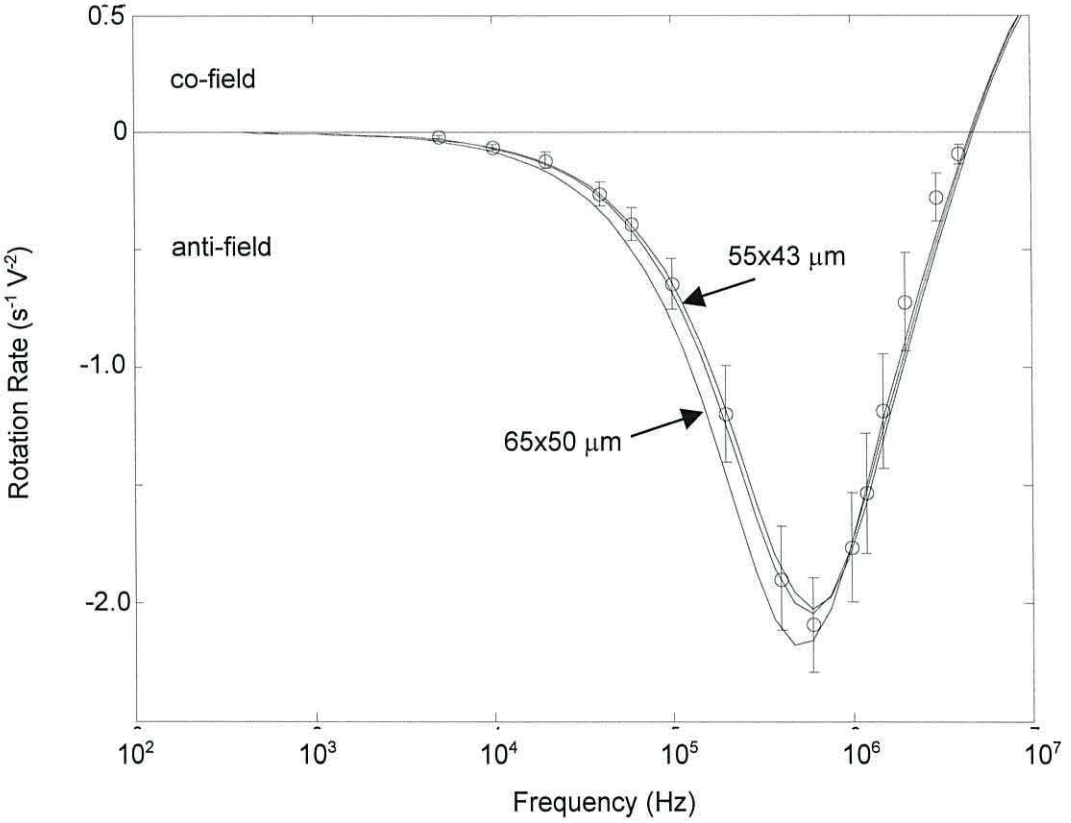

Figure 7.12 – Rotation spectra of 21 fertilised *A. suum* eggs with the peak rotation frequency 600 kHz. Solid lines show the best fit from the multi-shell model as listed in Tables 7.2 and 7.4. Error bars represent the mean rotation rate and one standard deviation (conductivity 0.65±0.1 mS/m).

7.6.5 Fertilised egg spectra – 1.5 MHz peak

To obtain the best fit of the model to the experimental data for the fertilised egg peak rotation frequency of 1.5 MHz, some parameters were once again changed (Table 7.5, Figure 7.13). The effects of the variations in size from the largest observed egg (62x48 μm) and the smallest egg (53x44 μm) are also shown. Only 22% of these eggs had internal contents that did not touch the egg wall.

	Initial values	New values
Lipid Membrane thickness (nm)	100 nm	200 nm
Lipid membrane conductivity (Sm^{-1})	1×10^{-7}	5×10^{-6}
Chitinous Layer conductivity (Sm^{-1})	0.05	0.09
Lipid membrane permittivity (ε_r)	6	3

Table 7.5 – Changes in parameter values from those listed in Table 7.2 needed to obtain the best fit of the model to the fertilised egg peak rotation frequency of 1.5 MHz shown in Figure 7.13.

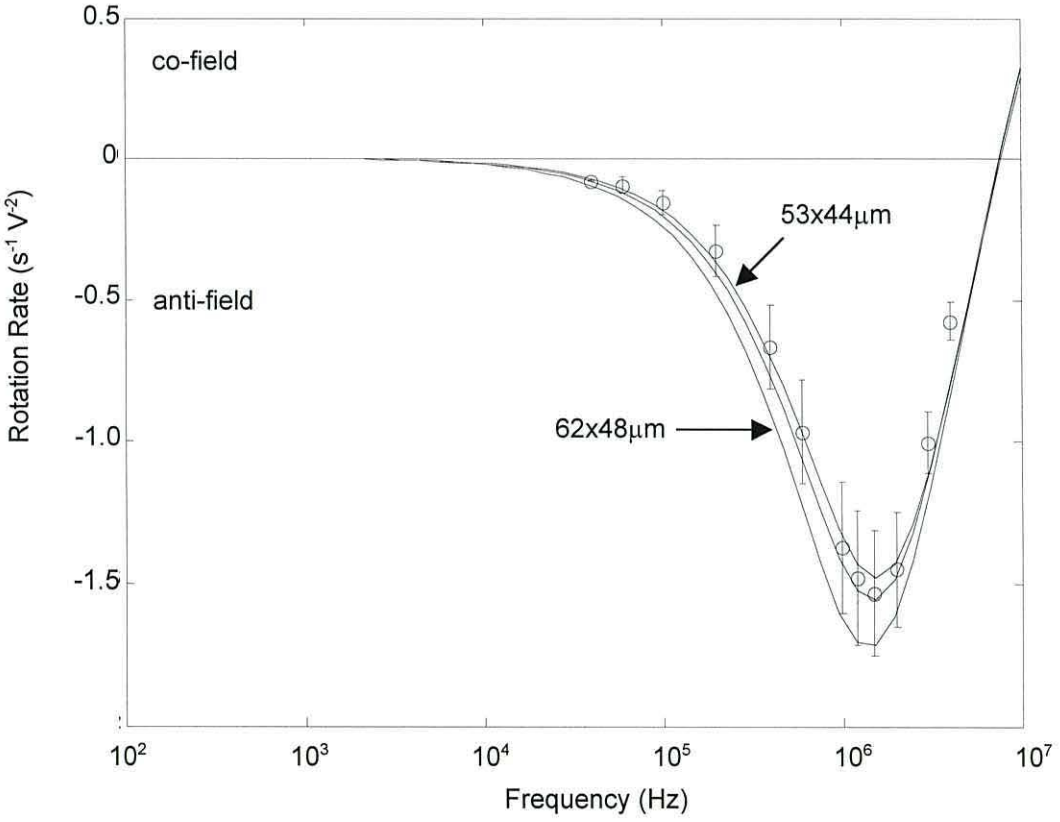

Figure 7.13 – Rotation spectra of 14 fertilised *A. suum* eggs with the peak rotation frequency 1.5 MHz. Solid lines show the best fit from the multi-shell model as listed in Tables 7.2 and 7.5. Error bars represent the mean rotation rate and one standard deviation (conductivity 0.65±0.1 mS/m).

7.6.6 Fertilised egg spectra discussion

The physiological changes occurring as an egg undergoes fertilisation, the formation of the lipid membrane etc., offers a possible explanation as to why there is so much variance between the fertilised egg spectra. The model indicates that the differences between the 3 anti-field peak rotation frequencies at 200 kHz, 600 kHz and 1.5 MHz are due to these physiological changes. All the eggs are viable, fertilised, unicellular and have similar lipid membrane conductivities, as expected of organisms of similar physiological state. Differences in their other dielectric properties indicate what physiological changes are *about* to occur. The cytoplasm conductivity increases with the peak rotation frequency, as does the thickness of the lipid membrane, while the permittivity of the membrane decreases. This can be attributed to changes in the egg development, from a unicellular internal organisation, to a more complex, multi-cellular organisation (Chapter 2, Figure 2.10), which contains, initially, two membrane bound cells. The distribution of the interior contents of the eggs appears to support this hypothesis (Table 7.6, Figure 7.14). As the frequency of the peak rotation frequency increases from 200 kHz to 1.5 MHz, more of the eggs have their internal contents touching the cell wall.

	1.5 MHz **(n=14)**	600 kHz **(n=21)**	200 kHz **(n=37)**
Contents touching cell wall (%)	78	29	8
Contents not touching cell wall (%)	22	71	92
Viable (%)	57	43	51
Non-viable (%)	43	57	49

Table 7.6 – Analysis of the data producing the three peak rotation frequency sets seen in Figures 7.11 to 7.13.

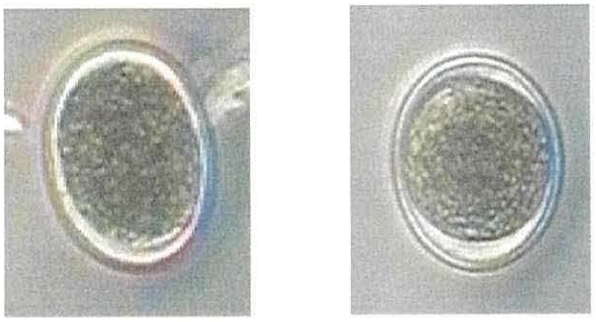

Figure 7.14 – An egg with the internal contents touching the egg wall (left)and an egg with internal contents retracted from the egg wall (right). Note that these are one sided captured images, and that when an egg rotates, the distinction is not as apparent or as large as these images might suggest.

7.6.7 Fertilised egg spectra - analysis by viability

As there were no clear reasons for the observed sets in the fertilised spectra the video data of all the experiments were taken to the Scottish Parasite Diagnostic Laboratory, in Glasgow, to have the viability and fertility state of the eggs confirmed by a clinical parasitologist. Not all eggs could be positively identified as viable or non-viable. Of the 104 fertilised egg spectra examined, the viability and development state of only 72 could be positively identified (Table 7.6). The spectra were then collated, analysed and found to have again three peak rotation frequency groupings around 200 kHz, 600 kHz and 1.5 MHz (Figures 7.15 to 7.17).

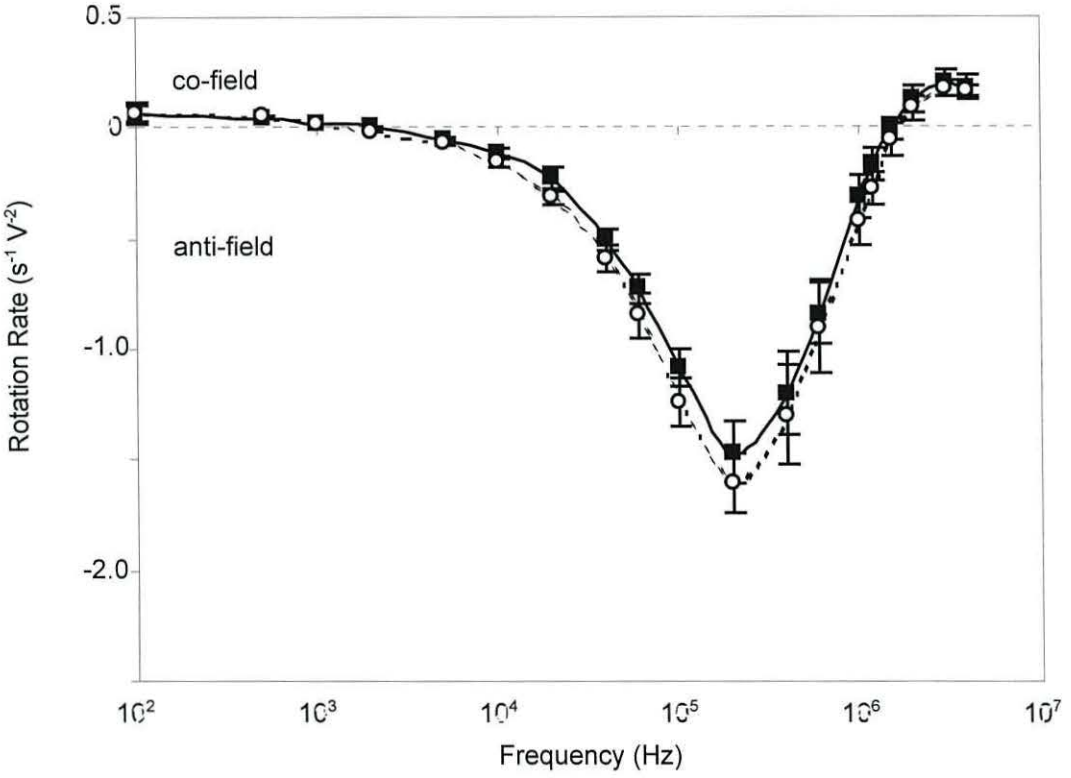

Figure 7.15 – Rotation spectra of 19 viable (○) and 18 non-viable (■) fertilised *A. suum* isolate A2 eggs at a peak rotation frequency of 200 kHz. Mean rotation rates shown, with error bars indicating one standard deviation (conductivity 0.65±0.1 mS/m).

Figure 7.15 shows electrorotational spectra of 37 eggs that had a peak rotation frequency of approximately 200 kHz and whose viability had been determined. The mean rotation rate of the viable eggs was found to be slightly higher than that of the non-viable eggs. However, the overlap of error bars shows that this is not a significant difference, and can be attributed to slight differences in physical size between the

eggs. The non-viable spectra bear no resemblance to that of ruptured egg spectra, seen previously in Figure 7.3, and suggest that while a fertilised egg may be biologically non-viable, it still possesses intact vitelline, chitinous and lipid layers which still have similar dielectric properties to viable eggs.

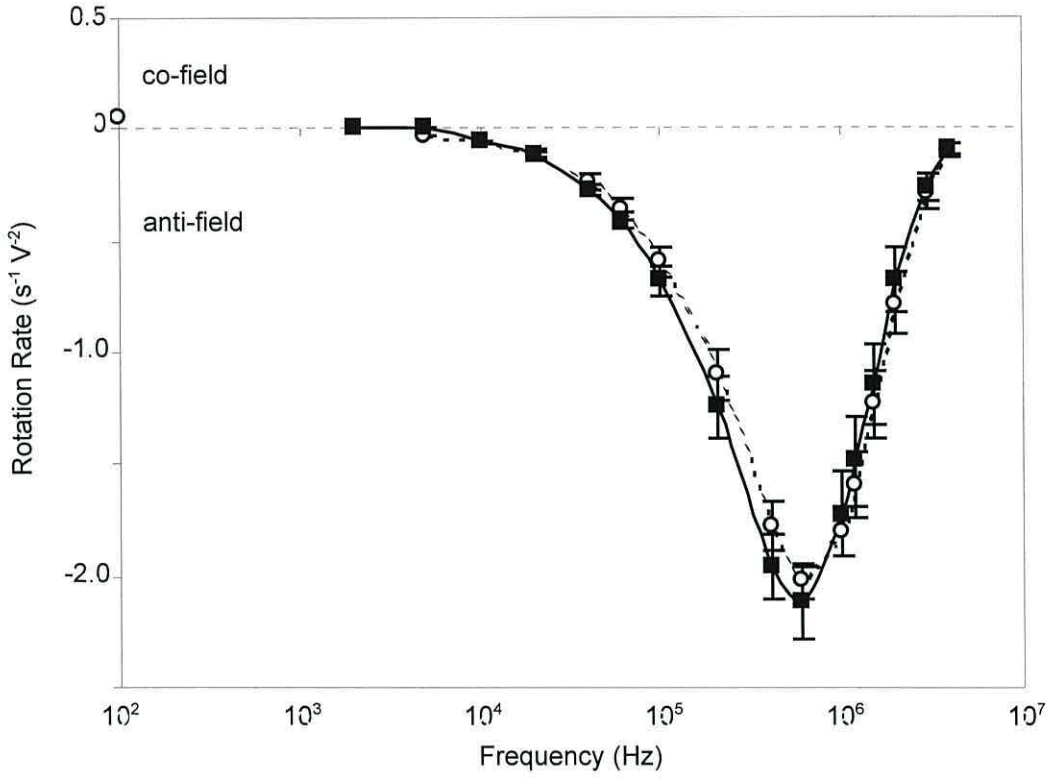

Figure 7.16 – Rotation spectra of 9 viable (o) and 12 non-viable (■) fertilised *A. suum* isolate A2 eggs at a peak rotation frequency of approximately 600 kHz. Mean rotation rates shown, with error bars indicating one standard deviation (conductivity 0.65±0.1 mS/m).

Figure 7.16 shows electrorotational spectra of 21 fertilised eggs that had a peak rotation frequency of 600 kHz and whose viability had been determined. The slight difference in the electrorotational responses between the two types of eggs can be attributed to variations in the egg sizes.

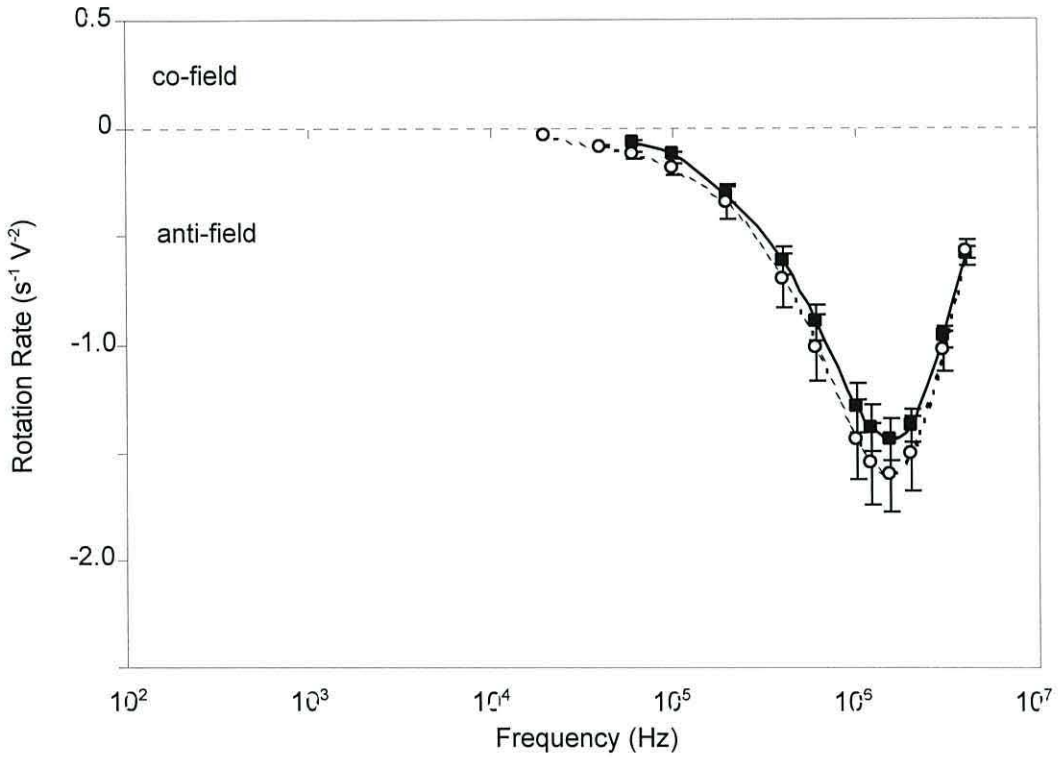

Figure 7.17 – Rotation spectra of 8 viable (o) and 6 non-viable (■) fertilised *A. suum* isolate A2 eggs at a peak rotation frequency of 1.5 MHz. Mean rotation rates shown, with error bars indicating one standard deviation (conductivity 0.65±0.1 mS/m).

Figure 7.17 shows electrorotational spectra of 14 fertilised eggs that had a peak rotation frequency of 1.5 MHz and whose viability had been determined. The mean rotation rate of the viable eggs is slightly higher than that of the non-viable eggs. However, the overlap of errors bars shows that this is not a significant difference.

7.7 Discussion

Decortication of the outer layer of the *A. suum* eggs is required before electrorotation experiments can proceed. The decortication process produces differing thicknesses of the vitelline layer, which greatly affects the spectra obtained, and so only spectra obtained from the same isolate which has been decorticated at the same time can be compared. In some instances, the decortication procedure removed the cell wall from the eggs completely. Thus decortication reduces the reproducibility of experimental data. However, decortication allows more accurate visual identification of an egg's fertilisations state (one/two cell stage or larval stage). Without decortiation, eggs adhere to the chamber and carry many particles of debris, which also affect reproducibility.

Fertilised eggs rotate at a more rapid rate and in the opposite direction to unfertilised eggs in the frequency window 10 kHz to 2 MHz (Figure 7.8). At 600 kHz, the average peak rotation rate of fertilised eggs are at a maximum in the anti-field region. Unfertilised eggs have a peak rotation frequency of 1 MHz in the co-field region, allowing for easy visual differentiation between the two types due to direction of rotation. This process can easily be automated using existing image processing techniques (Schnelle *et al.* 1997; DeGasperis *et al.,* 1998; Zhou *et al.*, 1998) and would create a quick and easy method for determining the contents of a mixed population, useful for screening water supplies.

Examination of the fertilised egg spectra indicated three possible sets, at 200 kHz, 600 kHz and 1.5 MHz (Figures 7.5 ,7.6, 7.11, 7.12 and 7.13). Attempts to correlate these sets with physical size, visible changes in life-cycle stage, and viability failed to identify the reason for the differences. The only factor that appears to correlate with the three sets of fertilised egg spectra is the distribution of the internal contents (Table 7.6). At the peak rotation rate ~1.5 MHz, 78% of the eggs have internal contents touching the cell wall. Corresponding figures at 600 kHz and 200 kHz are 29% and 8% respectively. It is highly likely that the cause is due to the changes in the physico-chemical nature of the eggs, such as the changes in the ascerosdies of the lipid layer as described in Chapter 2. This hypothesis is supported by the modelling data,

which indicates that changes in the lipid membrane and the cytoplasm properties can explain the different spectra. It must be noted though that an *Ascaris* egg is the most complex organism that has been attempted with this model. Previous organisms were simple structures such as yeast and red blood cells (as discussed in Chapter 4), and further investigation using multi-cellular fertilised eggs is recommended.

7.8 Conclusions

This is the first reported electrorotation study of a nematode, *Ascaris suum*. Electrorotation can readily distinguish between fertilised and unfertilised decorticated eggs, as confirmed using standard optical microscopy techniques. Spectra for fertilised eggs fall into three sets, probably reflecting three stages of egg development. However, the decortication process influences the spectra obtained, and limits the practical applications of the technique for this organism. Standardising the decortication process would be advantageous, but adds another level of complexity to the whole electrorotation process. However, electrorotation has been shown to be applicable to the important phylum, nematoda. The technique could be applied to similar organisms that do not require decortication, and which cannot easily be analysed using optical microscopy.

7.9 References

Asami, K., Hanai, T. and Koizumi, N. **(1976)** *J. Membrane. Biol.* **28** 169-180

Darben, P. **(2002)** *Personnel communication* based on unpublished, confidential commercial work carried out at the Queensland University of Technology, Australia

DeGasperis, G., Wang, X. B., Yang J., Becker, F. F., and Gascoyne, P. R. C. **(1998)** Automated Electrorotation: Dielectric characterisation of living cells by real time motion estimation. *Meas. Sci. Tech.* **9** 518-529.

Foor, W. E. **(1967)** Ultrastructural aspects of oocyte development and shell formation in *Ascaris lumbricoides. J. Parasitol* **53** 1245-1261

Gimsa, J., Glaser, R. and Fuhr, G. **(1991)** *In* Physical characterisation of biological cells Ed. Schutt, Berlin Gesundheit 295-323

Huang, Y., Hölzel, R., Pethig, R. and Wang, X.B. **(1992)** Differences in the ac electrodynamics of viable and non-viable yeast cells determined through combined dielectrophoresis and electrorotation studies. *Phys. Med. Biol.* **37(7)** 1499-1517

Schnelle, T., Glasser, H., and Fuhr, G. (**1997)** Opto-electronic technique for automatic detection of electrorotational spectra of single cells. *Cellular Engineering* **2** 33-41.

Wang, X-B, Huang, Y., Gascoyne, P. R. C., Becker, F. F., Holzel, R. and Pethig, R. **(1994)** Changes in Friend murine erythroleukaemia cell membranes during induced differentiation determined by electrorotation. *Biochim. Biophys. Acta.* 1193 330-344

Zhou, X-F., Burt, J. P. H., and Pethig, R. **(1998)** Automatic cell electrorotation measurements: Applied to studies of the biological effects of low-frequency magnetic fields and of heat shock. *Phys. Med. Biol.* **43** 1075-1090.

Chapter 8

Conclusions and Recommendations for Further Work

8.1 Conclusions

This thesis presents the results of the first investigation of two species of parasites that infect man, namely the protozoa *Cyclospora cayetanensis* and the nematode *Ascaris suum*, using the dielectric technique of electrorotation. This is also the first investigation of a member of the phylum nematoda. Chapter 1 described the global health implications of these two parasitic organisms, and details why electrorotation could be used as a rapid test of organism viability. The current status of research using the electrorotation technique was described, along with suggestions of potential applications in the field of parasitology and public health. It was noted that, with the exception of the work on *Cryptosporidium* and *Giardia* by Goater (1997 and 1999) and indirect work on *Plasmodium falciparum* (Gascoyne *et al.*, 1997), the protozoa, a group of more than 50,000 species (Pechenik, 1991), have been relatively ignored. Few thorough investigations have been undertaken to date of their dielectric properties, and no nematodes of the extant 20,000 species (Pechenik, 1991), have been investigated prior to the work presented here.

Both *Cyclospora* and *Ascaris* are of importance to human health as they can, for part of their life cycle, inhabit the intestine in a parasitic manner. Both species have been shown to be major causative agents of chronic diarrhoea in humans and other animals and so also can be of economic importance. Current techniques for the detection and viability determination of the transmissive stages of these parasites have their disadvantages, and so a sensitive detection method that could do both is seen, especially by the water industry, as a potentially useful tool. The transmissive forms of each organism, namely the oocysts of *Cyclospor*a and the eggs of *Ascaris*, are appropriate to study by electrorotation. The aim of the experimental work described in this thesis was to show that electrorotation could be used as such an identification and viability determination tool.

Chapter 2 contains a detailed review of the biological structure of the oocysts and eggs. Chapter 3 reviews the basic theory of AC electrokinetics, which provides the background to the electrorotation technique, and also briefly reviews the research performed into the dielectric properties of biological cells. Current mathematical models for simulating the behaviour of biological particles in rotating electric fields are described in Chapter 4.

The use of smaller electrode geometries, such as polynomial type electrodes of less than 0.5mm inter-electrode gap, have previously been demonstrated to assist positioning of particles prior to electrorotation analysis using negative dielectrophoresis. However, due to pre-sample handling and initial low concentrations of some of the organisms investigated here, only a fraction of the organisms in any sample could be assayed and the use of small electrode geometries was impractical. In some cases, no organisms from an aliquot of sample could be assessed, as none were positioned within the appropriate region of the electrode chamber. The electrode structure described in Chapter 5 attempts to overcome this problem by providing a uniform field over as large an area as possible, maximising the number of organisms exposed to the field, which can then be assessed.

In Chapter 6 it was demonstrated that electrorotation gives an indication of the viability of individual oocysts of *Cyclospora cayetanensis;* this correlated well with the work by Goater (1997) on a similar coccidian parasite, *Cryptosporidium parvum*, which was verified in that work by a twin dye permeability assay. This is an important result as to date, no vital dye has been described for *C. cayetanensis* oocysts (*cf.* DAPI and PI dyes for *C. parvum* oocysts). Such a dye technique would be valuable to compare with the electrorotation differences observed between morphologically similar oocysts of *C. cayetanensis* presented in this work, and many researchers are currently attempting to isolate such dyes (Eberhard *et al.,* 2000; Quintero-Bentacourt *et al.,* 2002). It has also been shown that electrorotation can determine the sporulation state of an oocyst, which is an important factor in assessing the potential risk of contaminated water, as only sporulated oocysts are infectious. Currently, only trained laboratory technicians can determine sporulation state. The electrorotation method can be automated, potentially allowing for faster and more

precise monitoring of water supplies. Simulation of the electrorotational response of *C. cayetanensis* oocysts has shown that the observed differences between viable and non-viable, and sporulated and unsporulated, oocyst spectra are consistent with their changing dielectric properties. The values from the model indicate that membrane conductivity of non-viable oocysts is significantly greater than that of viable ones ($2x10^{-5}$ S/m compared to $1x10^{-6}$ S/m, respectively). There is a corresponding decrease in the internal conductivity of the oocyst, from 0.5 S/m to 0.2 S/m, confirming that the loss of viability is associated with a physical degradation of the membrane and the loss of its ability to act as a barrier to passive ion flow. The membrane conductivity of a sporulated oocyst is greater than that of an unsporulated oocyst, as is the conductivity of the oocyst interior. This is consistent with the formation of the two membrane bound sporocysts during sporulation, which will increase the surface area of membrane within the oocyst.

In this work it was found that storage for up to 8 months in 2.5% potassium dichromate solution has minimal effect upon the electrorotation spectra of sporulated oocysts. However, an effect on the unsporulated oocysts was observed. Modelling indicated that the storage medium affected the surface charge on the wall of the unsporulated oocyst. The distinction between sporulated and unsporulated oocysts as indicated by the difference in their anti-field peak rotation rates remained. Only a limited number of oocysts could be investigated after storage, due to bacterial and particulate adhesion to the oocysts. The effect of the addition of a bacterium on the electrorotational response of an artificial particle has been shown by Hodgson (1998), for latex beads and on a biological particle by Goater (1999) for oocysts of *C. parvum.* The effect on the electrorotation spectrum of the adhesion of a small amount of faecal debris, not bacteria, reported in this work is not known to have been reported previously. A reduction in the anti-field rotation rate was observed, which, according to the model, could be ascribed to viscous drag alone, with the dielectric parameters of the oocyst unchanged. This result highlights an important limitation of the electrorotation technique; organisms under investigation need to be free of adherent debris and bacteria. This indicates that environmental samples will need to undergo rigorous cleaning procedures before they can be investigated, which could limit the effectiveness of the electrorotation technique, due to the inevitable losses that occur.

Cyclospora infects other primates, such as baboons (for a complete species list, see appendix A). Oocysts recovered from baboons are generally considered to be the same species as those recovered from humans, namely *C. cayetanensis.* However, a difference between the electrorotational response of human and baboon source oocysts was observed, but due to the very limited numbers of baboon source oocysts available, this difference could not be thoroughly investigated and may have been an effect of long term storage or biological variance. Recent work by Lopez *et al.* (1999), has indicated that there is indeed a difference between human and baboon source oocysts, and further investigation is required to determine if electrorotation is a sufficiently sensitive technique to distinguish between *Cyclospora* species.

In Chapter 7 it was demonstrated that electrorotation can indicate the fertilisation state of individual eggs of *A. suum.* Unfertilised eggs rotate in the co-field direction only, while fertilised eggs rotate in the anti-field direction only in the frequency range 200 kHz to 2MHz. Thus a mixed population can be rapidly and reliably assessed using the electrorotation method. Unfertilised eggs will never be biologically viable, and once egested by the female worm will never become fertilised. Modelling indicates that unfertilised eggs have very low internal conductivities, suggestive of non-viable organisms. However, the spectra of unfertilised eggs are not consistent with the spectra of eggs that had lost the majority of their contents through rupture. The latter had very low internal conductivities and were known to be non-viable. This indicates that unfertilised eggs, while biologically non-viable, possess functioning layers.

The outer, uterine layer of *Ascaris* eggs is very adhesive, and needs to be removed prior to investigation by electrorotation. This process, known as decortication, has the advantage of overcoming contamination of environmental samples by removing any debris along with the uterine layer. However, decortication has the disadvantage of removing varying thicknesses of the next layer of the egg, the vitelline layer, which affects the electrorotational response. Thus, only eggs from the same decortication sample were compared during electrorotation.

Three sets in the fertilised egg spectra were identified, which appear to be due to the distribution of the internal contents of the egg as it progresses though its life-cycle.

The model indicates that the changes are mainly due to the lipid membrane and chitinous layer properties. There is an apparent correlation between the three sets and the position of the interior contents in the egg with respect to the egg wall. The complex nature of the internal contents of a fertilised egg cannot be accurately modelled using the current model. However, it should be possible to model the effect of an electric field on a sphere containing a smaller sphere of differing electrical properties using a finite element modelling package, such as FemLab (COMSOL, UK). The inner sphere can be modelled touching and not touching the inner wall of the larger sphere, to see the effect this has on the electric field in the localised area. It is possible that, in the case for *Ascaris,* the internal contents effectively short circuit the egg wall where they touch it, causing a localised disruption to the field which affects the electrorotation spectra.

Ascaris is the first nematode to be investigated by the electrorotation technique, and is the most complex organism, in terms of the internal structure, to be modelled using the multi-shell model. The limitations of the multi-shell model for complex organisms were discussed in Chapter 4. At frequencies greater than 2 MHz, the recorded spectra were observed to deviate from the modelled spectra. However, the model is sufficiently accurate at frequencies below this for insights into the dielectric properties of the organism to be obtained.

Electrorotation overcomes the problems associated with vital dyes such as toxicity, the requirement for specialised storage and highly skilled microbiological training. Electrorotation is a non-invasive process, the undamaged oocysts/eggs can be tested further by other techniques, e.g. rDNA analysis, in the hope of determining the life-cycle and modes of transmission. Electrorotation also has the advantage of being versatile; the same experimental set-up can investigate many different organisms. Since electrorotation relies upon visual data analysis, the process is easily automated and several groups have published image processing procedures (Zhou *et al.*, 1998; DeGasperis *et al.*, 1998). These qualities of the electrorotation technique show that it has the potential to become a powerful investigative tool for microbiologists involved in the control of water and food -borne parasites.

8.2 Recommendations for Further Work

Placing an *Ascaris* egg in a rotation chamber and observing the changes to the electrorotation response as the egg undergoes embryonation over a period of several days would give an insight into the physico-chemical changes that occur during embryonation and clarify the cause of the three sets of anti-field spectra observed. Attempts to observe the changes occurring while an unsporulated oocyst of *C. cayetanensis* sporulates were attempted, but failed due to desiccation of the sample chamber. A redesigned electrorotation chamber to prevent drying is required. In addition, the chamber could incorporate inlet/outlet ports, which could be used to physically position the organism in the centre of the chamber by precise fluid flow. This would provide a low cost alternative to systems that have been used previously for accurate positioning, such as laser tweezers (Reichle *et al,* 2000), and would allow the majority of organisms in a sample to be analysed. Such a chamber was designed (Figure 8.1), and the recent advances in elastomer moulding, such as Polydimethylsiloxane (PDMS), mean that such a chamber can now be relatively easily fabricated.

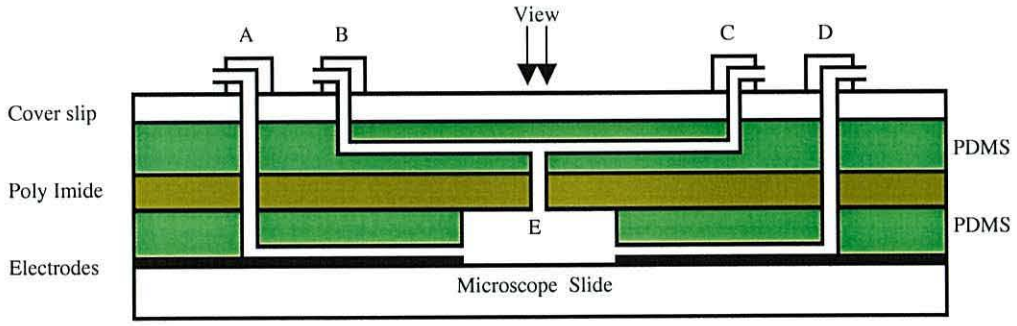

Figure 8.1 – Cross-section of a proposed low cost, microfabricated structure to capture and position single oocysts of *C. cayetanensis.* A and B – inlets, C and D –outlets, E - 100μm diameter hole.

To overcome problems associated with friction between the organism and the base of the chamber, the organism could be levitated using another set of electrodes by dielectrophoresis, as shown by Reichle *et al.* (1999). This is a very complicated solution, as the electrorotation fields and the dielectrophoretic fields interact, and there would be problems for large organisms such as *Ascaris* eggs. There are simpler

methods, such as placing the organism between two layers of solutions of different density (Fuhr and Kuzmin, 1986) or adjusting the suspending medium specific gravity so that the organism floats.

The *Ascaris* eggs examined in this initial investigation were removed from the uterus of female worms. To further the development of electrorotation as a tool for the water and food industries, eggs recovered from the environment need to be investigated and their electrorotational response compared to the data presented in this thesis.

A limitation of this work was the inability of the frequency generator to reliably provide four sinusoidally varying fields exactly 90° out of phase above 5 MHz. This prevented high frequency co-field rotation data to be obtained, although modelling of the organism response was limited above 2 MHz due to the complex internal structures involved. There are now commercially available frequency generators (such as the TGA 1244, 4 channel, 40 MHz arbitrary waveform generator, Thurlby Thandar Instruments, UK), which were not available until near the end of this work, that can provide reliable high frequencies. A lot of attention and modification of the model for low frequencies has been performed, as discussed in Chapter 4. However, the limitation of the model at high frequencies for complex organisms has not been significantly addressed and requires further investigation.

8.3 References

DeGasperis, G., Wang, X. B., Yang, J., Becker, F. F. and Gascoyne, P. R. C. **(1998)**, *Meas. Sci. Tech.* **9** 518

Eberhard, M. L., Pieniazek, N. J. and Arrowood, M.J. **(1997)** Laboratory diagnosis of *Cyclospora* infections. *Archiv. Pathol. Lab. Med.* **121** 792-797.

Fuhr, G. and Kuzmin, P. I. **(1986)** Behaviour of cells in rotating electric fields with account to surface charges and cell structures. *Biophys. J.* **50** 789-794

Gascoyne, P., Pethig, R., Satayavivid, J., Becker, F. F. & Ruchirawat, M. **(1997)** Dielectrophoretic detection of changes in erythrocyte membranes following malarial infection. *Biochim. Biophys. Acta -Biomembranes.* **1323** 240-252

Goater, A. D., Burt, J. P. H. and Pethig, R. **(1997)** A combined electrorotation and travelling wave device: applied to the concentration and viability of *Cryptosporidium. Journal of Physics D-Applied Physics.* **33:** L65-L70.

Goater, A. D. **(1999)** A.C. Electrokinetic Bioassays. Development of Electrorotation Assay for Analyets in Water. *Ph.D. Thesis,* University of Wales.

Hodgson, C. E. & Pethig, R. **(1998)** Determination of the Viability of *Escherichia coli* at the single organism level by electrorotation. *Clin. Chem.* **44** 2049-2051.

Lopez, F. A., Manglicmot, J., Schmidt, T. M., Yeh, C., Smith, H. V. and Relman, D. A. **(1999)** Molecular characterisation of *Cyclospora*-like organisms from baboons. *J. Infect. Dis.* **179** 670-676

Pechenik, J. A. **(1991)** *Biology of the Invertebrates 2nd Ed.,* Wm C. Brown,Dubuque, USA

Reichle, C., Schnelle, T., Müller, T., Leya, T. and Fuhr, G. **(2000)** A new microsystem for automated electrorotation measurements using laser tweezers. *Biochim. Biophys. Acta.* **1459** 218-229

Reichle, C., Müller, T., Schnelle, T. and Fuhr, G. **(1999)** Electrorotation in octopole micro-cages*J. Phys. D: Appl. Phys* **(32)** 2128-2135

Quintero-Bentacourt, W., Peele, E. R. and Rose, J. B. **(2002)** *Cryptosporidium parvum* and *Cyclospora cayetanensis* : a review of laboratory methods for detection of these waterborne parasites. *J. Microbiol. Meth.* **49** 209-224

Zhou, X-F., Burt, J. P. H. and Pethig, R. **(1998)**, *Phys. Med. Biol.,* **43** 1075.

8.4 Refereed Publications arising from this work

The full text of refereed publications are given in Appendix C, along with a list of conference presentations and posters.

Dalton, C., Goater, A. D., Drysdale, J. and Pethig, R. **(2001)** Parasite Viability By Electrorotation *Colloids and Surfaces A : Physicochemical and Engineering Aspects* **195** 263-268

Dalton, C., Goater, A. D., Pethig, R. and Smith, H. V. **(2001)** Viability of *Giardia intestinalis* cysts and viability and sporulation state of *Cyclospora cayetanensis* oocysts determined by Electrorotation. *Appl. Environ. Microbiol.* **67**(2) 586-590

Dalton, C., Pethig, R. and Smith, H. V. **(2000).** Electrorotation of *Ascaris suum. Trans. Royal Soc. Trop. Med. Hyg.* **94** 616-619

Dalton, C., Pethig, R., Paton, C. A. and Smith, H. V. **(1999)** Viability determination of *Cyclospora cayetanensis* oocysts. *Trans. Royal Soc. Trop. Med. Hyg.* **93** 461-463

Dalton, C., Pethig, R., Paton, C. A. and Smith, H. V. **(1999)** Electrorotation of oocysts of *Cyclospora cayetanensis. Inst. Phys. Conf. Ser.* **163** 85-88

8.5 Conference Presentations and Posters

Goater, A. D., Burt, J. P, H., Dalton, C. and Tame, J. A. **(2002)** AC Electrokinetics of Bioparticles in Water. **Oral presentation at the** *15th Meeting of the Microbiological Methods Innovation Forum*, 28th May, Campden & Chorleywood Food Research Association, Chipping Campden, UK.

Dalton, C. and Burt, J. P. H. **(2001)** Fertilisation state of ova of the nematode *Ascaris suum* determined by electrokinetic techniques. **Oral presentation at** *the first European Workshop on Electrokinetics and Electrohydrodynamics in Microsystems*, 6-8th September, Glasgow, UK.

Dalton, C., Burt, J. P. H., Cotterill, S. L., Goater, A. D., Zhou, X-F. and Pethig, R. **(2001)** Electrokinetic Particulate Laboratory-on-a-chip (Biofactory) Technology. **Poster presented at** *Molecular analysis : Analytical challenges for the life sciences*, 12-13th March, Warwick.

Dalton, C., Goater, A. D., Drysdale, J. and Pethig, R. **(2000)** Parasite Viability By Electrorotation. **Oral presentation at** the *International Symposium on Electrokinetic Phenomena* (ELKIN), Oct 2-6th, Dresden, Germany.

Dalton, C., Pethig, R. and Smith, H. V. **(2000).** Electrorotation of *Ascaris suum.* **Poster presented at** *The Royal Society of Tropical Medicine Meeting,* 17th May, Glasgow

Dalton, C., Pethig, R., Paton, C. A. and Smith, H. V. **(1999)** Viability determination of *Cyclospora cayetanensis* oocysts. **Poster presented at** *The Royal Society of Tropical Medicine Meeting.* 19th May, Edinburgh.

Dalton, C., Pethig, R., Paton, C. A. and Smith, H. V. **(1999)** Electrorotation of oocysts of *Cyclospora cayetanensis.* **Poster Presentation at** the IOP Electrostatics 1999 Conference, 28-31st March, Cambridge.

Appendix A – *Cyclospora* Species

In this appendix, the background and most recent research regarding *Cyclospora* is presented, along with the problems associated with investigating and controlling this organism.

Background

Although *Cyclospora cayetanensis* is a relatively newly described pathogen of humans, there are reports of cyclosporans being detected in the intestines of moles dating back to Eimer in 1870. The genus *Cyclospora* was named by Schneider in 1881, when he described a new species of coccidian parasite from a millipede, *Glomeris* spp. In 1902, Schaudinn reported the first life-cycle study, which showed that *Cyclospora caryolitica* developed in the intestines of moles and produced severe enteritis. Since then, fourteen species of *Cyclospora* have been described in moles, rodents, insectivores, snakes and primates (Table A.1).

Species	Host Species	Common Name	Oocysts size (μm)	Authorities
C. glomericola	*Glomeris sp.*	Millipede	25-36 x 9-10	Schneider, 1881
C. caryolytica	*Talpa europaea*	European Mole	16-19 x 13-16	Schaudinn, 1902
C. viperae	*Vipera aspis*	European Asp	16.8 x 12.6	Phisalix, 1923
C. babaulti	*Vipera berus*	Eurpoean Adder	16.8 x 10.5	Phisalix, 1924
C. tropidonoti	*Tropidonotus natrix (= Natrix natrix)*	Grass Snake	16.8 x 10.5	Phisalix, 1924
C. talpae	*Talpa europaea*	European Mole	12-19 x 6-13	(Pellérdy & Tanyi, 1968) Duszynski & Wattam, 1988
C. megacephali	*Scalopu aquaticus*	Eastern Mole	14-21 x 12-18	Ford & Duszynski, 1988
C. ashtabulensis	*Parascalops breweri*	Hairy-Tailed Mole	14-23 x 11-19	Ford & Duszynski, 1989
C. parascalopi	*Parascalops breweri*	Hairy-Tailed Mole	13-20 x 11-20	Ford & Duszynski, 1989
C. angimurinensis	*Chaetodipus hispidus*	Hispid Pocket Mouse	19-24 x 16-22	Ford, Duszynski & McAllister, 1990
C. cayetanensis	*Homo sapiens*	Human	8-10	Ortega, Gillman & Sterling, 1994
C. ceropitheci sp.n.	*Cercopithecus aethiops*	African Green / Vervet Monkey	8-10	Eberhard, da Silva, Lilley and Pieniazek, 1999
C. colobi sp.n.	*Colobus guereza*	Colobus Monkey	8-9	Eberhard, da Silva, Lilley and Pieniazek, 1999
C. papionis sp.n.	*Papio anubis*	Olive Baboon	8-10	Eberhard, da Silva, Lilley and Pieniazek, 1999

Table A.1 – Species of *Cyclospora*

The recognition of *Cyclospora* as a protozoan pathogenic to humans is relatively recent. Ashford *et al.* (1979) reported an *Isospora*-like coccidian infecting three humans in Papua New Guinea. From 1985, similar structures were found in faecal samples from patients with diarrhoea and were determined to be the causal agent. Due to the appearance and staining characteristics of the unsporulated oocysts, these infections were initially attributed to cyanobacterium-like bodies (blue-green algae) or coccidian-like bodies (CLBs). Ortega *et al.* (1993) characterised these CLBs as oocysts belonging to a species of *Cyclospora*. In 1994 the new species was designated as *C. cayetanensis*, after the location of Ortega's principle studies, Cayetano Heredia University in Lima, Peru (Ortega *et al.* 1994).

Epidemology

Organisms similar in appearance to *Cyclospora* have been found in patients with protracted diarrhoeal illness in North, Central and South America, the Carribean, Africa, Bangladesh, Southeast Asia, Australia, England, Germany and Eastern Europe (Figure A.1). The disease is endemic in Haiti, Nepal and Peru. Host ranges and reservoirs are as yet undefined (Miller and Paige, 1998). Most infections have been reported in tourists or expatriates visiting countries that normally have high diarrhoeal rates (Marshall *et al.*, 1997; Petry *et al.*, 1997). In recent years, the importance of *C. cayetanensis* as an emerging pathogen of humans has been highlighted by several outbreaks (Herwaldt, 2000). The first reported outbreak in the United States was in 1990, in a hospital dormitory in Chicago (Anon, 1991). Prior to that event, only sporadic cases had been reported (Soave *et al.*, 1998). In the spring of 1996, 1,465 cases were reported in the US and Canada, attributed to raspberries imported from Guatemala (Herwaldt *et al.*, 1997). Despite improved food safety measures, over 1,000 cases were again reported in 1997 due to the same source, and on May 30, 1997, the government of Guatemala and the Guatemalan Berries Commission voluntarily suspended exports of fresh raspberries to the United States (CDC, 1997). In May, 1998, Guatemalan berries were implicated in outbreaks in Ontario, Canada (CDC, 1998). To date, the mode of contamination of the raspberries has not been identified for any of these outbreaks. Mesclun, basil and blackberries have also been linked to *Cyclospora* infection in humans (Herwaldt, 2000).

In Peru, over a 6 year period, nearly all *Cyclospora* infections occurred between December and July (Ortega *et al.*, 1998). In Nepal, infections occurred most frequently from May to August (Schlim *et al.*, 1991; Hoge *et al.*, 1993). This seasonality corresponded to the rainy season, and one suggestion is that this seasonality is due to fluctuations in temperature and/or humidity (Soave *et al.*, 1998). However, this seasonality has yet to be defined. It is interesting to note that no outbreaks were associated with Guatemalan raspberries during Guatemala's autumn and winter export seasons in 1996 and 1997.

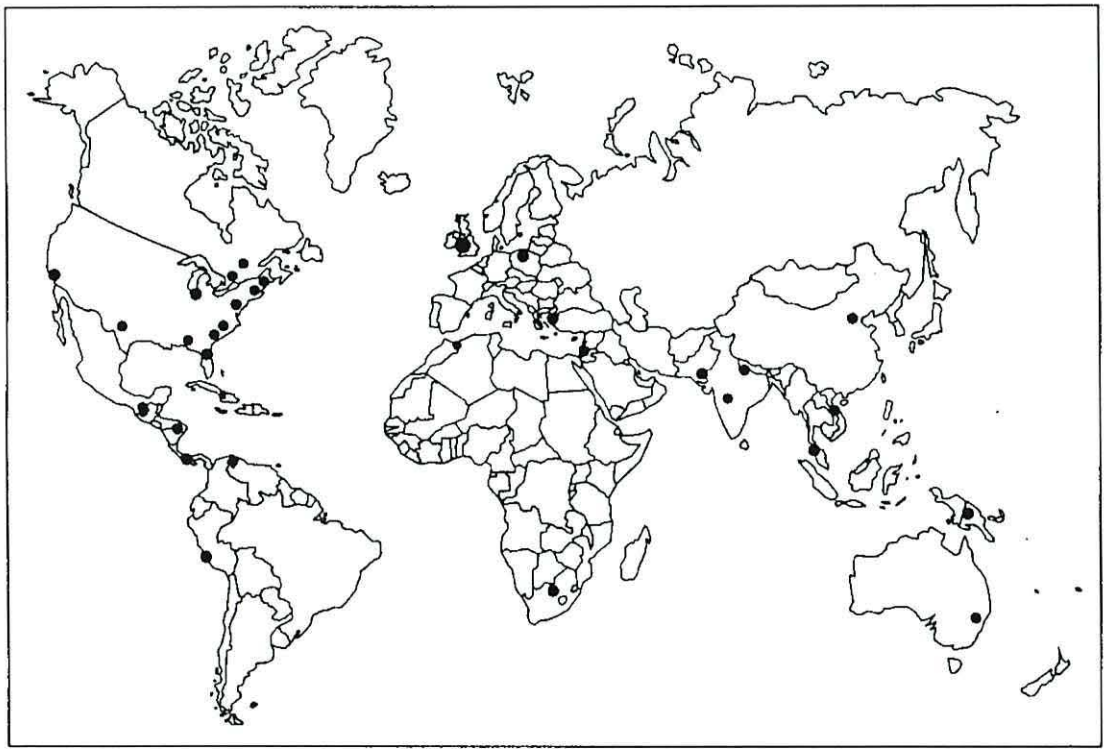

Figure A.1 – Map of the world showing sites of reported *C. cayetanensis* infection. (Ortega *et al.*, 1998).

In an outbreak in a military camp in Nepal in 1994, *C. cayetanensis* oocysts were recovered from the storage tank of an adequately chlorinated supply, indicating that *C. cayetanensis*, like *Cryptosporidium parvum*, is resistant to chlorination (Rabold *et al.*, 1994). *C. parvum* is also resistant to other halogens, such as iodine, and this may indicate that *Cyclospora* may also be resistant. Boiling appears to kill *Cyclospora* (Conner, 1997).

In the UK there have been no significant outbreaks associated with *Cyclospora* : only 44-66 laboratory reports of *C. cayetanensis* were reported per year between 1993 and

1998 (Cann *et al.*, 2000). However, only 68% of UK microbiology laboratories actively look for *Cyclospora*, and of those, only 58% correctly identified the organism when assessed, suggesting that *Cyclospora* may be under-diagnosed in the UK (Gill, 1997; Cann *et al.*, 2000). In the United States prior to the large multi-state outbreak in 1996, most laboratories did not routinely examine stool specimens for *Cyclospora*. Since then there has been better awareness for the need to perform the appropriate tests (Eberhard *et al.*, 1997), but a recent review states that most laboratories still only test for *Cyclospora* on request (Herwaldt, 2000).

Cyclosporiasis : the disease

Cyclosporiasis, the illness caused by infection with *C. cayetanensis,* is treatable, but is clinically indistinguishable from the illness caused by *Cryptosporidium parvum,* which is not treatable. This leads to confusion as to what care a patient requires if misdiagnosed.

Symptoms of *Cyclospora* infection occur approximately one week after ingestion of oocysts, and can persist for a month or more. The minimum number of oocysts required to infect an individual is thought to be between 10 to 100 (Adams and Ortega, 1999). It is not known how long the oocysts can survive under different environmental conditions.

Clinical manifestations include prolonged watery diarrhoea that occurs in a relapsing, cyclical pattern, sometimes alternating with constipation. Important associated symptoms include severe nausea, fever, vomiting, anorexia, myalgia, abdominal cramping and weight loss (mean weight loss associated with untreated infections is estimated to be 3.6 kg). Increased upper intestinal gas and bloating is frequently noted (Conner, 1997). The onset of illness has been reported as abrupt in 68% of adult patients with symptoms lasting an average 7 weeks (Marshall *et al.*, 1997). Although the illness is self-limited, it may be prolonged. Progressive fatigue, anorexia and weight loss may overshadow the presenting diarrhoeal symptoms (Soave, 1996; Conner, 1997). In patients suffering from acquired immune deficiency syndrome (AIDS), infection can last up to 4 months (Marshall *et al.*, 1997), is more severe and is associated with a high rate of recurrence that can be attenuated with long-term

suppressive therapy (Soave, 1996). Delay in diagnosis (which requires examination of a stool specimen) often occurs because upper gastrointestinal tract signs and the symptoms of profound fatigue predominate over the diarrhoeal symptoms by the time medical attention is sought. It has been reported that prior infection as a child can lead to possible immunity as an adult (Ortega *et al.*, 1998) and that children under 18 months can acquire protection from breast feeding (Conner, 1997).

The main site of infection is probably the small intestine and possibly the colon (Casemore, 1994). There is evidence from small animal studies on other cyclosporan species (*C .talpae*) of multiple organ involvement, including infection of the liver and bile duct (Casemore, 1994). Histological studies have provided evidence of the following characteristics of *Cyclospora* : the upper small bowel is the site of infection in the immuno-competent host; infection is associated with pronounced changes in histopathology; and the parasite is intracellular (Soave, 1996). Ultimately, nutrient malabsorption and increased secretion of fluids and electrolytes from the gut produces secretory and osmotic diarrhoea (Brown and Rotchafer, 1999).

Cyclosporiasis : Treatment

The recommended treatment for cyclosporiasis is a combination of two antibiotics, trimethoprim-sulfamethoxazole (TMP-SMX), also known as Bactrim, Septra, or Cotrim. (CDC, 2002). A study of 43 AIDS patients showed that TMP-SMX at 960mg (160mg TMP/800mg SMX) four times a day for 10 days was effective. Diarrhoea and abdominal pain stopped after 2.5 days. Recurrence of symptoms was observed 1-3 months post treatment in 44% of patients (Marshall *et al.*, 1997). In a double-blinded, placebo-controlled trial of TMP-SMX for *Cyclospora* infection in 20 expatriates in Nepal, oocysts and symptoms cleared after 7 days of treatment in 94% of the patients. After 7 days of crossover therapy, 91% of the patients in the placebo group cleared the infection (Marshall *et al.*, 1997). It is interesting to note that cyclosporiasis appears to have emerged in Nepal at a time when, because of growing resistance, quinolones replaced TMP-SMX for the treatment of bacterial enteritis (Hoge *et al.*, 1995). Alternative effective therapeutic agents have not yet been identified, which is unfortunate for sulfa-allergic patients, who have no treatment available to them (Brown and Rotchafer, 1999; Conner, 1997).

Taxonomy

C. cayetanensis is a coccidian pathogen, first reported in humans in 1979 (Ashford *et al.*, 1979). The name *C. cayetanensis* was first put forward by Ortega *et al.* in 1993, and was validated in 1994 when a complete morphological description was published (Ortega *et al.*, 1994). Prior to 1994, the organism was variously referred to as CLB (coccidian-like or cyanobacterium-like body), blue-green algae-like, fungal spores and large *Cryptosporidium* (Soave *et al.*, 1998). There have been various questions about the exact molecular taxonomy of *Cyclospora*, due in part to improvements in molecular diagnostic techniques and Duszynski *et al.* (1999) have questioned the exact structural description of the sporulated oocyst as made by Ortega *et al.* (1994). Despite this, *Cyclospora cayetanensis* is the preferred name for the organism in the literature and it has been classified as shown in Table A.2.

Kingdom	Protozoa (Goldfuss, 1818)	Predominantly unicellular
Phylum	Apicomplexa (Levine, 1970)	Possessing apical complex
Class	Sprozoasida	Asexual and sexual cycles, with oocyst formation
Sub-class	Coccidiasina	Life cycle with merogeny, gametogony and sporogony
Order	Eucoccidiorida (Leger & Duboscq, 1910)	
Suborder	Eimerioina	Independent microgamy and macrogamy
Family	Eimeriidae	
Genus	*Cyclospora* (Schneider, 1881)	2 sporocysts - 2 sporozoites each
Species	*cayetanensis* (Ortega *et al.* 1994)	Infects humans

Table A.2 – Taxonomic classification of *Cyclopora* species

Life Cycle and Transmission

Mechanisms of pathogenesis and potential virulence are not yet defined, although the faecal-oral route is probably the major one. Seasonality of infection is extremely strong. The life cycle has yet to be completely described.

Most reports (Hoge *et al.*, 1993; Rabold *et al.*,1994) dealing with the infection have come from cities and regions which are predominantly coastal, near both fresh and salt

water, suggesting *C. cayetanensis* is transmitted via the water-borne route (Figure A.1). The most likely explanation is that, like other coccidians, *C. cayetanensis*, is transmitted via the water- and food-borne routes. One suggestion for the contamination of the Guatemalan raspberries is that the berries were sprayed with insecticide diluted by contaminated ground water. A recent 12 month study of the water supply in Hanoi found *C. cayetanensis* oocysts in the water supply but could not confirm this was the mode of transmission of infection in the population (Cam *et al.*, 2001)

Unsporulated oocysts are shed in faeces, and up to 40% sporulated within 7-13 days under optimal laboratory conditions (Marshall *et al.*, 1997). As there are life cycle variations between *Cyclospora* species, it is difficult to predict the complete life cycle for *C. cayetanensis*, although exogenous sporulation closely resembles that of *C. talpae*. It also remains to be determined if humans are the only natural host. The potential existence of animal reservoir hosts, and the mechanisms of contamination of food and water, are still under investigation. (Eberhard *et al.*, 2000).

A proposed life cycle for *C. cayetanensis* is shown in Figure A.2 and described in Table A.3.

No. in Fig A.2	Description of life-cycle stage
1	When freshly passed in stools, the oocyst contains a spherical sporont and is not infective (thus, *direct* fecal-oral transmission cannot occur; this differentiates *C. cayetanensis* from another important coccidian parasite, *C. parvum*).
2	In the environment, sporulation occurs after days or weeks at temperatures between 26° C to 30° C , resulting in division of the sporont into two sporocysts, each containing two sporozoites.
3-4	Fruits, vegetables, and water can serve as vehicles for transmission.
5	The sporulated oocysts are ingested (in contaminated food or water). The oocysts excyst in the gastrointestinal tract, freeing the sporozoites which invade the epithelial cells of the small intestine.
6-7	Inside the cells the sporozoites undergo asexual multiplication and sexual development to originate mature oocysts which will be shed in stools in unsporulated form.

Table A.3 – Description of the proposed life-cycle of *Cyclospora cayetanensis*.

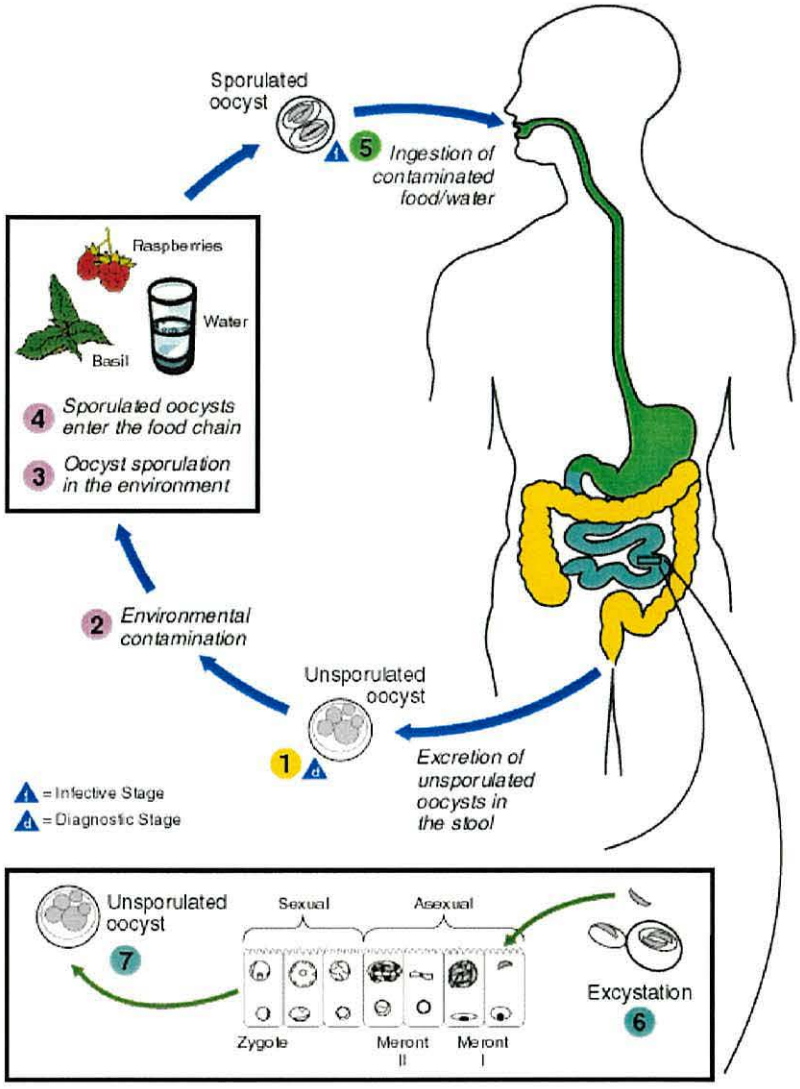

Figure A.2 - Proposed life cycle of *Cyclospora cayetanensis* (CDC, 2002).

References

Adams, A. and Ortega, Y. R. **(1999)** *Cyclospora.* In R. K. Robinson, C. A. Batt, and P.D. Patel (ed.), Encyclopaedia of Food Microbiology. Academic Press Limited, London, UK.

Anon **(1991)** Diarrheal diseases – outbreaks associated with cyanobacteria (blue-green algae)-like bodies – United States and Nepal. *Weekly Epidemiological Record* **66** 241-248.

Ashford, R. W., Warhurst, D. C. and Reid,G.D.F.**(1979)** Human infection with cyanobacterium-like bodies. *Lancet* **34** 1034.

Brown, G. H. and Rotchafer, J. C. **(1999)** *Cyclospora :* Review of an emerging parasite. *Pharmacotherapy* **19(1)** 70-75.

Cam, P. D., Sorel, N., Dan, L. C., Larher, E., Tassin, S., Barbier J. P. and Miegeville, M. **(2001)** A new contribution to the epidemiological survey of *Cyclospora cayetanensis* in Hanoi water supplied (View-Nam); A 12-month longitudinal study. *Med. Mal. Infect.* **31** 591-596.

Casemore, D. P. **(1994)** *Cyclospora :* Another 'new' Pathogen. *J. Med. Microbiol.* **41** 217-219.

Cann, K. J., Chalmers, R. M., Nichols, G., O'Brien, S. J. **(2000)** *Cyclospora* infections in England & Wales 1993-1998. *Commun.Dis & Public Health* **3(1)** 46-49.

CDC **(1997)** Update : Outbreaks of Cyclosporiasis – US and Canada. *Morbidity and Mortality Weekly* **46(23)** Centres for Disease Control, Atlanta.

CDC **(1998)** Outbreak of Cyclosporiasis – Ontario, Canada, May 1998. *Morbidity and Mortality Weekly* **47(38)** Centres for Disease Control, Atlanta.

CDC **(2002)** Centres for Disease Control and Prevention. Identification and diagnosis of parasites of public health concern. Retrieved May 14th, 2002, from the World Wide Web : http://www.dpd.cdc.gov/dpdx/HTML/Cyclosporiasis.htm

Conner, B. A. **(1997)** *Cyclospora* Infection : A review. *Annals Academic Med. Singapore* **26** 632-636.

Duszynski, D. W., Wilson, W. D., Upton, S. J. and Levine, N. D. **(1999)** Coccidia (Apicomplexa : Eimeriidae) in the primates and the scandentia. *Int. J. Primatology* **20(5)** 761 – 797.

Eberhard, M. L., Pieniazek, N. J. and Arrowood, M.J. **(1997)** Laboratory diagnosis of *Cyclospora* infections. *Archiv. Pathol. Lab. Med.* **121** 792-797.

Eberhard, M.L., Ortega, Y. R., Hanes, D. E., Nace, E. K., Do, R. Q., Robl M. G., Won, K. Y., Gavidia, C., Sass, N.L., Mansfield, K., Gozalo, A., Grigiths, J., Gilman, R. and Sterling C. R. **(2000)** Attempts to establish *Cyclospora cayetanensis* infection in laboratory animals. *J. Parasitol.* **86(3)** 577-582.

Eimer, T. **(1870)** Ueber die ei-und kugelformigen sogenannten Psorospermien der Wirbelthiere 1-58 *Wurzberg : A. Stuber's Verlangshandlung.*

Gill, N. **(1997)** Cyclosporiasis in Europe : Underdiagnosed? *EuroSurveillance Weekly* 21.8.97

Herwaldt, B. L. and Ackers, M-L. **(1997)** An outbreak in 1996 of cyclosporiasis associated with imported raspberries. *New Eng. J. Med.* 1548 – 1556.

Herwaldt, B. L. **(2000)** *Cyclospora cayetanensis* : A review focussing on the outbreaks of cyclosoriasis in the 1990s. *Clin. Infect. Dis.* **31** 1040-1057.

Hoge, C. W., Shlim, D. R., Rajah, R., Triplett, J., Shear, M., Rabold, J.G. and Echeverria, P. **(1993)** Epideminology of diarrhoeal illness associated with coccidian-like organism among travellers and foreign residents in Nepal. *Lancet* **341** 169-170.

Hoge, C. W., Shlim, D. R., Ghimire, M., Rabold, J. G., Pandey, P., Walch, A., Rajah, R., Gardiv, P. and Echeveria, P. **(1995)** Placebo-controlled trial of co-trimoxazole for *Cyclospora* infections among travellers and foreign residents in Nepal. *Lancet* **354** 691-693.

Marshall, M. M., Naumovitz, D., Ortega, Y.R. and Sterling, C. R. **(1997)** Waterborne Protozoan Pathogens. *Clin. Microbiol. Rev.* **10 (1)** 67-85.

Miller, M. A. and Paige, J. C. **(1998)** Other foodborne infections. *Veterinary Clinics of North America Food Animal Practice* **14(1)** 71-+.

Ortega, Y. R., Sterling, R., Gilman, R. H., Lama, V. A. and Diaz, F. **(1993)** *Cyclospora* Species – A New Protozoan Pathogen of Humans. *New Eng. J. Med.* 1306 – 1312.

Ortega, Y. R., Gilman, R. H. and Sterling, C. R. **(1994)** A new coccidian parasite (apicomplaxe:Eimeriidae) from humans. *J. Parsitology* **80(4)** 625-629.

Ortega, Y. R., Stirling, C. R. and Gilman, R. H. **(1998)** *Cyclospora cayetanensis. Adv. Parasitol.* **40** 399-418.

Petry, F., Hofstatter, J., Schulz, B. K ., Deitrich, G., Jung, M. and Schirmacher, P. **(1997)** *Cyclospora cayetanensis* : First imported infections in Germany. *Infection* **25(3)** 167-170.

Rabold, J. G., Hoge, C. W., Shlim, D. R., Kefford, C., Rajah, R. and Echeverria, P. **(1994)** *Cyclospora* outbreak associated with chlorinated drinking water. *Lancet* **344** 1360-1361.

Schaudinn, F. **(1902)** Studien uber krankheitserregende Protozoen. I. *Cyclospora caryolytica* Schaud. Erregar der perniciosen Enteritis des Maulwurfs. *Arbeiten aus dem Kaiserlichen Gesundheitsamte* **18** 378-416.

Schlim, D. R., Cohen, M. T., Eaton, M., Rajah, R., Long E. G. and Ungar, B. L. P. **(1991)** An algae like organism associated with an outbreak of prolonged diarrhoea among foreigners in Nepal. *Am. J. Trop. Med. Hyg.* **45** 383-389.

Schneider, A. **(1881)** Sur les psorospermies ovifirmes ou coccidies, especes nouvelles ou peu connues. *Archives de Zoologie Experimentale et Generale* **9** 387-404.

Soave, R. **(1996)** State of the Art Clinical Article : *Cyclospora,* and overview. *Clin. Inf. Dis.* **23** 429-437.

Soave, R. , Herwaldt, B. L. and Relman, D. A. **(1998)** *Cyclospora. Infect. Dis. Clin. N. America* **12(1)** 1-12.

Appendix B – *Ascaris* Species

Recognition that *Ascaris* infection is deleterious to health has prompted the World Health Organisation to develop and promote control strategies based on the prudent use of anthelminthic drugs, supported by appropriate health education and realistic sanitation (WHO, 1996). *Ascaris* infects both humans and pigs and swine parasitism exerts a significant economic impact worldwide – three of the six most common food-borne parasitic diseases in the United States are associated with pork consumption (Baker *et al.*, 1994). In this chapter, the background and most recent research regarding *Ascaris* is presented.

Background

Common parasitic roundworms of pigs and humans are in the genus *Ascaris.* The earliest recorded case of *Ascaris* infection in the UK appears to be 'Pete Marsh', whose 2,500 year old corpse, containing *Ascaris* worms, was found in a Cheshire bog (Owen, 1986). Tyson (1683) first described *Ascaris* in humans scientifically as *Lumbricoides teres*, but Linnaeus (1758) proposed that it be known as *A. lumbricoides*. Not long after, Goeze (1782) published his description of *Ascaris* in pigs, which he called *A. suum.* The two species continue to be discussed today as if they are separate, although there are difficulties in distinguishing them (Crompton, 1989) and there is a debate in the literature as to whether they are actually separate species or not (Crompton, 2001; Anderson, 2001).

The genus *Ascaris* comprises 17 species according to the classification of Yamaguti (1961) and 13 species according to that of Skryabin *et al.* (1991) (Table B.1).

Species	Host Species	Common Name	Distribution
*A. brevispiculum**	*Apodemus chevrieri*	Wood mouse	Former USSR
A. castoris	*Castor fiber*	Eurasian beaver	Europe
A. cebi	*Cebus capuucinus*	White throated capuchin monkey	Honduras to Columbia
A. columnaris	*Mephitis mephis* *Mustela erminea* *Procyon lotor*	Striped skunk Stoat Raccoon	Related mammals in N. America
A. dasypodina	*Dasypus gymnurus*	Armadillo	Paraguay
*A. devosi**	*Martes Americana*	American Martin	N. America
A. hippopotami	*Hippopotamus amphibious*	Hippopotomus	Sub-Saharan Africa
A. joffi	*Citellus pygmaeus*	Little souslik	Kazakhstan
*A. laevis**	*Marmota monax* *Citellus parryii*	Woodchuck Arctic ground squirrel	N. America
A. lumbricoides	*Homo sapiens* *Alouatta palliata* *Canis familiaris* *Callosciurus pygerythrus* *Gorilla gorilla* *Hylobates agilis* *Hylobates lar* *Macaca arctoides* *Macaca mulatta* *Pan paniscus* *Pan troglodytes* *Ratufa indica* *Sus domesticus*	Human Howling monkey Domestic dog Irrawaddy squirrel Gorilla Agile gibbon Gibbon Bear macaque Rhesus monkey Pygmy chimpanzee Chimpanzee Indian giant squirrel Domestic pig	Worldwide
A. ovis	*Ovis aries*	Domestic sheep	Australia, N. America, UK & former USSR
A. phacocheri	*Phacochoerus africanus*	Wart hog	D. R. Congo
A. schroederi	*Ailuropoda melanoleuca*	Giant panda	P. R. China
*A. spalacis**	*Spalax leucodon*	Blind mole rat	Balkans
A. suricattae	*Suricata suricatta*	Meerkat	Republic of South Africa
A. suum	*Sus domesticus* *Sus scrofa* *Bos Taurus* *Homo sapiens* *Erythrocebus patas*	Domestic pig Wild boar Domestic cattle Human Red monkey	Worldwide
A. tarbagan	*Marmota sibirica*	Siberian marmot	Siberia

Table B.1 – Host specificity of species of *Ascaris*. (* indicates the species is not listed in the Skryabin classification system) (Crompton, 2001).

Epidemology

In 1988 the estimated number of people infected with *A. lumbricoides* was 1 billion (Crompton, 1988). However, recent estimates have put the number at about 1.5 billion; the contribution from the third world being more than a billion alone (Crompton, 1999). *Ascaris* infection leads to morbidity in about 335 million of those infected, and is a global public health problem (Crompton, 2001). Cross infection of *A. suum* from pigs to humans has been reported (Crompton, 1989; Anderson, 1995). *Ascaris* infection is particularly prevalent in developing countries (Meeking *et al.*, 1996), with the list of countries with prevalences of 50% or more being longer than those countries reporting a decline in infections (Figure B.1) (Crompton, 1985).

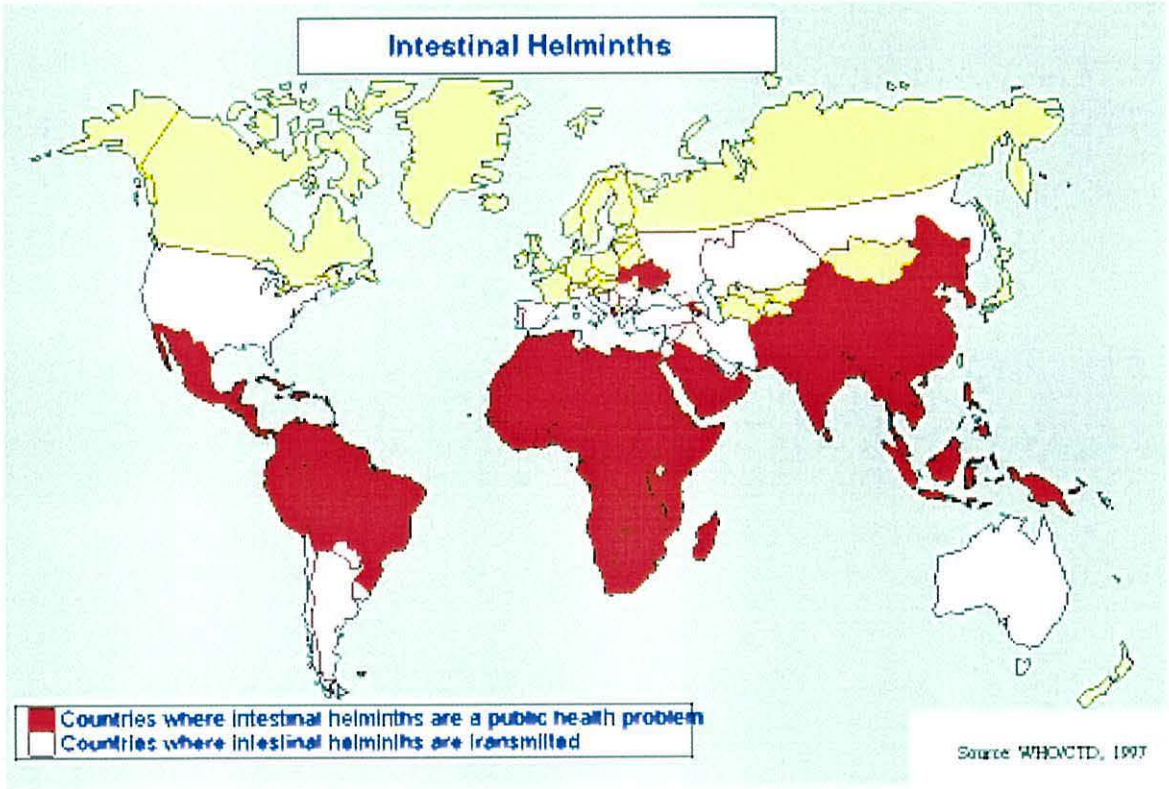

Figure B.1 – Map of the world showing the countries affected by helminth (intestinal worms) infection (WHO, 1995).

Once shed, the eggs can survive for 6-12 months in soils (Gaspard *et al.*, 1997). Eggs have even been reported to survive in sub-arctic regions (Embil *et al.*, 1984), and Krasnosos (1978) showed that some embryonated eggs were still viable after 14 years.

Ascaris Infection

The disease caused by *Ascaris* infection is called ascariasis. Infection occurs through the ingestion of embryonated eggs. In the presence of natural light and at 30°C, *A. lumbricoides* embryonate rapidly to the state in which they can infect man (Echenique *et al.,* 1997). The prepatent period, the time between the exposure of the host to the infective eggs and the detection of eggs in the hosts faeces, is 60-70 days. The infectious dose is unknown, but may be as low as 100 eggs. In a remarkable series of experiments in 1922, Koino infected himself with 2000 eggs and became seriously ill (Koino, 1922). Koino's younger brother, infected with 500 eggs, also became ill, but not as seriously.

Diagnosis of infection is by finding the characteristic eggs in faecal smears examined by bright field microscopy. The detection of eggs in stool samples can fail if there are only immature worms, males or old females are present in the small intestine as these worms do not produce eggs. There is at present no convenient method for discriminating between an egg of *A. lumbricoides* or *A. suum.*

A few adult worms in the intestine will not do much harm to the human host, except for occasional abdominal pain. Complications arise when there are large numbers of worms. Physical blockage of the intestine occurs, leading to serious intestinal complications. In such cases, surgery maybe required to remove the worms (Wasadikar *et al.,* 1997). It has been shown that *Ascaris* induced intestinal obstruction occurs about 30 times more frequently in children than adults (Ochoa, 1991) and that children aged 5-15 are at greater risk of morbidity than other groups in a community (Chan *et al.,* 1994).

Research has shown that heavy infection can lead to up to 25% non-utilisation of ingested calories by the host (Latham *et al.*,1977). Infection with *A. lumbricoides* has been strongly linked to retarded growth in children (Hlaing, 1993; Solomons, 1993; Ananthakrishnan *et al.,* 1997) and there is evidence that high numbers can affect mental performance (Watkins *et al.*,1997).

Ascaris treatment

The WHO recommends that four anthelminthic drugs should be used in programmes designed to reduce morbidity due to *A. lumbricoides* and other intestinal nematode infections – Albedendazole, Levamisole, Mebendazole and Pyrantel embonate (WHO, 1995). Treatment with Nitazoxanide to clear a specific infection (500 mg tablets administered orally, twice a day, for 7 days) can also be effective (Cabello *et al.*, 1997, Doumbo *et al.*, 1997). However, resistance to anthelmintics has appeared in some parasitic nematodes, but the mechanisms of this resistance remains to be determined (Martin *et al.*, 1996; Crompton, 2001). It is encouraging to note that, so far, no reports of drug resistant *A. suum* in pigs have been found (Taylor, 1992; Crompton, 2001).

Taxonomy of *Ascaris*

The accepted systematic scheme for the classification of *Ascaris* is set out in Table B.2.

Kingdom	Nemathelminthes	
Sub-kingdom	Metazoa	Multi-celled animals
Phylum	Nematoda	Roundworms (cylindrical body tapered at both ends, unsegmented)
Class	Secernetea	chemosensory structures located at the tail
Sub-class	Rhabditia	having a mouth & tripartite oesophagus
Order	Ascaridida	Large roundworms
Sub-order	Ascaridina	Roundworms of various arthropods, molluscs, and vertebrates (inc. humans)
Superfamily	Ascaridoidea	highly muscular oesophagus
Family	Ascarididae	well-developed lip region separated from the cervical region
Genus	*Ascaris*	three-lipped mouths
Species	*lumbricoides* (Linnaeus 1758) *suum* (Goeze 1782)	infects humans infects pigs

Table B.2 - Taxonomy of *Ascaris* species.

Lifecycle

The life cycle of *Ascaris lumbricoides* is by the direct faecal-oral route, with no intermediate host. Males and females live in the small intestine feeding on digested food of the human host. In order for eggs to start developing, they must be outside the host and the environmental temperature must be 30°C with moisture and oxygen being readily available. After 14 days the larvae are fully developed, but remain within the egg shell until swallowed by a human, usually either by ingesting contaminated soil or unwashed vegetables. Eggs can remain infective up to two years in the right conditions (CDC, 1999; Kazura, 2000).

The conditions required for hatching of the larvae are a temperature of about 37°C, moderately low-redox potential, high carbon dioxide concentration and neutral pH. These are the conditions found in the mammalian intestine. The full life cycle of *Ascaris lumbricoides* is shown in Figure B.2. Adult worms live in the intestine and females produce eggs which are passed in faeces. Fertile eggs embryonate and become infective in the right environmental conditions and are swallowed. The eggs take in water and the increased water concentration activates the larva, which secretes a variety of enzymes to help break down the egg shell. Once the egg shell is sufficiently weakened, the larva hatches out and starts to travel through the body. They pass through the intestinal wall and reach the lungs via the blood or lymphatic system. In the lungs, they pass into the air sacs, are carried up the bronchial tree, coughed into the pharynx and are re-swallowed to pass through the stomach and enter the small intestine, where they grow, mature and mate, producing more eggs that are excreted in faeces. An adult can live for 6 months to a year inside a human small intestine.

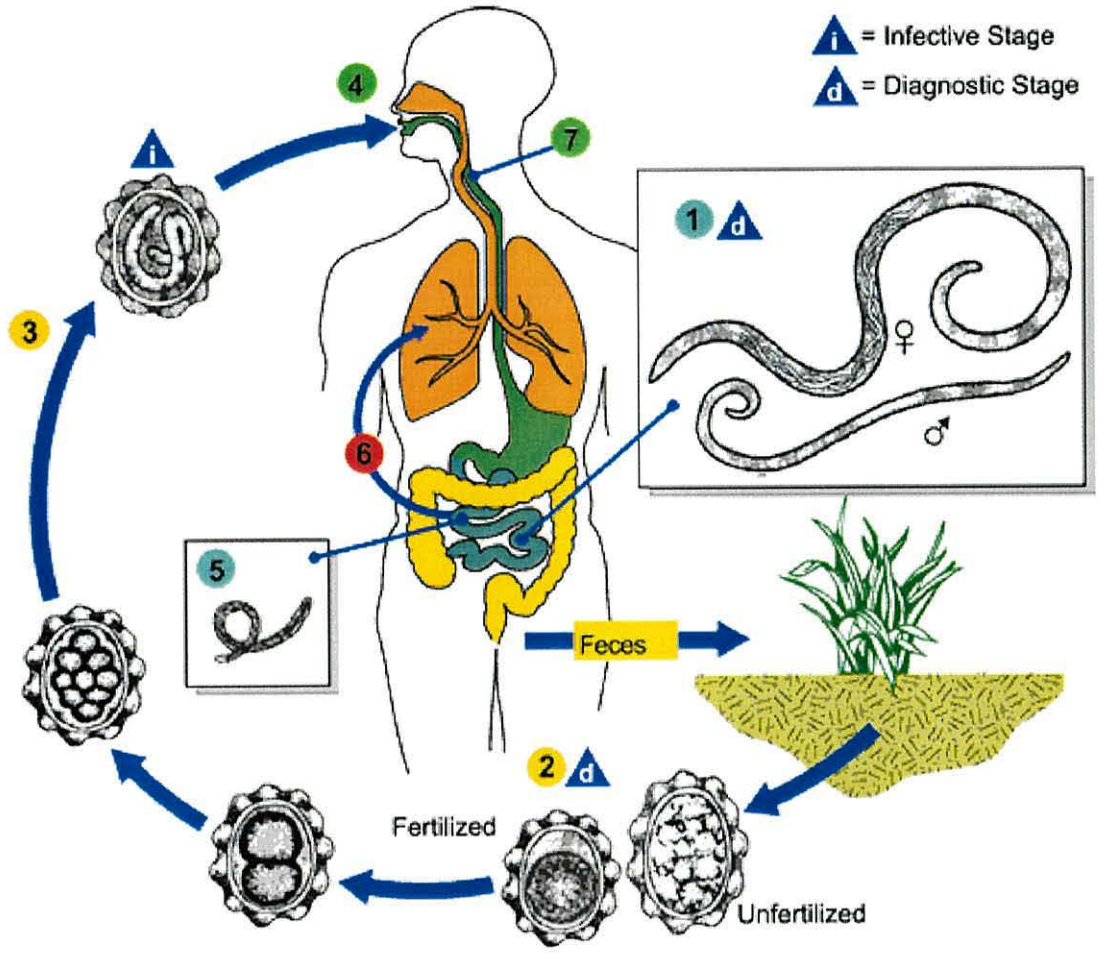

Figure B.2 – Life cycle of *Ascaris lumbricoides* (CDC, 2002).

References

Ananthakrishnan, S., Nalini, P. and Pani, S. P. **(1997)** Intestinal geohelminthiasis in the developing world. *National Medical Journal of India* **10(2)** 67-71

Anderson, T. J. C **(1995)** *Ascaris* infections in humans from North-America – molecular evidence for cross infection. *Parasitology* **110(2)** 215-219

Anderson, T. J. C **(2001)** The dangers of using single locus markers in parasite epidemiology : Ascaris as a case study. *TRENDS in Parasitology* **17(4)** 183-188

Baker, D. G., Bryant, J. D., Urban, J. F. and Lunney, J. K. **(1994)** Swine Immunity to selected parasites. *Veterinary immunology and immunopathology* **43(1-3)** 127-133

Cabello, R. R., Guerrero, L. R., Garcia, M. D. M. and Cruz, A. G. **(1997)** Nitazoxanide for the treatment of intestinal protozoan and helminthic infections in Mexico. *Trans. Royal Soc. Trop. Med. Hyg.* **91(6)** 701-703

CDC **(1999)** Centres for Disease Control and Prevention. *How to prevent transmission of intestinal roundworms from pets to people.* Retrieved January 9, 2000, from the World Wide Web: http://www.cdc.gov/ncidod/diseases/roundwrm/roundwrm.htm.

CDC **(2002)** Centres for Disease Control and Prevention. *Identification and diagnosis of parasites of public health concern.* Retrieved April 5th, 2002, from the World Wide Web : http://www.dpd.cdc.gov/dpdx/HTML/Ascariasis.htm.

Chan, M. S., Medley, G. F., Jamison, D. and Bundy, D. A. P. **(1994)** The evaluation of potential global morbidity attributable to intestinal nematode infections. *Parasitology* **109** 373-387

Crompton, D. W. T. (Ed.) **(1985)** *Ascariasis and its Public Health Significance.* Taylor & Francis, London.

Crompton, D. W. T. (**1988)** The prevalence of ascariasis. *Parasit.Today* **4** 162-169

Crompton, D. W. T. (**1989)** Prevalence of ascariasis. In : *Asariasis and it prevention and control.* Taylor and Francis, London.

Crompton, D. W. T. **(1999)** How much human helminthiasis is there in the world? *J. Parasitol.* **85 (3)** 397-403

Crompton, D. W. T. (**2001)** *Ascaris* and ascariasis. *Adv. Parasitol.* **48** 285-375

Doumbo, O., Rossignol, J. F., Pichard, E., Traore, H. A., Dembele, M., Diakite, M., Traore, F. and Dillo, D. A. **(1997)** Nitazoxanide in the treatment of cryptosporidial diarrhea and other intestinal parasitic infections associated with acquired immunodeficiency syndrome in tropical Africa. *Am. J. Trop. Med. Hyg.* **56(6)** 637-639

Echenique, C. G. and Magaro, H. M. **(1997)** Study of *Ascaris lumbricoides* in larval phases. *Acta Bioquimica Clinica Latino Americana* **31(1)** 23-27

Embil, J. A., Pereira, C. H. and White, F. H. **(1984)** Prevalence of *Ascaris lumbricoides* infection in a small Nova Scotian community. *Am. J. Trop. Med. Hyg.* **33** 595-598

Gaspard, P., Ambolet, Y. and Schwartzbrod, J. **(1997)** Urban sludge reused for agricultural purposes : Soils contamination and model development for the parasitological risk assessment. *Bulletin de L'Academie Nationale de Medicine* **181(1)** 43-57

Goeze, J. A. E. **(1782)** *Versuch einer Naturgeschichte der Eingeweidewurmer thierischer Korper.* Blankenburg : PA Pape.

Hlaing, T. **(1993)** Ascariasis and childhood malnutrition. *Parasitology* **107-SS** 125-136

Kazura, J. W. **(2000).** *Ascariasis (Ascaris lumbricoides).* In Behrman, R., Kliegman, R., and Jenson H. (Eds.). Nelson textbook of pediatrics (16th ed.) (pp. 1064-1065). Philadelphia: W.B. Saunders Company.

Koino, S. **(1922)** Experimental infections on human body with Ascarides. *Jpn. Med. World.* **2** 317-320

Krasnosos, L. N. **(1978)** Long term survival of ascarid eggs – *Ascaris lumbricoides* L. 1758 – in the soil of Samarkand. *Meditinskaya Parazitologicya I Parasitarnye Bolezni* **47** 103-105

Latham, L. and M. and Basta, S. S. **(1977)** The nutritional and economic implications of *Ascaris* infection in Kenya. *Staff working paper No. 271, International Bank for reconstruction and Development*, World Bank, Washington.

Linnaeus, C. **(1758)** *Systema Naturae* Laurentill Salvii, Holmiae

Martin, R. J., Valkanov, M. A., Dale, V. M. E, Robertson, A. P. and Murray, I. **(1996)** Electrophysiology of *Ascaris* muscle and anti-nematodal drug action. *Parasitology* **113-SS** 137-156

Meeking, H J., Stentiford, E. I. and Lee, D. L. **(1996)** The effect of sewage-sludge compost on the viability of the ova of a parasitic nematode. *Compost Sci. Util.* **4-2** 46-54

Ochoa, B. **(1991)** Surgical complications of ascariasis. *World J. Surgery* **15** 222-227

Owen, R. R. **(1986)** Parasites in Britain : a review. *J. Royal Soc. Health* **106** 41-43

Skryabin, K. I., Shikhobalova, N. P. and Mozgovoi, A. A. **(1991)** *Key to Parasitic Nematodes 2: Oxyurate and Ascaridata.* E. J. Brill, New York.

Solomons, N. W. **(1993)** Pathways to the impairment of human nutritional-status by gastrointestinal pathogens. *Parasitology* **107-SS** 19-35

Taylor, M. A. **(1992)** Anthelminthic resistance in helminth parasites of domestic animals. *Agricultural Zoology Reviews* **5** 1-50

Tyson, E. **(1683)** *Lumbricoides teres*, or some anatomical observations on the roundworm bred in human bodies. *Phil. Trans. Roal Soc. London* **13** 152-161

Wasadikar, P.P. and Kulkarni, A.B. **(1997)** Intestinal obstruction due to Ascariasis. *British Journal of Surgery* **84(3)** 410-412

Watkins, W. E. and Pollitt, E. **(1997)** 'Stupidity or worms' : Do intestinal worms impair mental performance? *Psychological Bulletin* **121(2)** 171-191

WHO **(1995)** *Drugs used in Parasitic Disease* 2nd Ed. WHO Model Prescribing Information, World Health Organisation, Geneva

WHO **(1996)** *Report of the WHO Informal Consultation on hookworm infection and anaemia in girls and women.* (WHO/CTD/SIP/96.1) World Health Organisation, Geneva.

Yamaguti, S. **(1961)** *Systema Helminthum III: The Nematodes of Vertebrates 1.* Wiley Interscience Publishers, London.

Appendix C – Publications

Refereed Publications arising from this work

Dalton, C., Goater, A. D., Drysdale, J. and Pethig, R. **(2001)** Parasite Viability By Electrorotation *Colloids and Surfaces A : Physicochemical and Engineering Aspects* **195** 263-268

Dalton, C., Goater, A. D., Pethig, R. and Smith, H. V. **(2001)** Viability of *Giardia intestinalis* cysts and viability and sporulation state of *Cyclospora cayetanensis* oocysts determined by Electrorotation. *Appl. Environ. Microbiol.* **67**(2) 586-590

Dalton, C., Pethig, R. and Smith, H. V. **(2000).** Electrorotation of *Ascaris suum. Trans. Royal Soc. Trop. Med. Hyg.* **94** 616-619

Dalton, C., Pethig, R., Paton, C. A. and Smith, H. V. **(1999)** Viability determination of *Cyclospora cayetanensis* oocysts. *Trans. Royal Soc. Trop. Med. Hyg.* **93** 461-463

Dalton, C., Pethig, R., Paton, C. A. and Smith, H. V. **(1999)** Electrorotation of oocysts of *Cyclospora cayetanensis. Inst. Phys. Conf. Ser.* **163** 85-88

Conference Presentations and Posters

Goater, A. D., Burt, J. P, H., Dalton, C. and Tame, J. A. **(2002)** AC Electrokinetics of Bioparticles in Water. **Oral presentation at the** *15th Meeting of the Microbiological Methods Innovation Forum*, 28th May, Campden & Chorleywood Food Research Association, Chipping Campden, UK.

Dalton, C. and Burt, J. P. H. **(2001)** Fertilisation state of ova of the nematode *Ascaris suum* determined by electrokinetic techniques. **Oral presentation at** *the first European Workshop on Electrokinetics and Electrohydrodynamics in Microsystems*, 6-8th September, Glasgow, UK.

Dalton, C., Burt, J. P. H., Cotterill, S. L., Goater, A. D., Zhou, X-F. and Pethig, R. **(2001)** Electrokinetic Particulate Laboratory-on-a-chip (Biofactory) Technology. **Poster presented at** *Molecular analysis : Analytical challenges for the life sciences*, 12-13th March, Warwick.

Dalton, C., Goater, A. D., Drysdale, J. and Pethig, R. **(2000)** Parasite Viability By Electrorotation. **Oral presentation at** the *International Symposium on Electrokinetic Phenomena* (ELKIN), Oct 2-6th, Dresden, Germany.

Dalton, C., Pethig, R. and Smith, H. V. **(2000).** Electrorotation of *Ascaris suum.* **Poster presented at** *The Royal Society of Tropical Medicine Meeting,* 17th May, Glasgow

Dalton, C., Pethig, R., Paton, C. A. and Smith, H. V. **(1999)** Viability determination of *Cyclospora cayetanensis* oocysts. **Poster presented at** *The Royal Society of Tropical Medicine Meeting.* 19th May, Edinburgh.

Dalton, C., Pethig, R., Paton, C. A. and Smith, H. V. **(1999)** Electrorotation of oocysts of *Cyclospora cayetanensis.* **Poster presented at** the IOP Electrostatics 1999 Conference, 28-31st March, Cambridge.

ELSEVIER

Colloids and Surfaces
A: Physicochemical and Engineering Aspects 195 (2001) 263–268

COLLOIDS AND SURFACES A

www.elsevier.com/locate/colsurfa

Parasite viability by electrorotation

C. Dalton, A.D. Goater *, J. Drysdale, R. Pethig

Institute of Bioelectronic and Molecular Microsystems, University of Wales, Dean Street, Bangor, Gwynedd, LL57 1UT, UK

Abstract

The safety of water supplies is threatened by waterborne protozoan pathogens of man. Many of these pathogens are highly resistant to standard disinfection methods, have low infectivity doses and cause protracted disease. Single organisms subjected to a uniform rotating electric field acquire an induced electric dipole moment. The dipole and field interact and can produce a torque that makes the organism spin. The rate and direction of spin is a sensitive function of the dielectric properties of the organism and the suspending medium, namely the conductivity and permittivity. During a pathogen's lifecycle, numerous physico-chemical changes occur, which alter its dielectric properties. Electrorotation can detect these changes, enabling the viability of the pathogen to be determined. Using a microfabricated planar gold electrode array optimised for electrorotation and energised with quadrature sinusoidal voltages, we investigated the electrorotational properties of two protozoan parasites; *Giardia muris* and *Cyclospora cayetanensis*. We present differences in their electrorotational response due to viability, which was confirmed by vital dye assay for *G. muris*. Based on this work, we propose that electrorotation can be used to determine the viability of *C. cayetanensis*, for which no vital dye assays are available. The potential of this technique as a rapid and precise assay for the determination of parasite viability is particularly applicable to the food, water and healthcare industries. Furthermore, electrorotation is a non-invasive technique, allowing organisms to be further analysed using, for example, DNA sequencing, to establish likely pathogen sources.

Keywords: Electrorotation; Viability; *Cyclospora cayetanensis*; *Giardia muris*

1. Introduction

Safe drinking water has been one of the major public health advances of the last century. People in developed countries take for granted that their water is safe to drink, a luxury that most of the world's population does not have. The leading cause of infant mortality in the developing world is infectious diarrhoea and the prevalence of diarrhoeal pathogens is largely influenced by the quality and quantity of clean water available for drinking and washing [1]. Until recently, modern water treatment had all but eliminated these concerns in developed nations. However, over the past 25 years, the safety of developed nations' water supplies has been threatened by contamination caused by protozoan parasites such as *Cryptosporidium parvum*, *Giardia intestinalis* and *Cyclospora cayetanensis*. These microscopic parasites, in very small quantities (< 100), can cause prolonged diarrhoea in healthy people, and have been known to cause death in the elderly, young

* Corresponding author. Tel.: +44-1248-382751x2711; fax: +44-1248-361429.
E-mail address: agoater@sees.bangor.ac.uk (A.D. Goater).

0927-7757/01/$ - see front matter
PII: S0927-7757(01)00850-0

children and immuno-compromised people, such as AIDS sufferers.

G. intestinalis is the most frequently detected protozoan parasite of man [2]. *Giardia muris* is a closely related species of *G. intestinalis* that infects rodents and cattle and is a good experimental substitute for *G. intestinalis*. The viability of *G. muris* cysts can be determined by vital dyes coupled with morphological inspection. This allows the determination of viability by electrorotation to be verified using existing and proven protocols. *C. cayetanensis* is a newly described protozoan of man [3] and causes diarrhoeal illness world-wide [4]. There is currently no vital dye method of determining the viability of oocysts of *C. cayetanensis* [5]. Electrorotation has earlier been successfully used to investigate the dielectric properties of the protozoan *C. parvum* [6]. Here, we have investigated the properties of *G. muris* and *C. cayetanensis*, and hence found that the physico-chemical changes that occur when a protozoan changes from a viable to a non-viable state can be clearly detected.

2. Electrorotation

If a bioparticle, such as a cell, bacterium or virus, is exposed to an external electric field, it becomes electrically polarised. If the electric field is uniform in nature, then the particle experiences no net electrostatic force. However, if the electric field is non-uniform, the particle experiences a dielectrophoretic force, which causes it to move to regions where it minimises its electrostatic energy. If the particle is subjected to a rotating uniform electric field, a torque will be exerted on the particle, causing it to spin. This effect was first described by Arnold [7] and Mischel [8] in 1982, and is called electrorotation.

Consider a particle suspended in the centre of a quadrature electrode system with each electrode energised by a sinusoidal voltage 90° out of phase with its adjacent electrodes. In this situation, the resultant electric field rotates at an angular velocity equal to the angular frequency, ω, of the applied sinusoidal voltages. The particle will experience a rotational torque, $\Gamma(\omega)$, the direction and magnitude of which is given by

$$\Gamma(\omega) = -\mathrm{Im}\{m(\omega)\}E \tag{1}$$

where Im indicates the imaginary component of the induced dipole moment $m(\omega)$ with,

$$m(\omega) = 4\pi\varepsilon_m f(\varepsilon_m^*, \varepsilon_p^*)R^3E \tag{2}$$

where E is the electric field strength, R is the radius of the particle and $f(\varepsilon_m^*, \varepsilon_p^*)$ is the Clausius–Mossotti factor, defined as:

$$f(\varepsilon_m^*, \varepsilon_p^*) = \frac{(\varepsilon_p^* - \varepsilon_m^*)}{(\varepsilon_p^* + 2\varepsilon_m^*)} \tag{3}$$

where ε_p^* and ε_m^* are the particle and suspending medium complex permittivities, respectively, defined as $\varepsilon^* = \varepsilon - j(\sigma/\omega)$ with ε the permittivity, σ the conductivity and $j = \sqrt{-1}$.

The dielectric properties of the particle are in turn related to the physico-chemical properties of the particle. Thus the induced rotation of the particle is a sensitive function of the particle's dielectric properties, namely the conductivity and permittivity of the organism's constituent components. These components include the cell wall (if present), the plasma membrane and the cytoplasm. The rotation is also a function of the conductivity and permittivity of the suspending medium. The membrane of a viable particle is (selectively) permeable to ions and non-lipid, soluble molecules. Upon cell death, membrane integrity is lost, and the cell freely exchanges material with the external suspending medium. Another result of cell death might be the loss of active transport mechanisms, causing transmembrane gradients to dissipate even if the membrane integrity is maintained. This greatly affects the rotation spectra produced, as less induced charge differences occur between the interior of the oocyst and the exterior medium. If the imaginary component of m is positive, then the torque produced will cause the particle to rotate in a direction that opposes that of the rotating field [9].

3. 'Bone' electrodes

A frequent practical problem with electrorotation is that the particle is seldom positioned in the

exact centre of the electrode array. Also, groups of particles cannot all be in the exact centre of the array, so many potential spectra are lost, as the uniformity of the field cannot be guaranteed over the whole region of the electrode chamber. In an attempt to over come this problem, we have designed a more efficient electrode geometry that provides a more uniform field over the central region of the electrode chamber (Fig. 1).

The 'bone' electrode design is optimised for electrorotation only by making the chamber enclosed by the electrode edges circular in shape. The electrode shapes are described by the 4th order polynomial:

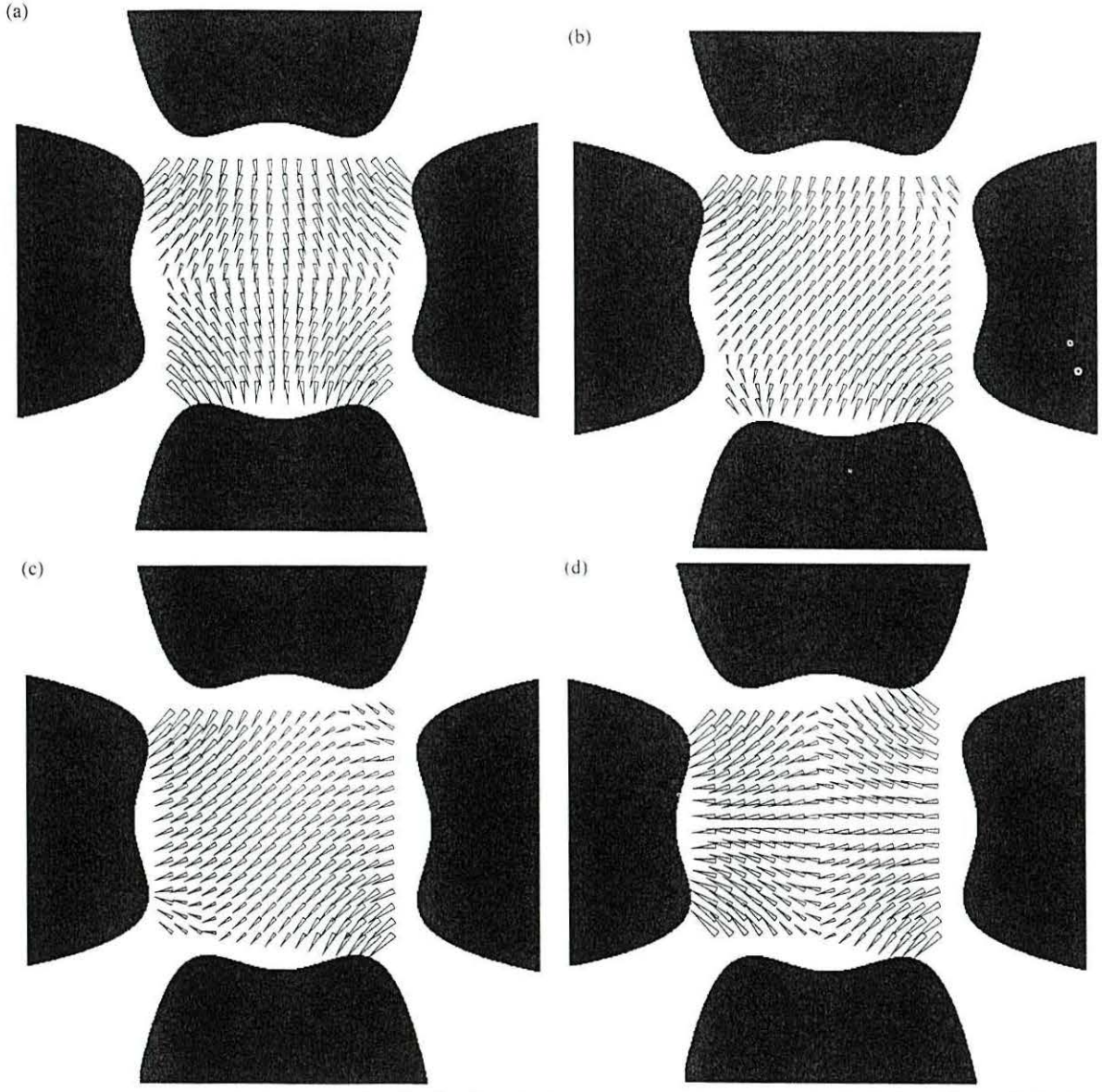

Fig. 1. (A–D) The bone electrode array as described by Eq. (4) with an electric field analysis in the $X-Y$ plane. The applied voltages progress through the first quarter of a cycle in 30° steps. (a) 0°; (b) 30°; (c) 60°; (d) 90°. The magnitude and direction of the vectors in the central region as the field changes direction remains constant.

$$y(x) = x^4 - 0.75x^2 + 1 \quad (4)$$

The shape provides a near uniform electric field in the central region and reduces unwanted dielectrophoretic forces that the organism may experience. This is confirmed by an electric field analysis in the $X-Y$ plane for the electrode system (Maxwell™, Ansoft) (Fig. 1(A–D)). The field vectors within the central section of the chamber do not change magnitude, confirming that the bone electrode design has a very uniform field within the central area. This allowed a greater number of spectra to be acquired during our analysis, which is especially important for obtaining data from organisms at low concentrations, such as the oocysts of *C. cayetanensis*. No animal model is available for the amplification of *C. cayetanensis* and so there are limited numbers available to work on.

4. Experimental setup

G. muris cysts were obtained from Waterborne Inc. (Louisiana, USA) via Professor H.V. Smith at the Scottish Parasite Diagnostic Laboratory (SPDL, Glasgow, UK). The cysts were transported packed in ice as a stock solution of 7 million cysts in 1 ml of reverse osmosis water. On arrival, the cysts were washed in ultra pure water and stored at 4 °C until required. The viability of *G. muris* cysts was determined following the approved protocol of Schupp and Erlandsen [10] of combining the fluorogenic vital dyes fluorescein diacetate (FDA) and propidium iodide (PI) with morphological inspection. Purified oocysts of *C. cayetanensis* were supplied from infected individuals from the Glasgow, Scotland area by Professor H.V. Smith. On arrival, the oocysts were washed in deionised water and stored at 4 °C in 2% potassium dichromate solution until required. Unsporulated (non-infectious, viable) oocysts of *C. cayetanensis* can be successfully sporulated to infectious, viable oocysts under laboratory conditions in 2.5% potassium dichromate solution [4]. The conditions for sporulation to occur in the environment are currently unknown [11]. The difference between sporulated and unsporulated oocysts is easily distinguished by light microscopy [4] and the electrorotational difference has been investigated and reported elsewhere [12]. All the oocysts used in this study were unsporulated and morphologically indistinguishable by light microscopy.

The (oo)cysts were washed three times in ultra pure water and suspended in dilute solutions of phosphate buffered saline (PBS) at a conductivity of 1.0 mS m^{-1} (PBS, pH 7.4, 10 mM Phosphate buffer, 27 mM KCl, 137 mM NaCl, Sigma Chemical Co.). The low conductivity of the suspending solution reduced electrolysis and heat production at the electrode edges. Working particle concentrations were 3×10^4 cysts ml^{-1} for *G. muris* and 5×10^3 oocysts ml^{-1} for *C. cayetanensis*. After each sample had been investigated, the chamber was washed prior to the next experiment with ultra pure water and dried under a stream of nitrogen.

The gold electrodes were manufactured by photolithography in a class II clean room onto a glass microscope slide with a 5 nm chromium adhesion layer and a 70 nm gold layer. The electrodes were energised using a computer controlled frequency generator with an output range of 100 Hz–10 MHz. Particle motion was visualised using phase contrast microscopy with a total magnification of $\times 400$ and recorded to video for later analysis and timing by stopwatch (Nikon Optiphot-2 microscope with JVC model TK-1280E colour video camera attachment).

5. Results

The electrorotation spectra obtained for $n = 37$ viable and $n = 5$ non-viable cysts of *G. muris* are shown in Fig. 2. There is a distinct difference between the two types of spectra obtained. In particular, there is the difference in the peak rotation rate, in the frequency window 60–600 KHz, where the viable cysts rotate at a much faster rate than the non-viable cysts. Also, at 400 KHz, the viable and non-viable cysts rotate in opposite directions, allowing for easy discrimination.

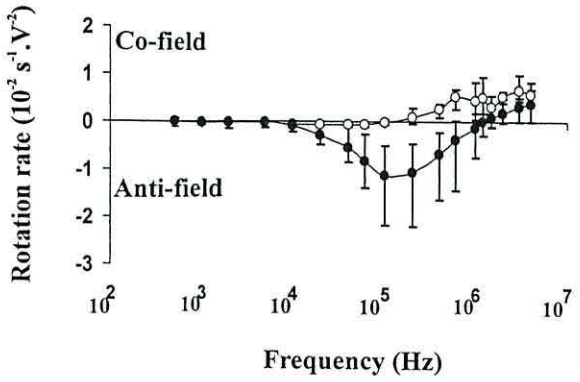

Fig. 2. Electrorotation spectra obtained for $n = 37$ (●) viable and $n = 5$ (○) non-viable cysts of *Giardia muris*. The mean rate of rotation is shown, with error bars indicating one standard deviation. Co-field and anti-field denote the sense of rotation of the particles relative to that of the applied field.

Fig. 3 shows the electrorotation spectra obtained for $n = 29$ viable and $n = 12$ non-viable oocysts of *C. cayetanensis*. The viable spectra are indicated by the shape of their response, which is similar to that of the viable *G. muris* spectra earlier shown.

All of the viable organisms possessed intact walls and refractile contents. The non-viable type spectra could be split into two groups—those that were morphologically non-viable (visible damage to the cell wall) and those morphologically indistinguishable from the viable organisms, but which gave the same spectra as the known non-viable cells. The ability to distinguish viable from non-viable by rotation in opposite directions is not possible, as there is overlap at the high frequency end of the spectra. However, the two groups can be distinguished by their rotation rates in the frequency window 40–400 KHz.

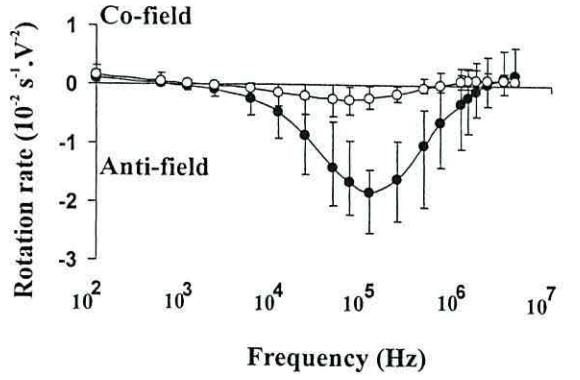

Fig. 3. Electrorotation spectra obtained for $n = 29$ (●) viable and $n = 12$ (○) non-viable oocysts of *Cyclospora cayetanensis*. The mean rate of rotation is shown, with error bars indicating one standard deviation. Co-field and anti-field denote the sense of rotation of the particles relative to that of the applied field.

A study of molecular mechanics to further understand the electrorotation behaviour between viable and non-viable protozoa would be of particular interest, especially the effect of membrane ion-transport. Related studies in the area of dielectrophoresis have been earlier reported [13].

6. Conclusions

Electrorotation can non-invasively determine the viability of cysts of *G. muris* and oocysts of *C. cayetanensis*. This allows the (oo)cysts to be further analysed by other methods, e.g. rDNA analysis. This method also has the advantage of being versatile—the same experimental setup can investigate many different organisms. Since electrorotation relies upon visual data analysis, the process is easily automated and several groups have published image processing procedures [14,15]. These qualities of the electrorotation technique show that it has the potential to become a powerful investigative tool for microbiologists involved in the control of water-borne parasites.

Acknowledgements

This work was supported by the Biotechnology and Biological Sciences Research Council, UK (Grant 97/B1/E/03539) and the National Foundation for Cancer Research, USA. We thank H.V. Smith and C.A. Paton, of the Scottish Parasite Diagnostic Laboratory for valuable discussions about the organisms and J.A. Tame for technical assistance with the electrode fabrication.

References

[1] T.S. Steiner, N.M. Theilman, R.L. Glerrant, Annu. Rev. Med. 48 (1997) 329.
[2] M.J.G. Farthing, A.-M. Cevallos, P. Kelly, in: G.C. Cook (Ed.), Manson's Tropical Diseases, 20th ed., Saunders, London, UK, 1996.
[3] R.W. Ashford, Ann. Trop. Med. Parasitol. 73 (1979) 497.
[4] Y.R. Ortega, C.R. Sterling, R.H. Gilman, V.A. Cama, F. Diaz, New Engl. J. Med. 328 (1993) 1308.
[5] M.L. Eberhard, N.J. Pieniazek, M.J. Arrowood, Arch. Pathol. Lab. Med. 121 (1997) 792.
[6] A.D. Goater, J.P.H. Burt, R. Pethig, J. Phys. D Appl. Phys. 30 (1997) L65.
[7] W.M. Arnold, U. Zimmermann, Z. Naturforsch 37c (1982) 908.
[8] M. Mischel, A. Voss, H.A. Pohl, J. Biol. Phys. 10 (1982) 223.
[9] A.D. Goater, R. Pethig, Parasitology 117 (1998) S177.
[10] D.C. Schupp, S.L. Erlandsen, J. Parasitol. 73 (1987) 723.
[11] A.M. Adams, K.C. Jinneman, Y.R. Ortega, in: R.K. Robinson, C.A. Bati, P.B. Patel (Eds.), Encyclopaedia of Food Microbiology, Academic Press, London, UK, 1999.
[12] C. Dalton, A.D. Goater, R. Pethig, H.V. Smith, Appl. Environ. Microbiol., 1062-00, 67 (2001) 586.
[13] J.P.H. Burt, R. Pethig, P.R.C. Gascoyne, F.F. Becker, Biochim. Biophys. Acta 1034 (1990) 93–101.
[14] X.-F. Zhou, J.P.H. Burt, R. Pethig, Phys. Med. Biol. 43 (1998) 1075.
[15] G. DeGasperis, X.B. Wang, J. Yang, F.F. Becker, P.R.C. Gascoyne, Meas. Sci. Tech. 9 (1998) 518.

APPLIED AND ENVIRONMENTAL MICROBIOLOGY, Feb. 2001, p. 586–590
0099-2240/01/$04.00+0 DOI: 10.1128/AEM.67.2.586–590.2001

Vol. 67, No. 2

Viability of *Giardia intestinalis* Cysts and Viability and Sporulation State of *Cyclospora cayetanensis* Oocysts Determined by Electrorotation

C. DALTON,[1] A. D. GOATER,[1]* R. PETHIG,[1] AND H. V. SMITH[2]

Institute of Molecular and Biomolecular Electronics, University of Wales, Bangor, Gwynedd LL57 1UT,[1] and Scottish Parasite Diagnostic Laboratory, Stobhill Hospital, Glasgow G21 3UW,[2] United Kingdom

Received 26 June 2000/Accepted 29 September 2000

Electrorotation is a noninvasive technique that is capable of detecting changes in the morphology and physicochemical properties of microorganisms. Electrorotation studies are reported for two intestinal parasites, *Giardia intestinalis* and *Cyclospora cayetanensis*. It is concluded that viable and nonviable *G. intestinalis* cysts can be differentiated by this technique, and support for this conclusion was obtained using a fluorogenic vital dye assay and morphological indicators. The viability of *C. cayetanensis* oocysts (for which no vital dye assay is currently available) can also be determined by electrorotation, as can their sporulation state. Modeling of the electrorotational response of these organisms was used to determine their dielectric properties and to gain an insight into the changes occurring within them. Electrorotation offers a new, simple, and rapid method for determining the viability of parasites in potable water and food products and as such has important healthcare implications.

Parasitism has a significant impact worldwide, both economically and in terms of human suffering. The environmental route of transmission (water, soil, or food) is important for many protozoan parasites. Increased demands made on natural resources increase the likelihood of encountering environments and food products contaminated with parasites. The development of new generic methods for simply and rapidly determining the viability of such parasites is therefore of importance.

Electrorotation is a new technique, in terms of its application to the study of microorganisms. During electrorotation, particles are subjected to a uniform rotating electric field that causes the particles to rotate (3, 20). The induced rotation of the particle is a sensitive function of the particle's dielectric properties, namely, the conductivity and permittivity of the organism's constituent components. These components include the wall (if present), the plasma membrane, and the cytoplasm. The rotation is also a function of the conductivity and permittivity of the suspending medium. Electrorotation has been successfully used to investigate the viability of oocysts of the protozoan *Cryptosporidium parvum* (12), and preliminary studies have been reported for oocysts of one human isolate of *Cyclospora cayetanensis* (8). Using an improved electrode design, we have investigated the electrorotational response of *Giardia intestinalis* cysts and have advanced our knowledge of the electrorotational response of oocysts of *C. cayetanensis*.

The flagellate *G. intestinalis* is the most frequently detected protozoan parasite in fecal samples from humans (11). Although an infected human can excrete up to 10^{10} cysts per day, the infective dose is low, between 25 and 100 cysts (26). In assessing water quality it is important not only to detect and identify cysts in low concentrations but also to determine their viability and therefore their potential for causing infection. Current methods for determining cyst viability include in vivo testing (27), in vitro excystation, vital dyes (32), phase-contrast microscopy (29), and heat shock mRNA analysis (1). In vivo methods are expensive, and while they give information about populations of cysts, none is obtained about individual cysts in a population, which is important when calculating the risk from parasites with low infectious doses. The in vitro methods are all lengthy procedures and/or subject to inaccuracies; for example, nonstaining was reported for one of four human isolates of *G. duodenalis* cysts tested (32), and excystation cannot be used for determining the viability of individual or small numbers of cysts (5). Smith (34) suggested that propidium iodide (PI) inclusion or exclusion and morphological assessment according to Schupp and Erlandsen (29) was the most suitable method for determining *G. intestinalis* cyst viability. Thompson and Boreham (36) also concluded that this was the most satisfactory way to proceed. We show that electrorotation can be used to determine the viability of *G. intestinalis* cysts, a conclusion supported using a combination of a vital dye and morphological indicators.

C. cayetanensis is a recently described protozoan parasite of humans (4, 21) and causes diarrheal illness worldwide. The exact mode of transmission is not yet known, but water- and food-borne routes have been implicated in recent outbreaks (35). The transmissive stage, a spherical oocyst with a diameter of 8 to 10 μm, is voided with the host feces in the unsporulated form. Sporulation occurs after 7 to 12 days of incubation at 25 to 30°C or within 6 months when maintained at 4°C; only sporulated oocysts are infectious. Identification of *C. cayetanensis* oocysts is through a combination of accurate size measurement, autofluorescence in UV light (450 to 490 nm and 365 nm), and excystation (22). Molecular techniques, for example, PCR, can be used for identification purposes (19), but

* Corresponding author. Mailing address: Institute of Molecular and Biomolecular Electronics, University of Wales, Dean St., Bangor, Gwynedd LL57 1UT, United Kingdom. Phone: 44 (0) 1248 351151, ext. 2711. Fax: 44 (0) 1248 361429. E-mail: agoater@sees.bangor.ac.uk.

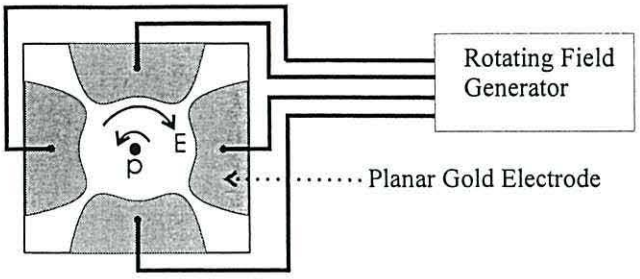

FIG. 1. A particle (p) suspended between four electrodes and subjected to a rotating electric field (E) (3, 13, 16, 20). Depending on the dielectric properties of the particle and the electrical frequency, the particle will rotate in either the same direction (cofield) or in the opposite direction (antifield) as the rotating field. Antifield rotation is depicted in this figure. The distance between opposing electrode faces was 2 mm.

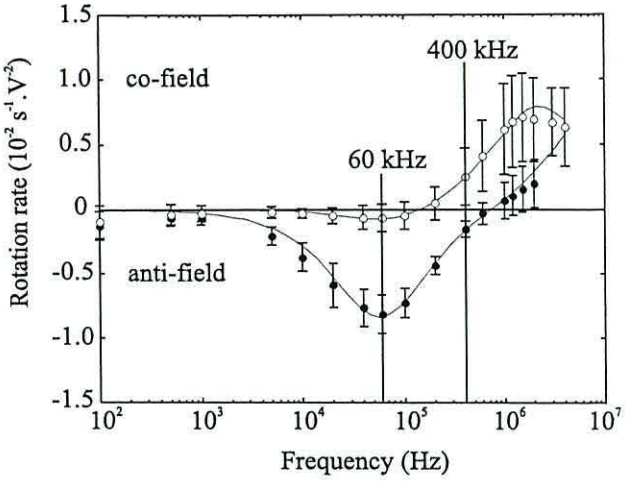

FIG. 2. Electrorotation spectra of *G. intestinalis* cysts at a suspending medium conductivity of 1 mS m^{-1} grouped according to inclusion or exclusion of the vital dye PI and morphology. Symbols show mean rotation rates and error bars indicate 1 standard deviation for $n = 8$ viable (solid symbols) and $n = 19$ nonviable cysts (open symbols). Solid lines show the best fits from the multishell model using the values listed in Table 1.

there are often distinct differences between laboratory and field data (33). No successful viability assays using vital dyes (10) or a suitable animal model have yet been reported for *C. cayetanensis* oocysts, and while the excystation method provides a means of viability determination, this typically takes between 1 and 2 weeks (21, 22), as the oocysts have to undergo sporulation first.

As the oocysts of *C. cayetanensis* are resistant to current water treatment procedures, including chlorination (25), and the infective dose is low, probably between 10 and 100 oocysts (2), there is a need for more-rapid viability assays that work at the single-organism level.

Based on our previous *C. parvum* study (12) and the current *G. intestinalis* data, we show strong evidence that, in the absence of a vital dye technique, the viability of *C. cayetanensis* oocysts can be determined by the electrorotation method. We also show that electrorotation can determine the sporulation state of an oocyst, which is important for assessing the potential risk of water contaminated with *C. cayetanensis*. Finally, we have analyzed the electrorotation response of the particles to determine their dielectric properties using the so-called dielectric multishell model, described elsewhere (18, 38).

MATERIALS AND METHODS

Cysts of *G. intestinalis* were obtained from human diarrheic samples provided by the public health laboratories of Gwynedd Hospital, Gwynedd, Wales, United Kingdom. Samples were purified by a water-ether sedimentation protocol followed by a sucrose flotation method (6). Cysts were then immediately washed in deionized water and stored at 4°C for use within 1 month. *G. intestinalis* cyst viability was determined morphologically by phase-contrast microscopy (29) and according to assays with the fluorogenic vital dye propidium iodide (PI) (30). A 100-μl aliquot of cyst suspension was incubated with 10 μl of PI (0.02 mg ml^{-1}) in phosphate-buffered saline (PBS), pH 7.4 (10 mM phosphate buffer, 27 mM KCl, 137 mM NaCl; Sigma Chemical Co.), for 30 min in a water bath at 37°C. Following the dye procedure the suspensions were washed in deionized water.

Purified *C. cayetanensis* oocysts were supplied by the Scottish Parasite Diagnostic Laboratory (SPDL) (Glasgow, United Kingdom). Samples were collected from three infected humans (two male, one female) in the Glasgow area who had recently traveled abroad. The samples were purified as for *G. intestinalis*. Oocysts were then washed in deionized water and stored at 4°C in 2% potassium dichromate solution.

To obtain reproducible electrorotation data, the particles are first washed and resuspended in a solution of well-defined chemical composition and conductivity. To reduce electrical heating effects, the magnitude of the rotating field should also be as low as possible. For the work reported here, PBS of conductivity 1 mS m^{-1} was used as the suspending medium to achieve easily measurable rotation rates for modest applied voltages in the convenient frequency range of 100 Hz to 10 MHz. The washing procedure (repeated three times) consisted of diluting a 100-μl aliquot of particle suspension in ultrapure water (conductivity, 0.1 mS m^{-1}) to 1.5 ml, vortexing for 30 s, microcentrifuging for 1 min (3,300 × *g*), and then aspirating to 100 μl. After the final wash, the sample was resuspended in PBS solution which had been diluted with ultrapure water to give a conductivity of 1 mS m^{-1}. The suspending medium conductivity was then checked by testing 200 μl of supernatant following centrifugation using a calibrated Hanna Instruments Pure Water Tester, modified to reduce the volume of the sample chamber. Working particle density concentrations were 3×10^4 cysts ml^{-1} for *G. intestinalis* and 5×10^3 oocysts ml^{-1} for *C. cayetanensis*.

Descriptions of the basic theory and experimental procedures of electrorotation are given elsewhere (13, 16). In brief, 20 μl of (oo)cyst suspension was pipetted into a chamber surrounded by four planar gold electrodes, as shown in Fig. 1. The so-called "bone" electrode design is described by a 4th-order polynomial and is optimized to create a uniform rotating electric field over as large an area as possible in the center of the chamber. The shape and magnitude of the spectra obtained are known to be affected by the particle position in the chamber and by the presence of debris on the particle surface (8). Particles were therefore excluded from analysis if they were positioned outside the middle third of the chamber, drifted more than three times their own diameter during the recording or possessed debris on their surface. These careful selection criteria, coupled with an electrode design that minimizes particle drift, improved the proportion of oocysts from which data could be obtained.

Particle identification and motion in the electric field were visualized using phase-contrast microscopy with a total magnification of ×400 (Nikon Optiphot microscope with JVC model TK-1280E color video camera attachment) and recorded by video for later analysis and timing by stopwatch. A minimum of 10 of behavior was recorded at each of 20, approximately equidistant, applied frequency points on a log scale over the range of 100 Hz to 10 MHz. After each aliquot had been examined and spectra had been recorded, the chamber was washed under pressure with ultrapure water from a wash bottle and dried under a stream of nitrogen gas.

RESULTS AND DISCUSSION

The electrorotation spectra obtained from 27 *G. intestinal* cysts, identified as possessing intact cyst walls with no debris adhering to the surface, are shown in Fig. 2. The spectra are grouped according to viability. It is clear that viable and non-viable cysts exhibit markedly different electrorotation behavio

TABLE 1. Particle dimensions and dielectric parameter values used in the modeling of electrorotation spectra

Parameter	*Giardia*[a]		*Cyclospora*			
	Viable	Nonviable	Unsporulated		Sporulated	
			Viable	Nonviable	Viable	Nonviable
Dimensions (μm)	9 × 6[b]	9 × 6[b]	9[c]	9[c]	9[c]	—[d]
Wall thickness (nm)	300[e]	300[e]	113[c]	113[c]	113[c]	—
Mean membrane thickness (midpoint ± range)(nm)	6 ± 0.5	6 ± 0.5	9 ± 0.5	9 ± 0.5	9 ± 0.5	—
Permittivity (ε_r)						
Interior	60[f]	60[f]	50[g]	50[g]	50[g]	—
Membrane (midpoint ± range)	6 ± 0.5	5 ± 0.5	4 ± 0.5	4 ± 0.5	4 ± 0.5	—
Wall	60[g]	60[g]	60[g]	60[g]	60[g]	—
Mean conductivity (midpoint ± range) (S m^{-1})						
Interior	0.8 ± 0.2	0.02 ± 0.002	0.8 ± 0.1	0.2 ± 0.03	0.8 ± 0.1	—
Membrane	$2 \times 10^{-6} \pm 0.8$	$1 \times 10^{-5} \pm 0.2$	$5.5 \times 10^{-6} \pm 0.3$	$1 \times 10^{-5} \pm 0.1$	$8 \times 10^{-6} \pm 0.5$	—
Wall	0.032 ± 0.002	0.05 ± 0.005	0.09 ± 0.01	0.01 ± 0.04	0.09 ± 0.01	—

[a] As determined by references 29 and 34.
[b] Measured values.
[c] From reference 21.
[d] —, none observed.
[e] From reference 31.
[f] From reference 15.
[g] From reference 16.

Spectrum profiles are in good agreement to those previously reported for the viability of isolated animal cells (14), biocide-treated yeast cells (*Saccharomyces cerevisiae* RXII) (37), and *C. parvum* oocysts (12).

Within the applied frequency range there is a frequency window, centered around 400 kHz, within which viable and nonviable cysts rotate in opposite directions. The terms "cofield" and "antifield" denote the sense of rotation of the particles relative to that of the applied field. At 400 kHz, cofield rotation thus characterizes nonviable cysts while antifield rotation characterizes viable cysts. The rotation direction, observed through a light microscope, is easily determined after a few seconds of observation and is aided by the ellipsoidal shape of the cysts. An alternative method of distinguishing the particle viability through electrorotation is by noting the significant difference in the magnitude of the antifield rotation peak. For these cysts (in a suspending medium of 1 mS m^{-1}), the peak antifield rotation, or characteristic frequency, is found at approximately 60 kHz. Although the greatest difference in rotational velocity for viable and nonviable cysts occurs at this frequency, determination of the viability of cysts by electrorotation alone requires accurate measurement of the rotational velocity and knowledge of the field strength. Automated image processing techniques that measure the rotational direction and velocity of particles have been demonstrated by several groups (9, 28, 38).

Modeling of the experimental data for *G. intestinalis* (Fig. 2) using an ellipsoidal two-shell model (37) allowed values of the electrical parameters of the different cell components to be estimated (Table 1). The most significant differences between viable and nonviable cysts are an increase in the membrane conductivity with a corresponding decrease in the interior conductivity. These findings are consistent with nonviable cysts having an impaired plasma membrane which allows ions to be exchanged more freely with the external media. This is also consistent with the response of PI dye, which only stains nonviable cysts as it cannot traverse intact biological membranes (17).

Initial electrorotation spectra for a second particle type of similar size, namely, the spherical oocysts of *C. cayetanensis*, are shown in Fig. 3. All of the $n = 19$ oocysts were in an unsporulated state and were morphologically indistinguishable. The spectra recorded, however, were of two distinct types. Similarities between these spectra and those shown in Fig. 2 for *G. intestinalis* cysts indicate the possibility that the

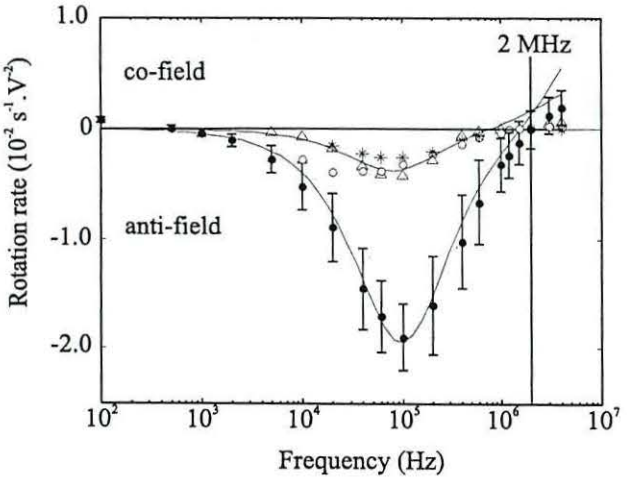

FIG. 3. Electrorotation spectra of unsporulated *C. cayetanensis* oocysts at a suspending medium conductivity of 1 mS m^{-1}. The spectra obtained from the $n = 19$ intact unsporulated oocysts were one of two distinct types. The first type, that characteristic of $n = 17$ oocysts, is summarized by the solid symbols and error bars representing the mean rotation rate and 1 standard deviation. The open symbols show the rotation rates of the $n = 2$ oocysts with the second distinct spectra type. Also shown is the electrorotation spectrum for an oocyst without internal contents (*). Solid lines show the best fit from the multishell model, using values listed in Table 1.

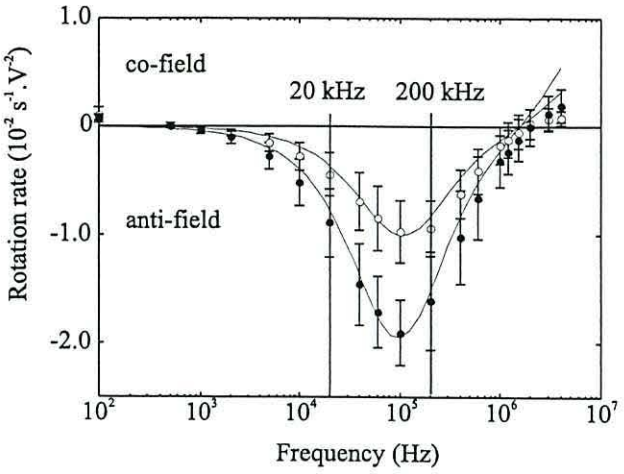

FIG. 4. Electrorotation spectra of *C. cayetanensis* oocysts at a suspending medium conductivity of 1 mS m^{-1} comparing sporulated and unsporulated intact oocysts. Symbols show mean rotation rates and error bars indicate 1 standard deviation for $n = 17$ unsporulated (solid symbols) and $n = 14$ sporulated (open symbols) oocysts. Solid lines show the best fit from the multishell model using values listed in Table 1.

two types of spectra shown in Fig. 3 are those of viable and nonviable oocysts. Discrimination of nonviable and viable *C. cayetanensis* oocysts by rotation in opposite directions at a specific frequency is not possible, due to overlap between the anti- and cofield crossover points and the very low rates of cofield rotation observed above 2 MHz.

The distinct $n = 2$ unsporulated intact-walled oocysts have a spectrum comparable to that of an oocyst that had no observable structural contents (Fig. 3) and which was considered nonviable. These spectra are similar over most of the frequency range, indicating that they are of a similar physiological state. The previous report on *C. cayetanensis* assumed that this type of response was due to a change in viability (8), but this could not be verified. Minor differences between spectra can be attributed to differing states of deterioration following oocyst death. Estimations of the electrical parameters of the different oocyst components for the viable and nonviable best model fits shown in Fig. 3 are listed in Table 1. Trends similar to those of the *G. intestinalis* cysts are found for the *C. cayetanensis* oocysts, namely, an increase in membrane conductivity with a corresponding decrease in the interior conductivity, providing further evidence that the change in shape of the spectra is indeed due to differences in physiological state.

Oocysts of *C. cayetanensis* were stored at room temperature (approximately 20°C) to induce sporulation. After 14 days, 30% were found to be sporulated. Excystation studies (21) on these sporulated oocysts performed at the SPDL showed that 75% excysted. An electrorotational comparison between unsporulated and sporulated oocysts of *C. cayetanensis* is shown in Fig. 4. The sporulation state was determined by the presence or absence of two sporocysts with the oocyst wall as identified using phase-contrast microscopy. Significant differences in the spectra are found in the frequency window from 20 to 200 kHz, with a much-reduced rotational velocity for the sporulated oocysts in this range. The previous report, for a single isolate of *C. cayetanensis*, indicated that at a frequency of 1 MHz, unsporulated and sporulated oocysts rotate in opposite directions (8). Although this previous conclusion was valid for that isolate, this distinction is not possible with mixed isolates. Importantly, however, the distinction based on the rate of rotation in the frequency window mentioned is confirmed. From the multishell model, the change in the spectra upon sporulation can be considered to be primarily associated with a slight increase in oocyst membrane conductivity. It must be noted, however, that whereas the multishell model enables accurate determinations to be made of the dielectric properties of the outermost membrane and wall of the oocysts, at best it can only provide a rough indication of any changes occurring in the properties or level of complexity of internal structures (7). From transmission electron microscopy studies (22), a sporulated oocyst is described as possessing a two-layered oocyst wall (63 and 50 nm thick, respectively) surrounding two sporocysts, each with 62-nm-thick walls surrounding a plasma membrane. Within each sporocyst are two membrane-bound sporozoites. These features may explain the deviation of the fitted lines in Fig. 4 from the experimental observations for *C. cayetanensis* at the higher frequencies, where the electrorotation properties are regarded as being more sensitive to the internal structure of particles (23).

In conclusion, we have demonstrated that the electrorotation technique can differentiate between viable and nonviable cysts of *G. intestinalis*. Two simple methods were identified for the rapid determination of cyst viability, the first of which involves only momentary observation of the particle to decide the direction of rotation. The second method involves determining the rotational velocity at a frequency close to the antifield maximum and may be more useful in environmental samples, as this feature is less sensitive to changes in the suspending medium conductivity. In using morphological inspection in conjunction with PI inclusion (36), we consider that our method for determining viability was sufficiently reliable in terms of deciphering the two distinct categories obtained in the electrorotation data.

In the absence of current viability surrogates for small numbers of organisms, we have also demonstrated that electrorotation velocity at the antifield maximum can be used to determine *C. cayetanensis* oocyst viability. The data presented in this paper for *G. intestinalis* cysts and from previously published electrorotation data from other protozoans (12), fungi (16), and animal cells (14) support this hypothesis. Indeed, where there is a need to develop viability assays for new pathogens or cells, by probing membrane integrity, electrorotation may provide a simple and rapid solution. Electrorotation also overcomes the problems associated with vital dyes, such as toxicity and the requirement for specialized storage.

The ability to determine the sporulation state of *C. cayetanensis* oocysts was also demonstrated with electrorotation. This is of importance as only following sporulation are the oocysts potentially infectious. Determining oocyst viability and sporulation state is therefore important in assessing the risk associated with potentially contaminated water. Currently only trained laboratory workers can identify the degree of sporulation, as oocysts of *C. cayetanensis* do not change their physical size upon sporulation.

Within the known limitations of the multishell model for

characterizing bioparticles of complex structure (7), the data (Table 1) indicate that the membrane conductivity of nonviable (oo)cysts is significantly greater than that of viable ones. The corresponding decrease in the internal conductivity of the (oo)cysts confirms that this is associated with a physical degradation of the membrane and the loss of its ability to act as a barrier to passive ion flow. It is also of interest to note from Table 1 that the best fit of the multishell model suggests that the *C. cayetanensis* membrane is thicker than that for *G. intestinalis* (9 and 6 nm, respectively). On the assumption that the chemical composition of the membrane remains constant, then the deduced reduction in the relative permittivity of the *G. intestinalis* membrane from a value of 6 ± 0.5 to $5 \pm 0.5\ \varepsilon_r$ also suggests that the effective surface area of the membrane is reduced on transition from the viable to nonviable state. A reduction in membrane surface area could correspond to a reduction in the complexity of the surface morphology, such as, for example, a reduction in membrane folding. Alternatively, the membrane polarizability could be reduced through a loss of protein function, for example, by the formation of protein complexes within the lipid bilayer (24).

ACKNOWLEDGMENTS

This work was supported by the Biotechnology and Biological Sciences Research Council, Swindon, United Kingdom (grant 97/B1/E/03539), and the National Foundation for Cancer Research, Bethesda, Md.

We thank C. A. Paton and J. A. Tame for technical assistance and M. Poole of the Public Health Laboratories, Bangor, United Kingdom, for supplying the *G. intestinalis* cysts.

REFERENCES

1. **Abbaszadegan, M., M. S. Huber, C. P. Gerber, and I. L. Pepper.** 1997. Detection of viable *Giardia* cysts by amplification of heat shock-induced mRNA. Appl. Environ. Microbiol. **63**:324–328.
2. **Adams, A., and Y. R. Ortega.** 1999. Cyclospora, p. 502–513. *In* R. K. Robinson, C. A. Batt, and P. D. Patel (ed.), Encyclopaedia of food microbiology. Academic Press Limited, London, United Kingdom.
3. **Arnold, W. M., and U. Zimmermann.** 1982. Rotating-field-induced rotation and measurement of the membrane capacitance of single mesophyll cells of *Avena sativa*. Z. Naturforsch. Teil C **37**:908–915.
4. **Ashford, R. W.** 1979. Occurrence of an undescribed coccidian in man in Papua New Guinea. Ann. Trop. Med. Parasitol. **73**:497–500.
5. **Bingham, A. K., E. L. Jarroll, E. A. Meyer, and S. Radulescu.** 1979. *Giardia* spp.: physical factors of excystation *in vitro* and excystation vs. eosin exclusion as determinants of viability. Exp. Parasitol. **47**:281–291.
6. **Bukhari, Z., and H. V. Smith.** 1995. Effect of three concentration techniques on viability of *Cryptosporidium parvum* oocysts recovered from bovine feces. J. Clin. Microbiol. **33**:2592–2595.
7. **Chan, K. L., P. R. C. Gascoyne, F. F. Becker, and R. Pethig.** 1997. Electrorotation of liposomes: verification of dielectric multi-shell model for cells. Biochim. Biophys. Acta **1349**:182–196.
8. **Dalton, C., R. Pethig, C. A. Paton, and H. V. Smith.** 1999. Electrorotation of oocysts of *Cyclospora cayetanensis*. Inst. Phys. Conf. Ser. **163**:85–88.
9. **DeGasperis, G., X. B. Wang, J. Yang, F. F. Becker, and P. R. C. Gascoyne.** 1998. Automated electrorotation: dielectric characterisation of living cells by real time motion estimation. Meas. Sci. Tech. **9**:518–529.
10. **Eberhard, M. L., N. J. Pieniazek, and M. J. Arrowood.** 1997. Laboratory diagnosis of *Cyclospora* infections. Arch. Pathol. Lab. Med. **121**:792–797.
11. **Farthing, M. J. G., A.-M. Cevallos, and P. Kelly.** 1996. Intestinal protozoa, p. 1255–1269. *In* G. C. Cook (ed.), Manson's tropical diseases, 20th ed. W. B. Saunders Ltd., London, United Kingdom.
12. **Goater, A. D., J. P. H. Burt, and R. Pethig.** 1997. A combined travelling wave dielectrophoresis and electrorotation device: applied to the concentration and viability of *Cryptosporidium*. J. Phys. D Appl. Phys. **30**:L65–L69.
13. **Goater, A. D., and R. Pethig.** 1998. Electrorotation and dielectrophoresis. Parasitology **117**:S177–S189.
14. **Gundel, J., D. Wicher, and H. Matthies.** 1989. Electrorotation as a viability test for isolated single animal cells. Stud. Biophys. **133**:5–18.
15. **Hölzel, R., and I. Lamprecht.** 1992. Dielectric properties of yeast cells as determined by electrorotation. Biochim. Biophys. Acta **1104**:195–200.
16. **Huang, Y., R. Hölzel, R. Pethig, and X.-B. Wang.** 1992. Differences in the AC electrodynamics of viable and non-viable yeast cells determined through combined dielectrophoresis and electro-rotation studies. Phys. Med. Biol. **37**:1499–1517.
17. **Jones, K. H., and J. A. Senft.** 1985. An improved method to determine cell viability by simultaneous staining with fluorescein diacetate and propidium iodide. J. Histochem. Cytochem. **331**:77–79.
18. **Kakutani, T., S. Shibatani, and M. Sugai.** 1993. Electrorotation of non-spherical cells—theory for ellipsoidal cells with an arbitrary number of shells. Bioelectrochem. Bioenerg. **31**:131–145.
19. **Lopez, F. A., J. Manglicmot, T. M. Schmidt, C. Yeh, H. V. Smith, and D. A. Relman.** 1999. Molecular characterisation of Cyclospora-like organisms from Baboons. J. Infect. Dis. **179**:670–679.
20. **Mischel, M., A. Voss, and H. A. Pohl.** 1982. Cellular spin resonance in rotating electric fields. J. Biol. Phys. **10**:223–226.
21. **Ortega, Y. R., C. R. Sterling, R. H. Gilman, V. A. Cama, and F. Diaz.** 1993. *Cyclospora species*: a new protozoan pathogen of humans. N. Engl. J. Med. **328**:1308–1312.
22. **Ortega, Y. R., R. H. Gilman, and C. R. Sterling.** 1994. A new coccidian parasite (Apicomplexa: Eimeriidae) from humans. J. Parasitol. **80**:625–629.
23. **Pethig, R.** 1991. Application of A.C. electrical fields to the manipulation and characterisation of cells, p. 159–185. *In* I. Karube (ed.), Automation in biotechnology. Elsevier, Amsterdam, The Netherlands.
24. **Pethig, R., and D. Kell.** 1987. The passive electrical properties of biological systems—their significance in physiology, biophysics and biotechnology. Phys. Med. Biol. **32**:933–970.
25. **Rabold, G., C. W. Hoge, D. R. Shlim, C. Kefford, R. Rajah, and P. Echeverria.** 1994. *Cyclospora* outbreak associated with chlorinated drinking water. Lancet **344**:1360.
26. **Rentdorff, R. C.** 1979. The experimental transmission of *Giardia lamblia* among volunteer subjects, p. 64–81. *In* W. Jakubowski and J. C. Hoff (ed.), Waterborne transmission of giardiasis. U.S. Environmental Protection Agency, Cincinnati, Ohio.
27. **Roberts-Thompson, I. C., D. P. Stevens, A. A. F. Moahmoud, and K. S. Warren.** 1976. Giardiasis in the mouse: an animal model. Gastroenterology **7**:57–61.
28. **Schnelle, T., H. Glasser, and G. Fuhr.** 1997. Opto-electronic technique for automatic detection of electrorotational spectra of single cells. Cell. Eng. **2**:33–41.
29. **Schupp, D. C., and S. L. Erlandsen.** 1987. Determination of *G. muris* cyst viability by differential interference contrast, phase, or brightfield microscopy. J. Parasitol. **73**:723–729.
30. **Schupp, D. C., and S. L. Erlandsen.** 1987. A new method to determine *Giardia* cyst viability: correlation of fluorescein diacetate and propidium iodide staining with animal infectivity. Appl. Environ. Microbiol. **53**:704–707.
31. **Sheffield, H. G., and B. Bjorvatn.** 1977. Ultrastructure of the cysts of *Giardia lamblia*. Am. J. Trop. Med. Hyg. **26**:23–30.
32. **Smith, A. L., and H. V. Smith.** 1989. A comparison of fluorescein diacetate and propidium iodide staining and *in vitro* excystation for determining *Giardia intestinalis* cyst viability. Parasitology **99**:329–331.
33. **Smith, H. V.** 1998. Detection of parasites in the environment. Parasitology **117**:S113–S141.
34. **Smith, H. V.** 1996. Detection of *Giardia* and *Cryptosporidium* in water: current status and future prospects, p. 195–225. *In* R. W. Pickup and J. R. Saunders (ed.), Molecular approaches to environmental microbiology. Ellis-Horwood, Chichester, United Kingdom.
35. **Sterling, C. R., and Y. R. Ortega.** 1999. *Cyclospora*: an enigma worth unravelling. Emerg. Infect. Dis. **5**:48–53.
36. **Thompson, R. C. A., and P. F. L. Boreham.** 1994. Discussants report: biotic and abiotic transmission, p. 131–136. *In* R. C. A. Thompson, J. A. Reynoldson, and A. J. Lymbery (ed.), *Giardia*: from molecules to disease. CAB International, Oxon, United Kingdom.
37. **Zhou, X.-F., G. H. Markx, and R. Pethig.** 1996. Effect of biocide concentration on electrorotation spectra of yeast cells. Biochim. Biophys. Acta Biomembr. **1281**:60–64.
38. **Zhou, X.-F., J. P. H. Burt, and R. Pethig.** 1998. Automatic cell electrorotation measurements: applied to studies of the biological effects of low-frequency magnetic fields and of heat shock. Phys. Med. Biol. **43**:1075–1090.

Royal Society of Tropical Medicine and Hygiene in Scotland Meeting at the University of Glasgow, Glasgow, 17 May 2000

Poster presentations

Acidic vesicles in *Schistosoma mansoni*

B. J. Cooke[1], P. Hagan[1], J. A. Thornhill[2], P. Carneiro-Santos[1] and J. R. Kusel[2] *Divisions of [1] Infection and Immunity, and [2] Biochemistry and Molecular Biology, IBLS, University of Glasgow, Glasgow G12 8QQ, UK*

Schistosomula of *Schistosoma mansoni* were stained with the fluorescent dye Lysotracker Red DND-99, which becomes protonated in acidic vesicles such as lysosomes (HAUGLAND, 1996: *Molecular Probes Handbook of Fluorescent Probes and Research Chemicals*, 6th edn. Oregon, USA: Molecular Probes Inc.). Accumulation of the dye was seen as brightly stained patches throughout the schistosomula, but did not occur in cercariae (P. Carneiro-Santos, unpublished). These novel organelles are a possible site of action of the drug praziquantel.

Methylene blue, a redox indicator, is coloured only when oxidized. Coloured methylene blue was seen to quench the fluorescence of Lysotracker within the acidic vesicles. This was visible as black spots in the fluorescent parasite, and demonstrated strongly oxidizing conditions within the vesicles. Addition of the oxidizing agent hydrogen peroxide revealed that the methylene blue was not accumulated in the vesicles, but that it was present throughout the parasite in its reduced form.

Quantitation of the vesicles in the schistosomula revealed a mean of 24·24, (SD 5·77). This number was seen to increase after 24, 48 and 72 h ($0{\cdot}05 > P > 0{\cdot}01$).

Addition of the methylene blue to the stained schistosomula can be used to demonstrate anaerobiasis in individual parasites with a high degree of sensitivity, and shows that conditions vary across the slide.

What is 'tropical medicine'?

S. Daga, C. L. Ewles, H. Javedan, F. C. Kerr, A. Maudgil and C. T. Roberts[1] (with David Stevenson[2] as group advisor) *[1] Second-year Students, The University of Edinburgh Medical School, Teviot Place, Edinburgh EH8 9AG, UK, [2] Honorary Fellow, Public Health Sciences, University of Edinburgh, UK*

Six second-year medical students formed a Special Study Module to determine the nature and relevance of 'tropical medicine' in the 21st century. It appears that since it was first established, the definition of 'tropical medicine' has remained ill-defined and poorly understood.

To improve understanding and resolve the dilemma, the evidence for both the speciality and the practice of medicine in the tropics was reviewed from geographical and social points of view and in relation to specific 'tropical diseases'.

Such analysis led to the conclusion that defining which factors are responsible for 'tropical diseases' is a difficult task. In addition, a more holistic approach should be taken, incorporating the changing health of the world and how the health of some areas affects others. In light of this, it may be an idea to think in terms of global health.

The complete report is available on the internet: http://www.bms.ed.ac.uk/medics/year2/group76

Electrorotation studies of *Ascaris suum*

C. Dalton[1], R. Pethig[1] and H. V. Smith[2] *[1] Institute of Molecular and Biomolecular Electronics, University of Wales, Bangor, Gwynedd LL57 1UT, UK; [2] Scottish Parasite Diagnostic Laboratory, Stobhill Hospital, Glasgow G21 3UW, UK*

We report electrorotation studies of ova of the nematode *Ascaris suum*. Electrorotation, the process of inducing controlled cellular spin by using rotating electric fields, is sensitive to the dielectric properties of microbiological organisms (ARNOLD, W. M. & ZIMMERMAN, U., 1988: *Journal of Electrostatics*, 21, 151–191). *A. suum* is the large roundworm infecting swine which can cross infect to humans (ANDERSON, T. J. C., 1995: *Parasitology*, 110, 215–219). An adult female worm can lay in excess of 200 000 fertilized ova per day into the environment, which in temperate climates can remain viable for 7 years. There are currently some 59 million people at risk of some morbidity from ascariasis (DE SILVA, N. R. *et al.*, 1997: *Tropical Medicine and International Health*, 2, 519–528).

We present distinct differences in the electrorotational response between fertilized and unfertilized ova of *A. suum*, which can be used for identification purposes in mixed populations. We also report variations within the fertilized ova spectra, which may be due to changes in the ova structure during the life-cycle. As electrorotation is a non-invasive process, after spectra have been acquired, the ova can be further analysed by conventional means.

Substrate recognition motifs of the *Trypanosoma brucei* nucleobase transporters

Lynsey J. M. McMurray and Harry P. de Koning *Division of Infection and Immunity, IBLS, University of Glasgow, Glasgow G12 8QQ, UK*

The P2 adenosine transporter has been used as a means of drug entry into *Trypanosoma brucei* (TYE, C.-K. *et al.*, 1998: *Bioorganic and Medicinal Chemistry Letters*, 8, 811–816). We decided to investigate the *T. brucei* nucleobase transporters as alternative 'doorways'. Low concentrations of free nucleobase in mammalian blood, and a high affinity of the parasite transporters for their nucleobase substrates, ensure selectivity of designed drugs. Nucleobase analogues have a distinguished history as anti-viral and anti-neoplastic agents, and a reservoir of known compounds exists. Bloodstream forms of *T. brucei* express 2 hypoxanthine transporters: the high-affinity H2 transporter and the lower-affinity H3 transporter (DE KONING, H. P. & JARVIS, S. M., 1997: *Molecular and Biochemical Parasitology*, 89, 245–258). Procyclic parasites express only the low-affinity H1 transporter (DE KONING, H. P. & JARVIS, S. M., 1997: *European Journal of Biochemistry*, 247, 1102–1110). Using an oil-spin technique to assay uptake, and by using nucleobase analogues, we will 'map' the different recognition motifs required for efficient hypoxanthine uptake by the H1 and H2 transporters.

Recovery of *Cryptosporidium* oocysts and *Giardia* cysts from large volumes of natural mineral waters

C. A. Paton, R. A. B. Nichols and H. V. Smith *Scottish Parasite Diagnostic Laboratory, Stobhill Hospital, Glasgow G21 3UW, UK*

Current European Union and UK legislation states that natural mineral waters should be free from parasites

TRANSACTIONS OF THE ROYAL SOCIETY OF TROPICAL MEDICINE AND HYGIENE (1999) 93, 461–463

Royal Society of Tropical Medicine and Hygiene in Scotland Meeting at the Pfizer Institute, Edinburgh, 19 May 1999

Poster presentations

Application of a murine model for contagious bovine pleuropneumonia (CBPP) to the in-vivo comparison of the virulence of European and African isolates

Malcolm J. Brodlie[1] and John B. March[2] *[1] Division of Biological Sciences, ICAPB, University of Edinburgh, King's Buildings, Ashworth Laboratories, West Mains Road, Edinburgh EH9 3JT, UK; [2] Moredun Research Institute, Pentland Science Park, Bush Loan, Penicuik EH26 0PZ, UK*

Contagious bovine pleuropneumonia (CBPP) is economically the most important cattle disease in Africa. The aetiological agent is *Mycoplasma mycoides* subspecies *mycoides* small colony variant (*MmmSC*). CBPP is generally considered to be more severe in Africa than in Europe—one explanation being that African strains are more virulent than European strains. Unfortunately *MmmSC* is a restricted pathogen in Britain rendering experiments involving cattle prohibitively expensive.

European strains have been shown to possess genotypic and metabolic differences from African strains; however, the relevance of these to virulence has not been demonstrated. In-vitro growth inhibition tests performed in this laboratory have suggested no difference in virulence between the 2 groups. In this study the virulence of European and African strains were compared *in vivo* using a murine model (SMITH, G. R., 1971: *Tropical Animal Health and Production*, 3, 169–172). No significant differences were found, suggesting that other factors such as improved husbandry and chemotherapy may be responsible for the more benign nature of CBPP in Europe.

An additional finding from this study was that strain M375, recently isolated from Botswana, was of significantly lower virulence in mice than the other *MmmSC* strains, providing further evidence that it behaves atypically for the species.

Molecular detection and characterization of *Cryptosporidium parvum* in human and wastewater samples

B. M. Campbell[1,2], R. A. B. Nichols[1], J. E. O'Grady[2] and H. V. Smith[1] *[1] Scottish Parasite Diagnostic Laboratory, Stobhill Hospital, Glasgow G21 3UW, UK; [2] University of Strathclyde, The Todd Centre, Department of Immunology, Glasgow G4 0NR, UK*

Cryptosporidium parvum causes gastrointestinal infection in both human beings and domestic livestock. Two genotypes have been described from analysis of 6 polymorphic genetic loci of *C. parvum*, namely genotype H (human) found only in humans, and genotype C (cattle) found in both human and non-human hosts. *C. parvum*-positive stool samples submitted to the Scottish Parasite Diagnostic Laboratory were purified and analysed by PCR-RFLP of the COWP gene (SPANO, F. *et al.*, 1997: *FEMS Microbiology Letters*, 150, 209–217) and characterized as either genotype H or C. Of 36 stool samples analysed, 27 were from sporadic cases and 9 were from 'outbreak' cases. Twenty four of the 27 sporadic cases were genotype C and 3 were genotype H, whereas all 'outbreak' cases were genotype C. Assay sensitivity for PCR-RFLP of the COWP gene was between 10 and 20 purified oocysts. Thirty sewage effluent samples were seeded with varying concentrations of oocysts (10, 100 and 1000) of an Iowa isolate (genotype C). The sensitivity of detection was between 100 and 1000 oocysts. Infectivity studies with genotypes H and C in ICR/CD1 neonate mice indicated that only genotype C oocysts caused infection. Improved PCR sensitivity could be achieved by genotyping the internal transcribed spacer 1 region or other multicopy gene. Genotyping small numbers of oocysts in both clinical and sewage effluent samples can assist in our understanding of *C. parvum* epidemiology.

Viability determination of *Cyclospora cayetanensis* oocysts

C. Dalton[1], R. Pethig[1], C. A. Paton[2] and H. V. Smith[2] *[1] Institute of Molecular and Biomolecular Electronics, University of Wales, Bangor LL57 1UT, UK; [2] Scottish Parasite Diagnostic Laboratory, Stobhill Hospital, Glasgow G21 3UW, UK*

Electrorotation, the process of inducing controlled cellular spin by using rotating electric fields, is sensitive to the dielectric properties of microbiological organisms (ARNOLD, W. M. *et al.*, 1988: *Journal of Electrostatics*, 21, 151–191).

Cyclospora cayetanensis is an emerging coccidian pathogen of humans, and is resilient to disinfection regimens used in water treatment. The viable, sporulated oocysts are not readily detected by the current methods used to assure the safety of water supplies. The oocysts are uniform in size and shape (spherical, 8–10 μm in diameter), making them ideal for electrorotational studies.

Using a microfabricated planar gold electrode structure, we investigated the electrorotational properties of oocysts of *C. cayetanensis*. We present variations in the response of morphologically similar oocysts, which are characteristic of a difference in oocyst viability (DALTON, C. *et al.*, 1999: *Institute of Physics Electrostatics '99 Conference Proceedings* [in press]). Differences in the electrorotational response of sporulated and unsporulated oocysts are also described. This rapid, non-invasive technique has potential applications in diagnostics.

Cryptosporidium oocyst manipulation, viability determination and capture using a combined travelling wave dielectrophoresis and electrorotation device

A. D. Goater[1], R. Pethig[1], C. A. Paton[2] and H. V. Smith[2] *[1] Institute of Molecular and Biomolecular Electronics, University of Wales, Bangor LL57 1UT, UK; [2] Scottish Parasite Diagnostic Laboratory, Stobhill Hospital, Glasgow G21 3UW, UK*

A micro-electrode device is described for manoeuvring single particles from a suspension for capture on to a membrane filter. Fabricated on a thin polyimide film by photolithography and laser ablation, the device is demonstrated here using oocysts of *Cryptosporidium parvum*, a waterborne pathogen of humans. The design allows the generation of both travelling wave and rotating electric fields by the same electrodes (GOATER, A. D. *et al.*, 1997: *Journal of Physics D: Applied Physics*, 30, L65–L69). Travelling wave dielectrophoresis (TALARY, M. S. *et al.*, 1996: *Journal of Physics D: Applied Physics*, 29, 2198–2203) is used to concentrate the particles into a central electrorotation (ARNOLD, W. M. *et al.*, 1988: *Journal of Electrostatics*, 21, 151–191) chamber where the physiolo-

Inst. Phys. Conf. Ser. No 163
Paper presented at the 10th Int. Conf., Cambridge, 28–31 March 1999

Electrorotation of oocysts of *Cyclospora cayetanensis*

C Dalton[1], R Pethig[1], C A Paton[2] and H V Smith[2]

[1]Institute of Molecular and Biomolecular Electronics, University of Wales, Dean Street, Bangor, Gwynedd, LL57 1UT, UK

[2]Scottish Parasite Diagnostic Laboratory, Stobhill NHS Trust Hospital, Springburn, Glasgow G21 3UW, UK

Abstract. Electrorotation is sensitive to the dielectric properties of microbiological organisms. Using a microfabricated planar gold electrode structure, we investigated the electrorotational properties of oocysts of the emerging coccidian pathogen, *Cyclospora cayetanensis*. We present differences in the electrorotational response of sporulated and unsporulated oocysts. Variations in the responses of morphologically similar oocysts, which are characteristic of a difference in oocyst viability, are also described. This rapid, non-invasive technique has potential applications in diagnostics.

1. Introduction

Cyclospora cayetanensis is a coccidian pathogen which causes prolonged diarrhoeal disease in both immunocompetant and immunocompromised hosts. Waterborne and foodborne routes have been implicated as likely routes of transmission. *Cyclospora* was first reported in humans by Ashford in 1979 [1] and is resilient to disinfection regimes used in water treatment. Viable, sporulated oocysts are responsible for the transmission of infection, and are not readily detected by current methods used to assure the safety of water supplies. Thus, distinguishing between non-viable and viable oocysts is of great significance to a variety of professionals, including epidemiologists, public health officials, and water industry personnel. The oocysts are remarkably uniform in size and shape (spherical, 8-10 μm diameter), making them ideal for electrorotational studies.

2. Electrorotation

As described by Pohl in 1978 [2], non-uniform (inhomogeneous) fields can induce a torque on a particle suspended in an electrolyte, causing it to spin. Arnold and Zimmerman [3] and Mischel *et al.* [4] first reported methods to induce controlled cellular spin by using rotating electric fields. A uniform rotating electric field can be generated by energising four electrodes with sinusoidal voltages, with 90° phase difference between adjacent electrodes (*figure 1*). The rate and direction of the induced electrorotation is determined by the imaginary component of the dipole moment m of the particle, which is itself dependant on the dielectric properties of the system as a whole. The rotational torque $\Gamma(\omega)$ exerted on a particle by the rotating electric field is given by :

$$\Gamma(\omega) = -\mathrm{Im}\{m(\omega)\}E$$

where *Im* indicates the imaginary component of the dipole moment *m* and *E* is the electric field strength. If the imaginary component of *m* is positive, then the torque exerted will be negative causing the particle to rotate in a direction that *opposes* that of the rotating field (*figure 1b*).

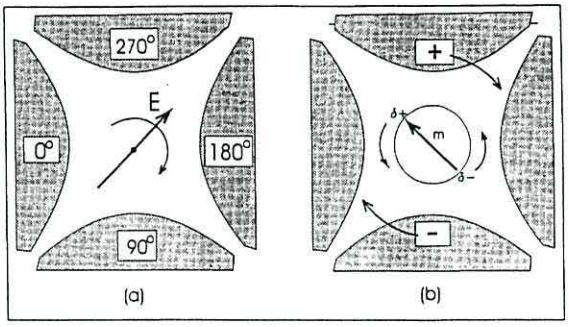

Figure 1 - (a) Rotating field generated by applying sinusoidal voltages to 4 electrodes, with phases spaced 90° apart. (b) The rotational torque acting on the particle will be either co- or anti- field, depending on the angle of the induced dipole moment. In the case represented here, the particle is rotating counter to the clockwise rotating field.

For biological particles, such as oocysts of *C. cayetanensis*, structures such as the oocyst wall and plasma membrane, along with the cytoplasm and its contents, each contribute to the overall electrical permittivity and conductivity of the particle.

3. Equipment and Materials

The electrodes were deposited by photolithography onto glass microscope slides, with a chromium adhesion layer of 5 nm and a gold layer of 70 nm. The inter-electrode analysis chamber was 2 mm in diameter. The electric fields were generated by a four phase sinusoidal signal generator, and applied to the electrodes in the frequency range 100 Hz to 10 MHz. Oocysts of *C. cayetanensis* were supplied by the Scottish Parasite Diagnostic Laboratory (SPDL), in either 2% potassium dichromate solution, or water. Oocysts were washed in ultra pure water and re-suspended in dilute solutions of normal phosphate buffered saline (Sigma Chemical Co.), which typically had conductivites of 0.6-1.0 mS/m, to reduce electrolysis and heat production at the electrodes. Sample results were visualised through a Nikon Optiphot 2 microscope using phase contrast microscopy with a magnification of x40 and a zoom of x2.25. Results were recorded to video tape for subsequent analysis using a JVC colour video camera head (model TK-1280E) attached to the microscope.

4. Results and Observations

Over 100 electrorotation spectra were obtained which facilitated the differentiation of sporulated and unsporulated oocysts of *C. cayetanensis*. Unsporulated oocysts rotate at a higher rate than sporulated oocysts (*figure 2*). The frequency at which the direction of rotation reverses from anti-field to co-field at high frequency (the so called cross-over frequency), is significantly different between sporulated and unsporulated oocysts. Thus, at 1MHz the unsporulated oocysts will rotate in the opposite direction to the sporulated oocysts, allowing rapid discrimination between the two types of oocyst.

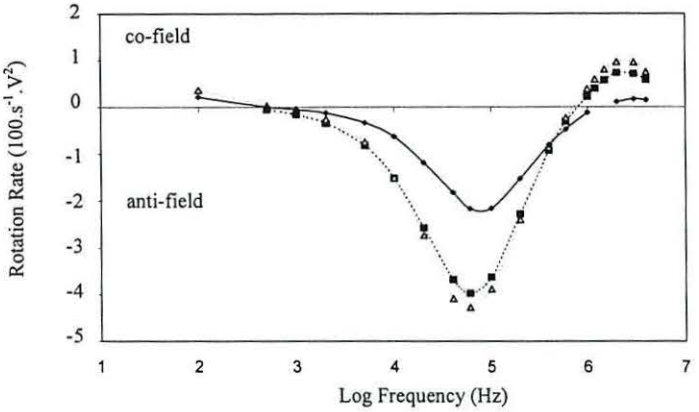

Figure 2 – Rotation spectra of unsporulated oocysts (dashed lines), which rotate at a higher rate than sporulated oocysts (solid line).

It is not possible to distinguish morphologically between viable and non-viable oocysts containing similar morula. Non-viable and viable oocysts can be either sporulated or unsporulated. The membrane of a viable oocyst is semi-permeable (selectively) to ions and non-lipid, soluble molecules. Upon cell death, membrane integrity is lost, and the cell freely exchanges material with the external suspending medium. This greatly affects the rotation spectra produced, as less induced charge differences occur between the inside of the oocyst, and the exterior medium. The peak rotation frequency was found to vary considerably for visibly similar, particulate free, unsporulated oocysts of *C. cayetanensis* (*figure 3*).

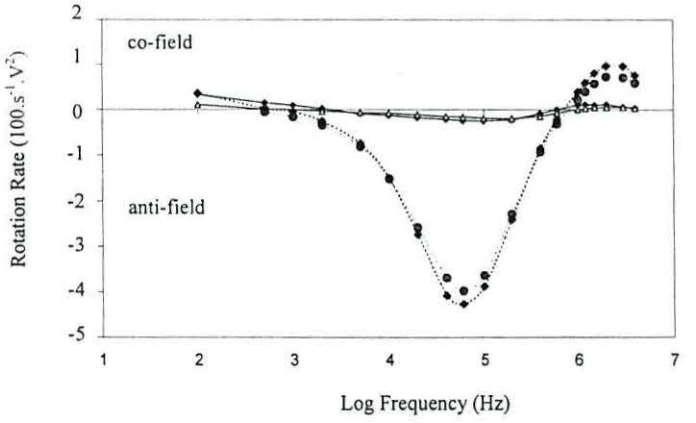

Figure 3 – Rotation spectra of unsporulated *C. cayetanensis* oocysts showing the difference between viable (dashed lines) and possibly non-viable (solid lines) oocysts.

This difference in the magnitude of rotation rate is similar to that reported by Goater *et al.* [5] for *Cryptosporidium parvum*, a smaller, but similar pathogen to *C. cayetanensis*. Goater confirmed that this observation was due to differences in oocyst viability by fluorogenic vital dye assay [6]. The viability of *C. cayetanensis* oocysts cannot be independently verified by such methods, because as yet none have been developed. Excystation of the oocysts at SPDL confirmed that 75% of the sporulated oocysts from the sample were viable.

The effect of small amounts of debris on the oocyst wall was investigated. The peak rotation frequency, and the rotation cross-over frequency values, for the debris-coated and uncoated oocysts, all remained the same (*figure 4*). The only difference was a slower rotation rate for the debris-coated oocysts. This can be attributed to viscous drag caused by the debris.

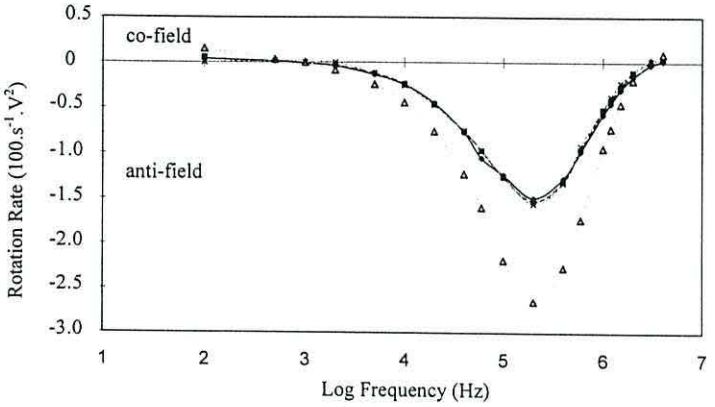

Figure 4 – Rotation spectra of uncoated (dashed line) and debris-coated (solid lines) sporulated oocysts of *C. cayetanensis*.

5. Conclusions

In this work, the sensitivity of the electrorotation assay in determining characteristic differences between morphologically indistinguishable oocysts of the pathogen *Cyclospora cayetanensis* has been shown. An important result has been the apparent ability of the assay to distinguish between viable and non-viable oocysts, previously not possible. As electrorotation is a non-invasive process, the undamaged oocysts can be tested further by other techniques in the hope of determining the life-cycle and modes of transmission.

6. Acknowledgements

We gratefully acknowledge the support of the BBSRC and NFCR, and thank A D Goater for valuable discussions and J Tame for technical assistance.

References

[1] Ashford R W 1979 *Annals of Tropical Medicine and Parasitology* **73** 497-500

[2] Pohl H A 1978 *Dielectrophoresis* (Cambridge: Cambridge University Press)

[3] Arnold W M and Zimmerman U 1988 *J. Electrostatics* **21** 151-191

[4] Mischel M, Voss A and Pohl H A 1982 *J. Biol. Phys.* **10** 223-226

[5] Goater A D, Burt, J P H and Pethig R 1997 *J. Phys. D : Appl. Phys.* **30** L65-L69

[6] Goater A D *personal communication*